



# THÈSE

En vue de l'obtention du

## DOCTORAT DE L'UNIVERSITÉ DE TOULOUSE

Délivré par **l'Institut Supérieur de l'Aéronautique et de l'Espace**  
Spécialité : Systèmes automatiques

---

Présentée et soutenue par **Alexander Peter FEUERSÄNGER**  
le 4 décembre 2007

**Contrôle d'un avion à stabilité réduite**  
**Control of Aircraft with Reduced Stability**

---

### JURY

M. Benoît Bergeon, président du jury - rapporteur  
M. Laurent Bovet  
M. Gilles Ferrères, co-directeur de thèse  
M. Dieter Schmitt, rapporteur  
M. Clément Toussaint, co-directeur de thèse  
M. Daniel Walker, rapporteur

---

École doctorale : **Systèmes**

Unité de recherche : **Équipe d'accueil SUPAERO-ONERA CSDV (ONERA-DCSD, centre de Toulouse)**

Co-directeurs de thèse : **M. Gilles Ferrères, M. Clément Toussaint**

## **Contrôle d'un avion à stabilité réduite**

Afin d'améliorer les performances et l'efficacité des avions civils, les développements actuels sont toujours plus orientés vers la réduction de la stabilité naturelle en combinaison avec un système de stabilisation automatique. Ceci permet de réduire de façon significative la traînée de l'avion en minimisant les surfaces stabilisatrices ou de voler avec des centrages plus avantageux.

Deux objectifs principaux définissent l'orientation de cette thèse. En première partie, on propose un ensemble de méthodes et d'outils pour évaluer l'impact d'une réduction de la stabilité naturelle de l'avion. Dans le cadre des critères de certification, nous examinons les paramètres qui jouent simultanément sur une augmentation de l'efficacité et une réduction de la stabilité, notamment la surface de la dérive et le centrage. En faisant cette évaluation dans le contexte d'avant-projet, nous aboutissons à des recommandations pour la conception de l'avion.

La deuxième partie traite de la synthèse d'un correcteur robuste de type back-up. On utilise une technique de synthèse polytopique qui garantit les qualités de vol nécessaires sur une large plage de centrages. Cette approche multi-objectif a pour but de limiter l'activité des actionneurs (critère Hinf) ainsi que de maximiser la positivité du système en boucle fermée pour garantir la stabilité en présence des saturations. Nous calculons les domaines d'attraction correspondants et proposons de synthétiser un correcteur de type anti-windup pour améliorer la performance du système saturé.

Finalement, une dernière partie traite des gains que l'on peut attendre avec les concepts d'avion à stabilité réduite. Sous quelques hypothèses, nous estimons les gains en masse, traînée et consommation de carburant pour démontrer l'intérêt des outils développés et de l'approche choisie.

*Mots Clés* : qualités de vol, stabilité réduite, actionneurs, correcteur statique robuste

## **Control of Aircraft with Reduced Stability**

In the ongoing competition for enhanced efficiency, major airplane manufacturers tend to incorporate a reduced flight dynamic stability or even instability in civil aircraft design. This allows for the installation of smaller vertical and horizontal stabilizers or a wider range of allowable center of gravity positions. As a consequence, the natural aircraft does not necessarily meet the handling quality requirements for certification. It can even be completely uncontrollable when stability augmentation systems fail. In that case, an autonomously operating back-up system has to guarantee minimum flying qualities.

Two overarching objectives define the road map for this dissertation. The first part deals with the assessment of the impact of reduced stability on airplane flight mechanics and dynamics. Within the context of certification requirements the influence of efficiency enhancing parameters that reduce stability has to be examined. Special focus is laid on the size of the vertical tailplane, and therewith on criteria linked to the minimum control speed VMC, as well as on aft center of gravity positions. An optimization of these parameters leads to a degradation in handling quality or a violation of certifying criteria which needs to be quantified at an early (future project) planning phase in order to timely incorporate design recommendations. Methods and tools enabling this assessment are presented.

The second part addresses the design of a robust static back-up control law for the naturally unstable airplane. The operational demands of this back-up system are sophisticated due to the considered degree of natural instability. The design is based on a polytopic (multi-model) technique assuring minimum handling qualities over a wide range of center of gravity positions in the presence of actuator saturations. The corresponding stability domains are computed and an anti-windup control scheme to enhance performance is presented. The final control law is validated with a three-axis nonlinear simulator.

An additional third part sets out to demonstrate that the potentials of reduced stability in civil transport aviation are assessable (under certain assumptions) with the developed methods and tools at an early stage. The estimated gains in mass, drag, and fuel consumption of the unstable aircraft in combination with the back-up controller are presented.

*Keywords* : handling qualities, reduced stability, actuators, static robust controller





*For my parents  
and for my brother*



---

## Acknowledgments

This thesis would not have been possible without the financial support I received from different sources. First of all, I would like to express my gratitude to the Erich-Becker-Stiftung (Frankfurt-Airport Foundation) for the unbureaucratic, fast and generous support. Second, my thanks go to the German Academic Exchange Service (DAAD), and finally I am indebted to ONERA (Office National d'Études et de Recherches Aérospatiales) who secured the funding of the last third of my thesis.

Furthermore, I would like to thank the members of my thesis committee. Many thanks go to the examiners who had the undoubtful pleasure of reading and examining my thesis report: to Prof. Dr. Benoît Bergeon, University of Bordeaux, who also presided the defense committee, to Prof. Dr.-Ing. Dr. h.c. Dieter Schmitt, University of Technology Munich and Airbus, and to Dr. Daniel Walker, University of Liverpool. I also would like to thank Dr. Laurent Bovet, Airbus, who joined the board of examiners for the thesis defense as an invited member.

I owe my thanks to my supervisors, Dr. Gilles Ferreres and Clément Toussaint, both researchers at the Systems Control and Flight Dynamics Department of ONERA Toulouse. Their expertise, understanding, and structured approach added considerably to the outcome of this project.

I am also very thankful to Dr. Carsten Döll, ONERA Toulouse: he was my initial contact at ONERA, helped me with housing problems and whenever I had trouble with French administration. Moreover, I appreciated his scientific support and advice a lot. My thanks go also to Dr. Jean-Marc Biannic for his ideas, shared-expertise, and support.

Very special thanks go out to Prof. Dr.-Ing. Wolfgang Schröder, Prof. Dr.-Ing. Wolfgang Alles, and Prof. Dr.- Ing. Dieter Jacob, all University of Technology Aachen (RWTH). Their encouragement, advice, support, and recommendations built the foundation for this project.

I would also like to thank all doctoral students at the Systems Control and Flight Dynamics Department, especially Nicolas Fezans and Patrice Antoinette, for proof reading and correcting the French short-version of my dissertation and the interesting conversations.

I will not forget my friends and colleagues Andreas Knauf and Sebastian Gaulocher. We spent uncountable hours together, filled with scientific, historical, philosophical, and enlightening conversations, experiences, voyages, and ideas. Thank you, indeed.

Finally, I wish to thank my family, my parents Hortange Antoinette and Gert-Peter, and my brother Grisca Peter, who have supported, encouraged, and motivated me throughout my entire life, and who gave me everything that was necessary (and much more) to pursue my way. Without them, none of this would have come true. And to Andrea, for her love and patience, thank you.

Toulouse, December 2007

Alexander P. Feuersänger



---

## Summary

Accepting a reduced flight dynamic stability or even instability in civil aviation seems promising with regard to drag, fuel consumption, and load charge flexibility. It allows for the installation of smaller vertical and horizontal stabilizers or a wider range of allowable center of gravity positions. As a consequence, the natural aircraft does not necessarily meet the handling quality requirements for certification. It can even be completely uncontrollable when stability augmentation systems fail. In that case, an autonomously operating back-up system has to guarantee minimum flying qualities.

Two overarching objectives define the road map for this dissertation. The first part deals with the assessment of the impact of reduced stability on airplane flight mechanics and dynamics. Within the context of certification requirements the influence of efficiency enhancing parameters that reduce stability has to be examined. Special focus is laid on the size of the vertical tailplane, and therewith on criteria linked to the minimum control speed  $V_{MC}$ , as well as on aft center of gravity positions. An optimization of these parameters leads to a degradation in handling quality or a violation of certifying criteria which needs to be quantified at an early (future project) planning phase in order to timely incorporate design recommendations. Methods and tools enabling this assessment are presented.

The second part addresses the design of a robust static back-up control law for the naturally unstable airplane. The operational demands of this back-up system are sophisticated due to the considered degree of natural instability. The design is based on a polytopic (multi-model) technique assuring minimum handling qualities over a wide range of center of gravity positions in the presence of actuator saturations. The corresponding stability domains are computed and an anti-windup control scheme to enhance performance is presented. The final control law is validated with a three-axis nonlinear simulator.

An additional third part sets out to demonstrate that the potentials of reduced stability in civil transport aviation are assessable (under certain assumptions) with the developed methods and tools at an early stage. The estimated gains in mass, drag, and fuel consumption of the unstable aircraft in combination with the back-up controller are presented.



# Contents

|          |  |           |
|----------|--|-----------|
| <b>1</b> | <b>Introduction</b>  | <b>1</b>  |
| 1.1      | Motivation . . . . .   | 1         |
| 1.2      | Flight Mechanics and Dynamics Analysis . . . . .               | 2         |
| 1.2.1    | Objectives . . . . .   | 2         |
| 1.2.2    | Outline . . . . .  | 3         |
| 1.3      | Robust Back-Up Control Design . . . . .                        | 4         |
| 1.3.1    | Objectives . . . . .   | 4         |
| 1.3.2    | Outline . . . . .  | 4         |
| 1.4      | Synthesis . . . . .  | 4         |
| <b>2</b> | <b>Framework</b>   | <b>7</b>  |
| 2.1      | Certification Criteria and Norms . . . . .                     | 7         |
| 2.2      | A Naturally Unstable Aircraft Concept: VELA . . . . .          | 9         |
| 2.2.1    | Aircraft Data . . . . .  | 9         |
| 2.2.2    | Equilibrium and Linearization . . . . .                        | 11        |
| <b>I</b> | <b>Flight Mechanics and Dynamics Analysis</b>                  | <b>13</b> |
| <b>3</b> | <b>Analytical Approach to Reduced Longitudinal Stability</b>   | <b>15</b> |
| 3.1      | Longitudinal Static Stability . . . . .                        | 16        |
| 3.1.1    | Neutral Point . . . . .  | 18        |
| 3.2      | Longitudinal Dynamic Stability . . . . .                       | 19        |
| 3.2.1    | 2nd Order Differential Equations in $\alpha$ and $q$ . . . . . | 20        |
| 3.2.2    | Limit of Natural SPO Stability . . . . .                       | 22        |
| 3.2.3    | General Stability Limit: Maneuver Point . . . . .              | 22        |

|          |   |           |
|----------|---|-----------|
| 3.2.4    | Handling Quality Characteristics versus C.o.G. Position . . . . . | 23        |
| 3.3      | Control of the Short-Period Oscillation . . . . .                 | 24        |
| 3.3.1    | Feedback of $\alpha$ . . . . .                                    | 24        |
| 3.3.2    | Feedback of $q$ . . . . .   | 25        |
| 3.3.3    | Combined Feedback of $\alpha$ and $q$ . . . . .                   | 25        |
| 3.4      | Robustness versus Center of Gravity Position . . . . .            | 26        |
| 3.5      | Integration of the Actuator Model . . . . .                       | 27        |
| 3.6      | Gain and Phase Margin . . . . .                                   | 28        |
| 3.6.1    | Gain Margin . . . . .   | 29        |
| 3.6.2    | Phase Margin . . . . .  | 30        |
| 3.7      | Illustration of Analytical Results . . . . .                      | 31        |
| <b>4</b> | <b>Longitudinal Stability and Actuator Activity/Fatigue</b>       | <b>35</b> |
| 4.1      | Modeling Aspects . . . . .  | 35        |
| 4.1.1    | SPO Properties . . . . .  | 36        |
| 4.1.2    | Actuator Model . . . . .  | 36        |
| 4.1.3    | Stabilizing Control Law . . . . .                                 | 37        |
| 4.1.4    | Model of the Turbulent Atmosphere . . . . .                       | 39        |
| 4.2      | Determination of Actuator Activity and Fatigue . . . . .          | 39        |
| 4.2.1    | Passage of a Random Signal Through a Linear System . . . . .      | 40        |
| 4.2.2    | Theory of Fatigue and Damage . . . . .                            | 41        |
| 4.3      | Application to the Aircraft . . . . .                             | 44        |
| 4.3.1    | Variables Influenced by Turbulence . . . . .                      | 44        |
| 4.3.2    | Complete Linearized Model . . . . .                               | 45        |
| 4.3.3    | Actuator Activity and Fatigue . . . . .                           | 47        |
| 4.4      | Results . . . . .   | 47        |
| 4.4.1    | Gain vs $X_g$ . . . . .   | 47        |
| 4.4.2    | Activity vs. $X_g$ . . . . .                                      | 49        |
| 4.4.3    | Damage vs. $X_g$ . . . . .  | 52        |
| 4.5      | Exemplary Application to a Mission Profile . . . . .              | 53        |
| 4.5.1    | Turbulence Intensities . . . . .                                  | 53        |
| 4.5.2    | Accumulated Mission Damage due to Turbulence . . . . .            | 56        |
| 4.5.3    | Summary . . . . .   | 59        |

|          |  |            |
|----------|--|------------|
| <b>5</b> | <b>Actuator Saturations and Longitudinal Stability</b>                             | <b>61</b>  |
| 5.1      | Simulations with Saturated Actuators . . . . .                                     | 61         |
| 5.1.1    | Actuator Modeling . . . . .  | 62         |
| 5.1.2    | Simulations . . . . .  | 62         |
| 5.2      | Aft C.O.G. Positions and Actuator Nonlinearities . . . . .                         | 64         |
| 5.2.1    | Stability in the Presence of Nonlinearities . . . . .                              | 65         |
| 5.2.2    | Application to the Aircraft . . . . .  | 67         |
| 5.2.3    | A Criterion for Aft C.o.G. Positions . . . . .                                     | 68         |
| 5.3      | Conclusion on Reduced Longitudinal Stability . . . . .                             | 72         |
| <b>6</b> | <b>Reduced Lateral Stability and <math>V_{MC}</math> Equilibrium</b>               | <b>73</b>  |
| 6.1      | An Analytical Approach Toward $V_{MC}$ -Computation . . . . .                      | 74         |
| 6.1.1    | Equilibrium Equations . . . . .  | 74         |
| 6.1.2    | Resolution . . . . .   | 76         |
| 6.1.3    | $V_{MC}$ Expressions . . . . .   | 77         |
| 6.1.4    | Interpretation and Physical Factors . . . . .                                      | 78         |
| 6.2      | Exploitation of the Analytical Approach . . . . .                                  | 80         |
| 6.2.1    | DC8 Classical Aircraft . . . . .   | 82         |
| 6.2.2    | VELA Blended-Wing Body Aircraft . . . . .  | 85         |
| 6.2.3    | Final Remarks on the Analytical Approach toward the $V_{MC}$ Equilibrium . . . . . | 88         |
| 6.3      | A Numerical Tool for $V_{MC}$ -Analysis . . . . .                                  | 90         |
| 6.4      | $V_{MC}$ -Equilibrium for a BWB Aircraft . . . . .                                 | 93         |
| 6.4.1    | Results . . . . .  | 93         |
| 6.4.2    | Variation of the C.O.G. Position . . . . .   | 97         |
| 6.4.3    | Variation of the Fin Surface Area . . . . .  | 99         |
| 6.4.4    | Key Aspects of the Utility . . . . .   | 99         |
| 6.5      | Summary on the $V_{MC}$ Equilibrium . . . . .                                      | 101        |
| <b>7</b> | <b>Dynamic Lateral Criteria and Reduced Stability</b>                              | <b>103</b> |
| 7.1      | Preliminary Analytical Developments . . . . .                                      | 103        |
| 7.1.1    | Decoupling and Parametrization . . . . .   | 105        |
| 7.1.2    | Dutch Roll Motion . . . . .  | 106        |
| 7.1.3    | Roll Motion . . . . .  | 108        |

|  |  |            |
|--|--|------------|
| 7.1.4  | Spiral Motion . . . . .  | 108        |
| 7.1.5  | Generic Modeling of a Roll Maneuver . . . . .                                    | 110        |
| 7.2  | Numerical Assessment of Dynamic Criteria . . . . .                               | 114        |
| 7.2.1  | Modal Evolution . . . . .  | 114        |
| 7.2.2  | 1st Maneuver . . . . .   | 115        |
| 7.2.3  | 2nd Maneuver . . . . .   | 116        |
| 7.2.4  | 3rd Maneuver . . . . .   | 117        |
| 7.3  | Summary on Dynamic Criteria . . . . .  | 118        |
| 7.4  | Conclusion on Reduced Lateral Stability . . . . .                                | 119        |
| 7.5  | Recommendation for the VELA Aircraft Design . . . . .                            | 120        |
| <br><b>II Robust Back-Up Control Design for an Aircraft with Reduced Stability</b> |  | <b>121</b> |
| <br><b>8 Introduction and Control Objectives</b>                                   |  | <b>123</b> |
| 8.1  | Aircraft Modeling . . . . .  | 124        |
| 8.1.1  | Aircraft Model . . . . .   | 124        |
| 8.1.2  | Linearized Longitudinal and Lateral Systems . . . . .                            | 125        |
| 8.1.3  | Plant Model for Controller Synthesis . . . . .                                   | 126        |
| 8.2  | Control Objectives . . . . .   | 128        |
| 8.2.1  | Summing Up . . . . .   | 128        |
| 8.2.2  | Control Objectives . . . . .   | 129        |
| <br><b>9 Robust Multi-Objective Feedback and Anti-Windup Design Technique</b>      |  | <b>131</b> |
| 9.1  | Introduction to the Control Philosophy . . . . .                                 | 131        |
| 9.2  | Modal and I/O Criteria . . . . .   | 132        |
| 9.2.1  | Modal Criterion (Pole Placement in an LMI Region of the Complex Plane) . . . . . | 132        |
| 9.2.2  | U-V-W Dissipativity Criterion . . . . .  | 134        |
| 9.2.3  | $H_\infty$ Criterion (Bounded Real Lemma) . . . . .                              | 137        |
| 9.2.4  | Positivity Criterion (Positive Real Lemma) . . . . .                             | 138        |
| 9.3  | Polytopic Multi-Objective Robust Control Design . . . . .                        | 139        |
| 9.4  | Stability and Performance Analysis in the Presence of Nonlinearities . . . . .   | 141        |
| 9.4.1  | Stability Analysis . . . . .   | 141        |

|            |  |            |
|------------|--|------------|
| 9.4.2      | Modification of the Stability Domain . . . . .                             | 143        |
| 9.4.3      | Convergence Speed . . . . .  | 144        |
| 9.4.4      | Stability in the Face of Exogenous Inputs . . . . .                        | 144        |
| 9.5        | Static Anti-Windup Control Scheme Toward Enhanced Performance . . . . .    | 146        |
| 9.5.1      | Plant Model for Anti-Windup Controller . . . . .                           | 146        |
| 9.5.2      | Design of a Robust Anti-Windup Controller . . . . .                        | 148        |
| <b>10</b>  | <b>Controller Design and Application</b>                                   | <b>151</b> |
| 10.1       | Preliminary Designs . . . . .  | 151        |
| 10.1.1     | Preliminary Design for Minimized Activity $\gamma_{1,min}$ . . . . .       | 152        |
| 10.1.2     | Preliminary Design Introducing Modal Constraints . . . . .                 | 153        |
| 10.2       | Robust Back-Up Controllers . . . . .                                       | 154        |
| 10.2.1     | Longitudinal Controller . . . . .  | 154        |
| 10.2.2     | Lateral Controller . . . . .   | 156        |
| 10.3       | Stability and Performance Analysis . . . . .                               | 158        |
| 10.3.1     | Longitudinal Stability and Performance . . . . .                           | 159        |
| 10.3.2     | Lateral Stability and Performance . . . . .                                | 161        |
| 10.4       | Simulations . . . . .  | 163        |
| 10.5       | Conclusion on the Robust Design Technique . . . . .                        | 163        |
| <b>III</b> | <b>Synthesis</b>   | <b>169</b> |
| <b>11</b>  | <b>Gains and Potentials</b>  | <b>171</b> |
| 11.1       | Parameters of a Naturally Stable and an Unstable Airplane Design . . . . . | 172        |
| 11.2       | Estimation of the Gain in Mass . . . . .                                   | 173        |
| 11.3       | Estimation of Drag Reduction . . . . .                                     | 176        |
| 11.3.1     | Friction and Form Drag . . . . .   | 177        |
| 11.3.2     | Induced Drag . . . . .   | 178        |
| 11.3.3     | Trim Drag . . . . .  | 179        |
| 11.4       | Estimation of the overall Gain in Fuel Burn . . . . .                      | 180        |
| 11.4.1     | Fuel Consumption and Drag . . . . .  | 180        |
| 11.4.2     | Fuel Burn Due to One Drag Count . . . . .                                  | 181        |
| 11.4.3     | Potential Fuel Burn Savings with Reduced Stability . . . . .               | 182        |

|  |            |
|--|------------|
| 11.5 Synthesis . . . . .   | 182        |
| <b>12 Conclusion and Outlook</b>                                     | <b>185</b> |
| <b>A Aircraft Data</b>   | <b>195</b> |
| A.1 VELA1 Blended-Wing Body . . . . .                                | 195        |
| A.1.1 Geometry and Mass Inertia . . . . .                            | 195        |
| A.1.2 Full Aerodynamic Model . . . . .                               | 196        |
| A.1.3 Simplified Aerodynamic Model . . . . .                         | 196        |
| A.2 Douglas DC8 . . . . .  | 198        |
| A.2.1 Geometry and Mass Inertia . . . . .                            | 198        |
| A.2.2 Simple Aerodynamic Model . . . . .                             | 198        |
| <b>B Certification Criteria and Norms</b>                            | <b>201</b> |
| B.1 Classical Criteria . . . . .                                     | 201        |
| B.1.1 Military Specifications . . . . .                              | 201        |
| B.1.2 FAR / JAR guidelines . . . . .                                 | 202        |
| B.2 Criteria Proposed by Industry . . . . .                          | 204        |
| B.2.1 Supplement to Take-Off and Landing Criteria . . . . .          | 205        |
| <b>C <math>V_{MC}</math> Equilibrium: Parametric Study in Detail</b> | <b>207</b> |
| C.1 DC8 . . . . .  | 211        |
| C.2 VELA1 . . . . .  | 215        |
| <b>D Aileron-Sideslip Coupling</b>                                   | <b>219</b> |

# List of Figures

|      |  |    |
|------|--|----|
| 2.1  | VELA1 aircraft. . . . .  | 9  |
| 3.1  | Possible variation of the aircraft pitching moment with $\alpha$ . Initial trim at A. . . . .  | 16 |
| 3.2  | A wing-tail combination. . . . .   | 17 |
| 4.1  | SPO poles as a function of the c.o.g. displacement $dx_g \in [-10\%, 10\%]$ . $\circ$ equal to $-10\%$ fwd, $\times$ to $0\%$ , and $+$ to $10\%$ aft. . . . . | 36 |
| 4.2  | Comparison of actuator models: Bode diagram. $T_{act} = 0.06$ . . . . .  | 37 |
| 4.3  | The Wöhler curves . . . . .  | 41 |
| 4.4  | SIMULINK scheme: SPO + actuator + controller + turbulence. . . . .   | 46 |
| 4.5  | Gains $K_\alpha, K_q$ as a function of $X_g$ and $T_{act}$ , $\xi = 0.7$ . . . . .   | 48 |
| 4.6  | Influence of modal specifications on gains. $T_{act} = 0.06$ s, $\xi = 0.3/0.7$ . . . . .  | 48 |
| 4.7  | Boundaries of the elevator deflection $\delta m$ . $T_{act} \in [0.06$ s; $0.48$ s]. . . . .   | 49 |
| 4.8  | Boundaries of the actuator rate $\delta \dot{m}$ . $T_{act} \in [0.06$ s; $0.48$ s]. . . . .   | 50 |
| 4.9  | Influence of modal specification onto elevator deflection boundaries. $T_{act} = 0.06$ s. Red: $\xi = 0.7$ , green: $\xi = 0.3$ . . . . .                      | 51 |
| 4.10 | Influence of modal specification onto elevator rate boundaries. $T_{act} = 0.06$ s. Red: $\xi = 0.7$ , green: $\xi = 0.3$ . . . . .                            | 51 |
| 4.11 | Normalized damage as a function of $dx_g$ . . . . .  | 52 |
| 4.12 | A dimensioning mission profile (simplified). . . . .   | 54 |
| 4.13 | Absolute damage of each flight phase for two different c.o.g. positions. . . . .   | 58 |
| 4.14 | Damage contribution of flight phases for an imposed damping ratio $\xi = 0.7$ . . . . .  | 58 |
| 4.15 | Damage inflicted upon the actuator per mission and resulting life expectancy. . . . .  | 58 |
| 5.1  | Actuator model with saturations on position and rate. . . . .  | 62 |
| 5.2  | Simulation. Saturation on position at $30^\circ$ and on rate at $30^\circ/s$ . Commanded (dashed) and actual (continuous) elevator rate/position. . . . .      | 63 |

|      |  |     |
|------|--|-----|
| 5.3  | Simulation. Saturation on position at $24^\circ$ and on rate at $30^\circ/s$ . Com-<br>manded (dashed) and actual (continuous) elevator rate/position. . . . .   | 64  |
| 5.4  | The Lur'e feedback interconnection problem. . . . .  | 67  |
| 5.5  | A graphical interpretation of the Popov criterion. . . . .   | 67  |
| 5.6  | Transformation of saturation into dead-zone nonlinearity. . . . .  | 68  |
| 5.7  | Transformation into Lur'e problem: linear parts SPO + actuator + con-<br>troller seen by nonlinearity. The $-1$ gain is introduced according to the<br>Lur'e scheme, Figure 5.4. . . . .   | 68  |
| 5.8  | Circle criterion and sector variable $k$ as a function of the c.o.g. position. . .   | 69  |
| 5.9  | From sector to stability region. . . . .   | 70  |
| 5.10 | Stability region for the dead-zone nonlinearity and maximum aft center of<br>gravity displacement $dx_g$ . The horizontal dashed line indicates the c.o.g.<br>position at the limit of natural stability (maneuver point). . . . . | 71  |
| 6.1  | Aircraft equilibrium with left outboard engine inoperative. . . . .  | 75  |
| 6.2  | DC8. $V_{MC}$ as a function of various parameters. . . . .   | 82  |
| 6.3  | VELA. $V_{MC}$ as a function of various parameters. . . . .  | 86  |
| 6.4  | Parameter impact on $V_{MC}$ for a classical and a BWB aircraft. . . . .   | 89  |
| 6.5  | $\beta, V$ -grid for the classical DC8 aircraft with critical engine failure. . . . .  | 90  |
| 6.6  | Evolution of flight parameters for maximum rudder deflection $\delta n = -30^\circ$<br>and the critical (left outboard) engine inoperative for a classical aircraft. . .   | 91  |
| 6.7  | The $V_{MC}$ as a function of the vertical fin size $S_D$ for a classical aircraft. . .  | 92  |
| 6.8  | $\beta, V$ -grid for the bwb aircraft model with critical engine failure. . . . .  | 94  |
| 6.9  | Evolution of flight parameters for the equilibrated VELA aircraft with max-<br>imum rudder deflection $\delta n = -30^\circ$ and the critical (left outboard) engine<br>inoperative. . . . .                                       | 95  |
| 6.10 | Evolution of $C_N^*$ as a function of aileron deflection $\delta l$ and angle of attack $\alpha$<br>for the BWB model . . . . .  | 96  |
| 6.11 | $V_{MC}$ equilibrium as a function of $X_g$ for $S_D = 2 \times 45m^2$ . . . . .   | 98  |
| 6.12 | Yaw angle $\beta$ corresponding the equilibrium at $V_{MC}$ as a function of $X_g$ for<br>$S_D = 2 \times 45m^2$ . . . . .   | 98  |
| 6.13 | $V_{MC}$ and its corresponding yaw angle as a function of the fin surface area<br>for $dx_g = -4.17\%$ fwd. . . . .  | 100 |
| 6.14 | $V_{MC}$ and its corresponding yaw angle as a function of the fin surface area<br>for $dx_g = +4.17\%$ aft. . . . .  | 100 |

|       |   |     |
|-------|---|-----|
| 7.1   | Impact of fin surface area and c.o.g. position on dutch-roll dynamics. . . . .  | 107 |
| 7.2   | Influence of c.o.g. position and fin size on sideslip during roll maneuvers. . .  | 113 |
| 7.3   | Lateral modes as a function of the vertical fin size. DC8: linearized at<br>$V = 44 \text{ m/s} = V_{MC}$ for $S_D = 100 \%$ , $S_D$ steps in $10 \%$ . VELA: $V =$<br>$V_{MC1} = 76 \text{ m/s}$ , $S_D = 2 \times (45 \text{ m}^2, 64 \text{ m}^2, 90 \text{ m}^2, \text{ and } 128 \text{ m}^2)$ . . . . . | 114 |
| 7.4   | 1st $V_{MC}$ maneuver. Indicated speeds denote the initial $V_{MC}$ equilibrium. .  | 115 |
| 7.5   | 2nd $V_{MC}$ maneuver. . . . .  | 116 |
| 7.6   | 3rd $V_{MC}$ maneuver. Indicated speeds denote the initial $V_{MC}$ equilibrium. .  | 117 |
| 8.1   | Open-loop poles for $dx_g = -10 \%$ fwd ( $\circ$ ) to $dx_g = +10 \%$ aft ( $+$ ). Left: Lon-<br>gitudinal system. SPO = Short-Period Oscillation. Right: Lateral System.<br>DR = Dutch Roll, SM = Spiral Mode, RM = Roll Mode. . . . .  | 126 |
| 8.2   | Transformation of saturation into dead-zone nonlinearity. . . . .   | 127 |
| 8.3   | Plant model used for controller design. . . . .   | 127 |
| 9.1   | An LMI region of the complex plane. . . . .   | 133 |
| 9.2   | Closed-loop structure with anti-windup controller. . . . .  | 147 |
| 9.3   | Transformed plant structure with anti-windup control scheme. . . . .  | 148 |
| 9.4   | Plant for anti-windup control design. . . . .   | 148 |
| 10.1  | $\gamma_1$ for two preliminary designs. . . . .   | 152 |
| 10.2  | Closed-loop poles for preliminary design #2 as a function of $X_g$ . . . . .  | 153 |
| 10.3  | Closed-loop poles. $\circ$ : $-7 \%$ fwd, $+$ : $+5 \%$ aft. Longitudinal motion. . . . .   | 155 |
| 10.4  | Magnitude (frequency response) of wind input to actuator outputs $T_{w_1 \rightarrow z_1}$<br>as a function of $dx_g$ . Longitudinal motion. . . . .  | 156 |
| 10.5  | Closed-loop poles. $\circ$ : $-7 \%$ fwd, $+$ : $+5 \%$ aft. Lateral motion. . . . .  | 157 |
| 10.6  | Magnitude (frequency response) of wind input to actuator outputs $T_{w_1 \rightarrow z_1}$<br>as a function of $dx_g$ . Lateral motion. . . . .   | 158 |
| 10.7  | Domain of attraction. Longitudinal motion. . . . .  | 159 |
| 10.8  | System performance. Longitudinal motion. . . . .  | 161 |
| 10.9  | Domain of attraction. Lateral motion. . . . .   | 161 |
| 10.10 | System performance. Lateral motion. . . . .   | 163 |
| 10.11 | Time response to command $\phi_c = 30^\circ$ . . . . .  | 164 |
| 10.12 | Time response to command $\phi_c = 30^\circ$ . . . . .  | 165 |
| 10.13 | Time response to command $\phi_c = 30^\circ$ in turbulent atmosphere. . . . .   | 166 |
| 10.14 | Time response to command $\phi_c = 30^\circ$ in turbulent atmosphere. . . . .   | 167 |

|      |   |     |
|------|---|-----|
| 11.1 | Open-loop poles of a VELA1 concept naturally stable in SPO and DR. . . .  | 172 |
| 11.2 | VTP dimensions and surface of supporting structure. . . . .   | 174 |
| 11.3 | Typical lift/drag polar. . . . .  | 176 |
| 11.4 | Typical contribution of different drag types. . . . .   | 177 |
| 11.5 | Elevator trim deflection and drag in cruise flight. Two exemplary c.o.g. ranges are indicated as well as the position of the neutral point. . . . .                                       | 179 |
| 11.6 | Distribution of total drag/cost reduction onto drag types. . . . .  | 184 |
|      |   |     |
| C.1  | DC8. Variation of the fin size. . . . .   | 211 |
| C.2  | DC8. Variation of the center of gravity position. . . . .   | 212 |
| C.3  | DC8. Variation of the mass. . . . .   | 212 |
| C.4  | DC8. Variation of $CY_{\beta, fuselage}$ . . . . .  | 213 |
| C.5  | DC8. Variation of $Cn_{\beta, fuselage}$ . . . . .  | 213 |
| C.6  | DC8. Variation of $\varepsilon_D$ . . . . .   | 214 |
| C.7  | VELA. Variation of the fin size. . . . .  | 215 |
| C.8  | VELA. Variation of the center of gravity position. . . . .  | 216 |
| C.9  | VELA. Variation of the mass. . . . .  | 216 |
| C.10 | VELA. Variation of $CY_{\beta, fuselage}$ . . . . .   | 217 |
| C.11 | VELA. Variation of $Cn_{\beta, fuselage}$ . . . . .   | 217 |
| C.12 | VELA. Variation of $\varepsilon_D$ . . . . .  | 218 |
|      |   |     |
| D.1  | VELA. Coefficient $C_n^*$ as composition of aileron deflection and angle of attack ( $C_{n\delta l}$ , $C_{n\delta l, \alpha}$ ). $S_D = 2 \times 45 m^2$ , $dx_g = -8.35\%$ . . . . .    | 220 |
| D.2  | VELA. Coefficient $C_n^*$ as composition of aileron deflection and angle of attack with reduced derivative $C_{n\delta l, \alpha}$ . $S_D = 2 \times 45 m^2$ , $dx_g = -8.35\%$ . . . . . | 220 |
| D.3  | VELA. Equilibrium at $\delta n = -30^\circ$ , $S_D = 2 \times 45 m^2$ , $dx_g = -0.0835$ and reduced $C_{n\delta l, \alpha}$ . . . . .  | 221 |
| D.4  | DC8. Introduction of derivative $C_{n\delta l, \alpha}$ into aircraft model. . . . .  | 222 |
| D.5  | DC8. Equilibrium at $\delta n = -30^\circ$ with modified modeling of aileron-sideslip-angle of attack coupling. . . . .   | 223 |

# List of Tables

|      |  |     |
|------|--|-----|
| 2.1  | VELA reference values. . . . .   | 10  |
| 4.1  | Characteristics of the Airbus Actuator Model. . . . .  | 36  |
| 4.2  | SPO specifications. . . . .  | 45  |
| 4.3  | A dimensioning mission profile (simplified). . . . .   | 55  |
| 4.4  | Vertical turbulence intensities. . . . .   | 55  |
| 4.5  | Turbulence intensities and probabilities $P_i$ of occurrence for levels $i = 1, 2,$<br>and 3 (light, medium, heavy). . . . . | 56  |
| 4.6  | A dimensioning mission profile (simplified). . . . .   | 57  |
| 6.1  | Main factors determining the $V_{MC}$ expressions and assumptions. . . . .   | 80  |
| 6.2  | Summary of analytic results for a classical aircraft. . . . .  | 84  |
| 6.3  | Summary of analytic results for the BWB VELA aircraft. . . . .   | 88  |
| 8.1  | VELA Reference Values . . . . .  | 124 |
| 10.1 | Longitudinal motion. Sector constraints for preliminary designs. . . . .   | 151 |
| 10.2 | Lateral Motion. Sector constraints for preliminary designs. . . . .  | 152 |
| 10.3 | Parameter-setting for the longitudinal control design. . . . .   | 154 |
| 10.4 | Longitudinal static robust controller. . . . .   | 155 |
| 10.5 | Results for the longitudinal robust control law. Valid for $dx_g \in [-7\%; +5\%]$ .155                                      |     |
| 10.6 | Parameter-setting for the lateral control design. . . . .  | 156 |
| 10.7 | Lateral static robust controller. . . . .  | 156 |
| 10.8 | Results for the lateral robust control law. Valid for $dx_g \in [-7\%; +5\%]$ . . .  | 157 |
| 10.9 | Lateral exchange rates. . . . .  | 162 |

|      |  |     |
|------|--|-----|
| 11.1 | Range of c.o.g. displacements $dx_g$ and reference surfaces of the fins $S_{vtp}$ for two VELA1 designs. . . . . | 172 |
| 11.2 | A380 vertical tailplane specifications, [50, 5]. . . . .   | 173 |
| 11.3 | VELA1 reduced vertical tailplane specifications. . . . .   | 175 |
| 11.4 | Potential fuel savings. . . . .  | 183 |
| A.1  | VELA reference values. . . . .   | 195 |
| A.2  | Mass inertia. . . . .  | 195 |
| A.3  | Coefficient $C_Z$ as a function of $\alpha$ and $\beta$ . . . . .  | 196 |
| A.4  | Simplified longitudinal coefficients. . . . .  | 197 |
| A.5  | Simplified lateral coefficients. . . . .   | 197 |
| A.6  | DC8 reference values. . . . .  | 198 |
| A.7  | Mass inertia. . . . .  | 198 |
| A.8  | Simplified longitudinal coefficients. . . . .  | 198 |
| A.9  | Simplified lateral coefficients. . . . .   | 199 |
| C.1  | Boundaries for $\varepsilon_D$ with $\kappa > 0$ , $\nu < 0$ . . . . .   | 211 |

# Publications

A. P. Feuersänger, G. Ferreres [37]

Robust Back-Up Control Design for an Aircraft with Reduced Stability and Saturated Actuators

In Proceedings: *IFAC Symposium: Automatic Control in Aerospace*

Toulouse, France, 2007

S. Gaulocher, A. Knauf, A. P. Feuersänger [42]

Self-Scheduled Controller Design for Relative Motion Control of a Satellite Formation

In Proceedings: *IMSM-IMAACA Multiconference*

Buenos Aires, Argentina, 2007

A. Knauf, S. Gaulocher, A. P. Feuersänger [52]

Innovative Controller Design for Systems with Parameter Variations

In Proceedings: *Deutscher Luft- und Raumfahrtkongress*

Braunschweig, Germany, 2006

A. P. Feuersänger, C. Döll, C. Toussaint [35]

Actuator Influence on Flying Qualities of a Naturally Unstable Aircraft

In Proceedings: *International Council of the Aeronautical Sciences, ICAS*

Hamburg, Germany, 2006

A. P. Feuersänger, G. Ferreres [36]

Design of a Robust Back-Up Controller for an Aircraft with Reduced Stability

In Proceedings: *Guidance, Navigation, and Control Conference and Exhibit*

Keystone, CO, USA, 2006

A. P. Feuersänger, G. Ferreres, C. Toussaint [39]

Synthèse d'un correcteur robuste de type back-up pour un avion à stabilité réduite

*Actes du congrès des doctorants EDSYS*

Tarbes, France, 2006

A. P. Feuersänger, C. Toussaint, C. Döll [38]

The Impact of Reduced Lateral Stability on the VMC Equilibrium and Manoeuvres during early Design Phases of an Aircraft

In Proceedings: *Deutscher Luft- und Raumfahrtkongress*

Friedrichshafen, Germany, 2005



# Chapter 1

## Introduction

### 1.1 Motivation

In the constant pursuit for enhanced efficiency, civil aircraft design has undergone a significant change in terms of its flight mechanical conception. Whereas the natural airplane used to satisfy virtually all flight performance and handling quality criteria, today's developments tend to incorporate a reduced natural flight mechanical and dynamic stability in combination with stabilizing control systems.

While the A320-aircraft family is still naturally stable, the A330/A340-family is already at the limit of natural stability with a mechanical back-up system in longitudinal mode and an emergency back-up stabilizer in lateral mode in the case of flight computer failure. The A380-family abandons virtually all mechanical back-up systems in favor of automatic stabilizing systems.

The goal is an increase in efficiency and performance. The philosophy of natural stabilization implies a certain size of vertical and horizontal stabilizers and hence a certain level of structural mass. Accepting a reduced natural stability or even instability in civil aviation seems therefore promising as it also allows for the installation of smaller vertical and horizontal empennages or a wider range of allowable center of gravity positions. This is beneficial with regard to drag, fuel consumption, and load charge flexibility.

As a consequence, the natural aircraft with reduced stability does not necessarily meet handling quality requirements for certification. It can even be completely uncontrollable in the case of a complete loss of stability augmentation systems.

An important objective is thus the assessment of the impact of reduced natural stability on the aircraft flight mechanics and dynamics. Within the context of certification norms and handling quality criteria the influence of efficiency enhancing parameters that reduce stability has to be examined.

Furthermore, since the natural aircraft with reduced stability does not realize handling quality requirements in the case of flight control computer failure, an autonomously op-

erating back-up control system has to be developed. The operational demands for such a back-up system are more sophisticated than those for current back-up systems (e.g. autonomous Back-Up Yaw Damper Units - BYDUs), as the considered degree of instability triggers accelerations of high amplitude of the natural aircraft when disturbances, such as turbulence, occur. Still, the system ought to be as simple as possible.

A third goal is the overall assessment of potential benefits and drawbacks that arise with accepting a reduced stability in favor of a more efficient aircraft design. This evaluation should incorporate aspects of both the flight dynamics analysis as well as the control design in order to draw a general conclusion on the subject.

Given the different nature of these three objectives, this dissertation is divided in three main parts, each of which is shortly presented hereafter.

## 1.2 Flight Mechanics and Dynamics Analysis

### 1.2.1 Objectives

Two parameters are identified as the main influencing factors in the conflicting area of efficiency and stability: the center of gravity (c.o.g.) position and the size of the vertical tailplane. Both have a significant influence on trim drag, surface drag, mass, or load charge flexibility [81, 76, 89, 102, 75, 77, 2].

An optimization of these parameters leads to a degradation in handling quality or a violation of certifying criteria which needs to be quantified in order to derive design recommendations or requirements for artificial stabilization. Furthermore, the degree of (in-)stability affects not only the airplane dynamics but also the stabilizing control system itself and, more precisely, the actuators [35]. This issue reveals to be worth examining since the actuators represent the link between automatic control system and excitation of aerodynamic surfaces.

The assessment of the impact of reduced natural stability is to be carried out during the future project planning phase of an airplane in order to timely incorporate design recommendations. The chosen aircraft concept is a model of the VELA1<sup>1</sup> airplane, which has been developed within the framework of a European research project. It represents a two-tailed blended wing-body configuration that surpasses the current A380 in mass/capacity as well as in geometry specifications [91, 6].

The first part of the dissertation is dedicated to the development of methods and tools allowing for an assessment of the impact of reduced stability at this early stage of airplane development.

---

<sup>1</sup>VELA - Very Efficient Large Aircraft.

### 1.2.2 Outline

Prior to Part I, Chapter 2 sketches briefly the framework of certification criteria and norms, and details some modeling aspects of the aircraft. Well known sources [94, 95, 93, 92, 96, 97, 30, 29] are presented as well as criteria specifically developed by industry [57].

Chapter 3, contributing to the flight dynamics analysis part, examines the effect of reduced stability on the longitudinal aircraft motion. An analytical approach aiming at the airplane's short period oscillation results in a set of equations allowing for an evaluation of the impact of c.o.g. position, actuator characteristics, and control of the aircraft motion. See also [90] for a similar approach. Suggested readings on the equations of flight are [22, 63, 44, 76, 89, 8, 20].

Chapter 4 develops a numerical tool which computes an estimate of control system activity and actuator fatigue damage caused by artificial stabilization [35, 48, 60, 66]. This technique is then used to compute an overall fatigue damage estimate for a typical vertical mission profile, demonstrating the applicability to airplanes in future project phase. In contrast to current techniques used by aircraft manufacturers [7], the developed technique delivers results quickly without involving any time consuming long scale numerical simulations.

Chapter 5 then develops a criterion relating c.o.g. position and minimum actuator requirements using classical automatic control stability criteria. The criterion relates the longitudinal c.o.g. position with minimum requirements for the elevator actuator saturation level [27].

Chapter 6 sets out to deal with the lateral aircraft criteria, and more precisely, with criteria associated to the equilibrium at  $V_{MC}$  (*minimum control velocity*). These criteria relate to straight flight with an inoperative external engine and are usually decisive for the sizing of the vertical tailplane. Again, an analytical approach leads the way into the subject and condenses in the presentation of a numerical tool [38]. The developed expressions in combination with the tool allow for an early evaluation of the capability of an aircraft to realize criteria linked to the minimum control speed.

A selection of dynamic criteria, notably those related to  $V_{MC}$ , are examined in Chapter 7 [27]. These are composed of maneuvers and handling quality requirements and are analyzed analytically and numerically. The chapter, and the flight mechanics and dynamics part, close with a list of recommendations for the VELA airplane design, demonstrating the convenience of the presented approaches.

## 1.3 Robust Back-Up Control Design

### 1.3.1 Objectives

Since the natural aircraft with reduced stability is hardly or not at all controllable a back-up control system has to be developed. The operational demands are challenging as the control system activity is expected to be high, as shown in Chapter 4, and control surfaces may be subject to saturation. In addition, the final controller has to be very simple.

The design of the back-up system must therefore incorporate multiple control objectives: it must guarantee minimum flying qualities necessary for certification over the whole range of possible center of gravity positions. Since high amplitudes of the control signals are expected, linear and nonlinear actuator characteristics have to be considered as well. Notably, saturations on the actuator position and rate outputs have to be taken into consideration and their possible impact on closed-loop stability and performance has to be minimized. Since the control architecture must be very simple (back-up system) one static control law which is robust versus saturations and a variation of c.o.g. positions is desirable.

### 1.3.2 Outline

The robust control design part of the dissertation starts with a short introduction to the problem from an automatic control point of view and presents a specifications list for a possible back-up control law (Chapter 8). This list is directly derived from the previous part which gave recommendations on the aircraft design.

Following the specified control objectives, Chapter 9 details a state-feedback polytopic design technique [23, 16, 36, 37] which reveals itself to be adaptable to this problem and to deliver adequate results quite efficiently. The control objectives are cast into LMI (Linear Matrix Inequality) form [78, 21, 41, 23, 24] and a convex design technique is presented. Special attention is given to the evaluation of the stability domain and the performance of the closed-loop system in the presence of actuator saturations [101, 17]. Furthermore, an option of minimizing the impact of saturations is portrayed with an anti-windup control scheme. In contrast to the works of, e.g. [86, 87, 101], here one static anti-windup controller is designed using a simple convex multi-model multi-objective design technique.

Chapter 10 is entirely dedicated to the application of the designed controller and the presentation of the results. Concluding remarks end the automatic control part.

## 1.4 Synthesis

In this final part of the dissertation, two configurations of the same aircraft type are compared in order to demonstrate the benefits of accepting a reduced stability. One

configuration is naturally stable and realizes certification criteria without an additional stability augmentation system. The other configuration has a reduced size of the vertical tailplane as well as a larger range of allowable c.o.g. positions. This naturally unstable configuration incorporates the designed robust back-up controller.

Using basic airplane design procedures [25, 89, 76, 75, 63, 51, 49, 53], an estimate of the gains in mass, drag, and fuel consumption is shown in Chapter 11. The potentials of reduced stability in civil transport aviation are proven to be assessable with the developed methods and tools at an early stage of aircraft conception.

A general conclusion is given and an outlook pointing out aspects worth examining in further research ends this dissertation.



## Chapter 2

# Framework

In order to assess the impact of reduced flight dynamic stability, the first step is to identify relevant certification and handling quality criteria. It is then possible to estimate possible conflicts between an efficient airplane design at the cost of reduced stability and certification issues. The earlier this conflict is identified the more can the aircraft manufacturer incorporate design changes at an early stage and, thus, reduce costs.

Section 2.1 presents criteria proposed by both official authorities and industry that play a potentially important role when designing an aircraft with reduced natural stability.

In order to conduct a relevant study, a future airplane concept is presented in Section 2.2. The airplane model is parametrized as to modify its degree of natural stability or instability. The flight mechanics and dynamics analysis will be subject of the following chapters.

### 2.1 Certification Criteria and Norms

Civil aircraft design and certification is based upon the *Federal Aviation Regulations* (FAR) which are distributed by the US-American *Federal Aviation Administration* (FAA). Within the FAR two guidelines are predominantly of interest for civil aircraft design:

- FAR Part 23 ‘*Airworthiness Standards: Normal, Utility, Acrobatic, and Commuter Category Airplanes*’ [97].
- FAR Part 25 ‘*Airworthiness Standards: Transport Category Airplanes*’ [96].

Both guidelines contain qualitative demands, i.e. these are often given without precise numbers. The idea is to give flexibility when developing aircraft, especially with regard to integration of new technologies.

The FAR are also background for the recently developed European certification guidelines, the *Joint Aviation Requirements* (JAR) [30, 29], which are not yet valid for all

member states of the European Union.

Design of military aircraft is often based on the US-American MIL-specifications from which the relevant demands and criteria for the actual project are combined. The so called *Design and Clearance Requirements* are given in:

- MIL-STD-1797A ‘*Military Standard – Flying Qualities of Piloted Aircraft*’ [94, 95].

In 1987 these guidelines replaced the former specification:

- MIL-F-8785 C ‘*Flying Qualities of Piloted Aircraft*’ [93].

Here, performance requirements depend on aircraft type (*class*), *flight phase*, quality grade (*level*) and *flight envelope*. The latter distinguishes speed, altitude, load factor and the *normal/failure state* of the airplane. Though made for military aircraft these guidelines are also used in civil aircraft design. As regards automatic control systems the demands and specifications are described in the MIL-F-9490D [92].

However, when approaching a new aircraft concept, these guidelines do often not suffice to describe all design and performance criteria needed for development. As a consequence, aircraft manufacturers exploit other sources, like NASA<sup>1</sup> *Technical Reports* or AIAA<sup>2</sup>-publications. In addition they provide their own criteria which are built on experiences with former aircraft designs or first calculations and testing.

Since this dissertation treats of aircraft with reduced stability, a composition of criteria to be analyzed will be limited to those which are directly affected by stability issues.

Section B.1 of Appendix B presents a selection of relevant criteria drawn from the sources mentioned above. Guidelines that include the subjective pilot opinion (like ‘good’, ‘difficult’, ‘to handle without greater problems’,...) are excluded from the list.

Section B.2 of Appendix B deals with additional criteria proposed by industry which fit the special configuration of a *blended wing-body* aircraft, as treated in the present work.

### Remarks.

(i) Most of these criteria find their origin in ‘classical’ sources like the FAR/JAR guidelines and the *military specifications*. Still, some requirements and limitations were introduced that originated from the very aircraft design itself.

(ii) The *military specifications* and FAR/JAR guidelines do not propose the same limitations for dynamic criteria. The MIL specifications are more demanding. Even if conceived for military aircraft, they present valuable guidelines when analyzing the aircraft eigenmotion, and especially when defining requirements for a control law.

The next step is the definition of a numerical model allowing for parametrization, simulation, and control design. Then the impact of reduced stability on longitudinal and

---

<sup>1</sup>NASA - National Aeronautics and Space Administration

<sup>2</sup>AIAA - American Institute of Aeronautics and Astronautics

lateral aircraft motions can be examined, notably the impact on the presented criteria list which is part of the qualification of an aircraft for civil transportation.

## 2.2 A Naturally Unstable Aircraft Concept: VELA

### VELA 1 General arrangement (actual wing tip with related span 99,6m not shown)

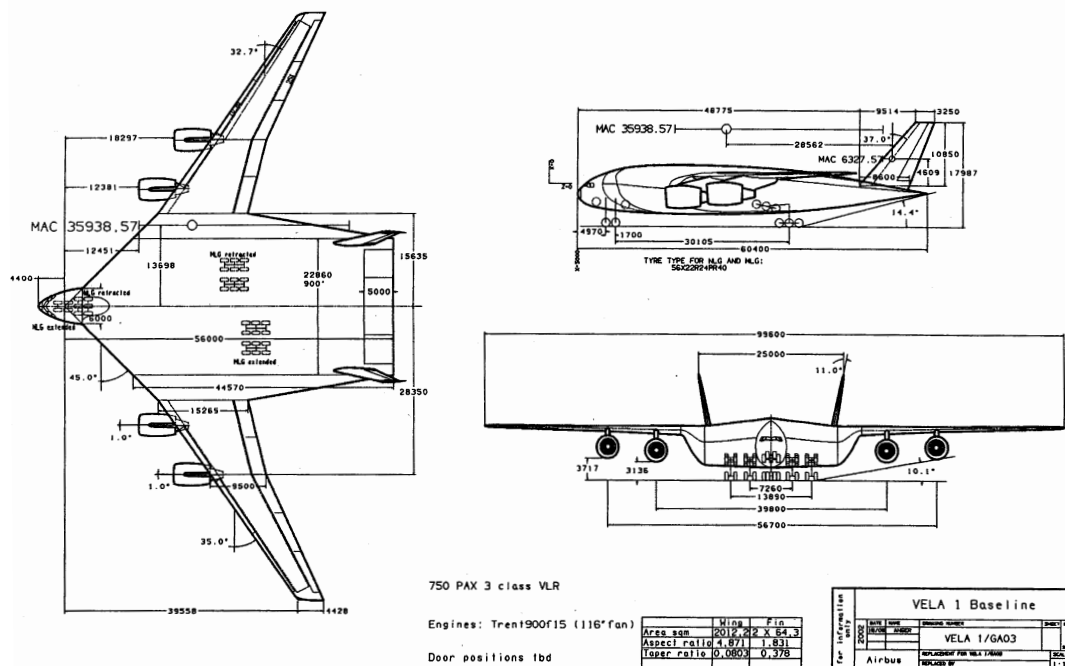


Figure 2.1: VELA1 aircraft.

The airplane chosen for application is the VELA1 blended-wing body aircraft which has been developed within the framework of the European VELA (=Very Efficient Large Aircraft) project. In this section, a description of the aircraft model is given. The aerodynamic and flight mechanical models are introduced. For the aerodynamic model, validated numerical data were directly drawn from the VELA project. The low speed aerodynamic data ensure modeling at a very detailed level for the flight phases of interest (take-off/approach). For the flight mechanical model the general rigid body equations of motion are considered.

### 2.2.1 Aircraft Data

The selected civil transport aircraft concept represents a blended wing-body configuration. The aircraft has a mass range  $M \in [550 t, 770 t]$  with a nominal inertia  $I_{yy,nom} = 44.8 \cdot 10^6 \text{ kgm}^2$ .

Made for civil transport the dimensions exceed those of the A380. Two fins whose size is not yet defined represent the vertical tailplane (VTP). The lever arm from fins and elevator to a nominal c.o.g. position is short ( $\approx 28.6 m$ ), especially when compared to the lever arm of the outboard engines ( $30 m$ ). Finally, the landing gear position and aircraft shape define a margin of  $14.4^\circ$  for *tailstrike*, i.e. the aircraft tail touches ground due a high pitch angle during take-off or landing. The reference data is listed in Table 2.1:

|  |     |       |              |       |
|--|-----|-------|--------------|-------|
| Mass range   | $M$ | $\in$ | $[550; 770]$ | $t$   |
| Reference surface                                      | $S$ | $=$   | 2012         | $m^2$ |
| Mean aerodynamic chord<br>( $\equiv$ Reference length) | $l$ | $=$   | 35.93        | $m$   |
| Wing span  | $b$ | $=$   | 99.60        | $m$   |

Table 2.1: VELA reference values.

### Flight Mechanical Model

The rigid body flight mechanics equations are expressed in the body frame coordinate system. The angular velocities of the aircraft are defined by the vector  $\vec{\Omega} = (p, q, r)^T$ , with  $p$  being the roll rate,  $q$  the pitch rate, and  $r$  the yaw rate.

With  $\vec{V}$  being the velocity vector of the aircraft in aircraft coordinates and  $J\vec{\Omega}$  the angular momentum (where  $J$  is the tensor of inertia), the dynamic equations are:

$$m\dot{\vec{V}} = \Sigma\vec{F}_{ext} + m\vec{\Omega} \times \vec{V} + m\vec{g} \quad (2.1)$$

$$J\dot{\vec{\Omega}} = \Sigma\vec{M}_{ext} + \vec{\Omega} \times (J\vec{\Omega}) \quad (2.2)$$

The external forces  $\vec{F}_{ext}$  and moments  $\vec{M}_{ext}$  exerted on the aircraft are produced by aerodynamic loads ( $\vec{F}_{aero}, \vec{M}_{aero}$ ) and thrust loads ( $\vec{F}_{thr}, \vec{M}_{thr}$ ). With the dimensionless aerodynamic coefficients, the aerodynamic loads read:

$$F_{aero} = \frac{1}{2}\rho S V_{aero}^2 \begin{pmatrix} C_X \\ C_Y \\ C_Z \end{pmatrix} \quad M_{aero} = \frac{1}{2}\rho S l V_{aero}^2 \begin{pmatrix} Cl \\ Cm \\ Cn \end{pmatrix} \quad (2.3)$$

where  $S$  and  $l$  are the reference area and reference length,  $\rho$  the density of the ambient air, and  $V_{aero}$  the aerodynamic speed. The coefficients are described in the body frame.

Whereas the  $Z$  force is positive downwards in direction of the aircraft  $z$ -axis, the lift force  $L$  and its coefficient  $C_L$  are positive upwards, perpendicular to the oncoming flow. Furthermore, the drag force  $D$  and its coefficient  $C_D$  are defined in direction of the oncoming flow, whereas  $X$  and  $C_X$  are positive in negative aircraft  $x$ -axis. For disambiguation,

the moment coefficient subscripts are denoted with small characters  $Cm$ ,  $Cn$ ,  $Cl$ .

The inertia tensor is symmetric with respect to the aircraft symmetry plane ( $x, z$ ) and reads:

$$J = \begin{pmatrix} A & 0 & -E \\ 0 & B & 0 \\ -E & 0 & C \end{pmatrix} \quad (2.4)$$

For the complete description of the model, the equations for pitch angle  $\theta$ , yaw angle  $\phi$ , heading  $\psi$ , and the kinematic equation for the vertical speed were also implemented. After a change of variables, one obtains the state vector with the nine state variables:

$$X = (V, \alpha, \beta, \theta, \phi, p, q, r, h)^T \quad (2.5)$$

The outputs of the model include the load factors  $n_X$ ,  $n_Y$  and  $n_Z$  in the body frame.

### Aerodynamic Model

The aerodynamic data are tabulated and allow for the reconstruction of all six aerodynamic coefficients ( $C_X$ ,  $C_Y$ ,  $C_Z$ ,  $Cl$ ,  $Cm$ , and  $Cn$ ). These are functions of the angle of attack  $\alpha$  successively combined with yaw angle  $\beta$ , rotational velocities  $p$ ,  $q$  and  $r$ , accelerations  $\dot{\alpha}$  and  $\dot{\beta}$ , and finally the control surface deflections (elevator, rudders - left and right - and wing control surfaces A1 to A10 - ailerons and spoilers)<sup>3</sup>. The aerodynamic data are given for flight at low speed, i.e. approach velocity ( $Mach = 0.2$ ) and for the reference point  $X_{ref}$  which is placed at 30.7% of the mean aerodynamic chord  $l$ . The model is parametrized as a function of the dimensionless c.o.g. displacement  $dx_g$  along the x-axis:

$$dx_g = \frac{X_g - X_{ref}}{l} \quad (2.6)$$

where  $X_g$  is the position of the center of gravity on the aircraft  $x$ -axis, positive in aft direction.

#### 2.2.2 Equilibrium and Linearization

The system dynamics can be linearized about the equilibrium  $f(X_{eq}, u_{eq}) = 0$  as follows:

$$\begin{aligned} \dot{X} &= f(X, u) \approx f(X_{eq}, u_{eq}) + \left. \frac{\partial f}{\partial X} \right|_{X_{eq}, u_{eq}} \bar{X} + \left. \frac{\partial f}{\partial u} \right|_{X_{eq}, u_{eq}} \bar{u} \\ Y &= g(X, u) \approx g(X_{eq}, u_{eq}) + \left. \frac{\partial g}{\partial X} \right|_{X_{eq}, u_{eq}} \bar{X} + \left. \frac{\partial g}{\partial u} \right|_{X_{eq}, u_{eq}} \bar{u} \end{aligned} \quad (2.7)$$

<sup>3</sup>Only elevator, rudder, and ailerons are used in this dissertation.

with  $\bar{X} = X - X_{eq}$  ( $\dot{\bar{X}} = \dot{X}$ ) and  $\bar{u} = u - u_{eq}$ . This leads to:

$$\begin{aligned}\dot{\bar{X}} &= A\bar{X} + B\bar{u} \\ \bar{Y} &= C\bar{X} + D\bar{u}\end{aligned}\tag{2.8}$$

with  $\bar{Y} = Y - Y_{eq}$ .

The partial derivatives  $\frac{\partial f}{\partial X}, \dots$  are calculated using the centered difference quotient:

$$\frac{\partial f}{\partial X_i}(X, u) = \frac{f(X + \varepsilon e_i, u) - f(X - \varepsilon e_i, u)}{2\varepsilon}\tag{2.9}$$

where  $e_i$  is the vector of the  $i$ -th component of the state vector  $X$ .  $\varepsilon$  gives the precision and is set to  $10^{-4}$ . For the sake of legibility the ‘bars’ will be omitted in future reference.

### Final Remarks on the Aircraft Modeling.

(i) As noted above, the model uses tabulated aerodynamic data. These were manipulated in order to generate different sizes for the vertical fin or produce a take-off/landing configuration.

(ii) The use of the whole aerodynamic data base is not always convenient. To that end, Toussaint et al. [91] provided a model with simplified aerodynamic data. The simplified data were obtained using linear regression on the aerodynamic data tables. This model has then been adapted by the author according to the needs.

(iii) When a comparison with the classical Douglas DC8 airplane is demonstrated, simplified DC8 aerodynamic and geometry data have been injected into the flight mechanics and dynamics model above. Both simplified aerodynamic models detail in Appendix A.

## Part I

# Flight Mechanics and Dynamics Analysis



## Chapter 3

# Analytical Approach to Reduced Longitudinal Stability

When speaking of reduced natural longitudinal stability in a flight mechanics context, usually two kinds of stability are distinguished: static and dynamic longitudinal stability. Even though the concept of distinguishing between these two types of stability is becoming more and more outdated it presents a thankful approach to the subject.

In flight mechanics, static stability is the initial tendency of an airplane to return to a given state of equilibrium, i.e. trim, when disturbed in its current flight path. Thus, the forces and moments evoked by the disturbance tend to return the aircraft to its equilibrium flight conditions. If the initial tendency of the airplane is to hold the disturbed position, the airplane is said to have neutral static stability. Finally, if the forces and moments cause the airplane to diverge even more from its initial flight condition, the airplane is statically unstable.

Furthermore, an airplane may undergo three forms of motion after disturbance: first, it may return to its former equilibrium condition in an aperiodic or oscillatory manner. The airplane is dynamically stable. Second, it may continue to perform a motion of constant amplitude. The airplane is said to have neutral dynamic stability. Third, it may diverge completely from its original equilibrium condition with increasing amplitude. The airplane is dynamically unstable. It is clear that an aircraft with reduced stability is either very difficult to control or not at all. In that case, a control system has to be conceived which guarantees acceptable handling qualities. This chapter is organized as follows:

Section 3.1 briefly presents what is commonly known as longitudinal static stability. Even though this definition of stability is conservative and presents just a special case of general, or dynamic, longitudinal stability, it is a viable approach to the subject and to the notion of the aircraft neutral point.

Section 3.2 then develops a more general definition of stability using analytic expressions of the short period mode of the longitudinal motion. The concept of the maneuver

point is introduced as the limit of flight dynamic stability.

Sections 3.3 to 3.6 elaborate on stabilizing feedback requirements according to the degree of instability. Moreover, elevator actuator bandwidth characteristics are considered as well as their influence on gain and phase margins for the controlled motion. The derived analytical expressions present a first set of tools to measure the impact of reduced stability. The chapter closes with an illustration of the developed results in Section 3.7.

### 3.1 Longitudinal Static Stability

If all forces, aerodynamic and gravitational, and aerodynamic moments exerted on an airplane are in balance about its c.o.g. then the airplane is in trim. In the longitudinal motion, this condenses to the statement that the sum of all pitching moments has to be zero. Figure 3.1 depicts quantitatively the pitching moment about the c.o.g. of an aircraft for two possible cases; first, where the aerodynamic moment increases as the angle of attack is increased and, second, where the moment decreases with increasing  $\alpha$ .

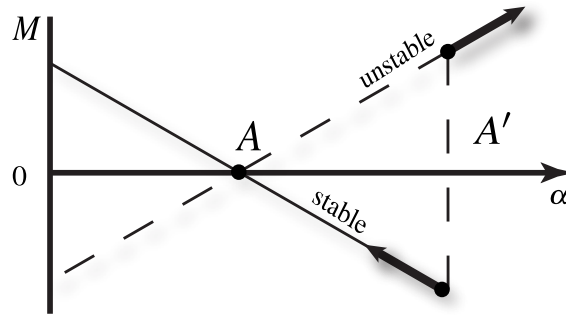


Figure 3.1: Possible variation of the aircraft pitching moment with  $\alpha$ . Initial trim at  $A$ .

For the  $\alpha$  value at point  $A$  the airplane is in trim. Here, the sum of all pitching moments  $M$  about the aircraft  $y$ -axis are zero. With a variation of  $\alpha$  the variation of  $M$  will be approximately linear. If  $M$  evolves to positive values with an increase of the angle of attack value to  $A'$ , then the pitching moments tend to increase  $\alpha$  even more (nose up). Obviously, the airplane is unstable. Conversely, if the moment decreases with  $\alpha$ , a down pitching moment is the result, tending to return  $\alpha$  to its trim value. Thus, two conditions must hold for an airplane to be *statically stable in pitch and in trim*:

$$\begin{aligned} \frac{dM}{d\alpha} &< 0 \\ M(\alpha_{trim}) &= 0 \end{aligned} \tag{3.1}$$



dimensionless longitudinal position of the aerodynamic center for the wing and  $x_{N,t}$  that for the horizontal tailplane.  $\eta_t$  is a factor taking into account a possible reduced aerodynamic pressure at the tail ( $\eta_t = 1$  in free stream).  $i_t$  stands for the tail incidence (or rigging) angle whereas  $S_t$  denotes the surface of the horizontal tail.  $S$  is the reference surface of the aircraft.  $\epsilon_\alpha$  presents the rate change of the wing induced downwash angle at the tail, varying linearly with the angle of attack:

$$\epsilon = \frac{w}{V} = \frac{d\epsilon}{d\alpha} d\alpha = \epsilon_\alpha \alpha \quad (3.7)$$

### 3.1.1 Neutral Point

As for wing and tail, there exist an overall aerodynamic center: if the c.o.g. is positioned at this point, the pitching moment stays constant, independent of the angle of attack. This position  $x_g = x_N$  is called the neutral point and can thus be determined by:

$$Cm_\alpha = 0 = (x_N - x_{N,w}) C_{L\alpha,w} - (x_{N,t} - x_N) \eta_t \frac{S_t}{S} C_{L\alpha,t} (1 - \epsilon_\alpha) \quad (3.8)$$

$$x_N = \frac{x_{N,w} + x_{N,t} \eta_t \frac{S_t}{S} \frac{C_{L\alpha,t}}{C_{L\alpha,w}} (1 - \epsilon_\alpha)}{1 + \eta_t \frac{S_t}{S} \frac{C_{L\alpha,t}}{C_{L\alpha,w}} (1 - \epsilon_\alpha)} \quad (3.9)$$

Expressing the lift coefficient change rate  $C_{L\alpha}$  in terms of wing and tail contribution gives:

$$C_{L\alpha} = C_{L\alpha,w} + \eta_t \frac{S_t}{S} C_{L\alpha,t} (1 - \epsilon_\alpha) \quad (3.10)$$

Inspection of the denominator in Eq. (3.9) shows its equality to  $C_{L\alpha}/C_{L\alpha,w}$ . Resubstitution of Eq. (3.9) in Eq. (3.6) delivers:

$$Cm_\alpha = (x_g - x_N) \cdot C_{L\alpha} \quad (3.11)$$

This important well-known result states that, for condition Eq. (3.2) to hold, *the center of gravity must be placed before the neutral point for an airplane to be naturally statically stable in the longitudinal motion.*

In the following, the center of gravity displacement will be expressed as the stability margin  $s_m$ :

$$s_m = -\frac{Cm_\alpha}{C_{L\alpha}} = -(x_g - x_N) = -\frac{X_g - X_N}{l} \quad (3.12)$$

Thus, the airplane is statically stable with positive  $s_m$  and unstable for  $s_m < 0$ . Some aerodynamic momentum coefficients can then be expressed via their value at the neutral point  $x_N$  and a force coefficient multiplied with the effective lever arm (static margin) of the aircraft:

$$\begin{array}{l} Cm_\alpha = \quad \quad \quad - s_m C_{L\alpha} \\ Cm_q = Cm_{q,x_N} - s_m C_{Zq} \\ Cm_{\delta m} = Cm_{\delta m,x_N} - s_m C_{L\delta m} \end{array} \quad (3.13)$$

Now that the limit of longitudinal static stability is well defined, the next paragraphs will deal with the dynamic stability. Here, we are interested in the short term response of the aircraft, assuming that long term responses can be handled by a pilot without any control system.

## 3.2 Longitudinal Dynamic Stability

Typically, two longitudinal oscillations can be distinguished. These oscillations, also known as modes, are called phugoid and short-period oscillation. The first presents a slow interchange of kinetic energy and potential energy about an equilibrium energy level. It incorporates a large amplitude variation of speed, pitch, flight path angle, and altitude, but at a constant angle of attack. Typically, the period is quite long (20-60 seconds) and the pilot can correct this motion even if it is unstable.

The short-period oscillation (SPO) is more interesting in this context, as this motion is difficult to control for the pilot when it becomes unstable. Typically, the SPO is a very fast, heavily damped, motion with a period of a few seconds or less. The motion is a rapid pitching of the aircraft about the center of gravity, resulting in a variation of angle of attack  $\alpha$  and pitch rate  $q$ .

The SPO can be derived from the lift force and pitch moment equations:

$$mV \frac{d\gamma}{dt} = L - W \cos \gamma + F \sin(\alpha + \sigma) \quad (3.14)$$

$$I_{yy} \frac{d^2\theta}{dt^2} = \sum M_Y \quad (3.15)$$

where  $L$  is the lift,  $W$  the weight and  $\sigma$  the thrust incidence. For  $\sigma \approx 0$  and assuming that the sum of moments  $M_Y$  about the  $y$ -axis is of aerodynamic nature only, this yields

(with  $\cos \gamma \approx 1$ ):

$$mV\dot{\gamma} = \frac{1}{2}\rho V^2 S \cdot C_L - mg + F \sin \alpha \quad (3.16)$$

$$I_{yy}\dot{q} = \frac{1}{2}\rho V^2 Sl \cdot C_m \quad (3.17)$$

Here, the relation  $\dot{\theta} = q$  is used, which is true for bank angle  $\phi$  and yaw rate  $r$  being zero. Now, the flight path angle can be expressed as  $\gamma = \theta - \alpha$ , and thus  $\dot{\gamma} = q - \dot{\alpha}$ .

Linearizing at an equilibrium condition and keeping only  $\alpha$ ,  $q$ , and elevator  $\delta m$  related terms gives a simplified system of the SPO:

$$\dot{\alpha} = -\frac{\bar{q}S}{mV}C_{L\alpha}\alpha + \left(1 - \frac{\bar{q}Sl}{mV^2}C_{Lq}\right)q - \frac{\bar{q}S}{mV}C_{L\delta m}\delta m + \frac{1}{V}\left(g - \frac{F}{m}\sin \alpha\right) \quad (3.18)$$

$$\dot{q} = \frac{\bar{q}Sl}{I_{yy}}C_{m\alpha}\alpha + \frac{\bar{q}Sl^2}{I_{yy}V}C_{mq}q + \frac{\bar{q}Sl}{I_{yy}}C_{m\delta m}\delta m \quad (3.19)$$

Here, the dynamic pressure  $\bar{q}$  has been introduced. For facilitated writing the following substitutions are made:

$$b_1 = \frac{\bar{q}S}{mV}, \quad b_2 = \frac{\bar{q}Sl}{I_{yy}}, \quad \varepsilon = b_1 \frac{l}{V}C_{Lq} \quad (3.20)$$

The term  $\frac{1}{V}(g - \frac{F}{m}\sin \alpha)$  presents the thrust contribution to the SPO. From experience we know, that this term only has a considerable effect for fighter aircraft flying at high angles of attack [22, 44, 63]. Furthermore, a relatively high glide ratio (as for civil long haul airplanes) reduces the influence of the thrust on the SPO even more. This term will thus be neglected from here on. The simplified short period oscillation system then reads in matrix notation:

$$\begin{pmatrix} \dot{\alpha} \\ \dot{q} \end{pmatrix} = \begin{pmatrix} -b_1 C_{L\alpha} & 1 - \varepsilon \\ b_2 C_{m\alpha} & b_2 \frac{l}{V} C_{mq} \end{pmatrix} \begin{pmatrix} \alpha \\ q \end{pmatrix} + \begin{pmatrix} -b_1 C_{L\delta m} \\ b_2 C_{m\delta m} \end{pmatrix} \delta m \quad (3.21)$$

This notation allows for a straightforward computation of the eigenvalues, and thus modal characteristics, of the SPO. For stability and closed-loop analysis purposes, the 2nd order differential equations are derived in the next paragraphs. Toussaint and Gimonet [90] have taken a similar approach with comparable results.

### 3.2.1 2nd Order Differential Equations in $\alpha$ and $q$

Derivation of the  $\alpha$ -equation and elimination of  $q$  delivers the differential equation for  $\alpha$ :

$$\begin{aligned} \ddot{\alpha} + [b_1 C_{L\alpha} - b_2 \frac{l}{V} C_{m_q}] \dot{\alpha} - b_2 [(1 - \varepsilon) C_{m_\alpha} + b_1 \frac{l}{V} C_{m_q} C_{L\alpha}] \alpha = \\ b_2 [(1 - \varepsilon) C_{m_{\delta m}} + b_1 \frac{l}{V} C_{m_q} C_{L\delta m}] \delta m - b_1 C_{L\delta m} \delta \dot{m} \end{aligned} \quad (3.22)$$

Proceeding in the same manner for  $q$  yields:

$$\begin{aligned} \ddot{q} + [b_1 C_{L\alpha} - b_2 \frac{l}{V} C_{m_q}] \dot{q} - b_2 [(1 - \varepsilon) C_{m_\alpha} + b_1 \frac{l}{V} C_{m_q} C_{L\alpha}] q = \\ b_1 b_2 [C_{L\alpha} C_{m_{\delta m}} - C_{m_\alpha} C_{L\delta m}] \delta m - b_1 C_{L\delta m} \delta \dot{m} \end{aligned} \quad (3.23)$$

Naturally, the eigendynamics described by the  $\alpha$  and  $q$  differential equations are identical. Only the inhomogeneous part (right-hand side) of the equations differ: these terms determine the particular solution superposed to the general solution, thus they take into account the respective influence of the elevator on the  $\alpha$  and  $q$  evolution. This will especially have an effect with respect to a closed-loop analysis. A short summary is given below:

Inhomogeneous linear differential equation of the short-period oscillation:

$$a_2 \ddot{x} + a_1 \dot{x} + a_0 x = \mathcal{F}_x(\delta m) \quad (3.24)$$

where

$$a_0 = -b_2 [(1 - \varepsilon) C_{m_\alpha} + b_1 \frac{l}{V} C_{m_q} C_{L\alpha}] \quad (3.25)$$

$$a_1 = b_1 C_{L\alpha} - b_2 \frac{l}{V} C_{m_q} \quad (3.26)$$

$$a_2 = 1 \quad (3.27)$$

with

$$b_1 = \frac{\bar{q}S}{mV}, \quad b_2 = \frac{\bar{q}Sl}{I_{yy}}, \quad \varepsilon = b_1 \frac{l}{V} C_{Lq} \quad (3.28)$$

The inhomogeneous parts  $\mathcal{F}_x(\delta m)$  for  $x = \alpha$  and  $x = q$  are:

$$\mathcal{F}_\alpha(\delta m) = b_2 [(1 - \varepsilon) C_{m_{\delta m}} + b_1 \frac{l}{V} C_{m_q} C_{L\delta m}] \delta m - b_1 C_{L\delta m} \delta \dot{m} \quad (3.29)$$

$$\mathcal{F}_q(\delta m) = b_1 b_2 [C_{L\alpha} C_{m_{\delta m}} - C_{m_\alpha} C_{L\delta m}] \delta m + b_2 C_{m_{\delta m}} \delta \dot{m} \quad (3.30)$$

### 3.2.2 Limit of Natural SPO Stability

**Theorem 3.1 (Adapted from the Hurwitz Criterion).** *A 2nd order dynamic system described by an inhomogeneous differential equation*

$$a_2 \ddot{x} + a_1 \dot{x} + a_0 x = c \neq 0$$

*is asymptotically stable if the following condition holds:*

$$a_n > 0, \quad n \in [0, 1, 2]$$

Applying this criterion to the SPO gives three stability conditions:

$$1. \quad a_0 = -b_2 [(1 - \varepsilon) C m_\alpha + b_1 \frac{l}{V} C m_q C_{L\alpha}] = \lambda_1 \cdot \lambda_2 > 0 \quad (3.31)$$

$$2. \quad a_1 = b_1 C_{L\alpha} - b_2 \frac{l}{V} C m_q = -(\lambda_1 + \lambda_2) > 0 \quad (3.32)$$

$$3. \quad a_2 = 1 > 0 \quad (3.33)$$

where  $\lambda_1$  and  $\lambda_2$  denote the eigenvalues of the system. The third condition is naturally fulfilled. Conditions 1 and 2 will deliver the natural dynamics stability limit. Introducing the c.o.g. dependency modeled in Eq. (3.13) yields:

$$1. \quad a_0 > 0 \Rightarrow (1 - \varepsilon) s_m C_{L\alpha} - b_1 \frac{l}{V} C_{L\alpha} (C m_{q,x_N} - s_m C_{Lq}) > 0 \quad (3.34)$$

$$2. \quad a_1 > 0 \Rightarrow b_1 C_{L\alpha} - b_2 \frac{l}{V} (C m_{q,x_N} - s_m C_{Lq}) > 0 \quad (3.35)$$

This leads to two conditions for the *stability limit in terms of the static margin  $s_m$* :

$$\boxed{\begin{array}{l} 1. \quad s_m > \frac{\rho S l}{2m} C m_{q,x_N} \\ 2. \quad s_m > \frac{C m_{q,x_N}}{C_{Lq}} - \frac{I_{yy}}{m l^2} C_{L\alpha} \end{array}} \quad (3.36)$$

The first condition is determining the c.o.g. static margin where the airplane is at the limit of dynamic stability. The second condition is not a physical constraint since  $C m_{q,x_N} < 0$ . It only guarantees that both eigenvalues  $\lambda_1$  and  $\lambda_2$  are actually negative, Eq. (3.31).

### 3.2.3 General Stability Limit: Maneuver Point

Eq. (3.36) demonstrates that the SPO (extracted from the longitudinal motion), can be stable for a negative static margin  $s_m$ , thus even when the airplane is statically unstable.

We therefore realize that the static stability notion is *conservative*, i.e. when placing the c.o.g. at  $x_g = x_N$  this does not necessarily mean that the aircraft is at its actual limit of stability. The stability limit lies  $|\frac{\rho S l^2}{2m} C m_{q,x_N}|$  behind the neutral point and is referred to as the *maneuver point*. With Eq. (3.12) the position of the maneuver point reads

$$X_{MP} = X_N - \frac{\rho S l^2}{2m} C m_{q,x_N} \quad (3.37)$$

This stability limit can also be interpreted as the c.o.g. position for which the necessary elevator deflection to command a load factor becomes zero.

$$\frac{\Delta \delta m}{\Delta n_Z} = 0 \quad (3.38)$$

Since the maneuver point is dependent on density  $\rho$  and mass  $m$ , it will have its most fwd, and thus most critical position at high altitude and high mass, i.e. at the beginning of cruise flight.

A dynamic margin  $d_m$  is thus defined as

$$d_m = -\frac{X_g - X_{MP}}{l} \quad (3.39)$$

### 3.2.4 Handling Quality Characteristics versus C.o.G. Position

The evolution of the handling quality determining parameters damping and frequency can now be traced as a function of the c.o.g. We assume that there exists a function describing the evolution of the frequency and damping from an aft c.o.g. position  $s_{m-}$  to more forward position  $s_m$ .

$$\exists f_{\omega^2}(s_m), \quad \omega_{s_m}^2 = \omega_{s_{m-}}^2 + f_{\omega^2}(s_m) \quad (3.40)$$

$$\exists f_{\xi\omega}(s_m), \quad \xi_{s_m} \omega_{s_m} = \xi_{s_{m-}} \omega_{s_{m-}} + f_{\xi\omega}(s_m) \quad (3.41)$$

We exploit the fact that in an oscillatory case:

$$a_{0s_m} = \lambda_{1s_m} \cdot \lambda_{2s_m} = \omega_{s_m}^2 \quad (3.42)$$

$$a_{1s_m} = -(\lambda_{1s_m} + \lambda_{2s_m}) = 2\xi_{s_m} \omega_{s_m} \quad (3.43)$$

Resolving for functions  $f_i(s_m)$  yields:

$$f_{\omega^2}(s_m) = [s_m - s_{m-}] b_2 C_{L\alpha} \quad (3.44)$$

$$f_{\xi\omega}(s_m) = \frac{1}{2} [s_m - s_{m-}] C_{Lq} \quad (3.45)$$

Resubstitution of the functions delivers the open-loop evolution of the damping and frequency characteristics of the system as a function of the c.o.g. position:

$$\omega_{s_m} = \sqrt{\omega_{s_{m^-}}^2 + [s_m - s_{m^-}] b_2 C_{L\alpha}} \quad (3.46)$$

$$\xi_{s_m} = \frac{2 \xi_{s_{m^-}} \omega_{s_{m^-}} + [s_m - s_{m^-}] C_{Lq}}{2 \sqrt{\omega_{s_{m^-}}^2 + [s_m - s_{m^-}] b_2 C_{L\alpha}}} \quad (3.47)$$

### 3.3 Control of the Short-Period Oscillation

This section will analytically analyze the feedback of aerodynamic variables  $\alpha$ ,  $q$ , and a combination of both.  $d_m$  denotes the dynamic stability margin, i.e. the relative margin in *mac* to the maneuver point.

#### 3.3.1 Feedback of $\alpha$

The feedback structure is as follows:

$$\delta m = K_\alpha \cdot \alpha \quad (3.48)$$

The closed-loop eigenvalues and coefficients of the differential equation become:

$$a_0^{cl} = \lambda_1^{cl} \cdot \lambda_2^{cl} = b_2 C_{L\alpha} d_m - K_\alpha b_2 [(1 - \varepsilon) C_{m_{\delta m, x_N}} + C_{L\delta m} d_m] \quad (3.49)$$

$$a_1^{cl} = -(\lambda_1^{cl} + \lambda_2^{cl}) = b_1 C_{L\alpha} - b_2 \frac{l}{V} (C_{m_{q, x_N}} - s_m C_{Lq, x_N}) + K_\alpha b_1 C_{L\delta m} \quad (3.50)$$

In the case of oscillatory modes the system damping can be derived from  $a_1 = 2\xi\omega$ . The gain  $K_\alpha$  contributes thus to the damping via the term  $K_\alpha b_1 C_{L\delta m}$ . Knowing that coefficient  $C_{L\delta m}$  is relatively small, and for a flying wing configuration even negligible, we can state that the feedback will not have a strong impact on the system damping but more on its frequency.

If the system had to be dynamically stabilized with a feedback on  $\alpha$ , the stabilizing gain would be:

$$K_\alpha^{stab} = \frac{C_{L\alpha} d_m}{(1 - \varepsilon) C_{m_{\delta m, x_N}} + C_{L\delta m} d_m} \quad (3.51)$$

### 3.3.2 Feedback of $q$

The feedback law for  $q$  is:

$$\delta m = K_\alpha \cdot q \quad (3.52)$$

This changes the eigenvalues of the system to:

$$a_0^{cl} = \lambda_1^{cl} \cdot \lambda_2^{cl} = b_2 C_{L\alpha} d_m - K_q b_1 b_2 C_{L\alpha} C m_{\delta m, x_N} \quad (3.53)$$

$$a_1^{cl} = -(\lambda_1^{cl} + \lambda_2^{cl}) = b_1 C_{L\alpha} - b_2 \frac{l}{V} (C m_{q, x_N} - s_m C_{Lq, x_N}) - K_q b_2 (C m_{\delta m, x_N} - s_m C_{L\delta m}) \quad (3.54)$$

Following the same reasoning as before, we can state that a  $q$  feedback will, in contrast to the feedback on  $\alpha$ , mainly alter the system damping properties. A stabilizing gain is found for

$$K_q^{stab} = \frac{d_m}{b_1 C m_{\delta m, x_N}} \quad (3.55)$$

### 3.3.3 Combined Feedback of $\alpha$ and $q$

When considering a combined feedback

$$\delta m = (K_\alpha, K_q) \cdot (\alpha, q)^T \quad (3.56)$$

one obtains a system of two linear equations with two unknowns  $K_\alpha$  and  $K_q$ . Exploiting the fact that in an oscillatory system

$$a_0^{cl} = \lambda_1^{cl} \cdot \lambda_2^{cl} = \omega_{obj}^2 \quad (3.57)$$

$$a_1^{cl} = -(\lambda_1^{cl} + \lambda_2^{cl}) = 2\xi_{obj} \omega_{obj} \quad (3.58)$$

the gains corresponding to a damping and frequency objective ( $\xi_{obj}$ ,  $\omega_{obj}$ ) can be calculated easily.

$$2\xi_{obj} \omega_{obj} = b_1 C_{L\alpha} - b_2 \frac{l}{V} (C m_{q, x_N} - s_m C_{Lq}) + K_\alpha b_1 C_{L\delta m} - K_q b_2 (C m_{\delta m, x_N} - s_m C_{L\delta m}) \quad (3.59)$$

$$\omega_{obj}^2 = b_2 C_{L\alpha} d_m - K_\alpha b_2 [(1 - \varepsilon) C m_{\delta m, x_N} + d_m C_{L\delta m}] - K_q b_1 b_2 C_{L\alpha} C m_{\delta m, x_N} \quad (3.60)$$

Under the hypothesis that the lift contribution of the elevator is negligible ( $C_{L\delta m} \approx 0$ ), the feedback gain on  $q$  can directly be determined from Eq. (3.59) for a given damping and frequency objective.  $K_\alpha$  is then obtained by substituting  $K_q$  in Eq. (3.60). The resulting expressions are not fully expanded for the sake of simplicity.

For a given damping and frequency objective, and under the hypothesis that  $C_{L\delta m} \approx 0$ :

$$K_q = \frac{a_1 - 2\xi_{obj}\omega_{obj}}{b_2 C m_{\delta m, x_N}} \quad (3.61)$$

$$K_\alpha = \frac{a_0 - \omega_{obj}^2 + (2\xi_{obj}\omega_{obj} - a_1)}{b_2(1 - \varepsilon) C m_{\delta m, x_N}} \quad (3.62)$$

Now that the base for SPO control is laid, robustness issues with a varying center of gravity position can be tackled conveniently.

### 3.4 Robustness versus Center of Gravity Position

The developed analytical expressions allow for analyzing the evolution of the system dynamics for a given feedback with a variation of the c.o.g. position. The approach is the same as for Eqs. (3.40) and (3.45). In that way specifications for the single feedback controller are determined which guarantee sufficient modal characteristics over a range of c.o.g. positions.

Inspection of Eqs. (3.59) and (3.60) shows that the functions describing the damping and frequency dependency on the c.o.g. are the same for open-loop and closed-loop systems if assumed that  $C_{L\delta m} \approx 0$ :

$$f_{\omega^2}^{cl}(s_m) = f_{\omega^2}^{ol}(s_m) = [s_m - s_{m-}] b_2 C_{L\alpha} \quad (3.63)$$

$$f_{\xi\omega}^{cl}(s_m) = f_{\xi\omega}^{ol}(s_m) = \frac{1}{2}[s_m - s_{m-}] C_{Lq} \quad (3.64)$$

$$\omega_{s_m}^{cl} = \sqrt{(\omega_{s_{m-}}^{cl})^2 + [s_m - s_{m-}] b_2 C_{L\alpha}} \quad (3.65)$$

$$\xi_{s_m}^{cl} = \xi_{min} = \frac{2 \xi_{s_{m-}}^{cl} \omega_{s_{m-}}^{cl} + [s_m - s_{m-}] C_{Lq}}{2 \sqrt{(\omega_{s_{m-}}^{cl})^2 + [s_m - s_{m-}] b_2 C_{L\alpha}}} \quad (3.66)$$

Since  $b_2 C_{L\alpha}$  in the denominator of Eq. (3.66) is much greater than  $C_{Lq}$  in the nominator, the damping  $\xi$  will diminish for a single fixed feedback gain for fwd c.o.g. positions. Conversely, the frequency will increase.

In order to demonstrate robustness with varying c.o.g. positions, a minimum damping constraint  $\xi_{min}$  has to be shown for the most fwd c.o.g. position as well as a maximum frequency limitation  $\omega_{max}$ . For aft c.o.g. positions it is convenient to consider a minimum

degree of stability objective  $\lambda_{min}^1$  for the SPO.

Since  $2\xi\omega = -(\lambda_1 + \lambda_2)$  a case differentiation according to whether the system is periodic  $\xi \leq 1$  or aperiodic  $\xi \geq 1$  has to be made in order to determine the minimum stability degree  $\lambda_{min}$ :

$$\omega_{s_{m-}}^{cl} \xi_{s_{m-}}^{cl} = \lambda_{min} \quad \text{for } \xi_{s_{m-}} \leq 1 \quad (3.67)$$

$$\omega_{s_{m-}}^{cl} (\xi_{s_{m-}}^{cl} - \sqrt{(\xi_{s_{m-}}^{cl})^2 - 1}) = \lambda_{min} \quad \text{for } \xi_{s_{m-}} \geq 1 \quad (3.68)$$

and hence

$$\omega_{s_{m-}}^{cl} = \frac{\lambda_{min}}{\xi_{s_{m-}}^{cl}} \quad \text{for } \xi_{s_{m-}} \leq 1 \quad (3.69)$$

$$\omega_{s_{m-}}^{cl} = \frac{\lambda_{min}}{\xi_{s_{m-}}^{cl} - \sqrt{(\xi_{s_{m-}}^{cl})^2 - 1}} \quad \text{for } \xi_{s_{m-}} \geq 1 \quad (3.70)$$

Reformulating Eq. (3.66) as to deliver the damping specifications needed for the most aft c.o.g. yields

$$\xi_{s_{m-}}^{cl} = \xi_{min} \sqrt{1 + \frac{1}{(\omega_{s_{m-}}^{cl})^2} [s_m - s_{m-}] b_2 C_{L\alpha} - \frac{1}{2\omega_{s_{m-}}^{cl}} [s_m - s_{m-}] C_{Lq}} \quad (3.71)$$

Thus, with Equations (3.69) to (3.71) the initial damping and frequency conditions for the most aft c.o.g. position can be determined (by iteration for example). Objectives  $\lambda_{min}$  and  $\xi_{min}$  are then guaranteed over the selected c.o.g. range.

Once the initial handling quality demands are set the corresponding robust feedback gain is easily obtained with the help of Eqs. (3.61) and (3.62).

### 3.5 Integration of the Actuator Model

The actuator model is represented by a first order differential equation

$$T_{act} \delta \dot{m} + \delta m = u_c \quad (3.72)$$

and characterized by the actuator time constant  $T_{act}$ .  $u_c$  is the commanded input of the actuator given by the control law

$$u_c = K_\alpha \alpha + K_q q \quad (3.73)$$

<sup>1</sup>The degree of stability of a state matrix  $A$  is  $-\max_i \text{Re}(\lambda_i)$ , where the  $\lambda_i$  are the eigenvalues of  $A$ .

The actuator output  $\delta m$  is the actual position of the elevator being at the same time the input to the airplane dynamics. For the ongoing analysis it seems promising to apply the Laplace transform and tackle the aircraft dynamics in the frequency domain. The aircraft input becomes

$$\delta m(s) = \frac{1}{T_{act}s + 1} \cdot [K_\alpha \alpha(s) + K_q q(s)] \quad (3.74)$$

where  $s$  is the complex variable. The differential equations for  $\alpha(s)$  and  $q(s)$  are given by Equations (3.24) to (3.30). When writing

$$\mathcal{F}_\alpha(U(s)) = z_{1\alpha} \cdot U(s) - z_{2\alpha} \cdot U(s) \cdot s \quad (3.75)$$

$$\mathcal{F}_q(U(s)) = z_{1q} \cdot U(s) + z_{2q} \cdot U(s) \cdot s \quad (3.76)$$

with

$$z_{1\alpha} = b_2 [(1 - \varepsilon) C m_{\delta m} + b_1 \frac{l}{V} C m_q C_{L\delta m}] \quad z_{2\alpha} = b_1 C_{L\delta m} \quad (3.77)$$

$$z_{1q} = b_1 b_2 [C_{L\alpha} C m_{\delta m} - C m_\alpha C_{L\delta m}] \quad z_{2q} = b_2 C m_{\delta m} \quad (3.78)$$

the transfer function from aircraft input  $U(s)$  to elevator actuator output becomes:

$$\frac{\delta m(s)}{U(s)} = G(s) = \frac{g_1 \cdot s + g_0}{(T_{act}s + 1)(s^2 + a_1 s + a_0)} \quad (3.79)$$

with

$$g_0 = K_q z_{1q} + K_\alpha z_{1\alpha} \quad (3.80)$$

$$g_1 = K_q z_{2q} - K_\alpha z_{2\alpha} \quad (3.81)$$

With this description it is now possible to analyze any impact of the control system and the actuator onto two stability relevant system characteristics: gain and phase margin.

### 3.6 Gain and Phase Margin

The *gain margin* is defined as the change in open-loop gain required to render the corresponding closed-loop system unstable. Systems with greater gain margins can withstand greater gain changes in system parameters before becoming unstable in closed-loop. The *phase margin* is defined as the change in open-loop phase shift required to make a closed-loop system unstable. The phase margin also measures the tolerance of the system to time delay. Since gain and phase margin are measures of relative stability the short-period oscillation in combination with a control law and an elevator actuator model will now be examined in view of these measures.

In short, the Bode stability criterion is recalled for reference.

**Theorem 3.2 Bode Stability Criterion.** Let  $\omega_{pc}$  be the phase crossover frequency of an open-loop system, i.e. the frequency where the phase shift is equal to  $-\pi$ . And let  $\omega_{gc}$  be the gain crossover frequency, i.e. the frequency where the amplitude ratio from input to output is 1 ( $= 0$  dB).

If at the phase crossover frequency, the corresponding system gain  $|G(i\omega_{pc})| < 0$  dB, then the closed-loop system is stable. The following stability margins are defined:

- *Gain Margin:* Let  $A_0 = |G(i\omega_{pc})|$ , then the gain margin is given by

$$GM = \frac{1}{A_0} \quad (3.82)$$

- *Phase Margin:* Let  $\varphi_0 = \arg G(i\omega_{gc})$ , then the phase margin is given by

$$PM = \pi + \varphi_0 \quad (3.83)$$

### 3.6.1 Gain Margin

Following the Bode criterion, the gain margin GM is only defined at the phase crossover frequency  $\omega_{pc}$ , thus for argument  $\varphi_0 = -\pi$ . Therefore, system gain is completely real. This fact is used to find  $\omega_{pc}$  by setting the imaginary part of the transfer function of Eq. (3.79) to zero. The Laplace variable is set to  $s = j\omega$ :

$$\omega^3 (T_{act}g_0 - T_{act}a_1g_1 - g_1) + \omega(g_1a_0 - T_{act}a_0g_0 - a_1g_0) = 0$$

This delivers

$$\omega_{pc} = \sqrt{\frac{T_{act}a_0g_0 + a_1g_0 - a_0g_1}{T_{act}(g_0 - a_1g_1) - g_1}} \quad (3.84)$$

Of course, the trivial solution  $\omega = 0$  exists: it provides the DC gain of the system but not the phase crossover frequency. Inserting this result into the real part of the transfer function gives the gain margin:

$$GM = \frac{1}{A_0} = \frac{a_1^2 T_{act} + a_1 a_0 T_{act}^2 + a_1}{a_1 g_1 T_{act} - g_0 T_{act} + g_1} \quad (3.85)$$

**Gain margin excluding actuator effects.** In a first step, an idealized actuator with unlimited bandwidth is assumed ( $T_{act} \rightarrow 0$ ). The crossover frequency becomes:

$$\omega_{pc} = \sqrt{a_0 - a_1 \frac{g_0}{g_1}} \quad (3.86)$$

and the gain margin for a ‘perfect’ actuator of unlimited bandwidth, i.e. with zero time constant is:

$$GM = \frac{a_1}{g_1} \quad (3.87)$$

A condition for the existence of the gain margin is derived:

$$\frac{a_1}{g_1} > 0 \quad (3.88)$$

If the natural aircraft is stable ( $a_1 > 0$ ), then consequently  $g_1 > 0$ , too, in order for the gain margin to be defined. If  $a_1 < 0$  the condition is inversed. This gives in the stable case:

$$g_1 > 0 \Rightarrow K_q z_{2q} - K_\alpha z_{2\alpha} > 0 \quad (3.89)$$

A larger positive feedback will thus reduce the gain margin which can therefore be adjusted according to the degree of instability given by  $a_1$  (determined by the center of gravity position of the airplane). A relation between feedback gains  $K_\alpha$  and  $K_q$  is implied (remember that  $z_{2q} < 0$ ):

$$K_q < K_\alpha \frac{z_{2\alpha}}{z_{2q}} \Rightarrow K_q < K_\alpha \frac{b_1 C_{L\delta m}}{b_2 C_{m\delta m}}$$

**Actuator impact on gain margin.** Applying the same approach to the gain margin of Eq. (3.85) gives two conditions: both the nominator and denominator can be set to zero in order to find a time constant. One condition delivers a time constant corresponding to the limit of stability, the other a value for which  $GM$  is not defined:

$$1. \quad T_{act}^2 + \frac{a_1}{a_0} T_{act} + \frac{1}{a_0} > 0 \quad (3.90)$$

$$2. \quad T_{act}(a_1 g_1 - g_0) + g_1 \neq 0 \quad (3.91)$$

Of course, only solutions with  $T_{act} > 0$  are of interest. The first condition only gives an upper limit for the time constant, if  $a_0 < 0$  (for an unstable airplane). Otherwise it does not deliver a constraint. At the same time, the second condition must hold for the gain margin to exist:

$$1. \quad T_{act_{max}} < -\frac{a_1}{2a_0} + \sqrt{\left(\frac{a_1}{2a_0}\right)^2 - \frac{1}{a_0}} \quad (3.92)$$

$$2. \quad 0 < T_{act} \neq \frac{g_1}{g_0 - a_1 g_1} \quad (3.93)$$

### 3.6.2 Phase Margin

The phase margin is computed for the gain crossover frequency  $\omega_{gc}$ , thus for the frequency where

$$|G(j\omega)| = \frac{|j\omega g_1 + g_0|}{|(j\omega T_{act} + 1)((j\omega)^2 + j\omega a_1 + a_0)|} = 1 \quad (3.94)$$

**Phase margin excluding actuator effects.** Again, in a first step we choose  $T_{act} \rightarrow 0$ .

Then a quadratic expression for  $\omega$  is obtained.

$$\omega^4 + \omega^2(a_1^2 - 2a_0 - g_1^2) + a_0^2 - g_0^2 = 0 \quad (3.95)$$

Its discriminant  $D$  delivers a first condition of existence:

$$D = (a_1^2 - 2a_0 - g_1^2)^2 - 4(a_0^2 - g_0^2) > 0 \quad (3.96)$$

Again, the positive solution is chosen, delivering the gain crossover frequency

$$\omega_{gc} = \frac{1}{\sqrt{2}} \left[ -(a_1^2 - 2a_0 - g_1^2) + \sqrt{D} \right]^{0.5} \quad (3.97)$$

Then the phase margin  $PM$  becomes:

$$PM = \pi + \varphi_0 = \pi + \arctan\left(\frac{g_1\omega_{gc}}{g_0}\right) - \arctan\left(\frac{a_1\omega_{gc}}{a_0 - \omega_{gc}^2}\right) \quad (3.98)$$

The maximum allowable time delay (or delay margin) within the system is inferred:

$$\tau_{max} = \frac{PM}{\omega_{gc}} \quad (3.99)$$

**Actuator impact on phase margin.** Expanding expression Eq. (3.94) and solving for  $\omega$  is not convenient due to the complexity of the resulting expressions. In order to provide a utility for analyzing the actuator impact also in this case, another approach is presented:

Eqs. (3.98) and (3.99) give the maximum allowable system time delay for an ideal actuator with  $T = 0$ . Eq. (3.90) gives the value  $T_{act}$  taking the system to the stability limit, thus a phase and gain margin of zero (and zero allowable delay) - if the aircraft is naturally unstable. Between those two extremal values of the actuator time constant, the allowable delays are computed via an  $\omega$ -grid satisfying simultaneously for Eqs. (3.94) and (3.100).

$$\arctan\left(\frac{g_1\omega}{g_0}\right) - \arctan\left(\frac{a_1\omega}{a_0 - \omega^2}\right) - \arctan(\omega T_{act}) = -\pi \quad (3.100)$$

### 3.7 Illustration of Analytical Results

This section is dedicated to a brief demonstration of the applicability of the developed analytical expressions. The VELA aircraft with reduced mass ( $m = 550t$ ) is equilibrated at low speed ( $Mach = 0.2$ ). The center of gravity position is varied as indicated.

Figure 3.3(a) displays the feedback necessary to put the system on the stability limit, computed with Eqs. (3.51) and (3.55). As expected, for the unstable SPO ( $s_m < -0.023$ ) the feedback needs to be positive.

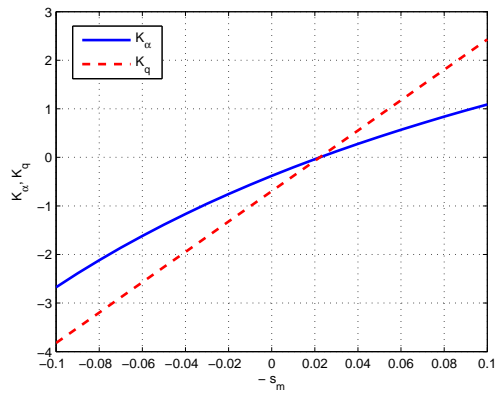
Figure 3.3(b) shows the evolution of the feedback gains for a given frequency and

damping objective (see Eqs. (3.61) and (3.62)).  $\omega = 0.8$  is kept constant and  $\xi$  varies between 0.1 and 1. As can be noted, a higher damping will lead to a smaller norm of the feedback gain. For a damping objective of 70 % (thick, red) at a c.o.g. position of 7 % aft, the gains  $K_\alpha = 1.32$  and  $K_q = 0.03$  are obtained.

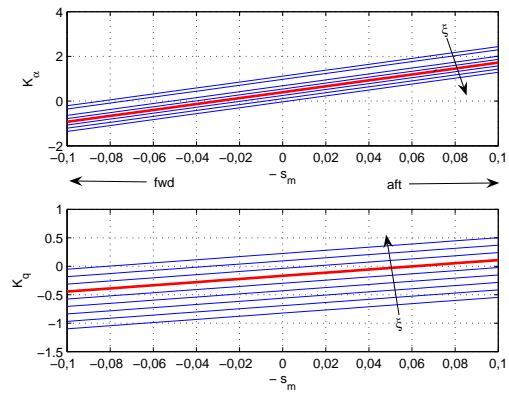
Figure 3.3(c) shows the analytically computed open-loop SPO poles whereas Figure 3.3(d) shows the closed-loop poles for this feedback.

Figure 3.3(e) demonstrates how frequency and damping evolve with the c.o.g. position when  $\omega = 0.8$  and  $\xi = 0.7$  at  $dx_g = 7\%$  aft (see Eqs. (3.46) and (3.47)).

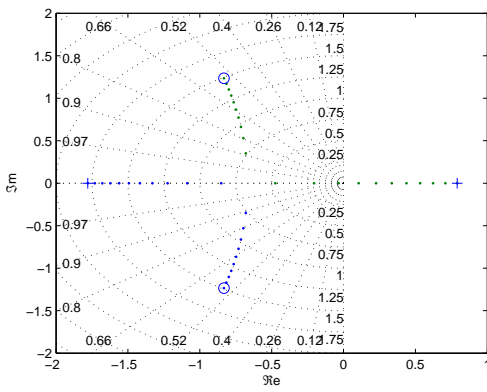
Finally, Figure 3.3(f) displays the time delay margin  $\tau$  as a function of the actuator time constant (normally  $T_{act} < 0.2$ ). A variety of dampings is given, 70 % damping is highlighted, and the frequency is kept constant. Clearly, a higher damping is favorable for the delay margin.



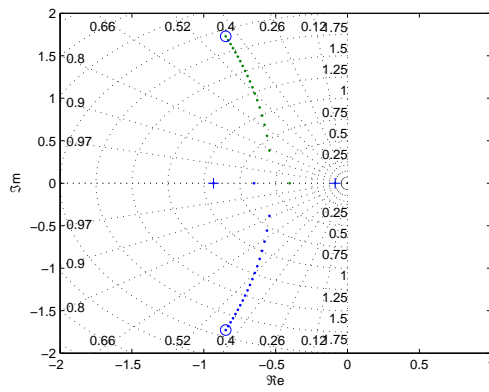
(a) Stability limit gains.



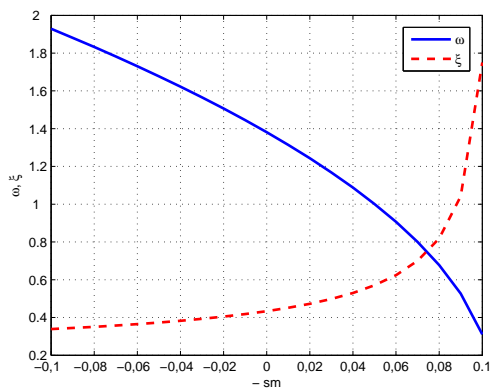
(b) Damping and frequency objective gains.



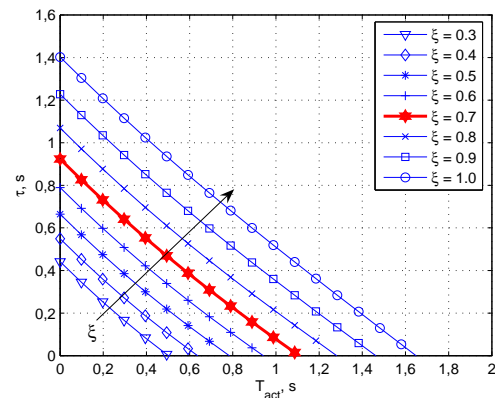
(c) Open-loop poles.



(d) Closed-loop poles.



(e) Damping and frequency evolution.



(f) Time delay margin.



## Chapter 4

# Longitudinal Stability and Actuator Activity/Fatigue

Chapter 3 built the bridge to the development of utilities based on numerical methods. In this chapter, a purely linear approach leads to the determination of the activity of a stabilizing control system. Special interest is laid on the physical link between flight mechanics and artificial stabilization: the actuator which transforms control commands into aerodynamic forces. A tool to analyze actuator fatigue and damage due to the control system activity is presented.

Section 4.1 addresses modeling aspects with regard to the closed-loop VELA aircraft in turbulent flight. A simple feedback controller, scheduled as a function of the center of gravity position, guarantees modal handling quality specifications for a wide c.o.g. range. Section 4.2 develops the necessary theory for actuator activity and fatigue determination. The corresponding application and results are presented in Sections 4.3 and 4.4. Special interest is laid on extremal fwd and aft positions as these impose a demanding task on the elevator actuator. Limits of c.o.g. positions are inferred from the interrelation of handling qualities, fluctuation of actuator deflection and rate during flight in turbulent atmosphere, and fatigue inflicted upon the actuator. The chapter ends with an exemplary application of the developed method to a mission profile in Section 4.5.

### 4.1 Modeling Aspects

The closed-loop behavior of the aircraft short-period oscillation (SPO) is scrutinized for flight in turbulent atmosphere during take-off and approach, i.e. low speed, as these flight phases are critical w.r.t. handling qualities. Therefore this section deals with modeling aspects of the SPO, the actuator, the control system, and the turbulent atmosphere.

### 4.1.1 SPO Properties

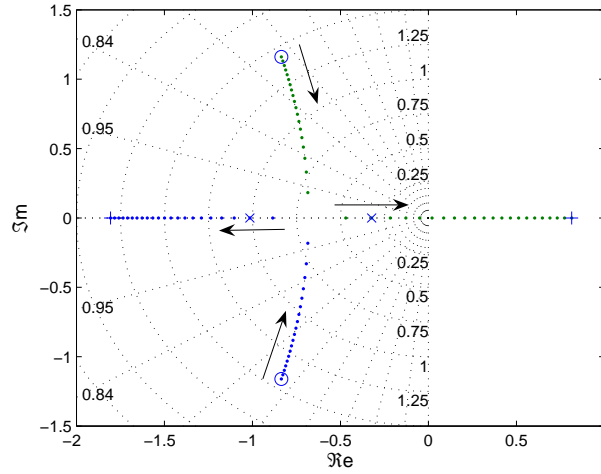


Figure 4.1: SPO poles as a function of the c.o.g. displacement  $dx_g \in [-10\%, 10\%]$ .  $\circ$  equal to  $-10\%$  fwd,  $\times$  to  $0\%$ , and  $+$  to  $10\%$  aft.

Figure 4.1 presents the poles of the short-period oscillation mode of the natural aircraft. The model has been parametrized<sup>1</sup> as a function of the c.o.g. position  $X_g$ . The center of gravity position is varied. The SPO becomes aperiodic for a displacement of  $-0.5\%$ . This numerically computed pole map shows very good coherence with the analytical solution of Section 3.7.

### 4.1.2 Actuator Model

For the time being, only linear aspects of the actuator are considered. Airbus proposes an elevator actuator model for analysis purposes with the following transfer function:

$$H_{act,Airbus}(s) = \frac{4.2s^2 + 530s + 26720}{s^3 + 55s^2 + 2229s + 26720} \quad (4.1)$$

where  $s$  is the Laplace variable. The eigenvalues, damping ratio, and frequency of this transfer function are given in Table 4.1.

| Eigenvalues         | Damping ratio | Frequency ( <i>rad/s</i> ) |
|---------------------|---------------|----------------------------|
| $-19.08 \pm 34.96i$ | 0.48          | 39.80                      |
| $-16.84$            | 1.00          | 16.84                      |

Table 4.1: Characteristics of the Airbus Actuator Model.

An analysis of the actuator dynamics reveals that a much simpler model can produce comparable dynamics. It also facilitates parametric studies. Eq. (4.2) describes a first

<sup>1</sup>Remember:  $dx_g = (X_g - X_{ref})/l$

order transfer function. If the parameter is set to  $T_{act} = 0.06 \text{ s}$  the eigenvalue of the transfer function is  $-16.7$ , and thus of similar magnitude as the aperiodic pole of the model proposed by Airbus.

$$H_{act}(s) = \frac{1}{T_{act}s + 1}. \quad (4.2)$$

The model behavior in terms of frequency and step response is also comparable: Figure 4.2 shows the unit input step response and the Bode diagram. The largest errors occur in phase. One has to acknowledge a loss in phase margin of up to  $45^\circ$  which has to be considered. Since we are basically interested in the actuator bandwidth<sup>2</sup> properties, the simplified model shall suffice for the sake of a facilitated analysis (the simplified model is pessimistic as concerns the gain margin).

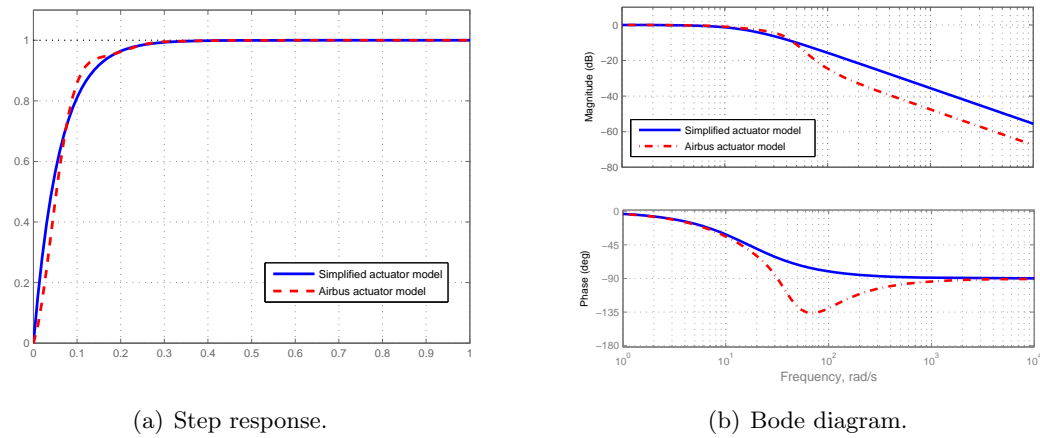


Figure 4.2: Comparison of actuator models: Bode diagram.  $T_{act} = 0.06$ .

### 4.1.3 Stabilizing Control Law

In order to guarantee consequently the same modal specifications for the SPO, a output-feedback controller is designed for each center of gravity position and actuator time constant occurring in the analysis. A modal design technique using only aerodynamic outputs  $\alpha$  and  $q$  is presented briefly. For output-feedback related problems with a non-zero feed-through matrix  $D$  and for further reading on this topic, refer to [61].

Consider the multi-input multi-output linear state-space system

$$\begin{aligned} \dot{x} &= Ax + Bu \\ y &= Cx + Du \end{aligned}$$

<sup>2</sup>The time constant  $T$  of a first order transfer with DC gain 1 is related to its bandwidth  $bw$  via  $bw \approx [0; \omega_c]$  with  $\omega_c = T^{-1}$ .

with  $n$  states ( $x \in \mathbf{R}^n$ ),  $m$  inputs ( $u \in \mathbf{R}^m$ ), and  $p$  outputs ( $y \in \mathbf{R}^p$ ).

With matrix  $D$  being zero and no initial input vector  $u_0$ , the feedback control law with static gain matrix  $K$  reads:

$$u = Ky \tag{4.3}$$

leading to:

$$\dot{x} = (A + BKC)x. \tag{4.4}$$

If one considers the following definitions:

$$\begin{aligned} \lambda_1 \dots \lambda_n &= \text{eigenvalues of } [A + BKC] \\ v_1 \dots v_n &= \text{right hand eigenvectors of } [A + BKC] \\ &\text{so that } (A + BKC)v_i = \lambda_i v_i \\ w_1 \dots w_n &\text{ with } w_i = KC v_i \end{aligned}$$

this retrieves to:

$$(A + BKC)V = V\Lambda \tag{4.5}$$

with

$$\Lambda = \begin{bmatrix} \lambda_1 & & 0 \\ & \ddots & \\ 0 & & \lambda_n \end{bmatrix}; \quad V = [v_1 \dots v_n]; \quad W = [w_1 \dots w_n].$$

so that with  $W = KC V$

$$(A - \Lambda I_n)V + BW = 0$$

The final expression then reads:

$$[A - \Lambda I_n \quad B] \begin{bmatrix} V \\ W \end{bmatrix} = 0, \quad W = KC V \tag{4.6}$$

Thus, the gain matrix  $K$  is found via  $K = W(CV)^{-1}$ . If  $C$  is identity, the resulting matrix  $K$  is the static state-feedback.

**Remark:** Since the system plant state matrix is a function of the c.o.g. displacement and actuator ( $A = f(dx_g, T_{act})$ ), a controller can be designed for each position and time constant according to the SPO modal specifications injected into  $\Lambda$ . The controller is designed to feed back only the SPO states ( $\alpha, q$ ), and NOT any actuator states. Therefore, the actuator pole will not be placed. After closing the loop an additional turbulence model is added.

#### 4.1.4 Model of the Turbulent Atmosphere

According to the military references MIL-F-8785C and MIL-STD-1797, turbulence is a stochastic process defined by velocity spectra, as if the aircraft flew through a ‘frozen’ turbulence field. Thus, flight in turbulent atmosphere can be modeled with the help of a filtered random signal (Gaussian white noise) at the input of the linearized aircraft. The filter represents a transfer function incorporating the atmospheric properties. A spectral Dryden representation Eq. (4.7) (i.e. the energies of the horizontal and vertical speeds of the turbulent atmosphere are functions of frequency) is used for simulation and analysis. The spectra and their corresponding transfer functions are given below:

$$\begin{aligned}\Phi_{W_x}(\omega) &= \frac{2\sigma_x^2 L_x}{V} \cdot \frac{1}{1 + \left(L_x \frac{\omega}{V}\right)^2} & \mapsto & H_x(s) = \sigma_x \sqrt{\frac{2L_x}{V}} \cdot \frac{1}{1 + \frac{L_x}{V}s} \\ \Phi_{W_z}(\omega) &= \frac{\sigma_z^2 L_z}{V} \cdot \frac{1 + 3\left(L_z \frac{\omega}{V}\right)^2}{\left[1 + \left(L_z \frac{\omega}{V}\right)^2\right]^2} & \mapsto & H_z(s) = \sigma_z \sqrt{\frac{L_z}{V}} \cdot \frac{1 + \frac{\sqrt{3}L_z}{V}s}{\left(1 + \frac{L_z}{V}s\right)^2}\end{aligned}\quad (4.7)$$

$\omega$  is the frequency in rad/s,  $L_x$  and  $L_z$  are characteristic scale lengths of the turbulence in  $x$  and  $z$  direction, respectively.  $\sigma_x$  and  $\sigma_z$  (turbulence intensity) are the associated standard deviations.  $s$  is the Laplace variable. Normalizing these spectra yields:

$$\frac{1}{2\pi} \int_{-\infty}^{\infty} \Phi_{W_{x/z}}(\omega) d\omega = \sigma_{x/z}^2. \quad (4.8)$$

For a first analysis, the atmospheric conditions are set to stormy conditions and are characterized by the following values:

$$L_x = L_z = 50 \text{ m} \quad \text{and} \quad \sigma_x = \sigma_z = 5 \text{ m/s}. \quad (4.9)$$

This is done as to take into account a dimensioning ‘worst case scenario’. At the end of this section, the technique will be applied to a typical mission profile and the turbulence characteristics will then eventually be adapted according to the specific flight phases.

## 4.2 Determination of Actuator Activity and Fatigue

This section provides the theoretical background needed to determine the actuator activity and fatigue related to a given equilibrium point depending on Mach number, altitude, and position of the center of gravity.

### 4.2.1 Passage of a Random Signal Through a Linear System

Consider a linear system whose input is a white Gaussian noise  $w$ . Then its state  $x$  and output  $y$  are also random signals. If the deterministic input is  $u(t) = 0$ , we can state the following theorem [68]:

**Theorem 4.1** *Consider a linear system:*

$$\dot{x}(t) = Ax(t) + Mw(t) \quad (4.10)$$

where  $w(t)$  is a stationary white Gaussian noise with a power spectral density  $W$ .  $m(t_0)$  represents the mean and  $P(t_0)$  the covariance of the initial random state  $x(t_0)$ . Therefore,  $x(t)$  is also a random signal

– with mean

$$m(t) = E[x(t)] = e^{A(t-t_0)}m(t_0) \quad (4.11)$$

– and covariance

$$P(t) = E[(x(t) - m(t))(x(t) - m(t))^T]. \quad (4.12)$$

These fulfill the differential equation:

$$\dot{P}(t) = AP(t) + P(t)A^T + MWM^T. \quad (4.13)$$

Assuming that the system is asymptotically stable it will tend toward steady-state behavior. Therefore  $\dot{P} = 0$  and  $P(t) = P$ . This yields the Lyapunov equation:

$$AP + PA^T + MWM^T = 0 \quad (4.14)$$

The output equation of the linear system  $y(t) = Cx(t)$  delivers the covariance matrix  $S(t)$  of output  $y(t)$ :

$$S(t) = CP(t)C^T \quad (4.15)$$

In steady-state, with  $\dot{S} = 0$  and  $S(t) = S$ , the standard deviation of the  $i$ -th state variable is the square root of the  $i$ -th diagonal element of  $S$ :

$$\sigma_i^2 = S_{ii} \quad (4.16)$$

This theorem is used in Section 4.3 to compute the standard deviation of the actuator state, presenting a measure of the actuator activity. Furthermore, the state deviation can be used to derive actuator fatigue damage, as presented in the next section.

### 4.2.2 Theory of Fatigue and Damage

#### Sinusoidal Stress

Consider a material exposed to stress  $e(t)$  (e.g. compression or torsion). The damage to a sinusoidal prompting of amplitude (level)  $\sigma$

$$e(t) = \sigma \sin(\omega t + \phi)$$

which is repeated during  $n$  cycles is

$$d = \frac{n}{N} \quad (4.17)$$

where  $N$  is the maximum number of cycles at level  $\sigma$  causing the first crack, i.e. rupture.  $N$  is usually given by the well-known Wöhler curves (Figure 4.3), see for example [54].

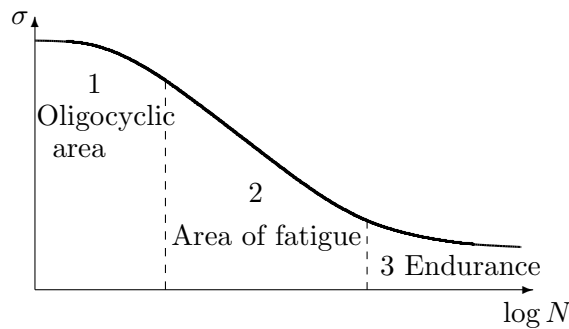


Figure 4.3: The Wöhler curves

We are interested in the so called *area of fatigue* of the Wöhler curve. The stress on the component does not cause plastic deformations but the repeated application debases the structure of the material and, eventually, triggers the appearance of the first crack.

The Basquin law,

$$N \sigma^b = C, \quad (4.18)$$

is an analytical approximation for the Wöhler curve within the fatigue area. It depends on two material constants<sup>3</sup>  $b$  and  $C$ .

One of the most commonly used rules to estimate the overall damage is the Palmgren–Miner theorem [54]. It states that the overall damage  $D$  is the sum of the damages  $d_i$  at different levels

$$D = \sum_i d_i = \sum_i \frac{n_i}{N_i} \quad (4.19)$$

which means that rupture occurs when  $D = 1$ .

<sup>3</sup>The material is assumed to be aluminum 6144 T4 with dimensionless constants  $b = 14.0$  and  $C = 2.26 \cdot 10^{78}$ .

### Stochastic Stress

Following Mouyon and Gaillet [66], the Palmgren–Miner theorem of Eq. (4.19) can be written as the mean damage  $D$

$$D = T n_p^+ \int_0^{+\infty} \frac{q(\sigma)}{N(\sigma)} d\sigma \quad (4.20)$$

for a stochastic stress  $e(t)$  applied during the time span  $T$  and with a probability density  $q(\sigma)$  for the occurrence of a positive extremum of level  $\sigma$ . The mean number of positive extrema during  $T$  is called  $T n_p^+ = T \int_0^{+\infty} q(\sigma) d\sigma$ . Using the Basquin law, Eq. (4.20) becomes

$$D = \frac{T n_p^+}{C} \int_0^{+\infty} \sigma^b q(\sigma) d\sigma \quad (4.21)$$

Lalanne [55] shows that the density function  $q(\sigma)$  for a Gaussian process  $e(t)$  is a combination of a Gaussian law  $G(0, \sqrt{1-r^2})$  and a Rayleigh distribution  $R(1)$  with the irregularity factor  $r$  as parameter.

Assuming that the signal is very regular, i.e.  $r \approx 1$  and hence  $q(\sigma)$  a Rayleigh law, Eq. (4.21) retrieves to

$$D \approx \frac{T n_p^+}{C} (\sqrt{2} \sigma_e)^b \Gamma\left(1 + \frac{b}{2}\right) \quad (4.22)$$

with  $\sigma_e$  the standard deviation of  $e(t)$ . In fact, this approximation is even still valid for small  $r$ . It will be used further on.

Assuming that the signal is irregular, i.e.  $r = 0$ ,  $q(\sigma)$  is Gaussian,  $n_p^+$  can be easily evaluated via

$$n_p^+ = \frac{1}{2\pi} \frac{\sigma_{\dot{e}}}{\sigma_e} \quad (4.23)$$

Combining Eqs. (4.23) and (4.22) delivers finally the relation of the mean damage  $D$  during  $T$

$$D \approx \frac{T}{2\pi C} \sqrt{2}^b \Gamma\left(1 + \frac{b}{2}\right) \sigma_{\dot{e}} \sigma_e^{b-1} \quad (4.24)$$

i.e. the mean damage  $D$  due to  $e(t)$  depends on the standard deviation  $\sigma_e$  of  $e(t)$  and the standard deviation  $\sigma_{\dot{e}}$  of  $\dot{e}(t)$ .

### Impact on the Actuator

The considered failure case of the elevator actuator is the rupture of the hydraulic jack due to stress. The stress  $e$  is hence the force acting on the jack  $F_j$  divided by its section  $S_j$

$$e = \frac{F_j}{S_j}.$$

The force  $F_j$  on the jack is given by the lever arm  $c_j$  between the jack and the elevator surface and the aerodynamic hinge moment  $M_{hinge}$  applied at the control surface:

$$e = \frac{M_{hinge}}{S_j c_j}$$

The hinge moment  $M_{hinge}$  is a function of the aerodynamic pressure  $\frac{1}{2}\rho V^2$ , the reference surface  $S$  of the control surface as well as its mean aerodynamic chord  $l$  and deflection  $\delta m$ . It also depends on the Mach number  $Ma$  and the configuration of the aircraft,  $conf$ . In a first linear approximation for  $M_{hinge}$ , it can be written

$$e \approx \frac{\frac{1}{2}\rho V^2 S l f(Ma, conf) \delta m}{S_j c_j} \approx K \delta m \quad (4.25)$$

which means that the stress  $e$  is almost proportional to  $\delta m$ . Because of this linearity, the standard deviations of  $e$ ,  $\dot{e}$  are also proportional to the standard deviations of  $\delta m$  and  $\dot{\delta m}$ . The mean damage Eq. (4.24) can hence approximately be expressed by the deflection  $\delta m$  and its speed  $\dot{\delta m}$  as follows:

$$D \approx K_g \sigma_{\dot{\delta m}} \sigma_{\delta m}^{b-1} \quad (4.26)$$

with

$$K_g = \frac{T}{2\pi C} \Gamma\left(1 + \frac{b}{2}\right) \left(\sqrt{2} K\right)^b \quad (4.27)$$

and

$$K = \frac{S}{S_j} \frac{l}{c_j} \frac{1}{2} \rho V^2 f(Ma, conf) \quad (4.28)$$

as shown in [66, 60].

The standard deviations of  $\delta m$  and  $\dot{\delta m}$  have already been determined with Eqs. (4.14) and (4.15) by a Lyapunov analysis of the closed-loop aircraft system. Hence, the associated damage can be directly computed using Eqs. (4.26)–(4.28).

### Accumulated Damage

Imbert and Mouyon [48], Mouyon and Gaillet [66], Losser and Mouyon [60] point out how flight missions can be divided into several phases  $i$ , each characterized by a certain aircraft model, control law, flight conditions, and stochastic filters  $W_i$  modeling the main excitations. Again, filtered white Gaussian noise is the input. As the damage is cumulative (as shown before), it suffices to evaluate each mean damage  $D_i$  separately using Eq. (4.24) and to sum the  $D_i$  to obtain the mission damage  $D_{mission}$  using some weighting factors  $w_i$ . The latter represent the time spent within the flight phase  $i$  compared to the total mission duration.

These weighting factors  $w_i$  can be determined when considering probabilistic data as in [47]. Turbulence of a certain deviation  $\sigma_{turb}$  are assumed to appear with a certain

probability  $P_\sigma$ . This value multiplied with the flight time within a mission segment of an aircraft gives the time during which the aircraft is probably exposed to a certain type of turbulence. Thus, one obtains a weighting factor of the examined damage-type compared to the aircraft service life.

Section 4.4 shows the damage results for low speed flight, comparable to take-off and approach phases. The focus is laid on a variation of the c.o.g. position and the actuator bandwidth. As a synthesis to this chapter, in Section 4.5 a complete civil aircraft mission profile will be used to demonstrate the applicability of the technique.

## 4.3 Application to the Aircraft

### 4.3.1 Variables Influenced by Turbulence

The aerodynamic speed  $V_a$  is composed of the inertial speeds  $v_x$  and  $v_z$  in combination with the wind components  $W_x$  and  $W_z$ :

$$\begin{aligned} v_{aX} &= v_X - W_x \cos \theta + W_z \sin \theta \\ v_{aZ} &= v_Z - W_x \sin \theta - W_z \cos \theta \end{aligned} \quad (4.29)$$

and hence

$$V_a = \sqrt{v_{aX}^2 + v_{aZ}^2} \quad (4.30)$$

$$\alpha_a = \tan^{-1} \left( \frac{v_{aZ}}{v_{aX}} \right) \quad (4.31)$$

For small wind perturbations, the linearized expression for variables speed  $V_a$  and angle of attack  $\alpha_a$  read:

$$V_a = V - W_x \cos \gamma + W_z \sin \gamma \quad (4.32)$$

$$\alpha_a = \alpha - \frac{W_z}{V} \cos \gamma - \frac{W_x}{V} \sin \gamma \quad (4.33)$$

In order to render the model more precise, the gradient of the vertical wind is taken into account, which has an effect onto the pitch rate of the aircraft. The aerodynamic pitch rate then becomes:

$$\begin{aligned} q_a &= q + q_w \quad \text{where} \\ q_w &= -(\dot{\alpha} - \dot{\alpha}_a) \\ &= -\frac{\dot{W}_z}{V} \cos \gamma - \frac{\dot{W}_x}{V} \sin \gamma \end{aligned} \quad (4.34)$$

The transfer function (pseudo-derivation) using the  $z$ -wind component to produce the extra wind pitch rate is:

$$H_{qw}(s) = \frac{s}{1 + \tau_{qw}s} \quad \text{with} \quad \tau_{qw} = \frac{4b}{\pi V}, \quad (4.35)$$

where the size of the aircraft is taken into account via its wing span  $b$ .

### 4.3.2 Complete Linearized Model

In order to synthesize a control law and successively adding actuator, controller, and wind models, the SPO is extracted from the full state-space representation. A reduced three-state longitudinal system (aircraft states  $\alpha$  and  $q$  and actuator state  $\delta m$ ) with vertical wind ( $w$ ) and elevator ( $\delta m$ ) as inputs is obtained:

$$\begin{aligned} \dot{x}_{red} &= A_{red} x_{red} + B_{red} u \\ y_{red} &= C_{red} y_{red} + D_{red} u \end{aligned} \quad (4.36)$$

with

$$x_{red} = \begin{pmatrix} \alpha \\ q \\ \delta m \end{pmatrix} \quad y_{red} = \begin{pmatrix} \alpha \\ q \end{pmatrix} \quad u = \begin{pmatrix} w \\ \delta m \end{pmatrix}$$

As the model has been parametrized as a function of  $X_g$ , this reduced system can be systematically calculated for each c.o.g. displacement  $dx_g$  within the considered target range. Static feedback controllers  $\delta m = (K_\alpha, Kq) \cdot (\alpha, q)^T$  are then synthesized as explained in Section 4.1 for each  $X_g$  assuring the specifications for the SPO in Table 4.2.

Two cases are presented. The first one presents a well damped SPO (damping ratio  $\xi = 0.7$ ). This choice is due to the analytical results showing clearly that a higher damping is favorable in terms of the norm of the feedback gain. It will be shown there that besides the better handling qualities also better results in terms of actuator activity and fatigue are obtained. Still, a lower damping case ( $\xi = 0.3$ ) is also considered as to demonstrate the influence of the modal specifications for the basic control law. This case assures only the minimum handling qualities during take-off and landing according to the military specifications [94].

|        | Damping ratio $\xi$ | Frequency $\omega$ |
|--------|---------------------|--------------------|
| case 1 | 0.7                 | 0.8 rad/s          |
| case 2 | 0.3                 | 0.8 rad/s          |

Table 4.2: SPO specifications.

The loop between aircraft states  $[\alpha, q]$  and elevator input  $\delta m$  can now be closed and the complete linearized system of SPO, actuator, controller, and wind can be rewritten as:

$$\begin{aligned} \underbrace{\begin{pmatrix} \dot{X}_w \\ \dot{X}_{CL} \end{pmatrix}}_{\dot{X}_{CLw}} &= \underbrace{\begin{pmatrix} A_w & 0 \\ B_{CL}C_w & A_{CL} \end{pmatrix}}_{A_{CLw}} \underbrace{\begin{pmatrix} X_w \\ X_{CL} \end{pmatrix}}_{X_{CLw}} + \underbrace{\begin{pmatrix} B_w \\ 0 \end{pmatrix}}_{B_{CLw}} e_w \\ \underbrace{\begin{pmatrix} u_w \\ Y_{CL} \end{pmatrix}}_{\dot{Y}_{CLw}} &= \underbrace{\begin{pmatrix} C_w & 0 \\ D_{CL}C_w & C_{CL} \end{pmatrix}}_{C_{CLw}} \underbrace{\begin{pmatrix} X_w \\ X_{CL} \end{pmatrix}}_{X_{CLw}} \end{aligned} \quad (4.37)$$

The subscripts  $CL$  and  $w$  denote the matrices and vectors associated to the closed-loop system and to the wind, respectively, where the only system input is the Gaussian white noise  $e_w$ .

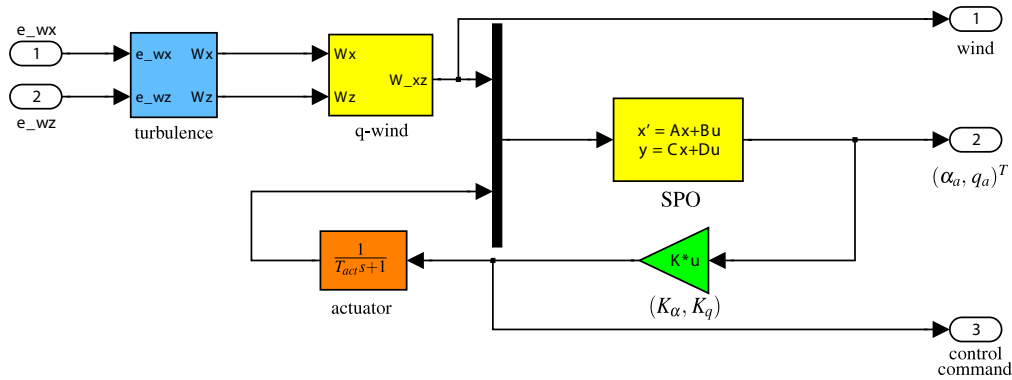


Figure 4.4: SIMULINK scheme: SPO + actuator + controller + turbulence.

**Remark:** Figure 4.4 presents the implementation of the aforementioned closed-loop system with exogenous wind input. Even though the controllers are computed for a feedback of the inertial states  $(\alpha, q)$ , the controller is implemented as to feed back the aerodynamic states  $(\alpha_a, q_a)$ . The analysis will thus show the actuator activity due to a feedback of aerodynamic variables which is close to a feedback of the unfiltered load factor.

### 4.3.3 Actuator Activity and Fatigue

The newly obtained system matrices  $A_{CLw}$ ,  $B_{CLw}$  and  $C_{CLw}$  are now considered for the calculation of the standard deviations. The Lyapunov equation Eq. (4.14) then becomes:

$$A_{CLw}P + PA_{CLw}^T + B_{CLw}B_{CLw}^T = 0 \quad (4.38)$$

The covariance matrix is derived from Eq. (4.39), which is evaluated for all  $dx_g$  in the range of interest  $[-10\%; 10\%]$ .

$$S = C_{CLw}PC_{CLw}^T. \quad (4.39)$$

With the help of these deviations calculated for specific flight conditions, we can infer the actuator activity as a function of  $dx_g$  as well as of the actuator time constant  $T_{act}$ .

## 4.4 Results

This section is dedicated to the presentation of the results. In a first step, the evolution of the necessary gains on the aircraft states  $[\alpha, q]$  is detailed. In a second step, the related actuator activity (in position and rate) is presented, from where we will derive the damage increment inflicted upon the actuator.

### 4.4.1 Gain vs $X_g$

The necessary gain to guarantee the SPO specifications depends on the specifications themselves as well as on the c.o.g. position  $X_g$  of the linearized aircraft and the selected actuator time constant  $T_{act}$ . Figure 4.5 shows this relation for a fixed damping ratio  $\xi = 0.7$ , the red thick line indicating the widest bandwidth with  $T_{act} = 0.06$  s.

As expected from the analytical results in Section 3.3, the gain  $K_\alpha$  rises with aft  $X_g$  as it predominantly affects the SPO frequency/module. The linearized poles of the natural aircraft tend to become aperiodic with aft  $X_g$  and to lose on the degree of stability  $\lambda$  and hence on the module which needs to be compensated by the gain. The actuator bandwidth causes small changes in gain. As concerns the gain  $K_q$ , which plays a major role w.r.t. the SPO damping, the impact of the actuator bandwidth is stronger: it can even cause a change of the algebraic sign of the necessary gain in order to obtain the same pole placement.

With  $T_{act}$  fixed, the effect of the choice of the imposed damping is visualized in Figure 4.6. The choice of a higher damping does, as predicted analytically, reduce the norm of the gains. This fact becomes clearer when recalling the natural behavior of the SPO poles. From being periodic for forward  $dx_g$  with damping ratio  $\xi \approx 0.3$ , the poles become aperiodic ( $\xi = 1$ ) for  $dx_g \approx 0$ , i.e.  $X_g \approx X_{ref}$ , and unstable for  $dx_g > +1.8\%$ . This states

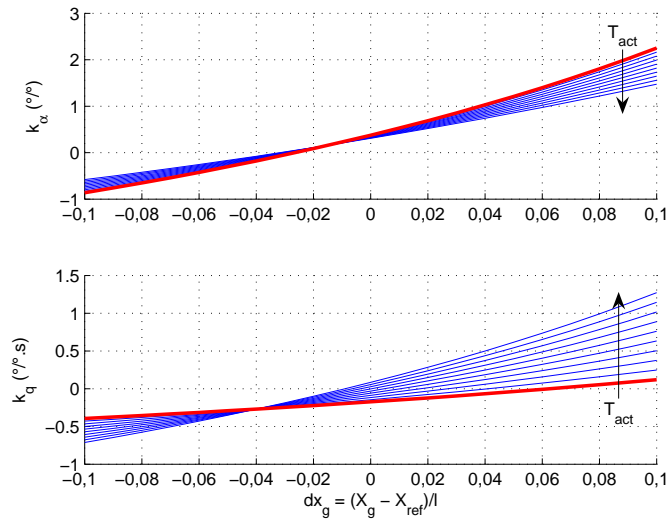


Figure 4.5: Gains  $K_\alpha$ ,  $K_q$  as a function of  $X_g$  and  $T_{act}$ ,  $\xi = 0.7$ .

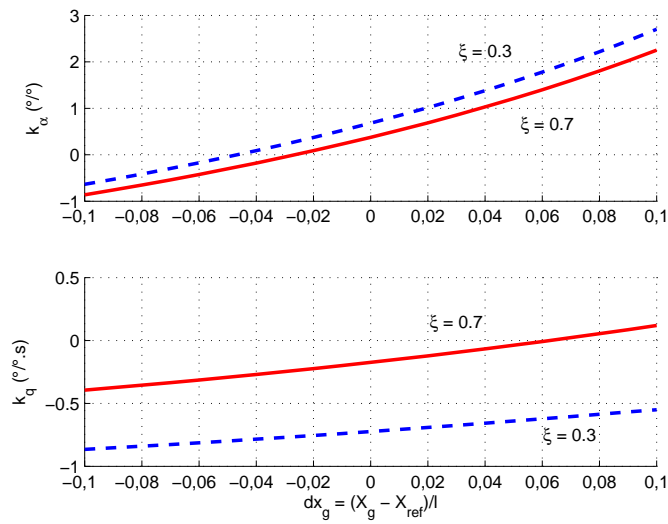


Figure 4.6: Influence of modal specifications on gains.  $T_{act} = 0.06$  s,  $\xi = 0.3/0.7$ .

that the natural damping ratio is quite high throughout a large part of the  $X_g$ -range, and hence less energy (gain) is needed to impose a damping ratio of 0.7 than for 0.3 with the same fixed frequency of  $0.8 \text{ rad/s}$ . In other words, choosing minimal handling qualities is not the best choice in order to obtain minimal gains.

**Remark:** Comparing with Section 3.3, the analytic results give a very precise forecast of the feedback requirements for small  $T_{act}$ . Furthermore, since  $K_\alpha$  tunes the system frequency  $\omega$  and  $K_q$  modifies the system damping  $\xi$ , it is interesting to state that there exist  $X_g$  for which the actuator does not have an influence on the frequency of the system and others for which there is no actuator influence on the system damping (Figure 4.5).

#### 4.4.2 Activity vs. $X_g$

As the considered VELA1 aircraft does not have a separate horizontal plane for trimming, the elevator is used to maintain the equilibrium. Thus, deviations of the elevator deflection in turbulent flight have to be added to the initial trim deflection.

Deflection or rate deviations are plotted for  $1\sigma$  (dashed), covering 68% of all fluctuations expected to be encountered, and  $3\sigma$  (continuous) covering 99.7%. These are functions of  $X_g$  and the actuator time constant. Red lines denote an actuator time constant of  $T_{act} = 0.06 \text{ s}$ .

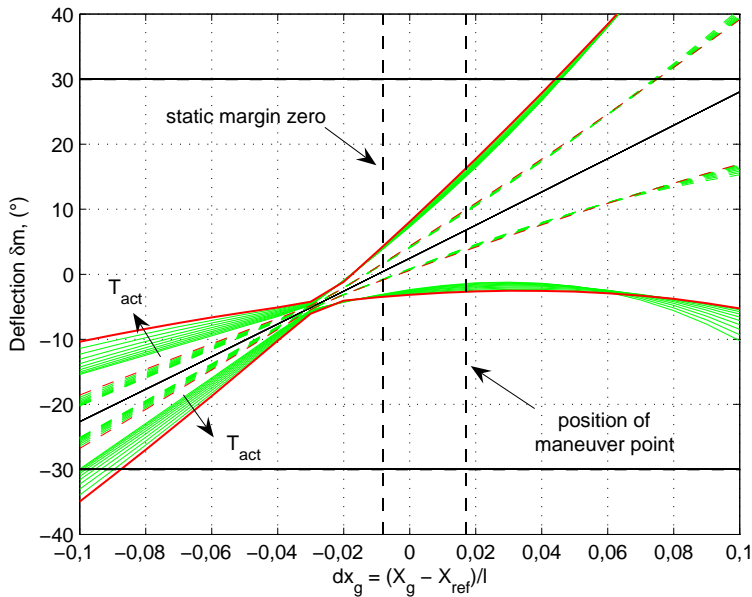


Figure 4.7: Boundaries of the elevator deflection  $\delta m$ .  $T_{act} \in [0.06 \text{ s}; 0.48 \text{ s}]$ .

Vertical dashed lines indicate two c.o.g. positions of interest: positions of maneuver point and zero static margin point. Horizontal continuous lines indicate typical values for saturation in position and rate of the elevator actuator.

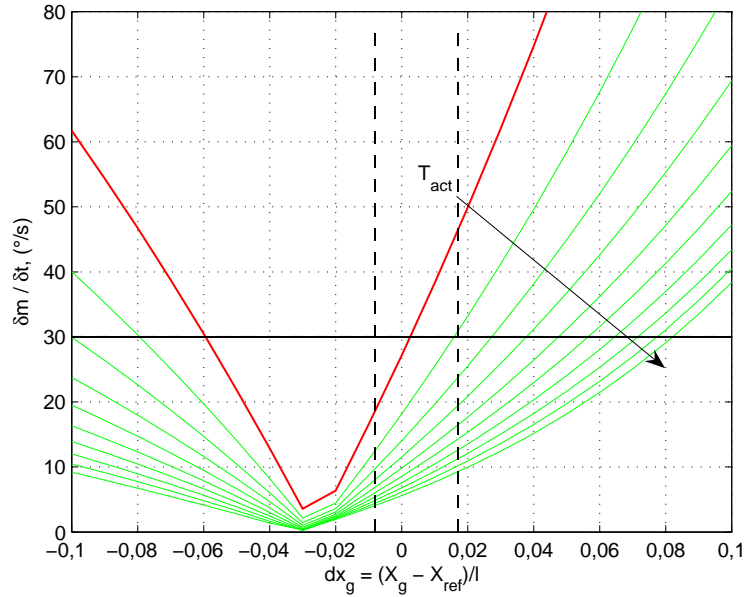


Figure 4.8: Boundaries of the actuator rate  $\delta\dot{m}$ .  $T_{act} \in [0.06 \text{ s}; 0.48 \text{ s}]$ .

Figure 4.7 displays the sum of elevator trim deflection and deviations with the modal specification  $\xi = 0.7$  which, as shown before, results in a smaller feedback gain. We can infer limits for the allowable  $X_g$  displacement  $dx_g$ , with 9% forward and 4.3% aft, according to where the deviations disrespect saturation constraints. The impact of the parameter  $T_{act}$  is negligible.

Figure 4.8 shows the actuator rate fluctuations for  $\xi = 0.7$ . The effect of the parameter  $T_{act}$  is very clear. A rapid actuator causes higher rate fluctuations and hence a very small range of  $X_g$ , whereas a slower actuator can widen the allowable c.o.g. range clearly. In that case, the actuator plays the role of a filter. Still, a rapid actuator is desired with regard to time delay and phase margins, see Section 3.7. If saturation in rate is to be avoided an actuator with a higher rate saturation limit ( $> 50^\circ/s$ ) is needed in order to have aft c.o.g. positions accessible.

Figs. 4.9 and 4.10 demonstrate the influence of the choice of the imposed damping ratio  $\xi$ : the  $X_g$  with minimum fluctuation is moved forward for a smaller damping ratio ( $\xi = 0.3$ ). As concerns actuator rate, a smaller damping ratio shifts the range of allowable  $X_g$  to fwd positions, but does not influence the range size. With regard to fluctuations in position though, a smaller damping increases fluctuation and therefore reduces the accessible c.o.g. area.

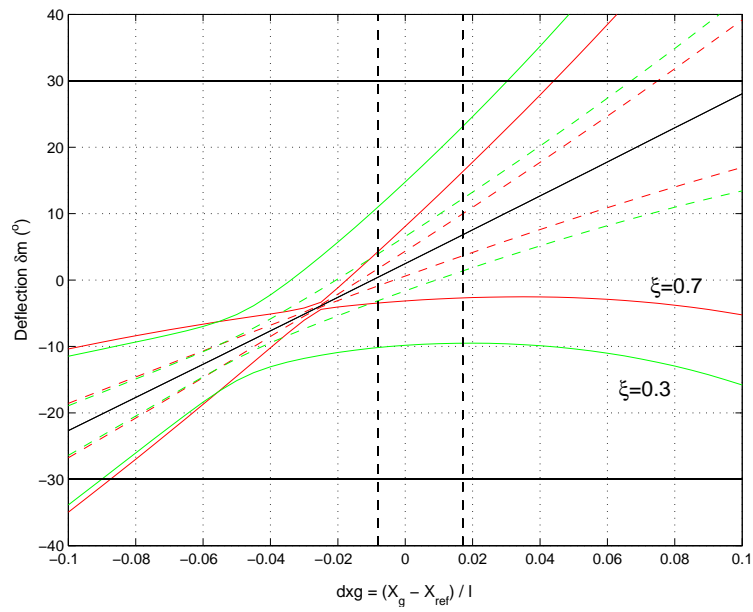


Figure 4.9: Influence of modal specification onto elevator deflection boundaries.  $T_{act} = 0.06$  s. Red:  $\xi = 0.7$ , green:  $\xi = 0.3$ .

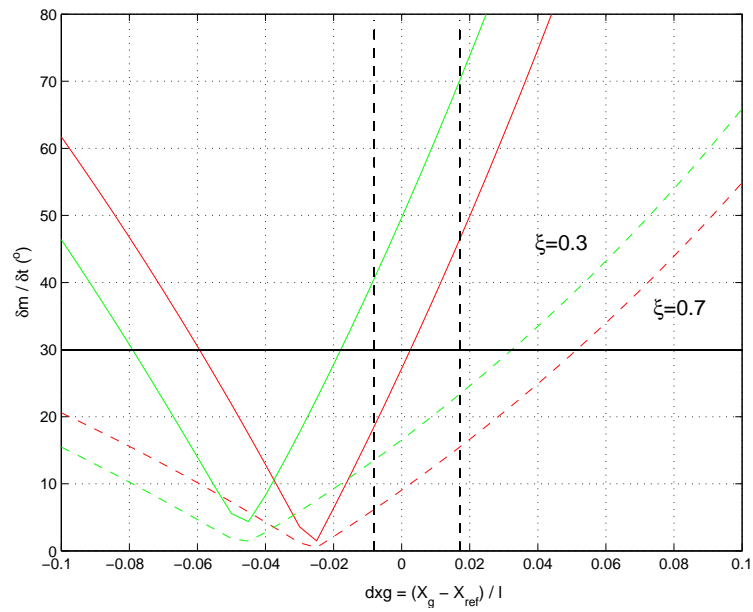


Figure 4.10: Influence of modal specification onto elevator rate boundaries.  $T_{act} = 0.06$  s. Red:  $\xi = 0.7$ , green:  $\xi = 0.3$ .

### 4.4.3 Damage vs. $X_g$

Figure 4.11 shows the normalized damage  $D_N$  for each c.o.g. displacement  $dx_g$  for both damping cases. The data are normalized with a reference damage for  $X_g = X_{ref}$ , minimum handling qualities ( $\xi = 0.3$ ), and  $T_{act} = 0.06$  s. The data are displayed logarithmically and show the enormous increase in damage for extreme aft  $X_g$ . The actuator time constant influence is visible and allows for damage differences of order  $10^1$  to  $10^2$  for forward  $X_g$ . The mean damage rises with a higher  $T_{act}$ , which becomes clear when recalling that deviations in position  $\delta m$  cause significantly higher damage than those in rate  $\delta \dot{m}$ . Compare with Eq. (4.26) and Figures 4.7 and 4.8.

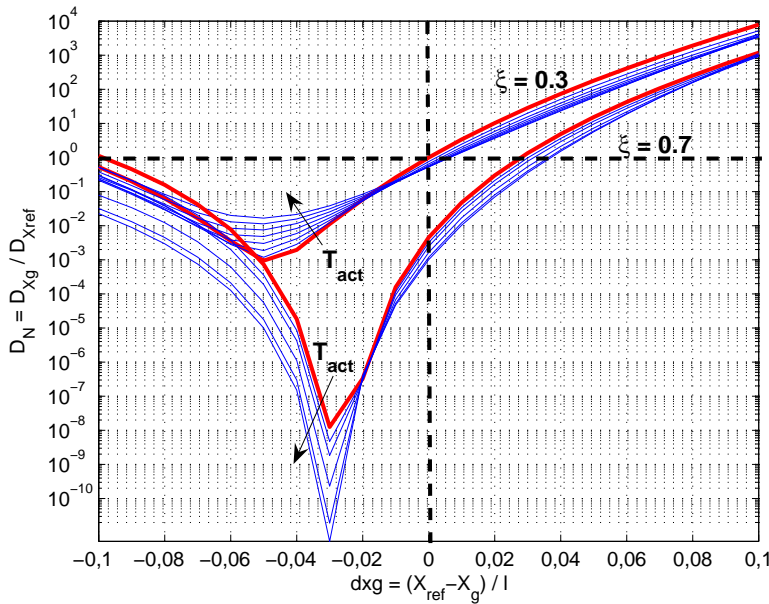


Figure 4.11: Normalized damage  $D_N = \frac{D_{Xg}}{D_{X_{ref}, \xi=0.3, T_{act}=0.06 s}}$  as a function of  $dx_g$ .  $T_{act} \in [0.06 \text{ s}; 0.48 \text{ s}]$ . Red (thick):  $T_{act} = 0.06 \text{ s}$ .

This figure also demonstrates the impact of the choice of the imposed damping ratio for a fixed  $T_{act}$ . For the sake of comparability, the damage values for damping ratio  $\xi = 0.7$  have been normalized with  $D_{X_{ref}, \xi=0.3}$  as well. Damage is notably lower for all displacements  $dx_g$  more aft than  $-4\%$ . Only extreme forward positions incorporate damage higher than the minimum handling quality case ( $\xi = 0.3$ ). But in that case a control system would not be used (aircraft naturally stable).

One should keep in mind, that these values are normalized. The absolute damage inflicted for  $T_{act} = 0.06$  s at the reference point  $X_{ref}$  is  $D_{X_{ref}, \xi=0.3} = 4.76 \cdot 10^{-5} \text{ s}^{-1}$  for  $\xi = 0.3$ . For  $\xi = 0.7$  it is only  $D_{X_{ref}, \xi=0.7} = 2.16 \cdot 10^{-7} \text{ s}^{-1}$ . As rupture of the component is expected at  $D = 1$ , the life expectancy at  $X_g = X_{ref}$  is  $T_{life} = D_{X_{ref}}^{-1}$ , if assumed that the fatigue is caused exclusively by the extreme turbulence so far examined during

take-off/approach. Under these circumstances, the actuator would break after 1286  $h$  of flight.

## 4.5 Exemplary Application to a Mission Profile

This section is dedicated to a brief demonstration of the benefits of the technique that has been developed in the previous paragraphs. This technique is especially interesting in the future project phase of an aircraft since fatigue estimations are so far determined by simulating a complete mission, then extracting the hinge moment evolution of the actuator, and finally computing the fatigue damage according to the Wöhler curves [4]. This is a very time consuming<sup>4</sup> process. The developed technique, once set-up, will allow for estimations after several minutes. This is due to the fact that all types of mission relevant parameters (turbulence, wind, maneuvers) can be modeled with stochastic processes, hence with a white bandwidth limited noise passing through a filter at the input of a linearized system. Further developments in the author's department [48] deal with modeling pilot commands as stochastic processes and even tackle nonlinearities (e.g. saturations) in the otherwise linear system. This section displays only the results related to the author's contribution to this subject, namely the estimation of turbulence induced fatigue damage to the elevator actuator due to a reduced natural stability.

A typical mission profile is taken from documents [74, 100] and displayed here (Figure 4.12) in a simplified manner. According to Airbus, this mission is comparable to a dimensioning mission for the actuator duty cycles of the A340-600 aircraft. The total mission time is 362 *min*, which corresponds roughly to a six hour flight from Frankfurt to Dubai. The mission is broken down into 14 different flight phases which are detailed in Table 4.3.

### 4.5.1 Turbulence Intensities

The values of the turbulence intensities are drawn from documents [3, 100]. These are the values which were used for the numerical calculation of the actuator fatigue of the A380. The corresponding norm is MIL-F-9785A. Three different levels of turbulence are considered: light, medium, and heavy.

The modeling via a Dryden spectrum is the same as in Section 4.1.4. Turbulence is used as to analyze the influence of a reduced stability on the elevator actuator.

Following the military norm, the characteristic wavelengths are function of the altitude:

|                       |                               |
|-----------------------|-------------------------------|
| $h < 1750 \text{ ft}$ | $L_x = 145\sqrt[3]{h}, [ft]$  |
|                       | $L_z = h, [ft]$               |
| $h > 1750 \text{ ft}$ | $L_x = L_z = 1750 \text{ ft}$ |

<sup>4</sup>Actually, the actuator fatigue estimations at the aircraft manufacturer can take up to several days, as of January 2007 [7].

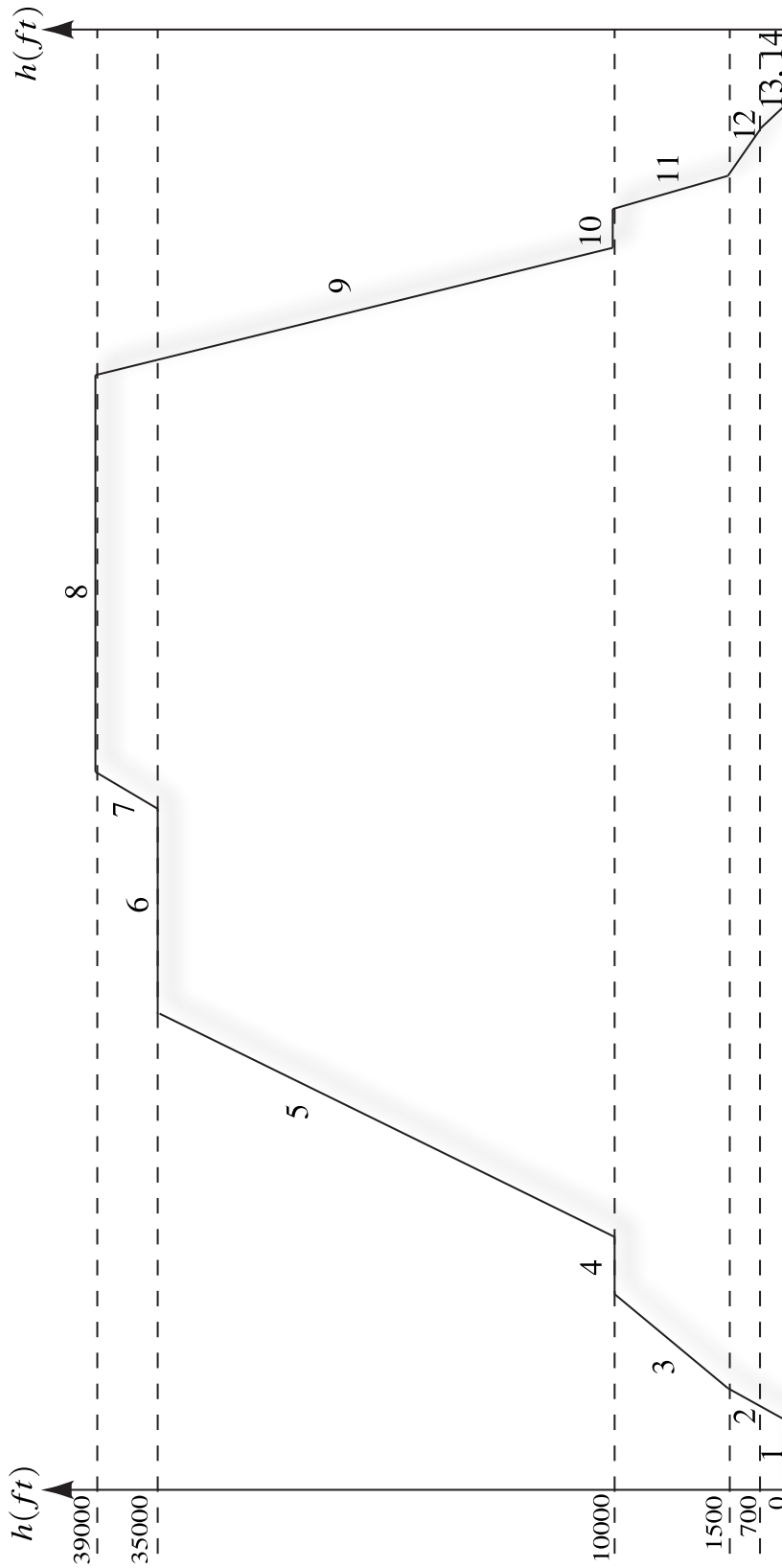


Figure 4.12: A dimensioning mission profile (simplified).

| Phase | Description                  | $V$ , [kt]/ <i>Mach</i> | Altitude $h$ , [ft] | Duration $t_p$ , [s] |
|-------|------------------------------|-------------------------|---------------------|----------------------|
| 1     | startup and taxi             | 10, 25                  | 0                   | 540                  |
| 2     | take-off and initial climb   | 80, 220                 | 0, 1500             | 96                   |
| 3     | climb                        | 220, 250                | 1500, 10000         | 162                  |
| 4     | acceleration in level flight | 250, 320                | 10000               | 42                   |
| 5     | climb                        | 320/0.82                | 10000, 35000        | 816                  |
| 6     | cruise flight                | 0.83                    | 35000               | 2334                 |
| 7     | climb                        | 0.83                    | 39000               | 276                  |
| 8     | cruise flight                | 0.83                    | 39000               | 16524                |
| 9     | descend                      | 0.83                    | 39000, 10000        | 738                  |
| 10    | deceleration at level flight | 310, 250                | 10000               | 60                   |
| 11    | descend                      | 250                     | 10000, 1500         | 390                  |
| 12    | approach                     | 250, 147                | 1500, 700           | 240                  |
| 13    | landing                      | 147, 45                 | 700, 0              | —                    |
| 14    | taxi-in                      | 30, 20                  | 0                   | 300                  |

Table 4.3: A dimensioning mission profile (simplified).

The vertical turbulence intensities as a function of  $h$  are given in Table 4.4.

| $h$ , (1000 ft)    | 1    | 5    | 10   | 15   | 20   | 25   | 30   | 35   | 40   |
|--------------------|------|------|------|------|------|------|------|------|------|
| $\sigma_z$ , [m/s] | 1.97 | 1.71 | 1.55 | 1.52 | 1.49 | 1.44 | 1.45 | 1.42 | 1.40 |

Table 4.4: Vertical turbulence intensities.

The longitudinal turbulence intensities are derived from the relation:

$$\frac{\sigma_x^2}{L_x} = \frac{\sigma_z^2}{L_z}$$

The three different turbulence grades are obtained as follows:

- medium turbulence corresponds to the norm:  $\sigma_2 = \sigma_{norm}$ ,
- light turbulence corresponds to:  $\sigma_1 = 0.5 \cdot \sigma_{norm}$ ,
- heavy turbulence corresponds to:  $\sigma_3 = 2 \cdot \sigma_{norm}$ .

As already mentioned in Section 4.2.2 probabilistic data will be used to determine the time during which the aircraft is exposed to a certain turbulence in each flight phase. Hoblit [47] gives a formula to determine the probability density for a type of turbulence to occur:

$$p(\sigma) = A_1 \sqrt{\frac{2}{\pi}} \frac{1}{b_1} e^{-0.5 \left(\frac{\sigma}{b_1}\right)^2} + A_2 \sqrt{\frac{2}{\pi}} \frac{1}{b_2} e^{-0.5 \left(\frac{\sigma}{b_2}\right)^2} \quad (4.40)$$

where  $A_1$ ,  $A_2$ ,  $b_1$ , and  $b_2$  are dependent on the altitude [47]. This probability density leads to the time fractions corresponding to each turbulence level. These are computed via:

$$P_2 = \int_{p_1}^{p_2} p(\sigma) d\sigma \quad (4.41)$$

$$P_3 = \int_{p_2}^{\infty} p(\sigma) d\sigma \quad (4.42)$$

$$P_1 = 1 - P_2 - P_3 \quad (4.43)$$

Thus, this model assumes that the aircraft will always encounter turbulence (probability of 1), Eq. (4.43). One can thus suppose that the model is pessimistic, as turbulence occurs at all times. Table 4.5 shows the intensities and their probabilities used for the damage computation.

| $h, [ft]$ | $\sigma_{norm}, [m/s]$ | $P_1$ | $P_2$ | $P_3$ |
|-----------|------------------------|-------|-------|-------|
| 1000      | 1.97                   | 0.613 | 0.286 | 0.101 |
| 5000      | 1.71                   | 0.741 | 0.177 | 0.082 |
| 10000     | 1.55                   | 0.951 | 0.033 | 0.016 |
| 15000     | 1.52                   | 0.966 | 0.023 | 0.011 |
| 20000     | 1.49                   | 0.981 | 0.013 | 0.006 |
| 25000     | 1.47                   | 0.987 | 0.009 | 0.004 |
| 30000     | 1.45                   | 0.993 | 0.005 | 0.002 |
| 35000     | 1.42                   | 0.995 | 0.004 | 0.001 |
| 40000     | 1.40                   | 0.997 | 0.002 | 0.001 |

Table 4.5: Turbulence intensities and probabilities  $P_i$  of occurrence for levels  $i = 1, 2,$  and  $3$  (light, medium, heavy).

#### 4.5.2 Accumulated Mission Damage due to Turbulence

Only in-flight phases, i.e. phases 2-12, will be used for this damage computation. Again, the damage will be computed for the whole range of c.o.g. positions, all with fixed modal conditions that are guaranteed by a control law. The conditions are the same as in the analysis beforehand with additional variations of altitude, Mach number, turbulence intensities and wavelengths. Table 4.6 notes the parameter settings for each flight phase that is analyzed. If the flight phase comprises more than one altitude or speed, the arithmetic mean value is chosen as for simplicity. Also, the time fraction derived from the probabilities multiplied with the phase duration are displayed.

Figure 4.13 displays in a stair diagram the absolute damage of each considered flight phase for a fwd c.o.g. position and an aft one for two different imposed damping ratios. The damage is displayed logarithmically. We notice that the damage for aft c.o.g. is significantly larger than for fwd ones. As shown beforehand, the higher damping causes less damage to the actuator. We also notice that most of the damage appears during take-off and approach phases. Even if the time during cruise flight is much longer, the effect

| Phase | $Mach$ | $h, [ft]$ | $\sigma_{norm}, [m/s]$ | $L_x$ | $L_z$ | $t_{P_1}, [s]$ | $t_{P_2}, [s]$ | $t_{P_3}, [s]$ |
|-------|--------|-----------|------------------------|-------|-------|----------------|----------------|----------------|
| 2     | 0.23   | 750       | 1.97                   | 1317  | 750   | 58.8           | 27.5           | 9.7            |
| 3     | 0.36   | 5750      | 1.71                   | 1750  | 1750  | 120.0          | 28.7           | 13.3           |
| 4     | 0.44   | 10000     | 1.55                   | 1750  | 1750  | 39.9           | 1.4            | 0.7            |
| 5     | 0.82   | 22500     | 1.49                   | 1750  | 1750  | 800.5          | 10.6           | 4.9            |
| 6     | 0.83   | 35000     | 1.42                   | 1750  | 1750  | 2322.3         | 9.3            | 2.3            |
| 7     | 0.83   | 37000     | 1.40                   | 1750  | 1750  | 275.2          | 0.6            | 0.3            |
| 8     | 0.83   | 39000     | 1.40                   | 1750  | 1750  | 16474.0        | 33.0           | 16.5           |
| 9     | 0.83   | 26500     | 1.47                   | 1750  | 1750  | 728.4          | 6.6            | 3.0            |
| 10    | 0.44   | 10000     | 1.55                   | 1750  | 1750  | 57.0           | 2.0            | 1.0            |
| 11    | 0.39   | 5750      | 1.71                   | 1750  | 1750  | 289.0          | 69.0           | 32.0           |
| 12    | 0.30   | 1100      | 1.97                   | 1496  | 1100  | 151.4          | 68.6           | 24.3           |

Table 4.6: A dimensioning mission profile (simplified).

of flying at low speed and higher turbulence outruns the accumulated damage during the long duration of cruise flight.

Figure 4.14 shows the contribution of the flight phases in percentages of the overall damage. It is interesting to see, that depending on the c.o.g. the partial contribution of the flight phases changes. Thus, the c.o.g. determines the sensitivity of actuator activity to a specific flight phase. The main damage is caused by phases 2 and 12, thus shortly after take-off and just before landing. As said before, this is ascribed to low speed effects, thus less elevator efficiency and a much higher probability of encountering heavy turbulence.

Figure 4.15 sums up all flight phase damages to an overall damage per single mission, depending on the center of gravity. Furthermore, if assumed that the aircraft performs 650 trips per year [65], the life expectancy of the actuator until rupture is displayed as a function of  $X_g$ . If the only damage were to be ascribed to the occurrence of turbulence, the diagram would read as follows: for an actuator life expectancy of 100 years, the damping ratio of  $\xi = 0.7$  allows for a 2% larger c.o.g. range in aft direction.

**Remark:** It shall be noted that the used VELA1 model is a low speed model. As a consequence, the model ignores all Mach related effects from which errors might occur. For each flight phase, the equilibriums are calculated and the dynamics are linearized. The corresponding controller is synthesized according to Section 4.1. The fatigue damage is then computed as in Sections 4.2 to 4.4 with the parameters of Table 4.6.

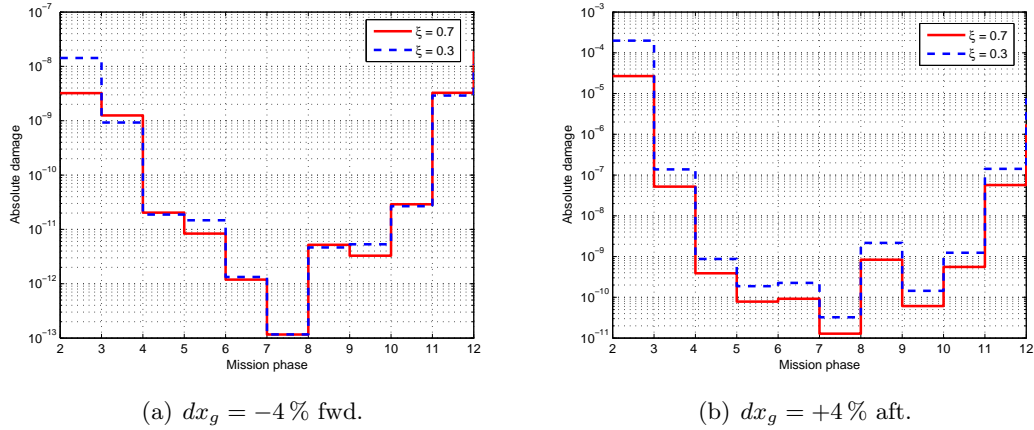


Figure 4.13: Absolute damage of each flight phase for two different c.o.g. positions.

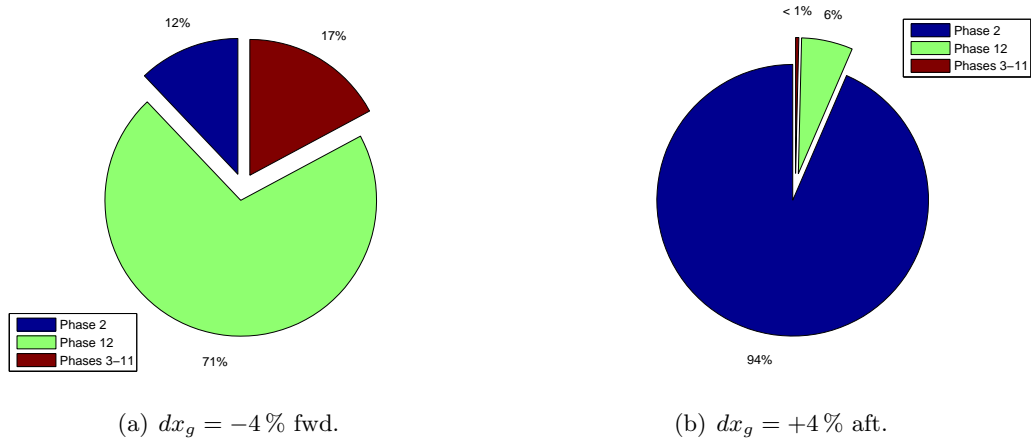


Figure 4.14: Damage contribution of flight phases for an imposed damping ratio  $\xi = 0.7$ .

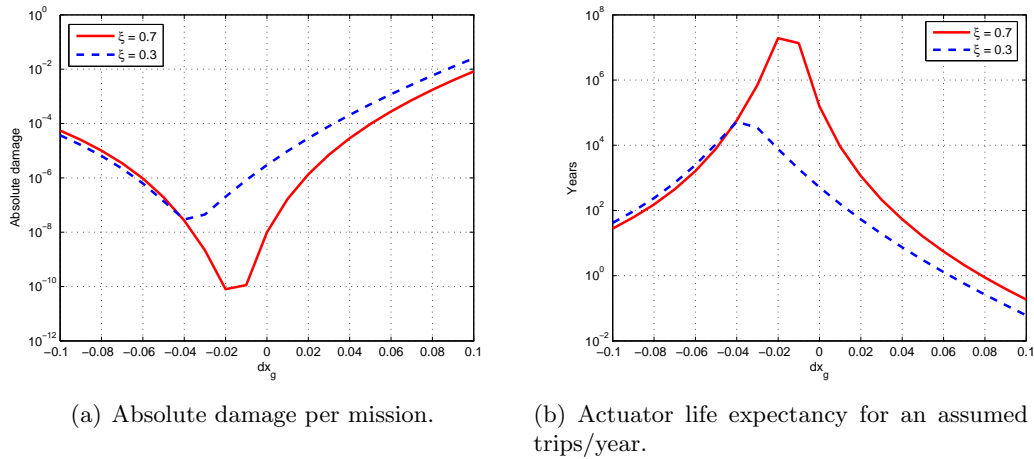


Figure 4.15: Damage inflicted upon the actuator per mission and resulting life expectancy.

### 4.5.3 Summary

Based on the analysis of a linearized longitudinal aircraft model in turbulent atmosphere, a set of tools has been developed allowing for the determination of actuator activity, fatigue, damage, and life expectancy, as well as their sensitivity to the degree of reduced stability. This approach can now be extended to including the lateral motion as well as maneuvers/pilot inputs. Thus, precise fatigue damage forecasts for a whole mission at an early development phase of the aircraft are now possible.



## Chapter 5

# Actuator Saturations and Longitudinal Stability

This fairly short chapter presents the integration of nonlinear actuator aspects into the context of reduced stability and develops a method to derive limits of controllability due to these nonlinearities. The closed-loop linear analysis in turbulent atmosphere allowed for the determination of actuator activity and fatigue of an aircraft with reduced stability whose flying qualities are guaranteed by a control law. By introducing saturation limits in position and rate, allowable ranges of center of gravity positions have been derived. The question that is posed in this section is: what happens if saturation is reached, and what impact do these nonlinear actuator characteristics have?

As an introduction to the topic, simulations are presented that show the influence of actuator saturations in rate and position. Of course, a simulation can only demonstrate the aircraft comportment during a limited time horizon for a specific flight attitude. Since the interest lies in the short term response, this approach is nonetheless justified and the simulations will give a good idea of the aircraft reaction. Finally, another approach addresses the actuator nonlinearities directly and a criterion for aft c.o.g. positions is derived. Concluding remarks to reduced longitudinal stability in general end this chapter.

### 5.1 Simulations with Saturated Actuators

As usual, the flight attitude parameters are set to very low speed and low altitude, since take-off and approach are the most critical flight phases. The selected speed is the safe take-off velocity  $V_{2,min} = 81.5 \text{ m/s}$ . The simulations are performed with Simulink, using the complete nonlinear aircraft model plus an actuator model which is specified below. The aircraft is stabilized with feedback  $\delta m = K_\alpha \alpha + K_q q$  guaranteeing a 30 % damping ratio and a  $0.8 \text{ rad/s}$  frequency. The time horizon is  $12 \text{ s}$  and turbulent wind is the only system entry.

### 5.1.1 Actuator Modeling

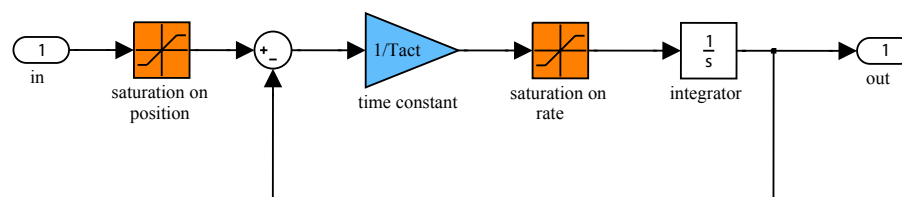


Figure 5.1: Actuator model with saturations on position and rate.

Figure 5.1 presents the model of the actuator. Instead of using a simple transfer function block with preceding saturations, a feedback representation is chosen where a saturation block before the integrator represents the saturation in actuator rate. This is done as to avoid the use of a rate limiter block which produces non negligible errors due to its initial condition zero setting. Furthermore, a saturation on position is modeled via a saturation block at the entry to the actuator model.

### 5.1.2 Simulations

Special attention has to be paid to the simulation integration time constant w.r.t. to the stochastic white noise generator. Naturally, the solver time step has to be significantly smaller than the noise sampling time: the former was set to  $8 \cdot 10^{-4}$ , the latter to  $1 \cdot 10^{-2}$  s.

The simulations show that for this aircraft saturation on elevator position is more critical than on rate. This stems from the fact that the BWB does not have a separate longitudinal trim plane. Therefore the longitudinal attitude has to be maintained with the elevator. Hence, all stabilizing commands coming from the controller are added to an initial trim deflection. Maximum elevator deflections are typically at  $\pm 30^\circ$ . By pushing back the c.o.g. step by step the position which causes divergence in  $\alpha$  or  $\theta$  of the saturated closed-loop system is found.

Figure 5.2(a) shows that the most aft c.o.g. displacement is  $dx_g = 8.5\%$ . The actuator already enters saturation in both position and rate, yet the aircraft does not diverge during 12 s. For 9% the relevant attitude angles diverge from 10 s onwards, see Figure 5.2(b). The elevator is constantly saturated which is equivalent to an open-loop system with a constant input.

How do these results relate to the predictions made by the closed-loop linear analysis approach? When comparing with Figures 4.9 and 4.10 in Section 4.4, the predictions are very close to simulation results when considering the  $1\sigma$  curves. There it was predicted that saturation is entered in position for a 7% aft c.o.g. displacement with a 30% imposed

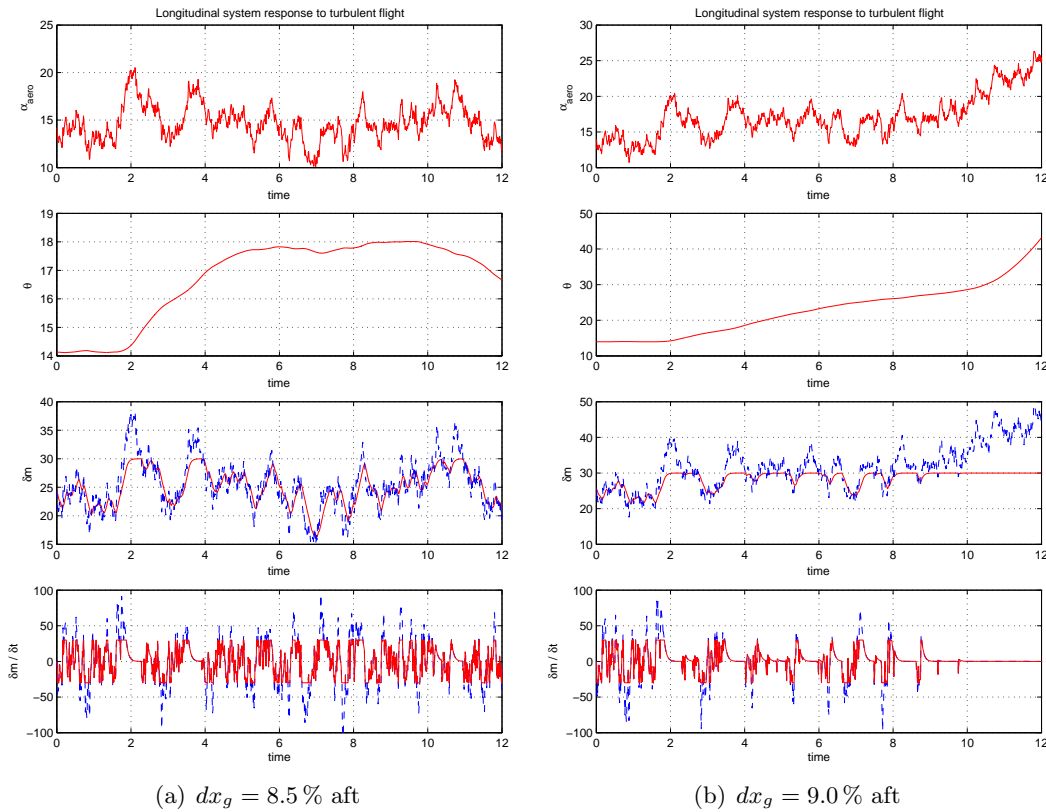


Figure 5.2: Simulation. Saturation on position at  $30^\circ$  and on rate at  $30^\circ/s$ . Commanded (dashed) and actual (continuous) elevator rate/position.

damping ratio which has been verified by simulations (not shown here). The simulations also show that there still rests a 1.5% margin until complete loss of controllability after saturation onset (Figure 5.2). Apparently, the  $3\sigma$  curves in the linear approach are conservative. Furthermore, the linear analysis does not allow for conclusions on the aircraft behavior when saturating.

It seems reasonable to introduce a safety margin which gives the pilot some authority. If a limit of  $\pm 24^\circ$  for the control system is set, the most aft c.o.g. displacement reduces to 7%. Figure 5.3 presents the corresponding simulations.

As regards rate saturation, both simulations reveal that the aircraft seems to be less sensitive. Even if the elevator saturates heavily in rate, the destabilization is always caused by saturation in position. Still, just from these simulations we cannot formulate a general statement concerning rate saturation. Therefore, the next section develops a general criterion for aft c.o.g. positions w.r.t. to nonlinear actuator specifications.

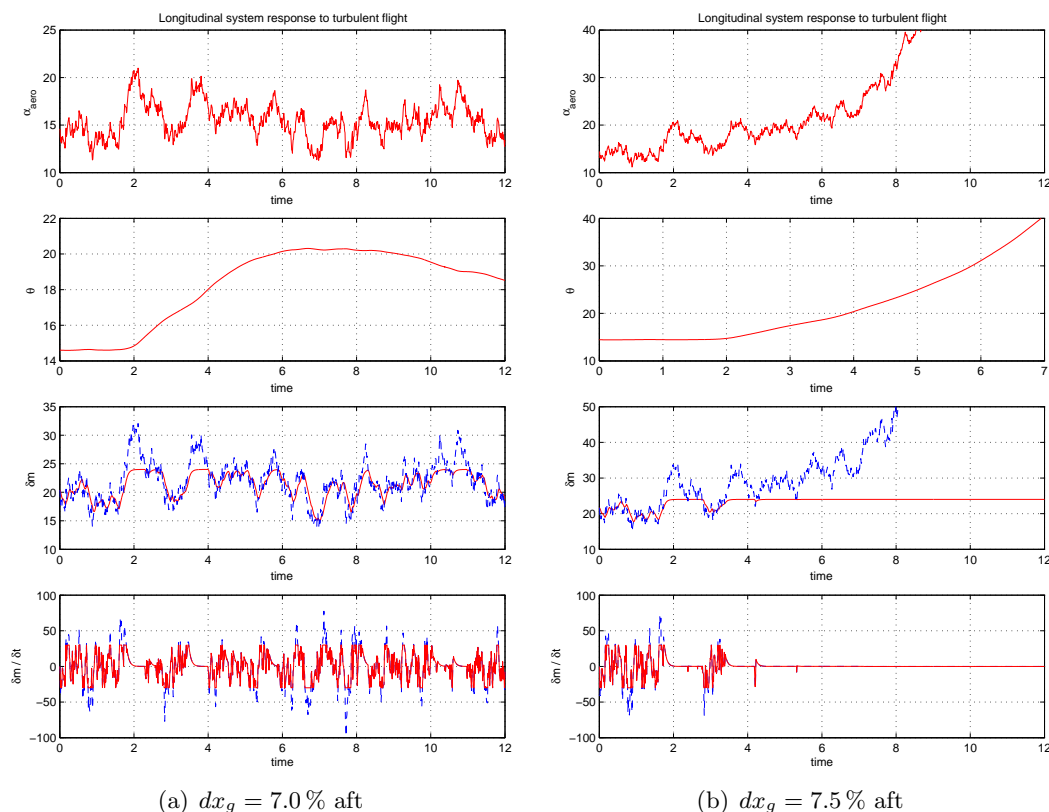


Figure 5.3: Simulation. Saturation on position at  $24^\circ$  and on rate at  $30^\circ/s$ . Commanded (dashed) and actual (continuous) elevator rate/position.

## 5.2 Aft C.O.G. Positions and Actuator Nonlinearities

The impact of saturation on the actuator position was easily illustrated via simulations. Saturation in position is to be avoided under all circumstances as it leads to divergence of the artificially stabilized VELA aircraft. This actuator characteristic limits thus the accessible range of center of gravity positions. The developed technique to estimate the expected actuator activity, as demonstrated in Section 4.2, is therefore a very useful tool because it computes the c.o.g. range which does not incorporate saturation when artificially stabilized. Therefore, the saturation on position case is clearly defined.

With regard to a rate saturation, simulations were less fruitful: even if the rate signal was completely saturated a destabilization has not taken place. Thus, the answer to the question whether the naturally unstable aircraft is sensitive to actuator rate saturation needs still to be found. Is it necessary, as for the position saturation case, to avoid all saturations in rate? To which degree can rate saturation be accepted?

These questions will be tackled with an analytical approach which is not limited to rate saturation, but includes all kinds of nonlinearities. Based on the Popov/circle criterion,

which stems from automatic control analysis and guarantees global stability in presence of nonlinearities, a criterion for aft c.o.g. positions will be derived in the context of an aircraft with reduced natural stability. The necessary theory is presented in the next section.

### 5.2.1 Stability in the Presence of Nonlinearities

At first, the notions  $L_2$  norm, space  $L_2$ , and  $L_2$  gain will be defined before presenting a criterion guaranteeing global stability in the presence of nonlinearities. These notions are widely used to assess the input/output stability of nonlinear systems.

**Definition 5.1**  *$L_2$  norm.* The  $L_2$  norm of a piecewise continuous function  $u : \mathbf{R}^+ \rightarrow \mathbf{R}^p$ , i.e.  $u$  is of the form

$$u(t) = \begin{bmatrix} u_1(t) \\ u_2(t) \\ \vdots \\ u_q(t) \end{bmatrix}$$

is defined as

$$\|u\|_{L_2} \stackrel{\text{def}}{=} \sqrt{\int_0^\infty [|u_1(t)|^2 + |u_2(t)|^2 + \dots + |u_q(t)|^2] dt} < \infty \quad (5.1)$$

**Definition 5.2** *Space  $L_2$ .* The space  $L_2$  consists of all piecewise continuous functions  $u : \mathbf{R}^+ \rightarrow \mathbf{R}^p$  satisfying the  $L_2$  norm.

Thus, the space  $L_2$  consists of all functions of  $t$  that are square integrable or, in other words, functions of finite energy. Finally, the notion of the  $L_2$  gain  $\gamma$  of a linear time-invariant (LTI) system  $H$  is introduced.

**Definition 5.3**  *$L_2$  gain.* The  $L_2$  gain of an LTI transfer matrix  $H$  is given by

$$\gamma(H) = \sup_x \frac{\|Hx\|_{L_2}}{\|x\|_{L_2}} \quad (5.2)$$

where

$$\|x\|_{L_2} = \left[ \int_0^\infty |x(t)|^2 dt \right]^{1/2} \quad (5.3)$$

**Remark.** The  $L_2$  gain is also called *induced  $L_2$  norm*. A remarkably readable reference on this subject is [62].

Being now familiar with the space  $L_2$  and the  $L_2$  gain a criterion making use of these notions and guarantees input/output stability is presented here. In this part of the dissertation, the criterion will be used from a flight dynamics engineer point of view. If the

reader is interested in a more general approach, notably from an automatic control theory point of view, further developments w.r.t. stability in combination with nonlinearities can be found in Chapter 9.

**Theorem 5.1 Popov Criterion.** *Consider the interconnection of a memoryless time invariant nonlinearity  $\phi(\cdot)$  with a SISO (single-input single-output) LTI (linear time invariant) system  $g(s)$ , also known as the Lur'e system, shown in Figure 5.4. Assume that the nonlinearity belongs to the sector<sup>1</sup>  $[0, k]$ , i.e.  $\phi(0) = 0$  and*

$$0 \leq \sigma\phi(\sigma) \leq k\sigma^2 \quad \forall \sigma.$$

*Assume furthermore that the transfer function  $g(s)$  is strictly proper<sup>2</sup>. Then, the system is  $L_2$  finite gain stable from  $u_1, u_2$  to  $y$  if there exist  $q \in \mathbf{R}$ , such that*

$$\inf_{\omega \in \mathbf{R}} \operatorname{Re}[(1 + j\omega q)g(j\omega)] + \frac{1}{k} > 0. \quad (5.4)$$

**Remarks:**

(i) There is a very practical graphical interpretation of the above theorem, in the case that  $g(s)$  and  $sg(s)$  are proper rational functions, see Figure 5.5.

(ii) If  $q$  in (5.4) is zero the criterion reduces to the more conservative circle criterion. In that instance the straight line through  $-1/k$  is the vertical tangent to  $g(j\omega)$  for all  $\omega$ . The circle criterion then reads:

$$\inf_{\omega \in \mathbf{R}} \operatorname{Re}[g(j\omega)] > -\frac{1}{k}. \quad (5.5)$$

(iii) The value  $-\frac{1}{k}$  obtained by the criterion is a measure of the so called *positivity* of a linear system. In general, the larger the positivity of the system the larger is a sector  $[0, k]$  for which stability is guaranteed. In that case, the circle criterion can produce more conservative positivity values than the Popov criterion (see Figure 5.5). For further reading on positivity and stability refer to Chapter 9.

In other words, the Popov (or circle) criterion relates the positivity characteristics of a linear system with an allowable nonlinearity sector, i.e. if the nonlinearity belongs to the sector defined by the positivity of the system, the system is globally stable. The issue is therefore to describe the relation between c.o.g. position, positivity and sector, and actuator rate saturation.

---

<sup>1</sup>All output signals of the nonlinearity stay within a sector defined by the x-axis and a straight line with slope  $k$  through zero.

<sup>2</sup>A strictly proper transfer function is a transfer function where the degree of the numerator is less than the degree of the denominator. This transfer function is asymptotically stable.

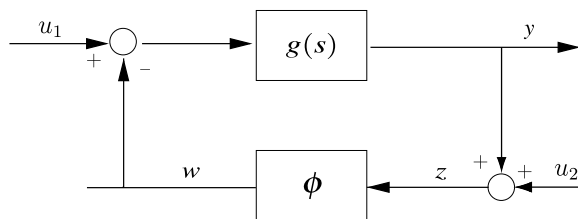


Figure 5.4: The Lur'e feedback interconnection problem.

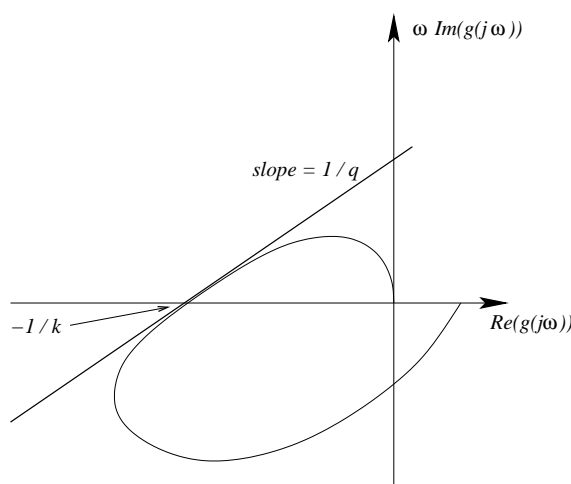


Figure 5.5: A graphical interpretation of the Popov criterion.

### 5.2.2 Application to the Aircraft

The transfer function that has to be analyzed according to Theorem 5.1 is the transfer function that is ‘seen’ by the nonlinearity  $\phi$ . Hence, the nonlinearity is to be cut out and its output and input become the input and output of  $g(s)$ , respectively. But due to the requirement of an asymptotically stable transfer function  $g(s)$  in Theorem 5.1, and since the open-loop aircraft model can be unstable, the saturation on the actuator rate output must be transformed into a dead zone nonlinearity, as indicated in Figures 5.6 and 5.7. By this means, stable closed loop behavior is guaranteed for  $g(s)$  which incorporates the closed-loop aircraft model stabilized by a control system. External inputs (such as wind and pilot inputs) are not shown in Figure 5.7. This will not affect the analysis results.

In the next steps, the simplified positivity constraint of Eq. (5.5) for the transfer function  $T_{w \rightarrow z}$  will be used. The nonlinearity is placed between  $w$  and  $z$  in Figure 5.7. It

is then possible to derive a direct relation between  $X_g$  and sector variable  $k$ .

$$\inf_{\omega \in \mathbb{R}} \operatorname{Re}[T_{w \rightarrow z}(j\omega)] > -\frac{1}{k} \tag{5.6}$$

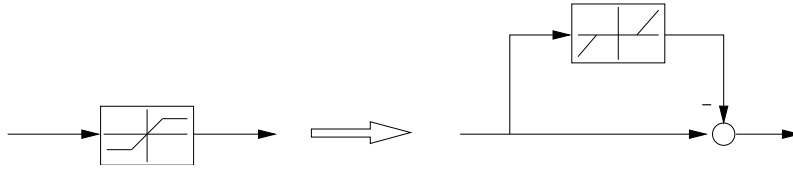


Figure 5.6: Transformation of saturation into dead-zone nonlinearity.

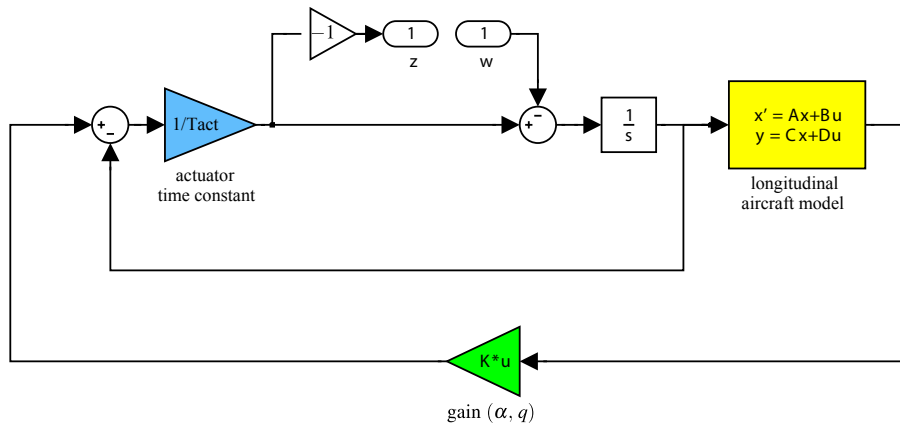


Figure 5.7: Transformation into Lur'e problem: linear parts SPO + actuator + controller seen by nonlinearity. The  $-1$  gain is introduced according to the Lur'e scheme, Figure 5.4.

### 5.2.3 A Criterion for Aft C.o.G. Positions

The circle criterion will deliver a sector  $[0; k]$ . If the nonlinearity that is placed between input and output of  $T_{w \rightarrow z}$  is fulfilling these sector conditions, global stability is obtained. However, the dead-zone nonlinearity belongs to sector  $[0; 1]$ . Physically, we can already state that this sector cannot be obtained: since saturation always results into an open-loop system (with maybe a constant input) we cannot expect global stability as a result as the natural aircraft is unstable. Thus, a smaller sector with  $k < 1$  will be obtained. But, depending on the saturation properties and the c.o.g. position, maybe a statement on the size of a *region of stability* can be made.

Applying the circle criterion, Eq. (5.6), leads to tracing the complex gain of the system in Figure 5.7 as a function of the frequency  $\omega$  and the center of gravity. Figure 5.8(a)

displays the Nyquist curves for the linear system seen by the nonlinearity for  $dx_g \in [-10\%, 10\%]$ .

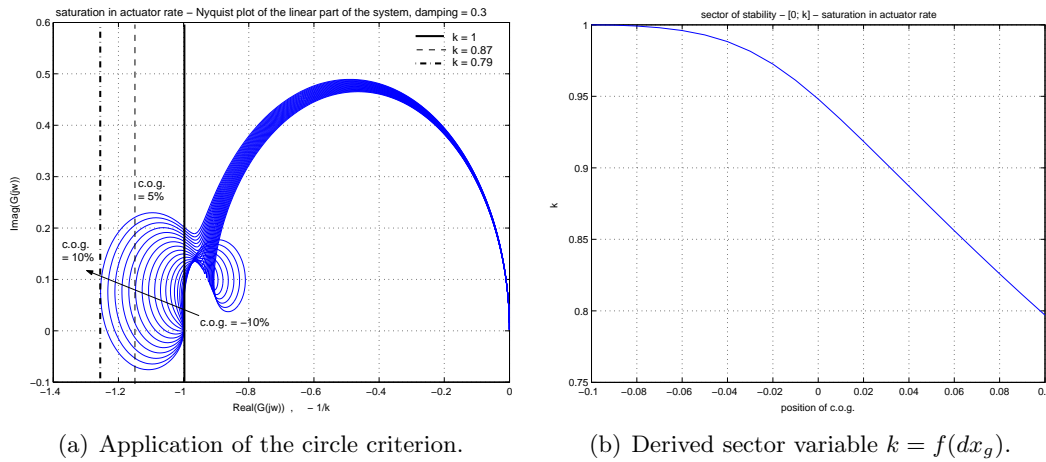


Figure 5.8: Circle criterion and sector variable  $k$  as a function of the c.o.g. position.

The diagram shows that a global stability cannot be guaranteed by any c.o.g. position ( $k < 1$ ): the Nyquist curves cross the  $-1/k$  limit, with  $k = 1$ , for all positions.

**Remark:** As the reader notices, global stability is also not guaranteed for c.o.g. positions that are naturally stable (even though the resulting  $k$  is very close to 1). The circle criterion is known to be conservative.

The following points are of interest:

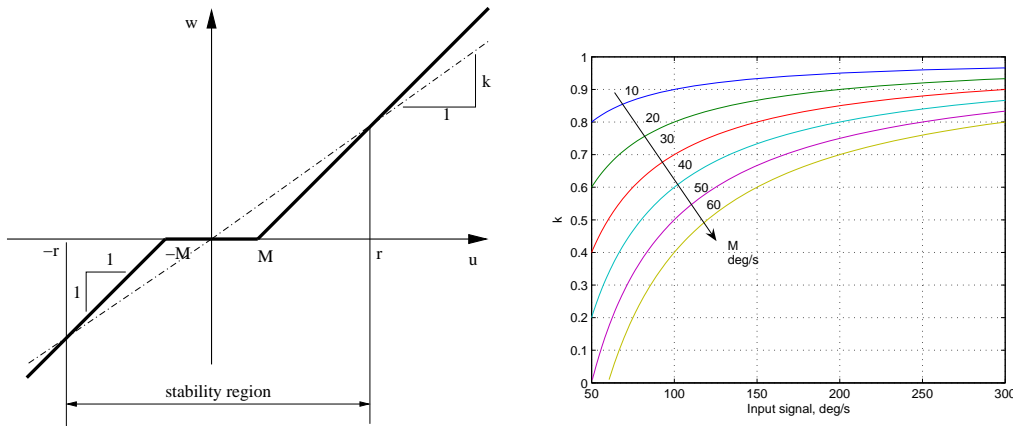
- The application of the circle criterion leads to a reduced sector  $[0; k]$  with  $k < 1$  (Figure 5.8(b)). As a consequence the input signal  $z$  of the nonlinearity has to be limited to the interval  $[-r; r]$  in order to maintain stability, see Figure 5.9(a). This interval shall be named stability region or stability domain.
- The stability region is defined by two parameters: the width of the dead-zone nonlinearity  $[-M; M]$  and the sector  $[0; k]$ . The latter is a function of the transfer matrix which represents the aircraft dynamics and thus depends directly on the c.o.g. position and the stabilizing control law.
- This relation leads to formulating a criterion. From Figures 5.8(b) and 5.9(a) we gain:

$$kr = -M + r \quad (5.7)$$

$$r = \frac{M}{1 - k} \quad (5.8)$$

which condenses into Figure 5.9(b) comprising a variation of parameter  $M$ .

These points allow for describing the relation of available elevator actuator rate and corresponding center of gravity range, and thus determine the controllability of the aircraft as a function of reduced stability and actuator properties.



(a) Dead-zone nonlinearity scheme with sector and stability region. (b) Relation of stability region, sector, and actuator rate saturation.

Figure 5.9: From sector to stability region.

**Lemma 5.1 Controllability Criterion in the Presence of Actuator Rate Saturation.** *If  $r$  is the maximum absolute value of all expected signal amplitudes entering the dead-zone nonlinearity, where its dead-zone is defined by  $M$  (Figure 5.9(a)), then a sector variable  $k$  is given by the relation Eq. (5.9):*

$$-\frac{1}{k} = -\frac{r}{r - M} \quad (5.9)$$

Furthermore, a system is  $L_2$  bounded-input/bounded-output stable if the Nyquist curve of its linear part in Lur'e representation (Figure 5.4) remains completely to the right hand side of the real value  $-1/k$ .

For a better comprehension, an example of an application of this criterion is presented:

- On the basis of the linear analysis of Chapter 4 (Figure 4.10) we know that high values in actuator rate have to be expected for aft c.o.g. positions. For a 10% aft position, the  $3\sigma$  curve can be extrapolated to an expected  $150^\circ/s$  command signal for the actuator during turbulent flight. When multiplying with a security factor of 2 a safe size of a stability region would be  $r = 300^\circ/s$ .
- Figure 5.9(b) gives the sector  $k$  as a function of this target stability region and of the choice of actuator.
- If one decides for an actuator capable of treating signals with a rate of  $30^\circ/s$ , a corresponding  $k$  of  $k = 0.9$  is found. With the help of Figure 5.8(b) the maximum

aft position for the c.o.g. is 3% aft. But if one decides for an actuator treating up to  $60^\circ/s$  the allowable range of c.o.g. positions is expanded up to 9.5% aft ( $k = 0.8$ ).

Thus, we present here a direct relation between actuator properties, reduced stability and load flexibility of the aircraft. The controllability criterion is summarized in Figure 5.10, where the relation is presented in one diagram which shows its comfortable application.

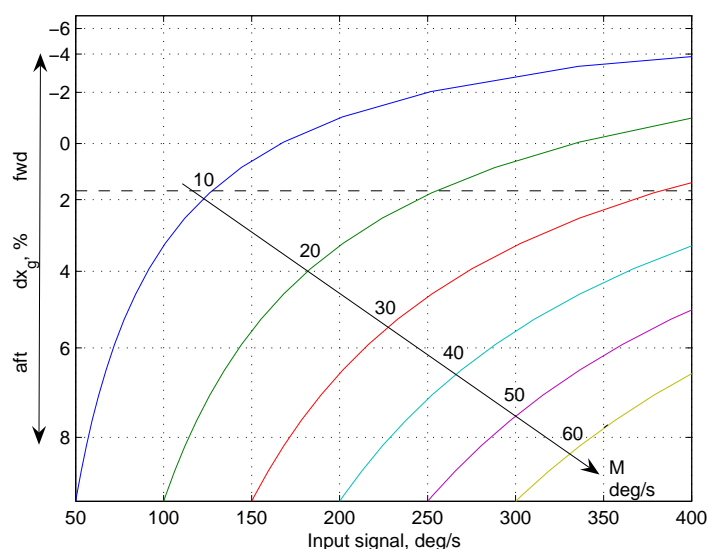


Figure 5.10: Stability region for the dead-zone nonlinearity and maximum aft center of gravity displacement  $dx_g$ . The horizontal dashed line indicates the c.o.g. position at the limit of natural stability (maneuver point).

**Remark:** For mathematical correctness one has to prove that the stability region lies inside a domain of attraction. The theory, application, and calculation of such domains of attraction is addressed in the 2nd part of this dissertation, Chapter 9. Furthermore, Chapter 10 demonstrates the relation between the size of such a domain of attraction and the value of the actuator rate limit.

### 5.3 Conclusion on Reduced Longitudinal Stability

As an introduction to the subject, the analytical approach of Chapter 3 revealed the main impact of a reduced longitudinal stability. The relation of c.o.g. position and modal properties, feedback gains, and robustness has been developed. This resulted in a set of analytical expressions allowing rapidly for a forecast on c.o.g., feedback, and actuator requirements.

Furthermore, a linear analysis approach in Chapter 4 assessed the influence of handling qualities and actuator properties within the context of reduced stability. In particular, the flight of the closed-loop aircraft with imposed handling qualities for the short-period oscillation in turbulent atmosphere has been analyzed. With the developed tools, limits for the center of gravity position have been derived from deflection and rate fluctuations as well as the fatigue and damage inflicted upon the actuator. As soon as stochastic models for pilot commands etc. exist as well as sufficiently precise linear models for all flight phases, a rapid and complete actuator fatigue damage estimation in relation with reduced stability is possible with the developed method.

Finally, a main nonlinear actuator aspect, the saturation, has been integrated into the context of reduced stability and limits of controllability in Chapter 5. A criterion has been developed combining linear analysis results and nonlinear stability theory. This condenses into a comfortable method to determine the trade-off between actuator saturation and degree of reduced stability in terms of the c.o.g. position. The method is expandable to other nonlinear characteristics. Reducing its conservatism is an option for further research.

## Chapter 6

# Reduced Lateral Stability and $V_{MC}$ Equilibrium

Minimizing stabilizing surfaces of an airplane, and therewith accepting lower natural stability, represents one way to reduce mass and drag and, thus, fuel consumption and environmental impact. An analysis of certifying sizing criteria during early phases of aircraft design is therefore an important goal as it enables an estimation of the influence of these criteria onto design parameters and vice versa.

In view of the above potentials, the goal is to assess the impact of a surface reduction of the vertical tailplane onto criteria associated with the *minimum control velocity*  $V_{MC}$ . The  $V_{MC}$  is the calibrated airspeed at which, when the critical engine is suddenly made inoperative, it is still possible to maintain minimum control of the airplane and straight equilibrated flight with a bank angle of not more than  $5^\circ$ , [96, 30].

The criteria related to the  $V_{MC}$ , as described in Chapter 2 and Appendix B, are playing a major role in aircraft certification. Since the  $V_{MC}$  is a measure of the capability of an aircraft to counter a yaw momentum, they are predominantly used for a first determination of the fin surface area.

Whereas Chapter 7 deals with dynamic criteria, this chapter focuses on equilibrated flight at  $V_{MC}$ . Due to a size reduction of the tailplane the capability of the aircraft to counter the engine induced moment is modified. The question is, to what extent can the influence of the fin size be assessed at an early design phase of an aircraft ? Which impact do other parameters, e.g. c.o.g. position and mass have?

Section 6.1 develops analytical formulas describing equilibrated flight with one engine inoperative. The analytical expressions are of different complexity and incorporate different physical effects. These expressions are used to conduct a parametric study identifying the main factors determining  $V_{MC}$  in Section 6.2.

Section 6.3 presents a tool as an aid to analysis and interpretation of the equilibrium with one engine inoperative. The equilibrium points of the aircraft are visually presented

within their context of physical limitations and certification constraints. The low speed flight domain is deduced and recommendations for the aircraft design can be given.

## 6.1 An Analytical Approach Toward $V_{MC}$ -Computation

This section is dedicated to the development of analytical expressions for the minimal control speed  $V_{MC}$ . Starting from the general rigid body equations, an analytical expression is derived and, step after step, simplified. These expressions allow for a better, physical comprehension of the problem and present a fruitful starting point for parametric studies.

### 6.1.1 Equilibrium Equations

$V_{MC}$  has to be shown with the critical (outboard) engine non-operational. The thrust of the still operating opposite engine produces a moment around the aircraft  $z$ -axis (moments around lateral and longitudinal axis are neglected for the time being). This moment has to be compensated (see Figures 6.1(a) and 6.1(b)). When the aircraft begins to slip, the fuselage and the vertical fin of a typical airplane produce a partially compensating moment. In order to equilibrate the aircraft, the rudder is deflected as well. Occurring roll moments are zeroed by deflecting the ailerons. Any induced lateral forces are countered by banking the aircraft, i.e. using its weight. At the same time, the FAR/JAR bank angle limit of  $5^\circ$  has to be respected. The  $V_{MC}$  and its related criteria are relevant in low speed flight phases (take-off and landing) as the efficiency of aerodynamic surfaces is low.

The lateral flight mechanics equations are reconsidered in the body frame. For equilibrated flight the equations read (compare with Section 2.2):

$$C\dot{r} - (A - B)qp - E(\dot{p} + rq) = \sum N = 0 \quad (6.1)$$

$$mV(\dot{\beta} + r \cos \alpha - p \sin \alpha) = \sum Y = 0 \quad (6.2)$$

$$A\dot{p} - (B - C)qr - E(\dot{r} + pq) = \sum L = 0 \quad (6.3)$$

$N$  represents the yaw moments,  $L$  the roll moments and  $Y$  the side forces exerted on the aircraft.  $N_{eng}$ ,  $Y_{eng}$  and  $L_{eng}$  are the moments and forces associated to the engine thrust. It is now assumed that the uncompensated engine only produces a yaw moment  $N_{eng}$  and that the side force and roll moment caused by this engine can be neglected ( $Y_{eng} = L_{eng} = 0$ ). Furthermore, the equations are linearized for small variations and for equilibrated steady flight (all derivatives zero as well as  $p = q = r = 0$ ). When normalizing the momentum equations by  $\frac{1}{2}\rho SIV^2$  and the force equation by  $\frac{1}{2}\rho SV^2$ , the equations read in coefficient notation:

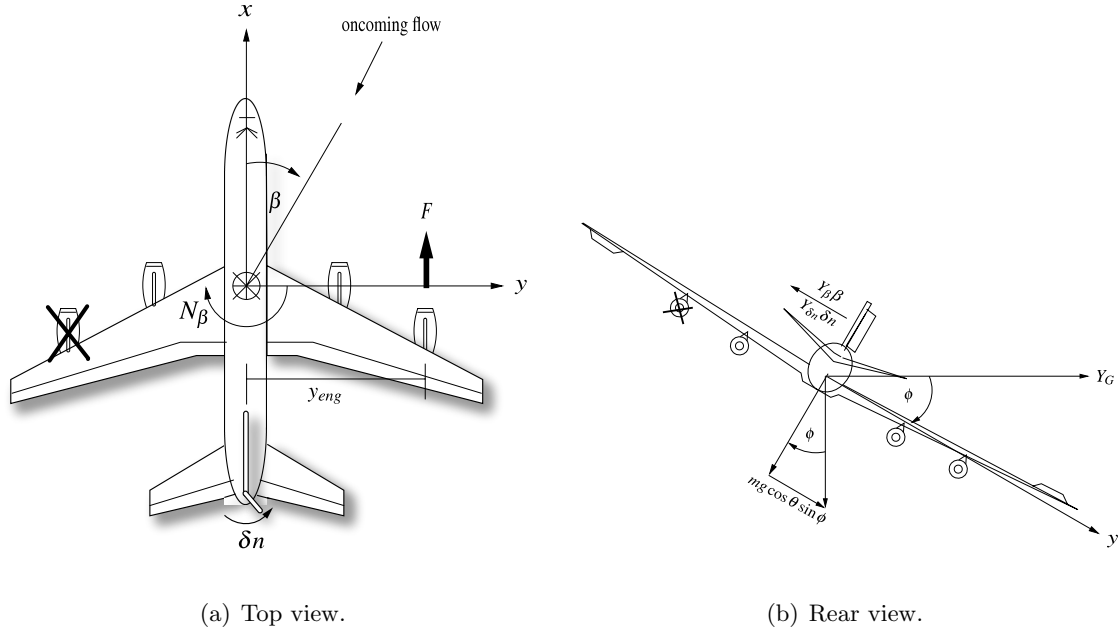


Figure 6.1: Aircraft equilibrium with left outboard engine inoperative.

$$0 = Cn_{\beta}\beta + Cn_{\delta n}\delta n + Cn_{\delta l}\delta l + Cn_F \quad (6.4)$$

$$0 = C_{Y\beta}\beta + C_{Y\delta n}\delta n + \frac{2m g}{\rho S V^2} \cdot \cos \theta \sin \phi \quad (6.5)$$

$$0 = Cl_{\beta}\beta + Cl_{\delta l}\delta l + Cl_{\delta n}\delta n \quad (6.6)$$

In favor of facilitated writing, here the pseudo-coefficient  $Cn_F = \frac{2y_{eng}F}{\rho S V^2}$  has been introduced which represents the induced moment due to engine failure.

In order to take into account the secondary effects of aerodynamic control surface deflections more precisely, corrective terms are introduced. These corrective terms  $\varepsilon$  affect the following coefficients (compare with [72]):

$$\tilde{C}n_{\beta} = Cn_{\beta}(1 - \varepsilon Cn_{\beta}) \quad (6.7)$$

$$\tilde{C}n_{\delta n} = Cn_{\delta n}(1 - \varepsilon_{\delta l}\delta n) \quad (6.8)$$

$$\tilde{C}Y_{\beta} = C_{Y\beta}(1 - \varepsilon C_{Y\beta}) \quad (6.9)$$

where

$$\varepsilon_{\delta l \delta n} = \frac{C_{n_{\delta l}} C_{l_{\delta n}}}{C_{l_{\delta l}} C_{n_{\delta n}}} \quad (6.10)$$

$$\varepsilon_{C_{n_{\beta}}} = \frac{C_{l_{\beta}} C_{n_{\delta l}}}{C_{n_{\beta}} C_{l_{\delta l}}} \quad (6.11)$$

$$\varepsilon_{C_{Y\beta}} = \frac{C_{Y_{\delta n}} C_{n_{\beta}}}{C_{Y_{\beta}} C_{n_{\delta n}}} \frac{1 - \varepsilon_{C_{n_{\beta}}}}{1 - \varepsilon_{\delta l \delta n}} \quad (6.12)$$

### 6.1.2 Resolution

When solving Eq. (6.6) for  $\delta l$  and placing it into Eq. (6.4) a first expression for the rudder deflection is obtained as a function of side-slip and, implicitly, engine moment and speed:

$$\delta n = -\frac{1}{1 - \varepsilon_{\delta l \delta n}} \cdot \left[ (1 - \varepsilon_{C_{n_{\beta}}}) \frac{C_{n_{\beta}}}{C_{n_{\delta n}}} \beta + \frac{C_{n_F}}{C_{n_{\delta n}}} \right] \quad (6.13)$$

Inserting this expression into Eq. (6.5) yields:

$$\sin \phi = -\frac{\rho S V^2}{2mg \cos \theta} \left[ C_{Y_{\beta}} (1 - \varepsilon_{C_{Y\beta}}) \beta - \frac{C_{Y_{\delta n}}}{1 - \varepsilon_{\delta l \delta n}} \cdot \frac{C_{n_F}}{C_{n_{\delta n}}} \right] \quad (6.14)$$

or

$$\beta = \frac{1}{C_{Y_{\beta}} (1 - \varepsilon_{C_{Y\beta}})} \left( \frac{C_{Y_{\delta n}}}{1 - \varepsilon_{\delta l \delta n}} \cdot \frac{C_{n_F}}{C_{n_{\delta n}}} - \frac{2mg \cos \theta \sin \phi}{\rho S V^2} \right) \quad (6.15)$$

Eq. (6.15) has a special interest as it determines the side-slip angle  $\beta$  directly, when speed and engine moment are known, since  $\phi$  is limited to  $|5^\circ|$ . Eqs. (6.13) to (6.15) can come in useful for undertaking parametric studies for varying speed, angles, and side-slip with regard to equilibrated flight with asymmetric thrust in general.

In order to derive one generic analytic expression for the minimum control speed  $V_{MC}$  itself, the solution for  $\beta$  is put into Eq. (6.13). An expression for the engine moment pseudo-coefficient  $C_{n_F}$  is obtained:

$$C_{n_F} = - \left[ 1 - \frac{2mg}{\rho S V^2} \frac{\tilde{\varepsilon}_D \cos \theta \sin \theta}{C_{Y_{\delta n}} \delta n} \right] \frac{(1 - \varepsilon_{\delta l \delta n})}{1 + \tilde{\varepsilon}_D} C_{n_{\delta n}} \delta n \quad (6.16)$$

with

$$\tilde{\varepsilon}_D = \frac{C_{Y_{\delta n}} C_{n_{\beta}}}{C_{n_{\delta n}} C_{Y_{\beta}}} \cdot \frac{1 - \varepsilon_{C_{n_{\beta}}}}{(1 - \varepsilon_{C_{Y\beta}})(1 - \varepsilon_{\delta l \delta n})}$$

All there remains to do now is to express  $C_{n_F}$  as a function of the thrust and its lever

arm:

$$Cn_F = -\frac{y_{eng}F}{\frac{1}{2}\rho SV^2} \quad (6.17)$$

where  $F$  is the thrust of the uncompensated engine and  $y_{eng}$  its lever arm around the aircraft  $z$ -axis. Solving the equality of Eqs. (6.16) and (6.17) for  $V$  gives a first analytic solution for  $V_{MC}$ . In this case, it is assumed that the thrust  $F$  is known.

**Remark.** For the sake of completeness, we consider the fact that the engine thrust can be modeled as [6]:

$$F = F_0 \left( \frac{\rho}{\rho_0} \right) \left( 1 - Ma + \frac{Ma^2}{2} \right) \quad (6.18)$$

where  $\rho$  is the density of the surrounding air and  $\rho_0$  the density at zero altitude.  $F_0$  equals the engine thrust on ground at zero speed and  $Ma = V/a$  is the Mach number ( $a$  being the speed of sound). Putting the thrust expression into Eq. (6.17) yields a quadratic equation when solving for  $V$ :

$$\boxed{AV^2 + BV + C = 0} \quad (6.19)$$

$$\text{with } \begin{cases} A = -y_{eng} \frac{F_0}{2a^2} \left( \frac{\rho}{\rho_0} \right) \frac{1+\tilde{\varepsilon}_D}{1-\varepsilon_{\delta l \delta n}} + \frac{1}{2}\rho Sl Cn_{\delta n} \delta n \\ B = y_{eng} \frac{F_0}{a} \left( \frac{\rho}{\rho_0} \right) \frac{1+\tilde{\varepsilon}_D}{1-\varepsilon_{\delta l \delta n}} \\ C = -y_{eng} F_0 \left( \frac{\rho}{\rho_0} \right) \frac{1+\tilde{\varepsilon}_D}{1-\varepsilon_{\delta l \delta n}} - mgl\tilde{\varepsilon}_D \cos \theta \sin \phi \frac{Cn_{\delta n}}{C_{Y\delta n}} \end{cases} \quad (6.20)$$

### 6.1.3 $V_{MC}$ Expressions

The first assumption shall be that the thrust remains constant and can be estimated to be close to  $F_0$ . Some arguments in favor of this assumption are: flight phases take-off/landing will be analyzed with the aircraft being close to the ground. Therefore  $\rho \approx \rho_0$ . With  $V$  small compared to the speed of sound  $a$ , Mach related effects can be neglected. The quadratic expression of Eq. (6.19) then reads (with  $F = F_0$ ):

$$\frac{1}{2}\rho Sl Cn_{\delta n} \delta n \cdot V^2 - y_{eng} F_0 \frac{1+\tilde{\varepsilon}_D}{1-\varepsilon_{\delta l \delta n}} - mgl\tilde{\varepsilon}_D \cos \theta \sin \phi \frac{Cn_{\delta n}}{C_{Y\delta n}} = 0 \quad (6.21)$$

A first  $V_{MC}$  expression is obtained:

$$V_{MC_{s1}} = \sqrt{\frac{2y_{eng}F}{\rho S l C n_{\delta n} \delta n} \cdot \frac{1 + \tilde{\varepsilon}_D}{1 - \varepsilon_{\delta l \delta n}} + \frac{2mg\tilde{\varepsilon}_D \cos \theta \sin \phi}{\rho S C_{Y\delta n} \delta n}} \quad (6.22)$$

A second simplification shall be obtained by neglecting all corrective terms, i.e.:

$$\varepsilon_{\delta l \delta n} = \varepsilon_{C n_{\beta}} = \varepsilon_{C_{Y\beta}} \approx 0$$

and thus  $\tilde{\varepsilon}_D$  is simplified to

$$\varepsilon_D = \frac{C_{Y\delta n} C n_{\beta}}{C n_{\delta n} C_{Y\beta}}$$

which yields

$$V_{MC_{s2}} = \sqrt{\frac{2y_{eng}F}{\rho S l C n_{\delta n} \delta n} \cdot (1 + \varepsilon_D) + \frac{2mg\varepsilon_D \cos \theta \sin \phi}{\rho S C_{Y\delta n} \delta n}} \quad (6.23)$$

Finally, a third simplification can be obtained when it is assumed that the engine momentum is only countered by the deflection of the rudder, i.e. neglecting all other interactions, hence  $\varepsilon_D \approx 0$ . This assumption leads to a well known formula which is often employed for a first estimation of the  $V_{MC}$  for standard airplanes with a long cigar-like fuselage and a large vertical tail-plane. Why this formula is only applicable to these types of airplanes will be explained later in this chapter.

$$V_{MC_{s3}} = \sqrt{\frac{2y_{eng}F}{\rho S l C n_{\delta n} \delta n}} \quad (6.24)$$

#### 6.1.4 Interpretation and Physical Factors

The reader notices that with simplifications less physical effects are taken into account. The next paragraphs explain the principal factors that characterize each of the three  $V_{MC}$  formulas. Some of the analytical expressions will be rewritten in a different form as to regroup physical effects. In that way, the equations are easily distinguishable by their influencing physical factors.

**Analysis of  $V_{MC_{s3}}$ .** The most simplified formula can also be obtained by neglecting all aileron and sideslip effects in Eq. (6.4)  $\delta l = \beta = 0$  and solving for  $V$ . When ignoring normalization variables  $\rho$ ,  $S$ ,  $l$ , the principal factors determining the speed are: the lever arm of the uncompensated engine,  $y_{eng}$ ; the thrust of the uncompensated engine,  $F$ ;

the coefficient describing the relation of rudder deflection and yaw momentum therewith produced,  $Cn_{\delta n}$  ( $< 0$ ); the deflection of the rudder,  $\delta n$  ( $< 0$  if  $y_{eng} > 0$  and vice versa).

$V_{MC_{s3}}$  is thus characterized by the balance between engine and rudder momentum.

**Analysis of  $V_{MC_{s2}}$ .** The formula for  $V_{MC_{s2}}$  can be expressed in terms of the most simplified formula for  $V_{MC_{s3}}$ :

$$(V_{MC_{s3}})^2 = \frac{2y_{eng}F}{\rho S l C n_{\delta n} \delta n} \equiv \kappa > 0 \quad (6.25)$$

With

$$v = \frac{2mg \cos \theta \sin \phi}{\rho S C_{Y\delta n} \delta n} \quad (6.26)$$

we can rewrite  $V_{MC_{s2}}$  as follows:

$$V_{MC_{s2}} = \sqrt{\kappa + \varepsilon_D \cdot (\kappa + v)} \quad (6.27)$$

This notation presents a regrouping of other influencing factors into the artificially introduced parameters  $\varepsilon_D$  and  $v$ . Having a closer look at  $\varepsilon_D$  the fraction reveals itself as the quotient of the distance between lateral aerodynamic neutral point and c.o.g. (which could be called a *lateral static stability margin*), and lever arm of the vertical fin. With Eq. (6.44) and the fact that

$$\frac{Cn_{\beta}}{C_{Y\beta}} = \frac{X_G - X_{N,lat}}{l} \underbrace{\leq 0}_{\text{usually}} \quad (6.28)$$

where  $X_{N,lat}$  is the lateral neutral point of the aircraft, we obtain:

$$\varepsilon_D = \frac{C_{Y\delta n}}{Cn_{\delta n}} \cdot \frac{Cn_{\beta}}{C_{Y\beta}} = \frac{X_G - X_{N,lat}}{X_G - X_{N,fin}} > 0 \quad (6.29)$$

For common airplanes  $\varepsilon_D$  is thus always positive since  $X_G < X_{N,lat} < X_{N,fin}$ . This pseudo-coefficient relates lateral stability margin and rudder lever arm. Its influence rises with a smaller lever arm and/or a larger lateral stability margin. As regards the latter, the geometry of the aircraft plays a major role in defining  $X_{N,lat}$ , especially for uncommon aircraft like the BWB. Notably the change of the fuselage type (long cigar-like vs. a very wide body) will have an effect on these parameters.

Remains factor  $v$ . The nominator features the aircraft mass and two angular functions depending on the aircraft equilibrium. The influence of the mass is therefore directly depending on the aircraft longitudinal and lateral trim.

Hence,  $V_{MC_{s2}}$  distinguishes itself from  $V_{MC_{s3}}$  through the consideration of mass, trim, and ratio of lateral neutral point position and rudder lever arm.

**Analysis of  $V_{MC_{s1}}$ .** The first of the presented  $V_{MC}$  formulas can be rewritten as

$$V_{MC_{s1}} = \sqrt{\tilde{\kappa} + \tilde{\varepsilon}_D \cdot (\tilde{\kappa} + v)} \quad (6.30)$$

with

$$\tilde{\kappa} = \frac{\kappa}{1 - \varepsilon_{\delta l \delta n}} = \kappa \cdot \gamma$$

and

$$\tilde{\varepsilon}_D = \varepsilon_D \cdot \frac{1 - \varepsilon_{C n_\beta}}{(1 - \varepsilon_{C_{Y\beta}})(1 - \varepsilon_{\delta l \delta n})} = \varepsilon_D \cdot \sigma \quad (6.31)$$

With factors  $\gamma$  and  $\sigma$  being the sole differences from  $V_{MC_{s2}}$ , *the most elaborate  $V_{MC}$  expression  $V_{MC_{s1}}$  takes into account all characteristics of the simplified expressions plus aileron and secondary effects.*

The characteristics of each of the analytical expressions are summarized in Table 6.1.

| $V_{MC_{s1}}$   | $V_{MC_{s2}}$   | $V_{MC_{s3}}$                                  |
|---|---|--|
| <i>engine moment</i><br><i>+ rudder moment</i><br><i>+ trim</i><br><i>+ mass</i><br><i>+ lateral neutral point/<br/> rudder lever arm</i><br><i>+ aileron effects</i><br><i>+ secondary effects</i> | <i>engine moment</i><br><i>+ rudder moment</i><br><i>+ trim</i><br><i>+ mass</i><br><i>+ lateral neutral point/<br/> rudder lever arm</i> | <i>engine moment</i><br><i>+ rudder moment</i> |

Table 6.1: Main factors determining the  $V_{MC}$  expressions and assumptions.

## 6.2 Exploitation of the Analytical Approach

This section presents a synthesis of a parametric study conducted with the developed  $V_{MC}$  expressions. For the sake of legibility of this document, details concerning the study are moved to Appendix C. The equations and parameters used for the parametric study are listed on the next page. As to take into account a possible c.o.g. displacement and variation of the fin size, the modeling of altered coefficients  $C_{Y\delta n}^*$  and  $C n_{\delta n}^*$  is displayed. The side force  $Y_{\delta n} \delta n$  is assumed to vary proportionally with the size of the fin, thus a proportionality factor  $S_D/S_{D,nom}$  is introduced,  $S_{D,nom}$  being the nominal size of the fin. The variation of the fin size and the c.o.g. position are also taken into account in coefficients  $C_{Y\beta}^*$  and  $C n_\beta^*$ . They are composed of a fuselage and a fin depending part, each of which can be modified separately. Furthermore, in order not to lose the link with the physical context, a recapitulation of the parameters and their physical meaning is listed as well.

**Equations and coefficient modeling for parametric study**

$$V_{MC_{s1}} = \sqrt{\tilde{\kappa} + \tilde{\varepsilon}_D \cdot (\tilde{\kappa} + v)} \quad (6.32)$$

$$V_{MC_{s2}} = \sqrt{\kappa + \varepsilon_D \cdot (\kappa + v)} \quad (6.33)$$

$$V_{MC_{s3}} = \sqrt{\kappa} \quad (6.34)$$

with

$$\kappa = \frac{2y_{eng}F}{\rho S l C n_{\delta n} \delta n} \quad (6.35)$$

$$\tilde{\kappa} = \kappa \cdot \gamma, \quad \text{where } \gamma = \frac{1}{1 - \varepsilon_{\delta l \delta n}} \quad (6.36)$$

$$v = \frac{2mg \cos \theta \sin \phi}{\rho S C_{Y \delta n} \delta n} \quad (6.37)$$

$$\varepsilon_D = \frac{C_{Y \delta n} C n_{\beta}}{C n_{\delta n} C_{Y \beta}} \quad (6.38)$$

$$\tilde{\varepsilon}_D = \varepsilon_D \cdot \sigma, \quad \text{where } \sigma = \frac{1 - \varepsilon_{C n_{\beta}}}{(1 - \varepsilon_{C_{Y \beta}})(1 - \varepsilon_{\delta l \delta n})} \quad (6.39)$$

$$C_{Y \delta n}^* = C_{Y \delta n, nom} \cdot \frac{S_D}{S_{D, nom}} \quad (6.40)$$

$$C n_{\delta n}^* = C n_{\delta n, X_{ref}} \cdot \frac{S_D}{S_{D, nom}} + dx_g \cdot C_{Y \delta n, nom} \cdot \frac{S_D}{S_{D, nom}} \quad (6.41)$$

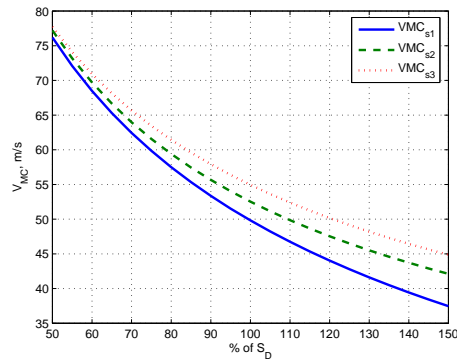
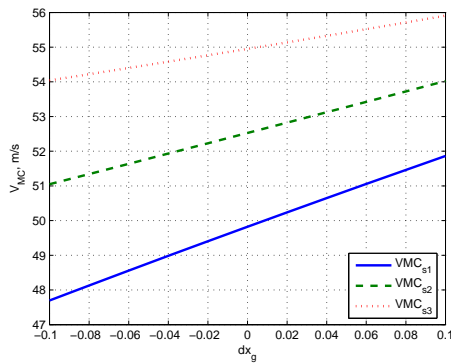
$$C_{Y \beta}^* = C_{Y \beta, fuselage} \cdot \left(1 + \frac{\Delta C_{Y \beta, fuselage}}{C_{Y \beta, fuselage}}\right) + C_{Y \beta, fin} \cdot \frac{S_D}{S_{D, nom}} \quad (6.42)$$

$$C n_{\beta}^* = C n_{\beta, fuselage} \cdot \left(1 + \frac{\Delta C n_{\beta, fuselage}}{C n_{\beta, fuselage}}\right) + C n_{\beta, fin} \cdot \frac{S_D}{S_{D, nom}} - dx_g \cdot C_{Y \beta, fin} \cdot \frac{S_D}{S_{D, nom}} \quad (6.43)$$

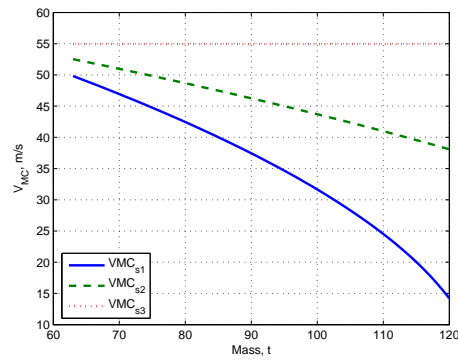
**Physical influence of parameters**

- $\kappa$  balance of rudder moment and engine thrust (in  $V_{MC_{s1}}$ ,  $V_{MC_{s2}}$ ,  $V_{MC_{s3}}$ )
- $v$  equilibrium angles and balance of mass and lateral force (in  $V_{MC_{s1}}$ ,  $V_{MC_{s2}}$ )
- $\varepsilon_D$  geometry, lateral neutral point (in  $V_{MC_{s1}}$ ,  $V_{MC_{s2}}$ )
- $\sigma, \gamma$  corrective terms and aileron effects (in  $V_{MC_{s1}}$  only)

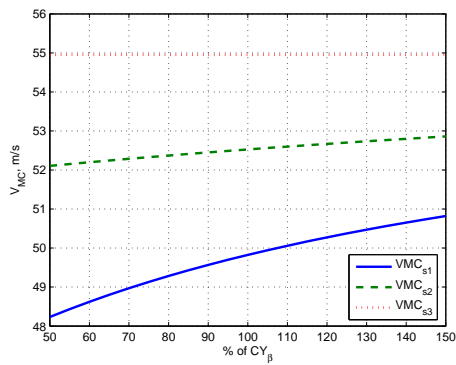
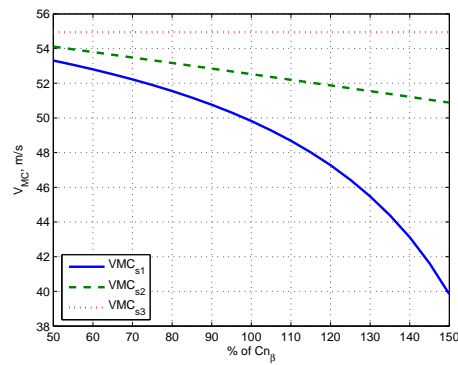
## 6.2.1 DC8 Classical Aircraft

(a) Fin size.  $S_{D,nom} = 29.3 m^2$ .

(b) Center of gravity.



(c) Mass.

(d)  $C_{Y_{\beta, fuselage}}$ .(e)  $C_{n_{\beta, fuselage}}$ .Figure 6.2: DC8.  $V_{MC}$  as a function of various parameters.

Only one parameter is varied at a time during the parametric analysis. The flight attitude is fixed to an initial set-up. The bank angle is set to  $\phi = 5^\circ$  which equals the maximum allowable bank angle for  $V_{MC}$  certification. The pitch angle is assumed to be zero ( $\cos\theta = 1$ ). The maximum rudder deflection is  $\delta n = 30^\circ$ . For the time being, the error caused by this approximation shall be assumed to be negligible. Variations of the pitch angle within reasonable limits ( $0^\circ$ – $20^\circ$ ) lead to an error of  $\Delta \cos\theta < 7\%$ . The maximum rudder deflection is set to  $30^\circ$ . The aircraft is at empty weight  $m = 63\text{ t}$  with the c.o.g. at reference position ( $dx_g = 0$ ). The nominal fin size is  $S_D = 29.3\text{ m}^2$ .

**Fin surface area.** The curves appearing in Figure 6.2(a) do not surprise. A larger fin leads to a smaller minimum control speed. The side force  $Y_{\delta n}\delta n$  produced by the rudder is assumed to be proportional to the size of the vertical fin and so is the produced rudder moment.

The figure shows that the three analytic  $V_{MC}$  expressions give coherent results. For larger fins, the differences between the three expressions become more apparent, up to a difference of 12%. The more elaborate the analytical  $V_{MC}$  formula, the lower the resulting speed. Thus, the most simplified expression seems to be somewhat conservative, which seems important with regard to certification. This becomes clear when considering that  $V_{MC_{s3}}$  only takes into account the rudder/fin produced moment to counter engine failure, thus with sideslip  $\beta = 0$ . With  $V_{MC_{s1}}$  incorporating trim ( $\beta, \phi \neq 0$ ) and secondary effects to produce a counter momentum, this expression results in the lowest minimum control speed.

**C.o.g.** The center of gravity is the parameter varying in Figure 6.2(b). This parameter appears in all three  $V_{MC}$  expressions in term  $\kappa$ , within the yaw momentum produced by the rudder  $Cn_{\delta n}\delta n$ . This moment can be expressed as a product of side force coefficient and lever arm of the rudder. This yields:

$$\underbrace{Cn_{\delta n}}_{<0} \delta n = \underbrace{\frac{X_G - X_{N,fin}}{l}}_{<0} \cdot \underbrace{C_{Y\delta n}}_{>0} \delta n = (x_g - x_{N,fin}) \cdot C_{Y\delta n} \delta n \quad (6.44)$$

with  $X_{N,fin}$  being the position of the neutral point of the fin. Hence, the influence of the center of gravity position  $X_G$  is obtained. The ratio  $\frac{X_G}{X_{N,fin}}$  is the indicator whether a c.o.g. displacement  $dx_g$  plays an important role or not with regard to  $V_{MC}$ . Again, we can guess that the  $V_{MC}$  of standard aircraft with long fuselages will not be affected very much by a c.o.g. displacement. Indeed, the influence of this parameter on the  $V_{MC}$  equilibrium of this aircraft is not of great importance. An enormous 20% change in  $mac$  of the c.o.g. incorporates a change in  $V_{MC}$  of less than 10%.

**Mass.** The next parameter subject to change is the mass. The aircraft mass influences directly term  $v$  which appears only in the less simplified analytic expressions. The mass varies between empty and maximum take-off weight. Naturally,  $V_{MC_{s3}}$  is not affected

| $P$                    |       | $av\Delta V_{MC}$ , [%] |   | main influence on:      |
|------------------------|-------|-------------------------|---|-------------------------|
| $S_D$                  | ↓     | +7.7                    | ↑ | $ \kappa / v $          |
| $dx_g$                 | → aft | +0.8                    | ↑ | $\varepsilon_D, \kappa$ |
| $m$                    | ↑     | -15.0                   | ↓ | $v$                     |
| $Cn_{\beta, fuselage}$ | ↑     | -3.8                    | ↓ | $\varepsilon_D$         |
| $CY_{\beta, fuselage}$ | ↓     | -0.8                    | ↓ | $\varepsilon_D$         |

Table 6.2: Summary of analytic results for a classical aircraft.

whereas  $V_{MC_{s2}}$  seems to reduce in a linear manner w.r.t. a mass change (Figure 6.2(c)).  $V_{MC_{s1}}$  decreases even more rapidly. This means that the aircraft including corrective terms and aileron effects is distinctively more sensitive to mass changes than simpler modelings. As anticipated, mass is an important factor w.r.t.  $V_{MC}$ . Since  $V_{MC}$  has to be shown with the most unfavorable configuration (i.e. reduced mass), it seems important to analyze the influence of this factor in advance on a non-simplified model.

**Fuselage.** Figures 6.2(d) and 6.2(e) display  $V_{MC}$  as a function of the variation of aerodynamic coefficients  $CY_{\beta}$  and  $Cn_{\beta}$ , respectively. In this case, only fuselage depending components of the coefficients, as stated in the list at the beginning of this section, are varied. Whereas an augmentation of  $CY_{\beta, fuselage}$  leads to a higher  $V_{MC}$  a rise in  $Cn_{\beta, fuselage}$  reduces  $V_{MC}$  notably. This is obvious since a higher equilibrating fuselage momentum adds to countering the engine induced moment.

Contrarily, a higher fuselage side force  $CY_{\beta}\beta$  compensates partially the compensating side force produced by banking the aircraft. Since banking is necessary due to  $\beta \neq 0$ , and therefore equilibrating at lower speed, an additional fuselage side force is counterproductive. These coefficients are related to each other via the center of gravity position and the lateral neutral point ( $\frac{Cn_{\beta}}{CY_{\beta}} = x_g - x_{N,lat}$ ). The most simplified formula does not show this effect which demonstrates again the necessity to apply the more complete expressions in future project phase.

For a classical aircraft, similar to the geometry of DC8, the main factors influencing  $V_{MC}$ , deduced from an analytical approach, are summarized in Table 6.2<sup>1</sup>:

- Parameters fin size and center of gravity position present the main parameters to be varied when aiming at higher efficiency at the cost of reducing stability. A smaller fin size and allowable aft c.o.g. positions will increase  $V_{MC}$ .
- The second section of the table summarizes the influence of other parameters. The mass is the most influencing parameter and is regrouped in the artificial parameter  $v$ . This parameter also incorporates the equilibrium conditions ( $\theta$  and  $\phi$ ). Thus, a

<sup>1</sup> $av\Delta V_{MC}$  is the average change of  $V_{MC_{s1}}$  in % per 10% variation of parameter  $P$ .  $\Delta V_{MC}$  [%] =  $\frac{(V_{MC, upper} - V_{MC, lower})}{V_{MC, upper}}$ ,  $\Delta P$  [%] =  $\frac{(P_{upper} - P_{lower})}{P_{upper}}$ ,  $av\Delta V_{MC} = \frac{\Delta V_{MC}}{\Delta P} \cdot 10\%$ .

slightly increased allowable maximum bank angle would have a direct impact on  $v$  and would virtually equal the effect of a higher mass (factor  $m \cdot \sin \phi$ ). This point will be reconsidered once more in the next section.

- Factors  $Cn_\beta$  and  $CY_\beta$  are listed for conceptual reasons. Since they are linked via the lateral neutral point of the fuselage they are characteristic for its shape. Their influence on  $V_{MC}$  is shown individually.
- Options that were not explicitly repeated here and have a direct impact on  $\kappa$  ( $= (V_{MC_{s3}})^2$ ) are: change of engine installation and thus reduction of thrust lever arm; higher rudder efficiency, e.g. double hinged rudder; use of other control surfaces to create an auxiliary momentum, e.g. spoilers ...

### 6.2.2 VELA Blended-Wing Body Aircraft

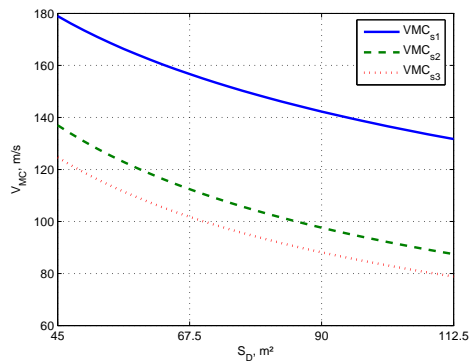
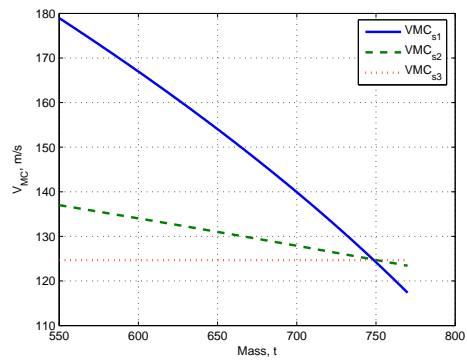
Again, only one parameter is varied at a time whereas the other ones are kept fixed. The bank angle is set to  $\phi = 5^\circ$ , the pitch angle to zero ( $\cos \theta = 1$ ) and the maximum rudder deflection to  $\delta n = 30^\circ$ . The reduced mass case is considered with  $m = 550 t$  and the c.o.g. at reference position ( $dx_g = 0$ ). The nominal (=minimal) fin size is  $S_D = 2 \times 45 m^2$  and the parametrization of the aerodynamic coefficients is as defined at the start of this section.

**Fin surface area.** Here, the results turn out to be quite different from the classical aircraft ones. Even though the tendency is the same, i.e. a larger fin leads to a smaller  $V_{MC}$ , Figure 6.3(a) shows that this time the most simplified formula delivers the lowest speeds. When recalling that the most simple expression equals an equilibrium at  $\beta = 0$ , we can infer that equilibrating the aircraft at a bank and sideslip angle does not reduce the VELA equilibrium speed.

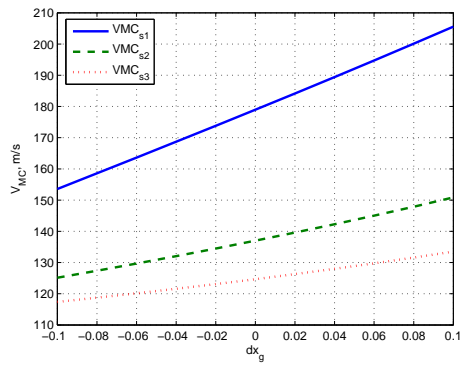
This means that the term  $\varepsilon_D \cdot (\kappa + v)$ , which distinguishes the more elaborated expressions from the most simplified one, is positive and therefore adds to an additional rise in minimum control speed. The crucial point is the relation of  $\kappa$  to  $v$ . Here, it seems that  $v$ , the term including the mass and attitude angles, is not sufficiently large and thus  $|\kappa|/|v| > 1$ .

In other words, it seems that the aircraft weight (at reduced mass) used for the  $V_{MC}$  equilibrium related to the engine-rudder moment ratio is not efficient. As shows the next paragraph, varying the mass supports this hypothesis.

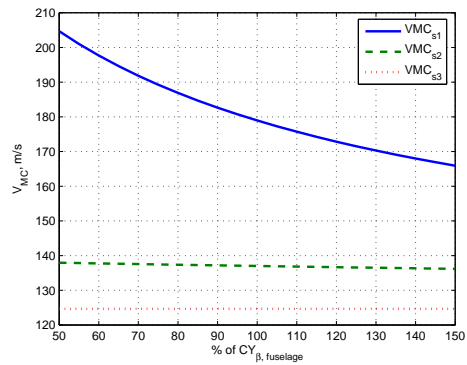
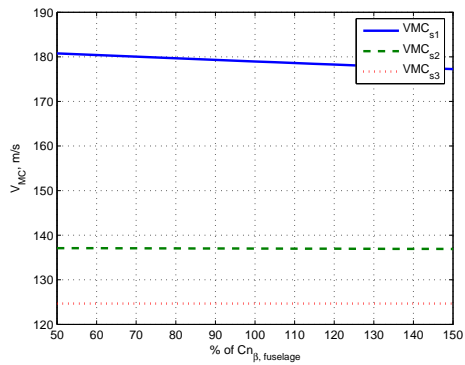
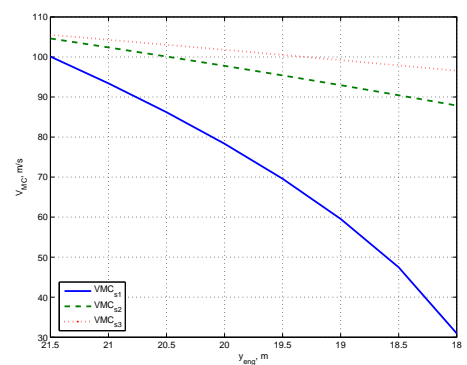
**Mass.** Like for the classical aircraft,  $V_{MC}$  is reduced with a mass increase. But here, term  $v$  can be enlarged with a higher mass until  $|\kappa|/|v| < 1$ , thus, changing the effect of  $\varepsilon_D \cdot (\kappa + v)$  and rendering it classical. Indeed, for a mass of  $750 t$  on, thus close to MTOW, the classical order of  $V_{MC}$  expressions is restored.

(a) Fin size.  $S_{D,nom} = 45 m^2$ .

(b) Mass.



(c) Center of gravity.

(d)  $C_{Y\beta, fuselage}$ .(e)  $C_{n\beta, fuselage}$ .(f)  $y_{eng}$ .Figure 6.3: VELA.  $V_{MC}$  as a function of various parameters.

For masses higher than 750 t, the aircraft behaves like a classical aircraft, in terms of the  $V_{MC}$  equilibrium.

The transitional mass is found by solving  $\kappa = -v$  for  $m$ .

$$m = -\frac{y_{eng}F}{gl \cos \theta \sin \phi} \cdot \frac{C_{Y\delta n}}{C_{n\delta n}} = \frac{y_{eng}F}{g \cos \theta \sin \phi} \cdot \frac{1}{X_{N,fin} - X_g} \quad (6.45)$$

Of course, a mass increase in order to render the aircraft ‘classical’ is not reasonable. But interestingly, the aircraft seems to be too light compared to the balance between thrust and rudder moment. In other words, the transitional mass decreases for a longer lever arm  $X_{N,fin} - X_g$ .

In that case, VELA cannot use its mass efficiently due to a short fin lever arm.

Thus two options arise in order to lower  $\kappa$ : either the thrust moment is reduced (engine installation) or the rudder moment drastically increased. Allowing for higher bank angles is an option for increasing  $v$ .

**C.o.g.** A change of the c.o.g. position has a much more dramatic effect than on a classical aircraft.  $V_{MC}$  increases strongly on this BWB aircraft for aft c.o.g. positions. Figure 6.3(c) illustrates this feature. The reason for this has to be ascribed to the much shorter lever arm of the vertical fin compared to the engine lever arm. The fuselage shape which is not longish cigar-like but rather short and wide (and therefore placing the outboard engine at a long distance to the aircraft  $x$ -axis) makes c.o.g. displacements much more influencing.

**Fuselage.** The effects of variations of  $C_{Y\beta, fuselage}$  and  $C_{n\beta, fuselage}$  are shown in Figures 6.3(d) and 6.3(e). It has to be noted that the  $C_{Y\beta, fuselage}$  variation has the opposite impact on  $V_{MC}$  as on a classical airplane:  $V_{MC}$  reduces with an increase in  $C_{Y\beta, fuselage}$ . The physical effect of an extra side force is the same as in the classical case but, since the aircraft is ‘too light’, ( $|\kappa|/|v| > 1$ ), this time the variation in  $\varepsilon_D$  will decrease the minimum control speed.

Furthermore, the main influence is on the corrective and aileron terms included in  $V_{MC_{s1}}$ , the reason for which the simplified formula show no or negligible variations in  $V_{MC}$ . The variations with  $C_{n\beta, fuselage}$  can be neglected on this airplane.

**Engine lever arm.** In one paragraph we briefly want to come back to the point of the airplane being too light compared to the created thrust and rudder moments. As said before,  $\kappa$  can be lowered significantly by reducing the lever arm of the uncompensated external engine. Figure 6.3(f) demonstrates the effect of a shortening lever arm. Instead of the initial position of  $y_{eng} = 30 m$ , a range from 21.5 m up to only 18 m of distance to the aircraft  $x$ -axis figures in the diagrams. In this range,  $|\kappa|/|v| < 1$ . If the external engine was placed even closer ( $y_{eng} < 18 m$ ), a smaller rudder deflection ( $|\delta n| < 30^\circ$ ) would suffice to equilibrate the aircraft. How this reduction of the lever arm is achieved (e.g. installation of the engines above the fuselage) shall be subject to research at another

| $P$                    |       | $av\Delta V_{MC}, [\%]$ |   | main influence on:      |
|------------------------|-------|-------------------------|---|-------------------------|
| $S_D$                  | ↓     | +4.4                    | ↑ | $ \kappa / v $          |
| $dx_g$                 | → aft | +2.5                    | ↑ | $\varepsilon_D, \kappa$ |
| $y_{eng}$              | ↓     | -42.3                   | ↓ | $\kappa$                |
| $m$                    | ↑     | -12.0                   | ↓ | $v$                     |
| $C_{Y\beta, fuselage}$ | ↑     | -2.9                    | ↓ | $\varepsilon_D$         |
| $C_{n\beta, fuselage}$ | ↑     | -0.2                    | ↓ | $\varepsilon_D$         |

Table 6.3: Summary of analytic results for the BWB VELA aircraft.

place.

A summary in numbers is given in Table 6.3. Some concluding remarks:

- The BWB aircraft presents the same tendencies as those of a classical aircraft when regarding smaller fins and aft c.o.g. positions. Both will increase  $V_{MC}$ . What is more striking is that a c.o.g. displacement triples  $\Delta V_{MC}$  compared to the classical aircraft. The source of this comportment is the relation of c.o.g. displacement and fin lever arm ( $dx_g/x_{SD}$ ). For the VELA BWB aircraft this quotient is significantly larger, hence is the impact.
- Another key difference is the shape of the fuselage. Factor  $C_{Y\delta n}/C_{n\delta n}$  determines, how much the attitude angles  $\phi$  and  $\theta$ , and therewith indirectly sideslip  $\beta$ , see Eq. (6.15), influence the the equilibrium. This determines also the mass influence. For VELA, this relation of engine moment to possible compensation by aircraft weight is very disadvantageous. Moreover, due to a wider (lifting) body, the outboard engine is placed far away from the c.o.g. creating a considerably higher moment.
- A logical solution is to reconsider the engine positioning, e.g. above the fuselage between the two fins.
- Remarks concerning mass and other options to reduce  $V_{MC}$  already mentioned for the DC8 aircraft are also true for this aircraft.

Finally, a direct comparison between classical and BWB aircraft is given in Figure 6.4.

### 6.2.3 Final Remarks on the Analytical Approach toward the $V_{MC}$ Equilibrium

This approach allows for the identification of the main factors influencing this equilibrium. It leads to a physical understanding of the problem. The juxtaposition of multiple factors in terms of efficiency on the one hand (fin size, aft c.o.g.), and in terms of certification criteria on the other (resulting  $V_{MC}$  speed, physical limitations), becomes visible and helps finding trade-offs.

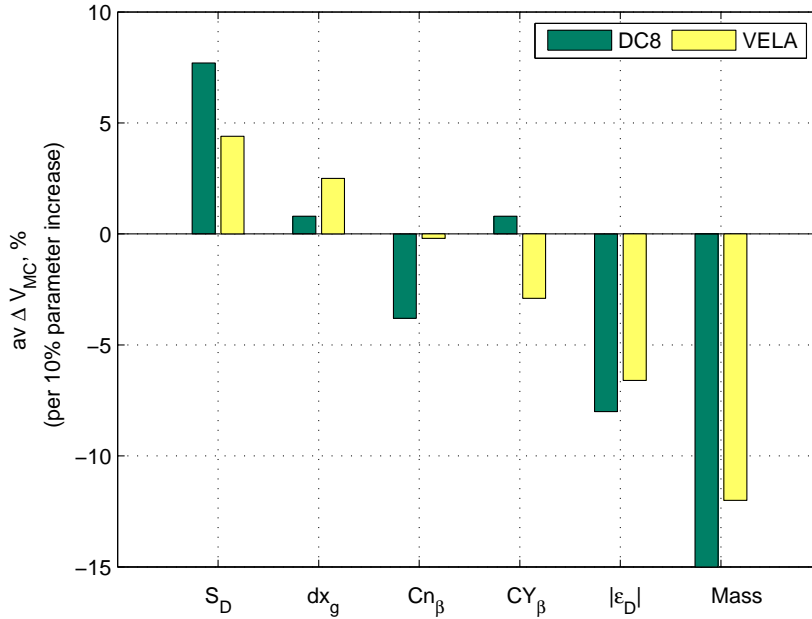


Figure 6.4: Parameter impact on  $V_{MC}$  for a classical and a BWB aircraft.

This approach also gives an idea on how much simplification can be allowed when dealing with certification criteria at an early stage of aircraft development. Whereas the effect of a varying vertical fin or the position of the c.o.g. can be estimated fairly well with the most simplified formula for the classical DC8 aircraft, the differences between these three  $V_{MC}$  expressions for the BWB concept are too large to be neglected. Furthermore, the impact of an important parameter like the mass can only be shown with the most elaborated  $V_{MC}$  expressions.

*One can retain that the most simplified expressions are too conservative for a classical aircraft and too optimistic for the VELA BWB. Whereas trim, mass, and secondary effects reduce  $V_{MC}$  even more for a classical aircraft, these effects are unfavorable for the BWB due to its unconventional shape (lateral neutral point, short fin lever arm).*

The application of the full  $V_{MC}$  expression  $V_{MC_{s1}}$  is necessary for a future project aircraft. Since the expression is complete, other flight equilibrium conditions can be taken into account as well, i.e. different pitch, bank, and rudder deflection angles.

In order to analyze the whole low speed flight domain of an aircraft, one would need to know the conditions for each equilibrium to apply these analytical expressions. Therefore it can be agreed upon that it is interesting to develop a numerical tool which allows to cover a whole domain of flight equilibriums. This tool should guide the way from the physical equation and intellectual understanding to a tangible, visual comprehension and help to find solutions. The next section will deal with this subject.

### 6.3 A Numerical Tool for $V_{MC}$ -Analysis

A Matlab tool has been developed which is based on the non-linear flight dynamic equations presented in Section 6.1. As it directly uses the analytic equations this tool is applicable to all aircraft models when sufficient aerodynamic data exist. Basically, the tool computes equilibrium points (trim points) for various flight parameters (i.e. bank angle, side-slip angle, altitude, speed, thrust setting) with the critical engine inoperative. This is done by iteratively solving the nine analytical equations of flight as described in Chapter 2. The tool then maps the low speed flight domain displaying criteria and physical limitations and helps identifying new and unexpected ones. Since the equilibriums are computed with the full longitudinal/lateral coupled model (including aerodynamic data depending on the trim), the results are expected to be somewhat different from the analytical approach, where so far the longitudinal motion has been taken into account only by an assumption for the pitch angle.

The procedure shall be explained by the means of an example.

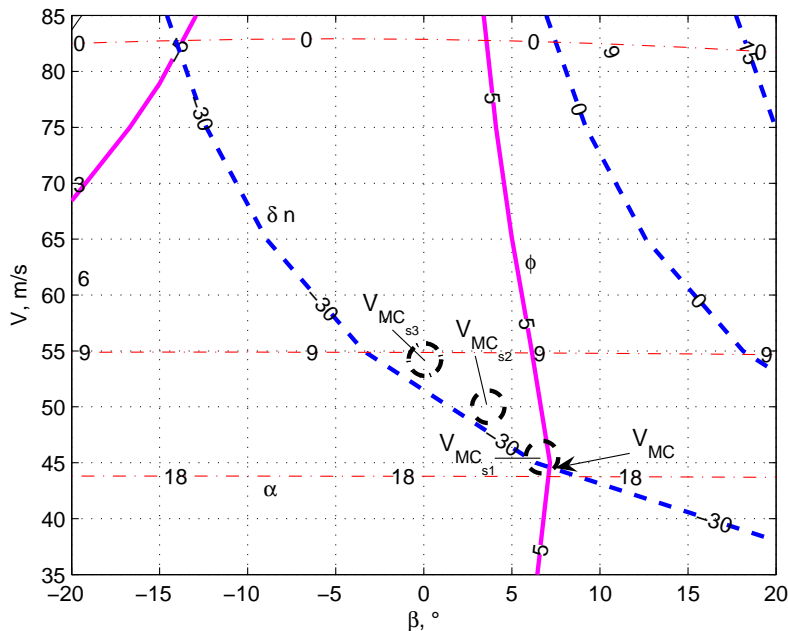


Figure 6.5:  $\beta, V$ -grid for the classical DC8 aircraft with critical engine failure.

Figure 6.5 presents the  $\beta, V$ -grid for a classical aircraft with engine failure at low speeds<sup>2</sup>. A grid of aircraft equilibriums for different speeds and side-slip angles is presented. Iso-lines interconnect equilibrium points of equal rudder deflection  $\delta n$  (blue, dashed,  $-30^\circ$  and  $0^\circ$ ), of equal bank angle  $\phi$  (magenta, thick,  $-5^\circ$  and  $5^\circ$ ) and of equal angle of attack  $\alpha$  (red, thin, from  $0^\circ$  to  $18^\circ$ ). The classical  $V_{MC}$  is situated at the intersection of the

<sup>2</sup>The DC8 aircraft model is used as a representative example for classically shaped airplanes.

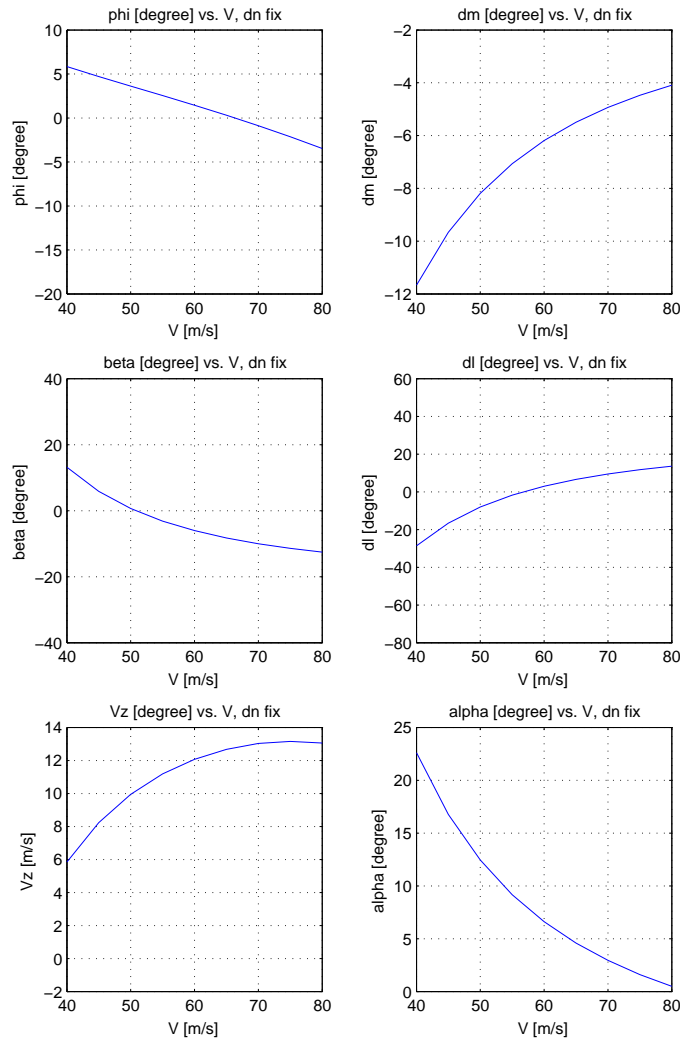


Figure 6.6: Evolution of flight parameters for maximum rudder deflection  $\delta n = -30^\circ$  and the critical (left outboard) engine inoperative for a classical aircraft.

$5^\circ$  bank angle iso-line and the  $-30^\circ$  rudder deflection iso-line. The bank angle limit is given by the FAR/JAR certification criterion and rudder deflection by physical actuator limitations. The intersection of both limits presents the lowest speed possible respecting all constraints. The  $V_{MC}$  is determined here by these two lateral criteria.

For comparison,  $V_{MC_{s1}}$ ,  $V_{MC_{s2}}$ , and  $V_{MC_{s3}}$ , resulting from the analytical expressions, are indicated as well. The trim conditions were injected into the analytical expressions. Consequently,  $V_{MC_{s3}}$  situated at  $\beta = 0^\circ$  is the fastest of the three speeds. A very good approximation is given with the full equation  $V_{MC_{s1}}$ . Minor differences have to be ascribed to coefficient modeling differences.

If one follows the  $-30^\circ$  rudder deflection iso-line, Figure 6.6 displays the evolution of angles, surface deflections and vertical speed for the constant rudder deflection at different

speeds. The figure depicts thus an intersection of the low speed flight domain for the rudder fixed at  $-30^\circ$ . The evolution of angles and deflections is monotone with increasing speed. The lowest speed fulfilling the criteria described in chapter 2 is  $V = 44 \text{ m/s}$ .

The evolution of the  $V_{MC}$  as a function of the fin size varying between 40 % and 140 % has been traced and is displayed in Figure 6.7. For  $S_{D,nom}$  a  $V_{MC}$  is found which is comparable to the analytic approach. Nevertheless, the impact of a change of the vertical tail plane is weaker here. The evolution is not as steep as in the analytical results and the numerical approach gives a lower  $V_{MC}$  for the initial fin size (cf. Figure 6.2(a)). Pialat and Loubignac [72] estimated the  $V_{MC}$  generally too high with an analytical approach compared to values provided by industry. These better results are to be ascribed to the consideration of the trim and the corresponding aerodynamic coefficients in the equilibrium computation, including any effects coming from a longitudinal and lateral coupling.

**Explanation:** In the analytical expression  $\cos \theta$  influences directly the amount of mass put into the equilibrium equation. Thus assuming  $\theta = 0$ , the effect of scaling of  $C_{Y\delta n}$  in the denominator with a varying fin size is directly influencing  $V_{MC}$  and leads to a steeper evolution. If now the longitudinal motion is taken into account as well by taking a closer look at the longitudinal equilibrium variables  $\alpha$  and  $V_Z^3$ , the reader will notice that  $\theta$  is far from being zero, especially at low speeds. Therefore, the effect of an increased fin size is partially countered by  $\cos \theta < 1$  and hence the less steep evolution of  $V_{MC}$ .

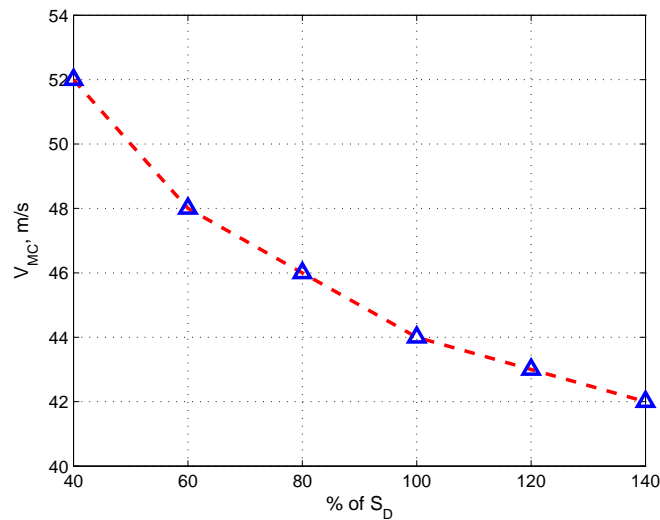


Figure 6.7: The  $V_{MC}$  as a function of the vertical fin size  $S_D$  for a classical aircraft.

This result can now be put into relation with the dynamic requirements and criteria given in Chapter 2. It is then possible to analyze the following trade-off: a reduction in mass and drag due to a smaller fin surface area vs. a degradation of handling qualities (reduced lateral stability) and/or a higher  $V_{MC}$ . Another aspect to consider would be the

<sup>3</sup>The climb angle  $\gamma = \tan V_Z$ . The pitch angle is defined as  $\theta = \alpha + \gamma$ .

implementation of an automatic control system to counter the degradation in handling quality due to a reduction in lateral stability. The dynamic criteria analysis will be part of Chapter 7.

**Summary.** This  $\beta, V$  - grid and the vertical section through this grid along a boundary (like the maximum rudder deflection) are a convenient representation for visualizing the allowable domain of flight. Other limitations, such as a maximum side force or minimal climb rate, can easily be introduced and visualized on the grid. When changing parameters, like in this case fin size and center of gravity position, the effects are displayed and the relation of these parameters with others becomes visible. Unexpected constraints can pop-up as well as unexpected potentials, yet unexploited.

This tool will now be utilized in the next section in order to conduct yet another analysis of the  $V_{MC}$  equilibrium for the BWB aircraft. This approach will provide new information that can be used to derive new restrictions, potentials, and therewith recommendations for the aircraft design.

## 6.4 $V_{MC}$ -Equilibrium for a BWB Aircraft

Only a summary of the results for the BWB aircraft will be shown in this section, for the sake of conciseness.

Again, flight at zero altitude and low speed is considered. Since the  $V_{MC}$  criteria are harder to realize with a lighter aircraft (compare with Section 6.1) the reduced mass case ( $m = 550 t$ ) is considered. The critical (left-outboard) engine is inoperative and the size of the vertical tailplane  $S_D$  and the position of the c.o.g. are varied.

The limitations known beforehand are:

- $|\delta l_{max}| = 30^\circ$  (maximum aileron deflection),
- $|\delta n_{max}| = 30^\circ$  (maximum rudder deflection),
- $|\phi_{max}| = 5^\circ$  (bank angle limitation),
- $|\alpha_{max}| = 14^\circ$  (*tail-strike*,  $0.4^\circ$  security margin).

Tail-strike occurs when the airplane tail touches the ground due to a high pitch angle.

### 6.4.1 Results

Figure 6.8 features the BWB aircraft with a c.o.g. at reference position ( $dx_g = 0\%$ ) and a fin surface area of  $2 \times 64 m^2$ . We can see that the flight domain is split into two regions by the  $5^\circ$  bank angle criterion. In the center of the grid, the bank angle is superior to  $5^\circ$ . The iso-lines form an intersection with other iso-lines, representing a different limiting criterion each.

The upper region is limited, like in the classical case, by bank angle and maximum

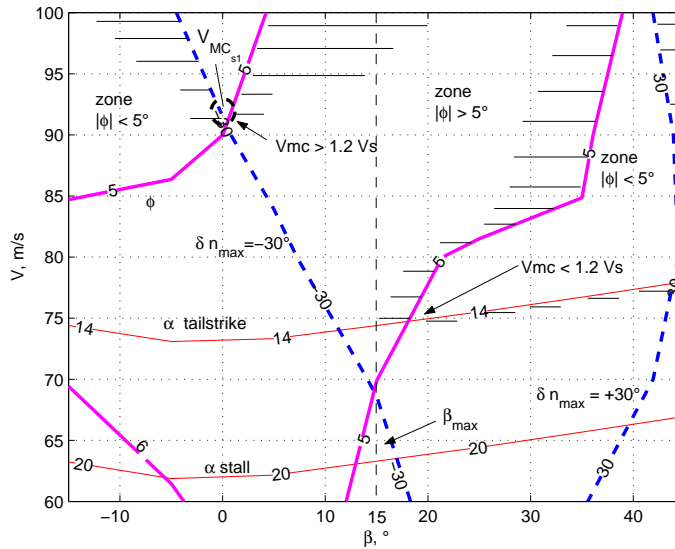


Figure 6.8:  $\beta, V$ -grid for the bwb aircraft model with critical engine failure.

rudder deflection. The  $V_{MC}$  is found at the intersection of these two limitations. For comparison, the analytical  $V_{MC_{s1}}$  is displayed as well. The corresponding trim conditions were inserted into the analytical equation. Especially the incidence angle has a strong influence on the aerodynamic coefficients due to their modeling (compare with Appendix A and the following paragraphs). As a consequence, the analytical result matches the numerical result very well.

The upper region is characterized by relatively high speeds and small sideslip. The lower region however, unlike classical aircraft, is limited by three different criteria: bank angle, rudder deflection and tail-strike or maximum angle of attack. The equilibrium is thus limited also by longitudinal criteria.

Even if equilibrated flight is possible at very low speeds with one engine failing (lower region), one has to consider very high sideslip angles. A new criterion will have to be introduced, defining a maximum side-slip angle  $\beta$ , e.g. vertical fin stall, marked here as an example with a black vertical dashed line.

This splitting into two, an upper and a lower flight domain, is caused by a very unique behavior of the bank angle which develops a maximum at a certain velocity and then drops back to smaller values, when flying with maximum rudder deflection (Figure 6.9). This behavior has its origin in a strong aileron-sideslip coupling which is inherent to the provided aircraft model. The complex relations and effects are described and explained in the next paragraphs.

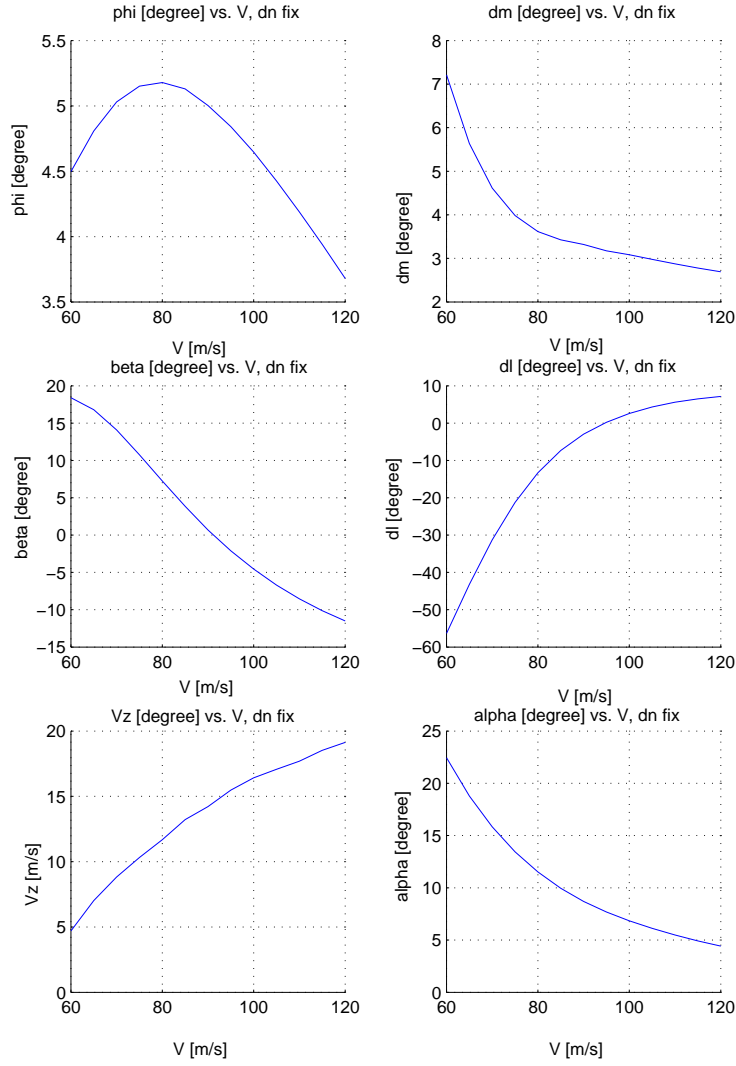


Figure 6.9: Evolution of flight parameters for the equilibrated VELA aircraft with maximum rudder deflection  $\delta n = -30^\circ$  and the critical (left outboard) engine inoperative.

### Bank Angle $\phi$

Contrarily to a classical airplane model the gradient of  $\phi$  is positive for low speeds and becomes eventually zero and then negative at a certain airspeed. In order to explain this phenomenon, a closer look is taken at Figure 6.10 which displays a pseudo-coefficient  $Cn^*$  as a composition of only aileron related effects, i.e. the yaw moment caused by aileron deflection. This momentum can be decomposed into a direct, deflection-dependent part (I), and a part (II) that also depends on the angle of attack.

$$Cn^* = (Cn_{\delta l 0} + Cn_{\delta l \alpha} \cdot \alpha) \cdot \delta l = \underbrace{Cn_{\delta l 0} \cdot \delta l}_I + \underbrace{Cn_{\delta l \alpha} \cdot \alpha \cdot \delta l}_{II} \quad (6.46)$$

We realize that the ailerons produce a partially compensating (thus positive) moment for speeds inferior to  $110\text{ m/s}$  and that the  $\alpha$ -related part  $C_{n\delta l\alpha} \cdot \alpha \cdot \delta l$  adds the most to the positive momentum caused by the aileron deflection.

The most particular behavior of the bank angle, which comprises a maximum in its evolution, becomes comprehensible. At low speeds the aircraft is equilibrated at a high angle of attack. This angle increases thus the effect of an aileron-sideslip coupling, as the derivative depending on  $\alpha$  shows (Figure 6.10). The ailerons contribute to a compensating moment and equilibrate thus the lack of rudder efficiency at low speed.

With increasing speed, the rudder becomes more effective, producing a larger momentum and more side force, and thus the aircraft needs to be banked more (rise in  $\phi$ ) to counter lateral force. For higher speeds, the angle of attack decreases and thus the ailerons contribute less to a counter-momentum.  $\phi$  reaches a maximum and then turns over to a classical evolution. Eq. (6.14) in Section 6.1 shows that  $\phi$  depends directly on sideslip angle  $\beta$  but also on aileron effects, shown as corrective term  $\epsilon_{\delta l\delta n}$ . Once this corrective term becomes zero (thus at higher speeds and smaller angle of attack  $\alpha$ ) the evolution becomes classical:  $\phi$  decreases with  $\beta$ . Interestingly, this equation shows that the influence of the ratio engine/rudder moment is also determined by this secondary effect. Apparently, for the VELA airplane model, this effect is not secondary. As a result,  $\phi$  cuts through the  $|\phi| = 5^\circ$ -bank angle limit twice, thus creating two allowable domains of flight.

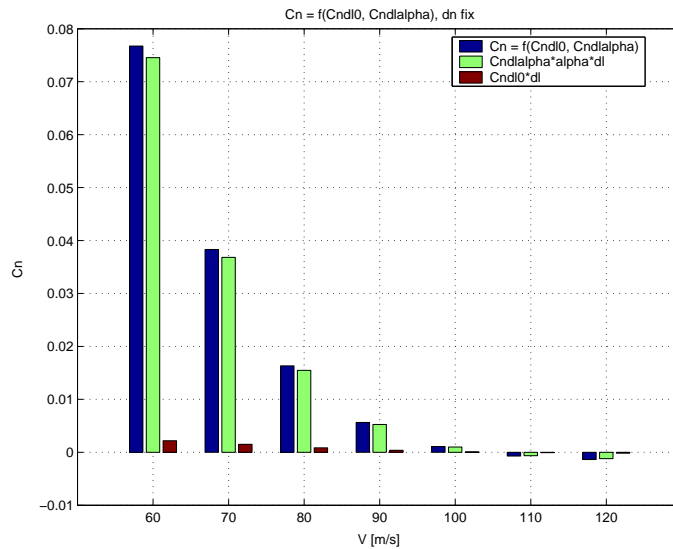


Figure 6.10: Evolution of  $C_N^*$  as a function of aileron deflection  $\delta l$  and angle of attack  $\alpha$  for the BWB model

In order to demonstrate this result more clearly, firstly the aerodynamic model of the BWB aircraft has been modified: the derivative  $C_{n\delta l\alpha}$  has been changed from  $-0.15$  to  $-0.015$ , thus reducing this coupling by factor 10. As a result, the evolution of  $\phi$  becomes classical: a monotonously decreasing function (Figures D.2 and D.3 in Appendix C).

Secondly, this  $\alpha$ -induced aileron-yaw momentum coupling has been introduced into the DC8 aircraft model which led to a similar behavior of  $\phi$  compared to that of a BWB aircraft. Compare with Figures D.4 and D.5.

**Remark:** Normally, the aileron-yaw coupling ( $Cn_{\delta l}$ ) is positive in the aerodynamic coordinate system. In fixed aircraft coordinates however, the lift vector is inclined by  $\alpha$  which can cause the contrary effect. This negative aileron-yaw coupling is of course defined by the aircraft modeling and the question remains, whether the magnitude of  $Cn_{\delta l}$ , provided by a CFD software<sup>4</sup>, is realistic.

### Aileron Deflection $\delta l$

The roll equation, Eq. (6.6) in Section 6.1, shows that, with  $\delta n$  fixed, the aileron deflection depends directly on  $\beta$ . Sideslip is very high for low speeds and so is the aileron deflection (Figure 6.9). Speeds below 70 m/s result in unrealistically high aileron deflections. When  $\beta$  becomes zero, the aileron deflection tends to zero as well.

### Elevator Deflection $\delta m$

From the longitudinal momentum equation we know that for equilibrated flight  $\delta m = -\frac{Cm_{\alpha}}{Cm_{\delta m}}\alpha$ . The evolution is therefore clear: at low speeds a high angle of attack leads to high elevator deflections and vice versa.

### Main Differences: Classical vs. BWB

The main difference reveals itself in the composition of the boundaries defining  $V_{MC}$ : the minimum control speed is not necessarily defined by two lateral criteria or limitations. Figure 6.8 shows that there can be a combination of lateral and longitudinal constraints.

These data are valuable as they allow for an exploitation of the potentials (possibility of choosing a  $V_{MC}$  equilibrium that appears to fit best) at an early stage. The trade-off between low side-slip in combination with higher speeds for the upper domain and lower speeds with higher yaw angles is visible.

Now, variations of the c.o.g. position and the size of the vertical tailplane shall be taken into account which might provide a better compromise/solution and result in a recommendation for the aircraft design.

#### 6.4.2 Variation of the C.O.G. Position

The examined BWB aircraft features a relatively short lever arm between the vertical fins and the center of gravity. Consequently, a displacement of the c.o.g. has a noticeable

<sup>4</sup>CFD software: Computational Fluid Dynamics Software Lattice-beta, V1.1

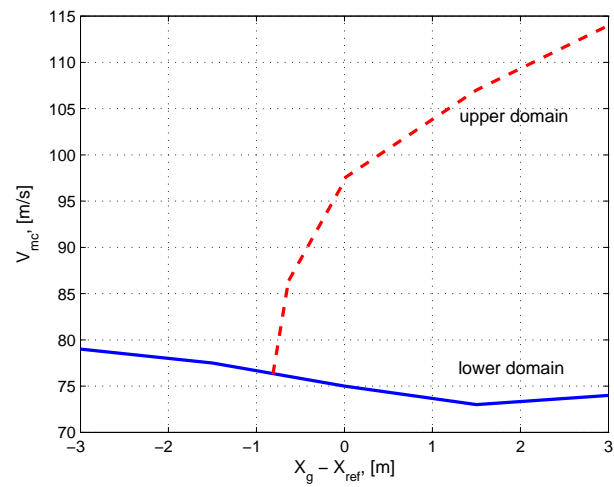


Figure 6.11:  $V_{MC}$  equilibrium as a function of  $X_g$  for  $S_D = 2 \times 45m^2$ .

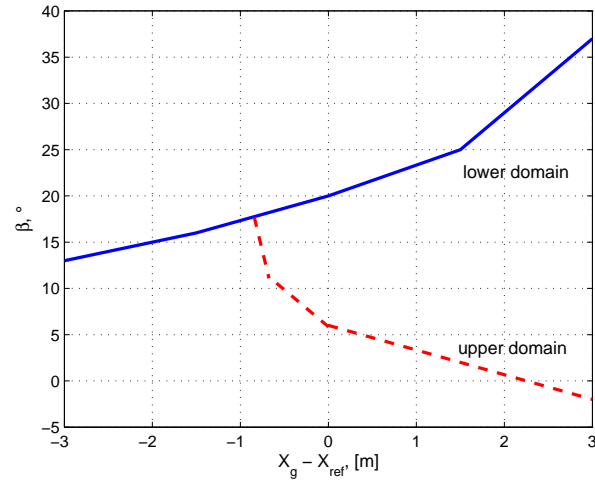


Figure 6.12: Yaw angle  $\beta$  corresponding the equilibrium at  $V_{MC}$  as a function of  $X_g$  for  $S_D = 2 \times 45m^2$ .

impact as already shown in the analytic approach section.

When moving  $X_g$  in aft direction, the maximum bank angle criterion splits the  $\beta, V$ -grid in two areas:

- an upper, classical domain where  $V_{MC}$  is defined by two lateral criteria (rudder deflection and bank angle),
- a lower domain where  $V_{MC}$  is defined by mixed criteria (bank angle and tailstrike).

With regard to the upper domain,  $V_{MC}$  rises for  $X_g$  displacements in aft direction. Contrarily, in the lower domain  $V_{MC}$  diminishes for  $X_g$  displacements in aft direction. The iso-lines for the rudder deflection move to the right-hand side of the grid, i.e. the overall yaw angle at  $V_{MC}$  increases with a displacement of the c.o.g. in aft direction for the lower domain. The upper domain incorporates diminishing yaw angles.

Figures 6.11 and 6.12 show a summary of the effects described so far. The transition point between lower and upper domain is associated to a c.o.g. position for which the bank angle curve is tangent to the  $|5^\circ|$  bank angle limit. Further aft, two domains exist in the  $\beta, V$ -grid divided by a bank angle zone of  $|\phi > 5^\circ|$ .

The upper domain is at very high speeds. If the aircraft has to be certified with  $V_{MC} \leq V_{2min} = 1.2 V_S = 81.5 \text{ m/s}$  the criterion is not realized within the upper domain. The lower domain realizes the criterion. Only a limitation in yaw angle (like *fin stall*) would limit c.o.g. positions to fwd ones.

**Remark.** For very aft center of gravity positions, the most constraining longitudinal limitation can be given by a maximum elevator deflection. Due to the short lever arm of this aircraft, elevator deflections  $\delta m$  become critical when equilibrating the aircraft.

### 6.4.3 Variation of the Fin Surface Area

As Figures 6.13 and 6.14 show, for fwd c.o.g. positions  $V_{MC}$  is reduced with a larger fin surface up to the splitting point in an upper and lower domain. Concerning this fact, a large fin can cause effects similar to a c.o.g. displacement. A large fin will produce strong lateral forces which are equilibrated by banking the aircraft. At low speeds this produces the bank angle phenomenon described earlier. Interestingly, in the upper domain  $V_{MC}$  does not decrease with a larger fin size and a fwd c.o.g. position.

For aft c.o.g.  $V_{MC}$  decreases clearly with a larger fin size for the upper domain. The lower domain is not affected as it is limited longitudinally, hence not influenced by the fin.

### 6.4.4 Key Aspects of the Utility

The advantage of the developed tool is clearly its representation of the computed equilibriums. This allowed for conveniently identifying the separation into two flight domains.

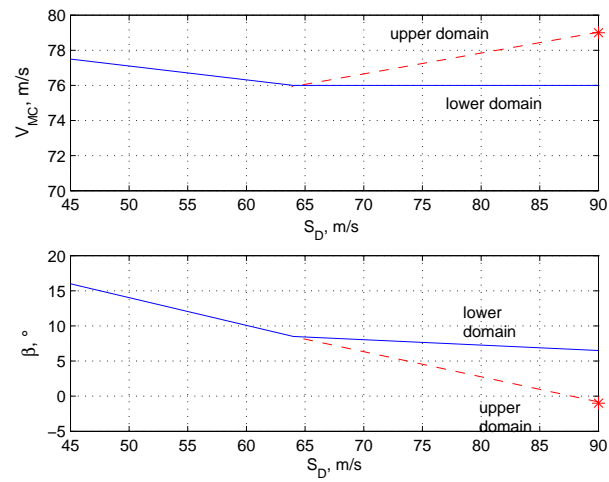


Figure 6.13:  $V_{MC}$  and its corresponding yaw angle as a function of the fin surface area for  $dx_g = -4.17\%$  fwd.

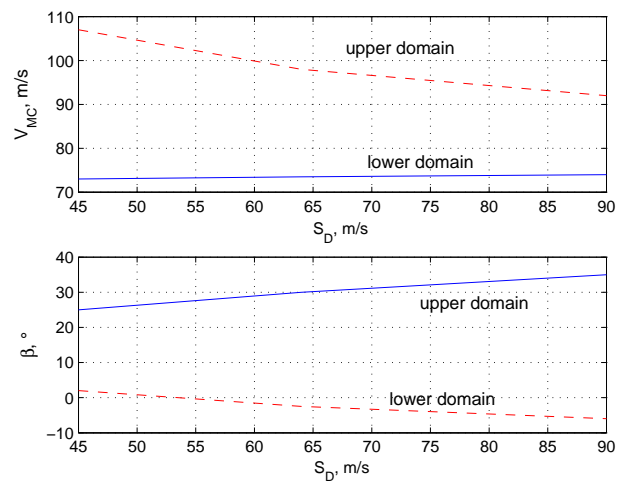


Figure 6.14:  $V_{MC}$  and its corresponding yaw angle as a function of the fin surface area for  $dx_g = +4.17\%$  aft.

In addition, this method unveils specific modeling characteristics, such as the aileron coupling, which can then be analyzed.

## 6.5 Summary on the $V_{MC}$ Equilibrium

The two proposed analysis techniques are complementary and prove to be applicable to the examination of equilibrated flight with asymmetric thrust. The certification relevant case of engine failure during low altitude and low speed flight (landing/take-off) has been examined with these techniques. Whereas the analytical part delivers more physical/flight mechanical insights, the numerical tool incorporates boundaries, limitations, and the aircraft equilibrium and allows for a visual interpretation of the problem.

The  $V_{MC}$  equilibrium-related criteria are critical on the VELA aircraft. Nevertheless, the conducted analysis reveals several options to achieve a better performance at an early stage of the aircraft design. Unlike classical aircraft, the position of the center of gravity is very important in this context. The relative short lever arm has a strong influence on the equilibrium.

Furthermore, the assumption that  $V_{MC}$  is always defined by maximum bank angle and maximum rudder deflection is proven to be false. The presented lower flight domain incorporates a mix of longitudinal and lateral limits. These new limitations are e.g. tailstrike, maximum elevator deflection or a maximum sideslip angle in order to prevent an aerodynamic stall at the fin. A solution would be to choose a fin profile which is designed for high angles of attack and/or to define a maximum allowable sideslip angle (e.g.  $\beta_{max} \approx 15^\circ$ ). In that case, dynamic criteria have to be examined since a reduced fin size will cause greater sideslip during roll maneuvers. The next chapter will assess this issue and other dynamic criteria that are influenced by a reduced lateral stability.

**Remark:** It should be noted that if the bank angle restriction of  $\phi = \pm 5^\circ$  was relaxed just a little to  $\phi = \pm 6^\circ$  the results concerning the BWB would appear to be quite different. This is due to the relatively small changes of bank angle with different speeds and sideslip angles. An interrogation of industry and aviation authorities could clarify if such a relaxation is possible. If this is the case,  $V_{MC}$  will not at all be defined by the typical limitations (rudder and bank angle). Instead, it will always be a combination of rudder deflection and several other, untypical, boundaries (e.g. angle of attack, fin stall, elevator deflection).



## Chapter 7

# Dynamic Lateral Criteria and Reduced Stability

This chapter is dedicated to the examination of dynamic sizing criteria, such as maneuvers that have to be carried out at  $V_{MC}$  and others imposed by certification authorities.

Chapter 2 lists the dynamic criteria which are critical in the context of an aircraft with reduced natural stability. One criterion represents a modal constraint in damping ratio and frequency and relates directly to lateral handling qualities. Three other criteria are directly related to  $V_{MC}$  and represent maneuvers that have to be carried out under special conditions.

Firstly, the development of analytical expressions describing the aircraft lateral dynamics will be given, followed by a brief analysis with respect to certification criteria. The influence of a change of the fin surface area is examined. Secondly, numerical results are presented to confirm the analytical results for both the classical DC8 aircraft and the VELA BWB aircraft.

The last section of this chapter concludes in a possible parameter setting (fin size, possible center of gravity positions) for the future project BWB aircraft VELA1, demonstrating the trade-off between performance and reduced lateral stability. Final remarks end this chapter.

### 7.1 Preliminary Developments Toward an Analytical Examination of Dynamic Criteria

In this subsection we seek to analytically describe the impact of a change in fin size and position of the c.o.g. onto the aircraft flight dynamics. Therefore, beginning with the lateral flight mechanics equations, the eigenvalues ('modes') of the lateral movement will be developed and related to the aforementioned parameters.

The lateral flight mechanics equations in the body frame read (compare with Chapter 2, under the assumption that  $V$  and  $\alpha$  are constant):

$$mV(\dot{\beta} + r \cos \alpha - p \sin \alpha) = \sum Y = mg \sin \phi \cos \theta + \frac{1}{2}\rho S V^2 C_Y \quad (7.1)$$

$$C\dot{r} - (A - B)qp - E(\dot{p} + rq) = \sum N = \frac{1}{2}\rho S l V^2 C_n \quad (7.2)$$

$$A\dot{p} - (B - C)qr - E(\dot{r} + pq) = \sum L = \frac{1}{2}\rho S l V^2 C_l \quad (7.3)$$

The sum of side forces  $Y$ , yaw moments  $N$ , and roll moments  $L$  are described in form of aerodynamic coefficients  $C_Y$ ,  $C_n$ , and  $C_l$ , respectively. When linearizing for small variations we obtain for these coefficients in the body frame:

$$C_Y = C_{Y\beta}\beta + C_{Yp}\frac{pl}{V} + C_{Yr}\frac{rl}{V} + C_{Y\delta l}\delta l + C_{Y\delta n}\delta n \quad (7.4)$$

$$C_n = C_{n\beta}\beta + C_{np}\frac{pl}{V} + C_{nr}\frac{rl}{V} + C_{n\delta l}\delta l + C_{n\delta n}\delta n \quad (7.5)$$

$$C_l = C_{l\beta}\beta + C_{lp}\frac{pl}{V} + C_{lr}\frac{rl}{V} + C_{l\delta l}\delta l + C_{l\delta n}\delta n \quad (7.6)$$

Rotational velocities  $p$  and  $r$  (roll and yaw rate) are made dimensionless by factor  $\frac{l}{V}$ . If furthermore it is assumed that  $\cos \beta = 1$ ,  $\sin \beta = \beta$ , pitch rate  $q = 0$  and  $E = 0$ , then a system of four linearized equations describing the aircraft lateral dynamics is obtained:

$$\begin{pmatrix} \dot{\beta} \\ \dot{r} \\ \dot{p} \\ \dot{\phi} \end{pmatrix} = \begin{bmatrix} \frac{Y_\beta}{V} & -\cos \alpha & \sin \alpha & \frac{g \cos \theta}{V} \\ N_\beta & N_r & N_p & 0 \\ L_\beta & L_r & L_p & 0 \\ 0 & \tan \theta & 1 & 0 \end{bmatrix} \begin{pmatrix} \beta \\ r \\ p \\ \phi \end{pmatrix} + \begin{bmatrix} \frac{Y_{\delta l}}{V} & \frac{Y_{\delta n}}{V} \\ N_{\delta l} & N_{\delta n} \\ L_{\delta l} & L_{\delta n} \\ 0 & 0 \end{bmatrix} \begin{pmatrix} \delta l \\ \delta n \end{pmatrix} \quad (7.7)$$

This notation has been chosen for facilitated writing. With  $\bar{q} = \frac{\rho}{2}V^2$ , the terms in the matrices are:

$$\begin{aligned}
Y_\beta &= \frac{1}{m} \bar{q} S C_{Y\beta} & Y_{\delta n} &= \frac{1}{m} \bar{q} S C_{Y\delta n} \\
Y_{\delta l} &= \frac{1}{m} \bar{q} S C_{Y\delta l} \\
N_\beta &= \frac{1}{C} \bar{q} S l C n_\beta & N_r &= \frac{1}{C_V} \bar{q} S l^2 C n_r \\
N_p &= \frac{1}{C_V} \bar{q} S l^2 C n_p & N_{\delta n} &= \frac{1}{C} \bar{q} S l C n_{\delta n} \\
N_{\delta l} &= \frac{1}{C} \bar{q} S l C n_{\delta l} \\
L_\beta &= \frac{1}{A} \bar{q} S l C l_\beta & L_r &= \frac{1}{A_V} \bar{q} S l^2 C l_r \\
L_p &= \frac{1}{A_V} \bar{q} S l^2 C l_p & L_{\delta n} &= \frac{1}{A} \bar{q} S l C l_{\delta n} \\
L_{\delta l} &= \frac{1}{A} \bar{q} S l C l_{\delta l}
\end{aligned}$$

### 7.1.1 Decoupling and Parametrization

Even though it might not always be possible to isolate three distinct dynamics of this lateral system, it is common to name the following different characteristic motions (eigen-dynamics), see e.g. [63, 22, 8, 20]:

- **Dutch Roll:** lateral-directional oscillations, medium-fast, weakly damped.
- **Roll:** fast aperiodic motion around the longitudinal axis.
- **Spiral:** slow aperiodic motion, often instable.

Principally, the systems dynamics are characterized by the eigenvalues of system Eq. (7.1). The characteristic equation is:

$$(\lambda^2_{1,2} + 2\xi\omega_0\lambda_{1,2} + \omega_0^2)(\lambda_3 + \frac{1}{T_R})(\lambda_4 + \frac{1}{T_S}) = 0 \quad (7.8)$$

where  $\xi$  and  $\omega_0$  are the damping ratio and natural frequency of the dutch roll motion,  $T_R$  the roll time constant, and  $T_S$  the time constant of the spiral motion.

By separating the system dynamics, the next paragraphs will briefly show how these are influenced by a change in the size of the vertical tailplane and the position of the center of gravity.

The coefficients implied in system Eq. (7.1) that are sensitive to these variations are mainly  $Cn_\beta$ ,  $Cn_r$ , and  $C_{Y\beta}$ . A very simple parametrization will allow for a brief analysis. If fuselage and wing effects are neglected for the time being, then these coefficients can reasonably be modeled in favor of a facilitated study (compare with Section 6.1 and [32, 8, 20]):

**Parametrization**

$$C_{Y\beta}^{**} = C_{Y\beta,fin} \cdot \frac{S_D}{S_{D,nom}} \quad (7.9)$$

$$Cn_{\beta}^{**} = x_{SD} \cdot C_{Y\beta}^{**} \quad (7.10)$$

$$Cn_r^{**} = -x_{SD}^2 \cdot C_{Y\beta}^{**} \quad (7.11)$$

$$x_{SD} = \frac{(X_G - X_{N,fin})}{l} \quad (7.12)$$

$x_{SD}$  is the normalized lever arm of the fin and thus negative.

**Remark:** Decoupling the eigenvalues will cause non-negligible errors, since the dutch-roll dynamics can be coupled with the spiral dynamics when close to instability. Nevertheless, this section does not seek to find a better analytical approximation to the dynamics. The goal is instead to use simple expressions that lead to a physical understanding of the impact of a variation of fin surface area or c.o.g. position. Further reading on more sophisticated analytical descriptions can be found in [9, 14, 31, 59, 71, 85, 99].

**7.1.2 Dutch Roll Motion**

A simplifying approximation ( $\cos \alpha = 1$ ,  $Y_{\delta l} = 0$  and all coupled terms, e.g.  $g \cos \theta / V$  zero) gives the differential equation of the dutch roll oscillation:

$$\begin{pmatrix} \dot{\beta} \\ \dot{r} \end{pmatrix} = \begin{bmatrix} \frac{Y_{\beta}}{V} & -1 \\ N_{\beta} & N_r \end{bmatrix} \begin{pmatrix} \beta \\ r \end{pmatrix} + \begin{bmatrix} 0 & \frac{Y_{\delta n}}{V} \\ N_{\delta l} & N_{\delta n} \end{bmatrix} \begin{pmatrix} \delta l \\ \delta n \end{pmatrix} \quad (7.13)$$

The characteristic equation is:

$$\det(\lambda I - A) = \lambda^2 - (N_r + \frac{Y_{\beta}}{V})\lambda + (N_{\beta} + N_r \frac{Y_{\beta}}{V}) = 0 \quad (7.14)$$

This delivers (with  $N_r \frac{Y_{\beta}}{V} \ll N_{\beta}$ ):

- natural frequency:  $\omega_0 = \sqrt{N_{\beta} + N_r \frac{Y_{\beta}}{V}} \approx \sqrt{N_{\beta}} = V \cdot \sqrt{\frac{\rho S l}{2C}} \sqrt{Cn_{\beta}}$ .

- damping ratio:  $\xi = -\sqrt{\frac{\rho S C}{8l}} \frac{1}{\sqrt{Cn_{\beta}}} (l^2 Cn_r + \frac{C_{Y\beta}}{m})$

**Influence of Fin Surface Area and C.o.G. Position**

With the modeling presented above, the expressions for damping ratio and frequency can be rewritten as (remember that  $C_{Y\beta}$  is negative as well):

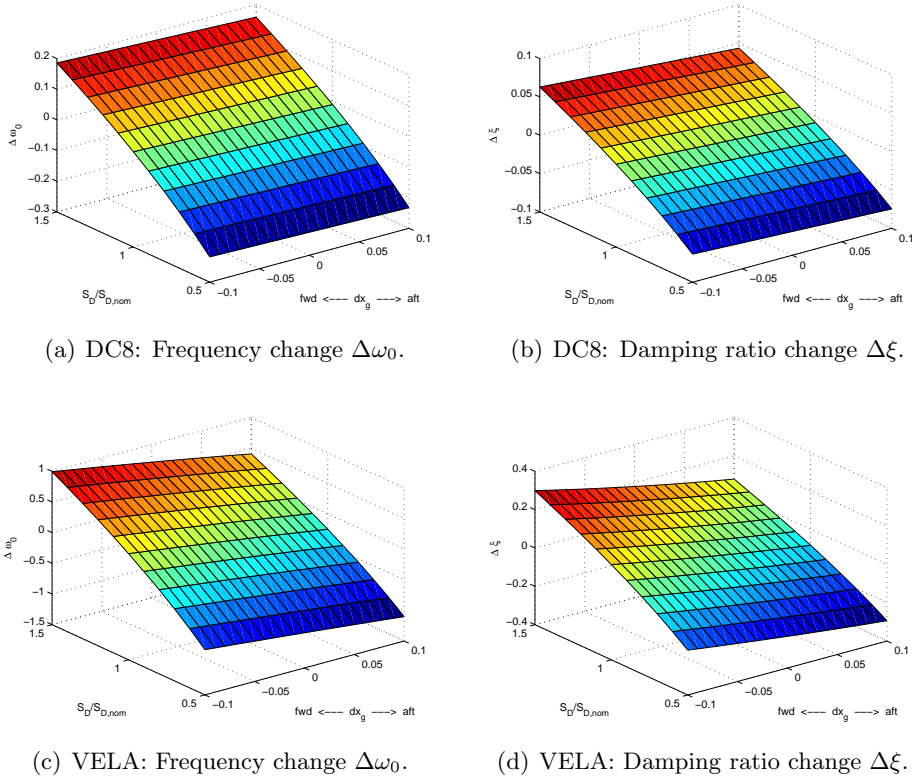


Figure 7.1: Impact of fin surface area and c.o.g. position on dutch-roll dynamics.

$$\omega_0 = V \cdot \sqrt{\frac{\rho S l}{2C}} \sqrt{\frac{|C_{Y\beta,fin}|}{S_{D,nom}}} \cdot \sqrt{|x_{SD}| \cdot S_D} \quad (7.15)$$

$$\xi = \sqrt{\frac{\rho S C}{8l}} \sqrt{\frac{|C_{Y\beta,fin}|}{S_{D,nom}}} \cdot \left( \frac{l^2}{C} |x_{SD}|^{3/2} + \frac{1}{m} \cdot \frac{1}{\sqrt{|x_{SD}|}} \right) \cdot \sqrt{S_D} \quad (7.16)$$

Hence, damping ratio and frequency evolve with:

$$\begin{cases} \omega_0 = k_1 \cdot \sqrt{|x_{SD}| \cdot S_D} \\ \xi = k_2 \cdot \sqrt{|x_{SD}| \cdot S_D} \cdot \left( \frac{l^2}{C} \cdot |x_{SD}| + \frac{1}{m} \cdot \frac{1}{|x_{SD}|} \right) \end{cases} \quad (7.17)$$

where  $k_1$  and  $k_2$  regroup flight attitude and aircraft dependent factors.

According to these formulas, fin lever arm and fin size have the same impact on the dutch-roll frequency. A shorter lever arm, which corresponds to a more aft c.o.g. position, decreases the oscillation frequency. So does also a smaller fin surface area. As concerns the damping ratio, the evolution is less obvious: it comprises the evolution of  $\omega_0$  which is

then multiplied by a term relating mass, inertia, and c.o.g. position.

Figure 7.1.2 shows how frequency and damping evolve with a parameter variation for the DC8 and VELA aircraft. The differences in frequency and damping ( $\Delta\omega_0$ ,  $\Delta\xi$ ) are displayed. We notice that the effect of changing the c.o.g. is much more important for the BWB aircraft. Moving the c.o.g. aft causes a considerable loss in damping and frequency. The fin size has its main impact on the frequency, causing a 1 Hz rise for a 50% larger fin. Damping varies by some 30%.

*Remember:* As mentioned before, due to the simplified analytical expressions these results are only reliable if the aircraft is not close to the transition stability–instability. This will be verified later on with the numerical analysis.

### 7.1.3 Roll Motion

An approximation for the roll motion is given by the following equation:

$$\begin{pmatrix} \dot{p} \\ \dot{\phi} \end{pmatrix} = \begin{bmatrix} L_p & 0 \\ 1 & 0 \end{bmatrix} \begin{pmatrix} p \\ \phi \end{pmatrix} + \begin{bmatrix} L_{\delta l} & L_{\delta n} \\ 0 & 0 \end{bmatrix} \begin{pmatrix} \delta l \\ \delta n \end{pmatrix} \quad (7.18)$$

This yields the characteristic equation:

$$\lambda(\lambda - L_p) = 0 \quad (7.19)$$

which delivers the roll time constant:

$$T_R \approx -\frac{1}{L_p} = -\frac{AV}{\bar{q}Sl^2Cl_p} = -\frac{2A}{\rho Sl^2VCl_p} \quad (7.20)$$

**Influence of fin surface area and c.o.g. position.** As  $Cl_p$  is virtually unaffected by these parameters, the roll time constant will not be influenced by any change in surface or position.

### 7.1.4 Spiral Motion

It is assumed that weight and centrifugal force in the body frame y-axis are balanced. For small angles, the following can be assumed [8, 22]:

$$\begin{aligned} g\phi &\approx Vr \\ Y_\beta\beta &\approx 0 \\ \dot{\beta} &\approx 0 \end{aligned}$$

The spiral motion is then approximated with the homogeneous state-equation:

$$\begin{pmatrix} 0 \\ \dot{r} \\ \dot{p} \\ \dot{\phi} \end{pmatrix} = \begin{bmatrix} 0 & -1 & 0 & \frac{g}{V} \\ N_\beta & N_r & N_p & 0 \\ L_\beta & L_r & L_p & 0 \\ 0 & 0 & 1 & 0 \end{bmatrix} \begin{pmatrix} \beta \\ r \\ p \\ \phi \end{pmatrix} \quad (7.21)$$

This yields the characteristic equation:

$$\lambda^2 - \lambda \left( L_p - \left( N_p - \frac{g}{V} \right) \frac{L_\beta}{N_\beta} \right) + \frac{g}{V} \frac{1}{N_\beta} (N_r L_\beta - N_\beta L_r) = 0 \quad (7.22)$$

This equation incorporates the roll dynamics as well, so it corresponds to

$$\left( \lambda + \frac{1}{T_R} \right) \left( \lambda + \frac{1}{T_S} \right) = \lambda^2 + \left( \frac{1}{T_R} + \frac{1}{T_S} \right) \lambda + \frac{1}{T_R T_S} = 0 = \lambda^2 + a_1 \lambda + a_0$$

Comparing the coefficients with the roll motion eigenvalue  $\lambda_r = L_p \approx -\frac{1}{T_R}$ , and using the fact that  $\frac{1}{T_R} \gg \frac{1}{T_S}$  with  $\frac{1}{T_S}$  close to zero, one obtains the following approximation:

$$\begin{aligned} \frac{1}{T_R} &\approx a_1 = -L_p \left( \frac{N_p - \frac{g}{V}}{L_p} \frac{L_\beta}{N_\beta} \right) \approx L_p \\ \frac{1}{T_R} \frac{1}{T_S} &\approx a_0 = \frac{g}{V} \frac{1}{N_\beta} (N_r L_\beta - N_\beta L_r) \\ &\Rightarrow \frac{1}{T_S} = T_R \cdot \frac{g}{V} \frac{1}{N_\beta} (N_r L_\beta - N_\beta L_r) \\ &\Rightarrow T_S = \frac{V}{g} \cdot \frac{Cl_p Cn_\beta}{Cn_\beta Cl_r - Cl_\beta Cn_r} \end{aligned} \quad (7.23)$$

This translates easily into a **spiral stability criterion** (pole on the left-half plane):

$$\boxed{Cl_\beta Cn_r > Cn_\beta Cl_r} \quad (7.24)$$

since  $Cl_p Cn_\beta < 0$  and  $Cn_\beta Cl_r > 0$ .

**Influence of fin surface area and c.o.g. position.** The spiral mode is adjusted via coefficients  $Cl_\beta$  and  $Cl_r$  which refer to the dihedral effect (aircraft wings not in plane with the body frame  $x$ - $y$ -plane). Rewriting the criterion using Eq. (7.9) leads to a guideline to adjust the dihedral as a function of the c.o.g. position and the fin lever arm, respectively:

$$-Cl_\beta x_{SD}^2 C_{Y\beta,fin} \cdot \frac{S_D}{S_{D,nom}} > Cl_r x_{SD} C_{Y\beta,fin} \cdot \frac{S_D}{S_{D,nom}} \quad (7.25)$$

$$Cl_\beta > -\frac{Cl_r}{x_{SD}} \quad (7.26)$$

The corresponding simplified time constant expression is then:

$$T_S = \frac{V}{g} \cdot \frac{Cl_p}{x_{SD} Cl_\beta + Cl_r} \quad (7.27)$$

In this simplified representation, as the reader might notice, the surface of the vertical fin does not influence the spiral time constant which lets us see Eq. (7.27) with some skepticism. The influence of the fin size will be verified numerically in the next section.

Still, it is interesting to assess the spiral stability criterion. According to the norm, the bank angle must not double within 12 s starting from an initial  $\phi = 20^\circ$ , [96, 30]. Translating this into analytical terms will approximately give (assuming that the spiral pole is in the positive half plane, hence unstable):

$$\begin{aligned} \dot{\phi}(t) - \lambda_S \phi(t) &= 0, \quad \phi(0) = \phi_0 \\ \Rightarrow \phi(t_1) &= \phi_0 \cdot e^{\lambda_S t_1} \\ \phi(t_2) &= 2 \cdot \phi_0 \cdot e^{\lambda_S t_2} \\ \Rightarrow \lambda_S &= \frac{\ln 2}{t_2 - t_1} \end{aligned} \quad (7.28)$$

This yields:

$$\boxed{-\frac{1}{T_S} \approx \frac{g}{V} \cdot \frac{x_{SD} Cl_\beta + Cl_r}{Cl_p} < \frac{\ln 2}{12 \text{ s}} \approx 0.058 \text{ s}^{-1}} \quad (7.29)$$

### 7.1.5 Generic Modeling of a Roll Maneuver

The previous paragraphs have dealt with the analytical description of the lateral dynamics of the aircraft. This description allows for an analysis with respect to modal handling criteria, considering the fin size and the c.o.g. position as parameters.

Other important lateral certification criteria are presented in form of maneuvers. These are basically roll maneuvers the aircraft has to carry out under certain conditions, e.g. at  $V_{MC}$  or  $V_2$  with one engine non-operational. In this context, especially roll maneuvers in direction of the non-operational engine are of interest for the following reason: as an initial condition, the rudder will be fully deflected to counter the engine induced yaw momentum. Hence, side slip cannot be controlled during the roll maneuver and its increase might be unacceptably high. It is thus interesting to use a generic analytical description of a roll

maneuver in order to examine the sensitivity of the aircraft to these criteria with varying parameters.

Two simplifying assumptions are made:  $\alpha = \theta = 0^\circ$  and  $Y_{\delta l} = 0$ . From Eq. (7.7) we obtain the linearized lateral dynamics system:

$$\begin{pmatrix} \dot{\beta} \\ \dot{r} \\ \dot{p} \\ \dot{\phi} \end{pmatrix} = \begin{bmatrix} \frac{Y_\beta}{V} & -1 & 0 & \frac{g}{V} \\ N_\beta & N_r & N_p & 0 \\ L_\beta & L_r & L_p & 0 \\ 0 & 0 & 1 & 0 \end{bmatrix} \begin{pmatrix} \beta \\ r \\ p \\ \phi \end{pmatrix} + \begin{bmatrix} 0 & \frac{Y_{\delta n}}{V} \\ N_{\delta l} & N_{\delta n} \\ L_{\delta l} & L_{\delta n} \\ 0 & 0 \end{bmatrix} \begin{pmatrix} \delta l \\ \delta n \end{pmatrix} \quad (7.30)$$

The pilot will give a stick command to perform a roll. This command translates into a roll rate command, with  $p_0$  being the roll rate objective. The goal is therefore to analytically describe a roll maneuver with a commanded roll rate  $p_0$ . Considering the pure roll motion, with  $p_0$  as entry, Eq. (7.18) gives

$$\begin{pmatrix} \dot{p} \\ \dot{\phi} \end{pmatrix} = \begin{bmatrix} L_p & 0 \\ 1 & 0 \end{bmatrix} \begin{pmatrix} p \\ \phi \end{pmatrix} + \begin{bmatrix} -L_p \\ 0 \end{bmatrix} p_0 \quad (7.31)$$

Remember that  $L_p < 0$ .

Comparing the  $\dot{p}$ -expressions in Eqs. (7.30) and (7.31) leads to the following expression of the necessary aileron deflection  $\delta l$  to obtain roll rate  $p_0$ :

$$\delta l = -\frac{L_\beta}{L_{\delta l}}\beta - \frac{L_r}{L_{\delta l}}r - \frac{L_{\delta n}}{L_{\delta l}}\delta n - \frac{L_p}{L_{\delta l}}p_0 \quad (7.32)$$

Substituting the aileron deflection  $\delta l$  in the lateral equation system, Eq. (7.30), with the above expression yields:

$$\begin{pmatrix} \dot{\beta} \\ \dot{r} \\ \dot{p} \\ \dot{\phi} \end{pmatrix} = \begin{bmatrix} \frac{Y_\beta}{V} & -1 & 0 & \frac{g}{V} \\ N_\beta - \frac{N_{\delta l}}{L_{\delta l}}L_\beta & N_r - \frac{N_{\delta l}}{L_{\delta l}}L_r & N_p & 0 \\ 0 & 0 & L_p & 0 \\ 0 & 0 & 1 & 0 \end{bmatrix} \begin{pmatrix} \beta \\ r \\ p \\ \phi \end{pmatrix} + \begin{bmatrix} 0 & \frac{Y_{\delta n}}{V} \\ -\frac{N_{\delta l}}{L_{\delta l}}L_p & N_{\delta n} - \frac{N_{\delta l}}{L_{\delta l}}L_{\delta n} \\ -L_p & 0 \\ 0 & 0 \end{bmatrix} \begin{pmatrix} p_0 \\ \delta n \end{pmatrix} \quad (7.33)$$

Finally, state variables  $\beta$  and  $r$  can be expressed in terms of the roll rate and bank angle. Since the roll rate derivative  $\dot{p}$  and bank angle derivative  $\dot{\phi}$  were modeled with the

pure roll motion a solution is found easily:

$$\begin{cases} \dot{p} = L_p \cdot (p - p_0) \\ \dot{\phi} = p \end{cases} \xrightarrow{f} \begin{cases} p = p_0 - p_0 e^{-\frac{t}{T_R}} \\ \phi = p_0 \cdot (t - T_R) + p_0 \cdot T_R \cdot e^{-\frac{t}{T_R}} \end{cases} \quad (7.34)$$

with  $T_R = -\frac{1}{L_p}$ . Formulating  $\dot{\beta}$  and  $\dot{r}$  in terms of  $p$  and  $\phi$  leads to:

$$\begin{pmatrix} \dot{\beta} \\ \dot{r} \end{pmatrix} = \begin{bmatrix} \frac{Y_\beta}{V} & -1 \\ N_\beta - \frac{N_{\delta l}}{L_{\delta l}} L_\beta & N_r - \frac{N_{\delta l}}{L_{\delta l}} L_r \end{bmatrix} \begin{pmatrix} \beta \\ r \end{pmatrix} + \begin{bmatrix} 0 & \frac{Y_{\delta n}}{V} \\ -\frac{N_{\delta l}}{L_{\delta l}} L_p & N_{\delta n} - \frac{N_{\delta l}}{L_{\delta l}} L_{\delta n} \end{bmatrix} \begin{pmatrix} p_0 \\ \delta n \end{pmatrix} + \begin{bmatrix} \frac{g}{V} \cdot \phi \\ N_p \cdot p \end{bmatrix} \quad (7.35)$$

And with Eq. (7.34) this gives:

$$\begin{pmatrix} \dot{\beta} \\ \dot{r} \end{pmatrix} = \begin{bmatrix} \frac{Y_\beta}{V} & -1 \\ N_\beta - \frac{N_{\delta l}}{L_{\delta l}} L_\beta & N_r - \frac{N_{\delta l}}{L_{\delta l}} L_r \end{bmatrix} \begin{pmatrix} \beta \\ r \end{pmatrix} + \begin{bmatrix} -\frac{g}{V} T_R & \frac{Y_{\delta n}}{V} \\ N_p - \frac{N_{\delta l}}{L_{\delta l}} & N_{\delta n} - \frac{N_{\delta l}}{L_{\delta l}} L_{\delta n} \end{bmatrix} \begin{pmatrix} p_0 \\ \delta n \end{pmatrix} + \begin{bmatrix} \frac{g}{V} p_0 \cdot (t - T_R e^{-\frac{t}{T_R}}) \\ -N_p \cdot p_0 \cdot e^{-\frac{t}{T_R}} \end{bmatrix} \quad (7.36)$$

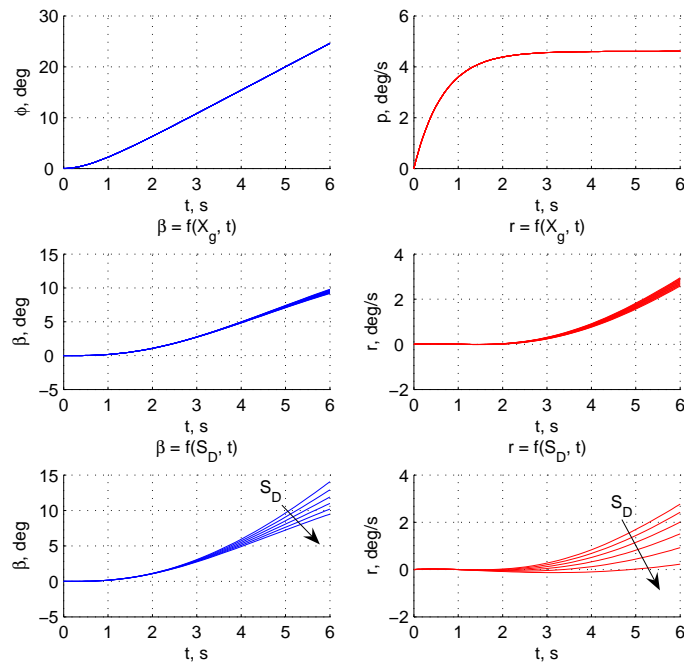
This equation can now be solved numerically with initial conditions set to zero ( $\beta_0 = r_0 = 0$ ).

The necessary roll rate to command is calculated as follows:

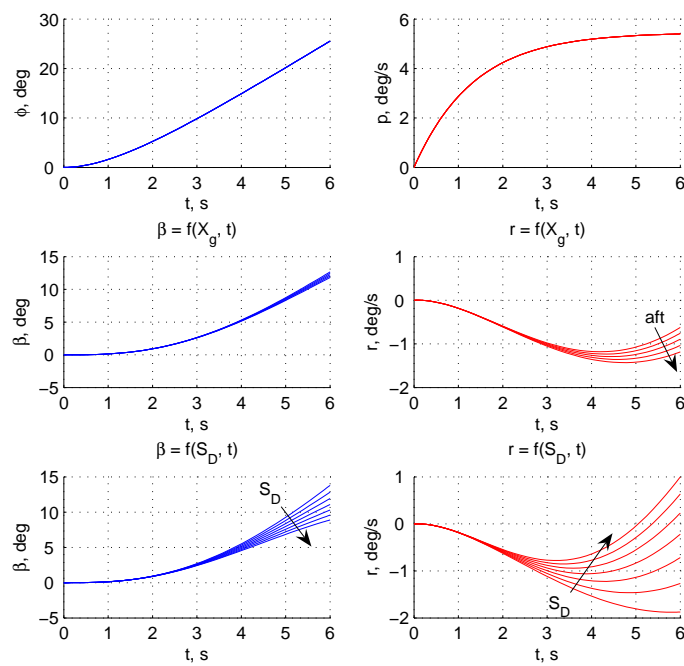
$$p_0 = \frac{\phi_{obj}}{t_{obj} - T_R + T_R e^{-\frac{t_{obj}}{T_R}}} \stackrel{T_R \ll t_{obj}}{\approx} \frac{\phi_{obj}}{t_{obj} - T_R} \quad (7.37)$$

Here,  $\phi_{obj}$  equals the bank angle to be attained in maneuver time  $t_{obj}$ . The next simulations which stem from the analytical maneuver description incorporate a bank angle objective of  $20^\circ$  in 5 s. Since the roll mode itself has been decoupled it is completely untouched by fin or c.o.g. variations.

For both aircraft (Figures 7.2(a) and 7.2(b)), a significant increase in sideslip angle  $\beta$  of the order of  $10^\circ$  occurs. When considering that this increase has to be added to an initial bank angle due to the  $V_{MC}$  equilibrium this evolution is problematic. A variation of the center of gravity position has potentially a negligible impact onto roll maneuvers.



(a) DC8



(b) VELA

Figure 7.2: Influence of c.o.g. position and fin size on sideslip during roll maneuvers.

## 7.2 Numerical Assessment of Dynamic Criteria

After a preliminary analytical assessment of the lateral aircraft dynamics with varying fin size and varying position of the center of gravity, thus considering a reduced natural stability, the relevant certification criteria are now assessed numerically with the complete aircraft models.

The results are shown for a neutral c.o.g. position,  $dx_g = 0\%$ , and a reduced mass, i.e. of  $63t$  for the classical DC8 airplane and  $550t$  for the VELA BWB. All simulations are carried out with SIMULINK. The initial equilibrium is calculated as shown in Chapter 2. The maneuvers are then simulated with the simplified nonlinear aircraft model. The control surface deflections (ailerons  $\delta l$  and rudder  $\delta n$ ) are limited to  $\pm 30^\circ$  each.

### 7.2.1 Modal Evolution

A handling quality criterion to be met is a minimum damping ratio of 10% for the dutch-roll motion. If this cannot be achieved ‘naturally’ a control system, e.g. a back-up yaw-damper unit, has to be implemented to assure this minimum damping ratio. Figure 7.3 displays the evolution of the lateral modes of the aircraft with a variation of the fin size.

The aircraft model is linearized at the minimum control speed for the nominal fin size. Then the modal evolution of the dutch-roll poles is traced as a function of a varying fin size<sup>1</sup>.

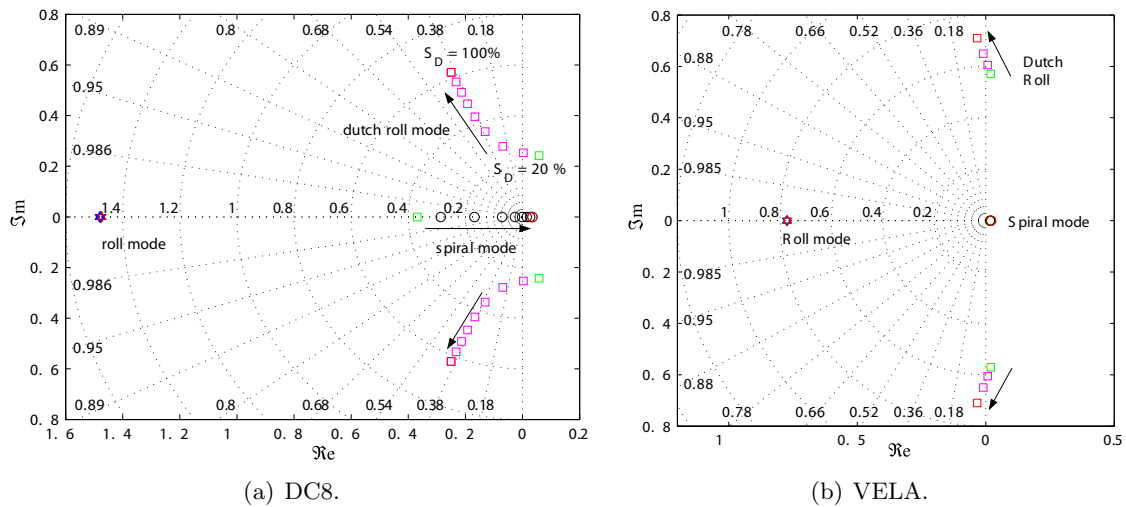


Figure 7.3: Lateral modes as a function of the vertical fin size. DC8: linearized at  $V = 44\text{ m/s} = V_{MC}$  for  $S_D = 100\%$ ,  $S_D$  steps in 10%. VELA:  $V = V_{MC_1} = 76\text{ m/s}$ ,  $S_D = 2 \times (45\text{ m}^2, 64\text{ m}^2, 90\text{ m}^2, \text{ and } 128\text{ m}^2)$ .

<sup>1</sup>Actually, the aircraft would need to be linearized at the corresponding equilibrium  $V_{MC}$  to each fin size. The linearization inaccuracy due to the small change in speed is negligible.

**DC8:** The dutch roll damping is practically constant at about 38% for a fin surface reduction of up to 50%. Up to this point, mainly the frequency of the dutch roll mode is reduced by reducing the fin area. A further reduction leads to instability at 30% of the nominal size.

The roll mode is virtually not influenced whereas the impact on the spiral mode is clearly visible. A smaller fin size leads to stabilization of the spiral mode. The mode becomes stable between 70% and 80% of  $S_D$ . Thus, the simplified analytical expression Eq. (7.27) is not valid for this classical aircraft.

**VELA:** Except for the largest fin size the VELA aircraft is unstable in the dutch-roll mode. Both damping (slightly) and frequency (mainly) are influenced by the fin area. The roll mode of the aircraft stays unaffected as well as the spiral mode. Here, the analytical expressions are coherent with the VELA aircraft modeling.

### 7.2.2 1st Maneuver

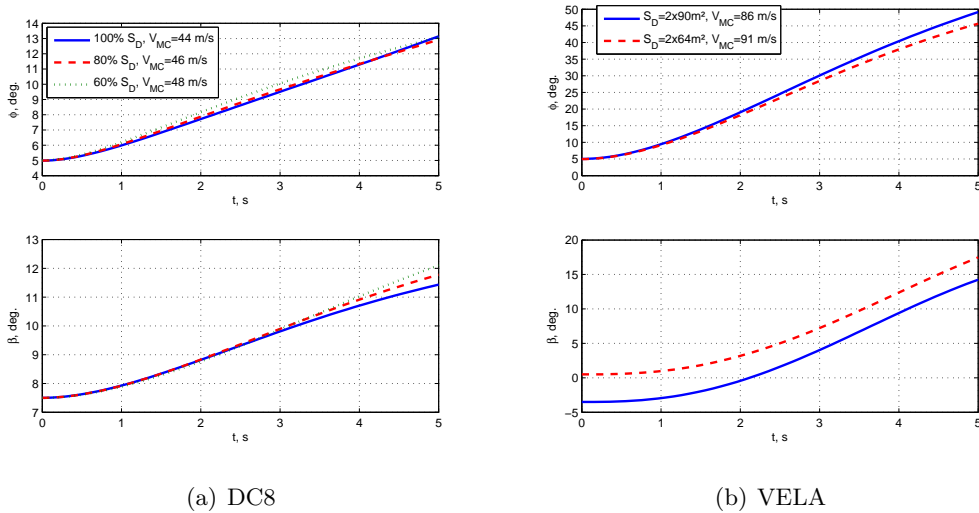


Figure 7.4: 1st  $V_{MC}$  maneuver. Indicated speeds denote the initial  $V_{MC}$  equilibrium.

Following the criterion definition given in Chapter 2, the aircraft has to roll in direction of the operational engines (with one external engine inoperative) beginning at an equilibrium at  $V_{MC}$  (thus with the rudder fully deflected to compensate the engine momentum). The bank angle has to increase by  $20^\circ$  in less than 5 s. The corresponding equilibrium speeds are shown in Figure 7.4.

**DC8: Figure 7.4(a).** This maneuver cannot be realized under the presented conditions. The speed of the initial equilibrium at  $V_{MC}$  is too slow and therefore aerodynamic surfaces are not efficient enough to create a sufficient roll rate. An augmentation in speed is still possible since any speed that is smaller as  $V_{2min}$  can be certified as minimum control

speed. The aircraft realizes the criterion for speeds  $V \geq 50 \text{ m/s}$  with the largest fin size ( $S_D = 100\%$ ). This slightly higher speed also reduces the side slip angle during the maneuver.

**VELA: Figure 7.4(b).** The time responses for two different sizes of the vertical tailplane are presented. The criterion is easily realized. The initial equilibriums were chosen to be classical, i.e. limited by maximum bank angle and rudder deflection. The aircraft flies thus within the upper domain (compare with Section 6.4).

**Reduction of the Fin Size.** A smaller fin size leads to a slight increase in sideslip angle and some minor oscillations in bank. The occurrence of these lateral-directional oscillations is linked to a reduced lateral dynamic stability due to a smaller fin size. Compare with Section 7.2.1 where the direct relation of fin size and dynamic stability is shown. Still, a fin size increase is disproportionate to the achieved sideslip reduction.

What is important to notice is that, since the rudder is already fully deflected, the sideslip angle cannot be controlled any further when rolling in the direction of the operational engines. This issue has been addressed in Section 7.1. The analytical results already gave a hint of the sideslip development. It will thus be very important to be able to equilibrate the aircraft with small sideslip angles before performing roll maneuvers. Furthermore, it will be crucial to give the rudder a control authority margin, in order for a stability augmentation system to guarantee dynamic stability.

### 7.2.3 2nd Maneuver

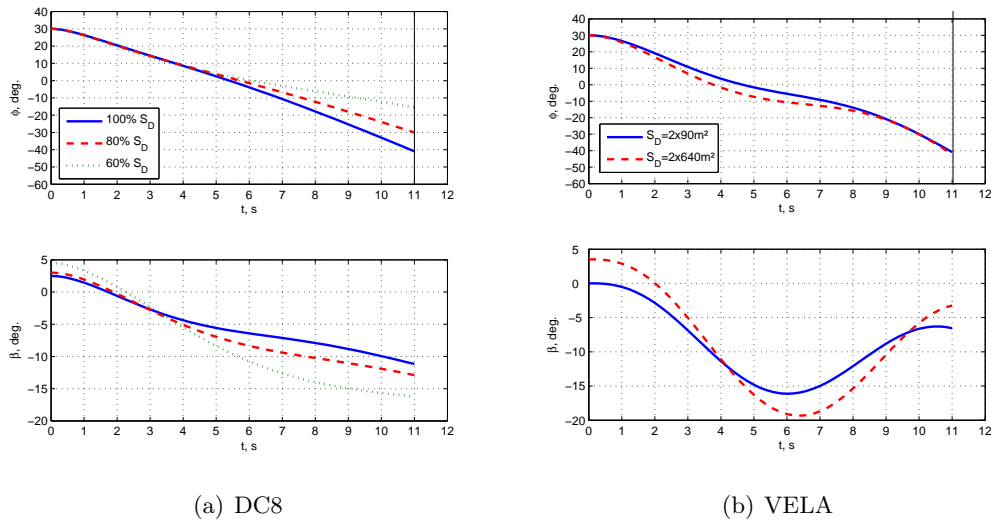


Figure 7.5: 2nd  $V_{MC}$  maneuver.

The aircraft has to roll  $60^\circ$  roll in 11 s in direction of the non-operational engine starting from  $30^\circ$  in bank. The speed for the initial equilibrium is set to  $V_{2min} = 52.5 \text{ m/s}$

(DC8) and  $V_{2min} = 81.5 \text{ m/s}$  (VELA) according to the criterion. The speeds are equal for all fin sizes since the speed is in this case related to the stalling speed  $V_S$  and hence not influenced by the fin size<sup>2</sup>. The exact conditions can be looked up in Chapter 2.

**DC8: Figure 7.5(a).** This criterion is realized except for the smallest fin size. In this maneuver, the rudder could be used to counter the growing sideslip angle since the aircraft rolls into the opposite direction. A fin size reduction leads, as before, to a decrease in roll rate and an amplification of lateral-directional oscillations. Whereas this is not critical for the two larger fin sizes, the aircraft would have to be certified with a higher  $V_{MC}$  and thus with a higher take-off related speed  $V_2$  to realize this criterion when opting for the smallest fin size.

**VELA: Figure 7.4(b).** Again, this criterion is realized. The rudder has authority to tackle upcoming oscillations in sideslip. A fin size reduction leads to significantly higher sideslip. Whereas with the larger fin size the aircraft can be equilibrated with zero sideslip, this is not possible for the smaller one. This contributes even more to an augmentation in  $\beta$ . Strong oscillations occur at all times and the use of a control system is advisable/necessary.

### 7.2.4 3rd Maneuver

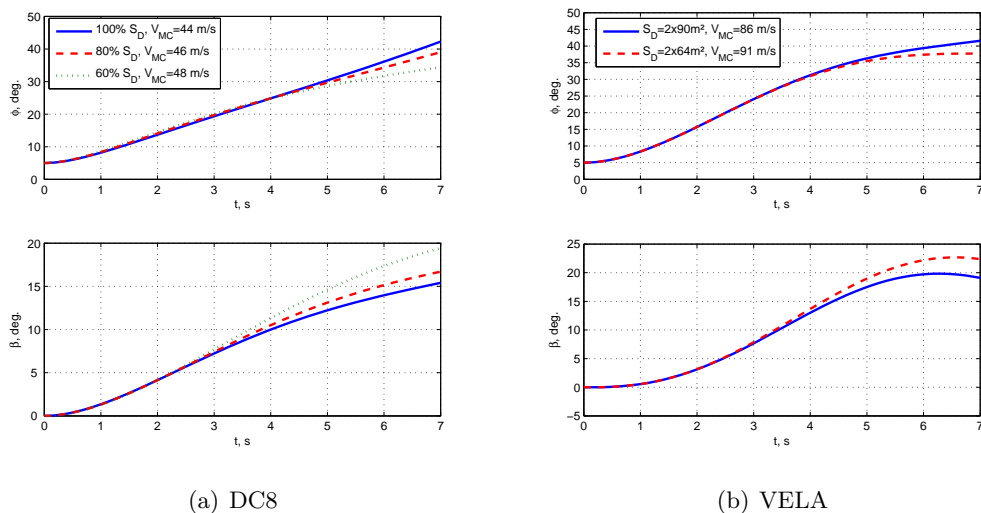


Figure 7.6: 3rd  $V_{MC}$  maneuver. Indicated speeds denote the initial  $V_{MC}$  equilibrium.

This criterion is purely related to the roll capacity of the aircraft. At  $V_{MC}$  the airplane has to be capable to perform a  $20^\circ$  roll with all engines operative. The aircraft is equilibrated at  $\phi = 5^\circ$  with zero sideslip angle since no engine momentum is induced. The rudder has full authority in both directions.

<sup>2</sup>This is true if a weight reduction due to a smaller fin size is neglected as well as any secondary lift effects of the fin for a banked aircraft.

The criterion is easily realized for all fin sizes for both aircraft. The sideslip angle increases significantly. But since the rudder has full authority, this sideslip angle would be countered either by a pilot or a control system.

**Reduction of the Fin Size.** An increase in sideslip is noticeable for the smallest fin size. The reader can guess that the pilot workload increases as well. In order to benefit from a smaller fin size the implementation of control system seems necessary.

## 7.3 Summary on Dynamic Criteria

### Classical Aircraft

The analytical and the numerical approach delivered good comparable results with regard to the dutch-roll mode. This can be ascribed to the fact that this mode is naturally stable and not close to instability. A smaller fin size leads to a reduction of the frequency but hardly influences the damping (true down to 50% of the original fin size). As regards the maneuvers, a smaller fin size is accompanied by larger sideslip angles. This is notably disturbing for roll maneuvers in direction of the operational engines, as the rudder does not have any authority to counter an augmentation in sideslip.

### VELA BWB Aircraft

Unlike the DC8 the simplified analytical expressions did not deliver good results for the dutch-roll mode (Figures 7.1.2 and 7.3). The numerical analysis revealed that the aircraft is either unstable in the dutch-roll mode or close to instability. As explained, the simplified analytical expressions are imprecise in this region of the complex plane. The numerical trace of the eigenvalues shows that the damping ratio is barely affected by a variation of the fin surface area.

The simulated maneuvers show a common point with classical aircraft: a smaller fin size leads to larger sideslip angles. Even more than for the classical aircraft this poses a problem when engine failure occurs. For all roll maneuvers in direction of the operational engines the rudder may be close to saturation. Unlike classical aircraft, the spiral mode is not affected and maneuverability stays high for all fin sizes. Moreover, a control system has to be installed to guarantee minimum handling qualities.

Two solutions to the increasing sideslip angle during rolling with a saturated rudder are thinkable. The first one is to equilibrate the aircraft at  $V_{MC}$  with less or even zero sideslip. To achieve this, the aircraft either has to have a larger fin (more mass and drag) or needs to be certified for higher take-off and landing speeds (eventually longer field length necessary). The second option would be the use of spoilers and other aerodynamic surfaces in order to tackle sideslip and keep a small fin size with a small rudder at low speeds. But this will involve new systems with their own additional weight and certification needs.

Finally, the most effective solution to reduce sidelsip for the  $V_{MC}$  equilibrium is a different engine installation closer to the  $x$ -axis of the aircraft.

Handling criteria issues (minimum damping ratio, frequency) should be handled with an automatic control system. When opting for a small fin size a simple and reliable back-up system will be needed. Designing this back-up control unit, which will guarantee acceptable flying qualities and at the same time allows for a wide range of c.o.g. positions, will be an interesting task.

## 7.4 Conclusion on Reduced Lateral Stability

This chapter has dealt with criteria that are predominantly influenced by a reduced lateral stability. The reduction of lateral stability is the consequence of reducing the size of the vertical tailplane and in some cases, when the c.o.g. is placed to aft positions. The aim of such modifications is to obtain a better performance, i.e. a more efficient aircraft. A smaller fin means less surface drag, less mass, and thus less fuel consumption. A c.o.g. which is situated around the neutral point will reduce the pitching moment of the aircraft due to the lift. Therefore the horizontal tailplane and trim drag can be reduced which again implies benefits for the performance.

The examined criteria are related to the minimum control speed  $V_{MC}$ . The  $V_{MC}$  certification requires the complex realization of several criteria which distinguish themselves by relating either to the aircraft statics or to the aircraft flight dynamics.

The static  $V_{MC}$  criteria were analyzed with an analytical and a numerical approach. For the latter a convenient visual representation has been developed which helps identifying particular constraints defining the minimum control speed. Both techniques in combination allow for a good examination of the aircraft performance w.r.t. to the  $V_{MC}$  equilibrium at an early stage of the aircraft development.

Dynamic criteria were also addressed in this bi-directional way. Preliminary analytical developments derived simple expressions to demonstrate the physical impact of a varying fin size or c.o.g. position. Nevertheless, these revealed to be insufficient and can only be considered as a compliment to simulations and parameter studies with a more complex model. This is especially true for a BWB aircraft which is constantly in (or close to) the zone of dynamic instability.

In order to exploit the potentials of the VELA BWB the most, a list of recommendations has been derived from the analysis of a reduced lateral stability for this future project aircraft (see next page).

## 7.5 Recommendation for the VELA Aircraft Design

The following suggestions are given as to take advantage of accepting a reduced lateral stability. In the following (non-exhaustive) list items can be combined to establish a trade-off:

- + Selection of a small fin size, approximately between  $2 \times 45 m^2$  to  $2 \times 64 m^2$ .
- + The range of c.o.g. positions is set around the longitudinal neutral point. To gain in flexibility the allowable center of gravity displacement shall be between  $3 m$  ( $\approx 7\%$  in  $mac$ ) fwd and  $1.5 m$  ( $\approx 5\%$  in  $mac$ ) aft.
- To compensate the degradation in handling quality, a back-up control system has to be developed which guarantees sufficient handling qualities for the given target specifications (fin, c.o.g. position) when normal flight control laws fail.
- To counter the small fin size and its short lever arm statically, the aircraft is certified for higher approach and landing speeds.

Furthermore, the following is thinkable:

- Design of a rudder with higher efficiency (e.g. double-hinged),
- Development of a control system to counteract gust effects at the fin for smaller rudder security margins,
- Development of a control system to use ailerons and spoilers to counteract engine failure rapidly in order to simplify the task of the fin and rudder without producing extra side force.

**Remark:** These recommendations are appropriate for the given BWB aircraft model. If larger modifications are thinkable then a relocation of the engines to a smaller distance to the aircraft  $x$ -axis will improve the  $V_{MC}$  performance immensely. Instead of fighting the symptoms, attacking the cause (the engine induced yaw moment) might be a fruitful approach.

The design of a back-up control law which is robust versus a large range of center of gravity positions for a highly unstable BWB aircraft is necessary. As Chapter 4 demonstrated, a reduced stability will trigger high amplitude control law activity and may cause saturation and fatigue of the control surface actuators. The design of a robust control law countering these effects is the goal of the 2nd part of this dissertation.

## Part II

# Robust Back-Up Control Design for an Aircraft with Reduced Stability



## Chapter 8

# Introduction and Control Objectives

*The second part of this dissertation is dedicated to the design of a robust back-up control law for the future aircraft concept VELA (Very Efficient Large Aircraft) which is naturally unstable in its low-speed flight domain. The design is based on a polytopic technique and assures minimum handling qualities over a wide range of center of gravity positions for both longitudinal and lateral aircraft motions.*

This chapter presents the context and poses the problem whereas Chapter 9 is dedicated to the controller design technique followed by its application in Chapter 10.

Accepting a reduced flight dynamic stability or even instability in civil aviation seems promising with regard to drag, fuel consumption, and load charge flexibility. It also allows for the installation of smaller vertical and horizontal empennages. As a consequence, the natural aircraft is not controllable in the case of a complete loss of electrical power, when stability augmentation systems fail. Therefore, an autonomously operating back-up control system has to be developed which guarantees minimal flying qualities. The operational demands for such a back-up system are more sophisticated than those on current back-up systems (e.g. autonomous Back-Up Yaw Damper Units - BYDUs), as the degree of instability rapidly triggers accelerations of high amplitude of the natural aircraft when disturbances, such as turbulence, occur. Still, the system ought to be as simple as possible.

The control system will be designed for the future aircraft concept VELA1<sup>1</sup>, representing a two-tailed blended wing-body configuration. The VELA1 concept is very sensitive to c.o.g. displacements in the longitudinal motion and unstable in its dutch-roll mode during low-speed flight due to a reduced size of the vertical tail-plane, as shown by [35, 91, 34].

---

<sup>1</sup>See Section 2.2 for details on the VELA1 aircraft.

The linear and nonlinear characteristics of the elevator, rudder, and aileron actuators are considered, including amplitudes of position and rate outputs as well as the associated saturations.

Section 8.1 first gives the basic facts on the aircraft modeling. Then it presents the necessary modifications for the control design. Section 8.2 discusses the objectives for the back-up controller and condenses into a list of requirement specifications.

## 8.1 Aircraft Modeling

For the aerodynamic model, validated numerical data were directly drawn from the VELA project. The low-speed aerodynamic data ensure modeling at a very detailed level for the flight phases of interest (take-off/approach) (additional information can be found in Chapter 2 and Appendix A).

### 8.1.1 Aircraft Model

For the flight mechanical model, the general rigid body equations of motion are considered. Reference data of the blended wing-body civil transport concept are listed once more in Table 8.1.

|  |     |       |            |       |
|--|-----|-------|------------|-------|
| Mass range   | $M$ | $\in$ | [550; 770] | $t$   |
| Reference surface                                      | $S$ | $=$   | 2012       | $m^2$ |
| Mean aerodynamic chord<br>( $\equiv$ Reference length) | $l$ | $=$   | 35.93      | $m$   |
| Wing span  | $b$ | $=$   | 99.60      | $m$   |

Table 8.1: VELA Reference Values

The **aerodynamic data** are parametrized as a function of the dimensionless displacement of the c.o.g. position  $X_g$ :

$$dx_g = \frac{X_g - X_{ref}}{l} \quad (8.1)$$

along the aircraft  $x$ -axis.  $X_{ref}$  is the reference point placed at 30.7% of the mean aerodynamic chord  $l$ .  $dx_g$  is thus negative for c.o.g. positions forward of the reference point and positive for aft positions.

The longitudinal static margin at low speed ( $Mach = 0.2$ ) and zero altitude is approximately zero for  $X_g = X_{ref}$ , thus  $dx_g = 0$ . The  $dx_g$  parametrization allows thus for a simple differentiation between longitudinally stable cases ( $dx_g < 0$ , fwd) and unstable cases ( $dx_g > 0$ , aft).

The state vector  $X$  of the complete nonlinear model has nine state variables

$$X = (V, \alpha, \beta, \theta, \phi, p, q, r, h)^T \quad (8.2)$$

where  $V$  is the aerodynamic speed and  $h$  the altitude. The outputs of the model include the load factors  $n_x$ ,  $n_y$  and  $n_z$  in the body frame.

The **equilibrium** is chosen to be straight, level, symmetric flight at zero altitude  $h$  (take-off, approach), low speed ( $Mach = 0.2$ ), low mass  $M = 550 t$ , and with  $\dot{h} = V_z = 0$  m/s. The system dynamics are linearized at the equilibrium:

$$f(X_{eq}, u_{eq}) = 0 \quad (8.3)$$

where  $f(X, u)$  computes the derivative of the state vector  $\dot{X} = dX/dt$  as a function of state  $X$  and inputs  $u$ .

### 8.1.2 Linearized Longitudinal and Lateral Systems

After linearization, the aforementioned full state-space representation can be transformed and reduced to a two-state longitudinal system  $(\alpha, q)$  with vertical wind ( $w_z$ ) and elevator ( $\delta m_c$ ) as inputs, as well as a four-state lateral system  $(\beta, r, p, \phi)$ , with lateral wind ( $w_y$ ), aileron ( $\delta l_c$ ), and rudder ( $\delta n_c$ ) inputs.

When assuming that the aircraft is in back-up mode, no sophisticated  $\alpha$ - or  $\beta$ -estimation can be expected. Since acceleration measurements are quite reliable and relatively simple to perform, the state-space representation is transformed in order to describe horizontal and vertical load factors  $n_y$  and  $n_z$  (normally included in the output vector  $Y$ ) as pseudo-system states  $\tilde{n}_y$  and  $\tilde{n}_z$  in  $\tilde{X}_{lat}$  and  $\tilde{X}_{lon}$ , respectively.

Consider the initial linear state-space model:

$$\begin{aligned} \dot{X} &= A X + B_1 w + B_2 u \\ Y &= C X + D_1 w + D_2 u \end{aligned} \quad (8.4)$$

Decoupled in longitudinal and lateral motions, the states, outputs, and control and exogenous (wind) inputs are:

$$X_{lon} = (\alpha, q)^T \quad Y_{lon} = (n_z, q)^T \quad w_{lon} = w_z \quad u_{lon} = \delta m_c \quad (8.5)$$

$$X_{lat} = (\beta, r, p, \phi)^T \quad Y_{lat} = (n_y, r, p, \phi)^T \quad w_{lat} = w_y \quad u_{lat} = (\delta l_c, \delta n_c)^T \quad (8.6)$$

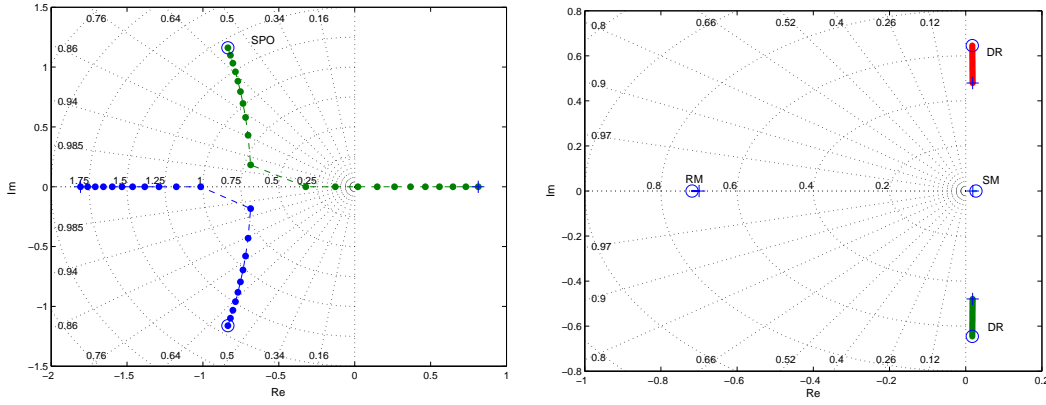


Figure 8.1: Open-loop poles for  $dx_g = -10\%$  fwd ( $\circ$ ) to  $dx_g = +10\%$  aft ( $+$ ). Left: Longitudinal system. SPO = Short-Period Oscillation. Right: Lateral System. DR = Dutch Roll, SM = Spiral Mode, RM = Roll Mode.

Introducing  $\tilde{X} = C X$  yields:

$$\begin{aligned}\dot{\tilde{X}} &= \underbrace{CAC^{-1}}_{\tilde{A}} \tilde{X} + \underbrace{CB_1}_{\tilde{B}_1} w + \underbrace{CB_2}_{\tilde{B}_2} u \\ Y &= \tilde{X} + D_1 w + D_2 u\end{aligned}\quad (8.7)$$

with

$$\tilde{X}_{lon} = (\tilde{n}_z, q)^T \quad (8.8)$$

$$\tilde{X}_{lat} = (\tilde{n}_y, r, p, \phi)^T \quad (8.9)$$

The open-loop poles of the resulting two linear state-space models are given in Figure 8.1 as a function of the c.o.g. displacement  $dx_g$ .

**Remark:** The final plant model for the controller design will incorporate first-order transfer functions modeling elevator, rudder, and aileron actuators. As a consequence, the resulting transfer matrix between control inputs and system outputs is strictly proper. Remaining entries in matrix  $D$  only denote the feedthrough of the wind input, which are neglected for the controller synthesis. More details are given in the next section.

### 8.1.3 Plant Model for Controller Synthesis

Systems incorporating symmetric saturation nonlinearities can easily be rewritten so as to incorporate the complementary dead-zone nonlinearity (indicated in Figure 8.2). This is relevant since the output of the dead-zone nonlinear operator  $\phi(\cdot)$  is null when no saturation occurs and thus the closed-loop state matrix  $A_{cl}$  describes the nominal (linear)

behavior of the system including any stabilizing control laws. This  $A_{cl}$  matrix is therefore Hurwitz. This modification is needed for the controller design as well as for the stability analysis. Section 5.2.2 already demonstrated this transformation in order to apply the Popov/circle criterion.

The complete plant model is shown in Figure 8.3. Indeed, the transfer function block  $G(s)$ , into which the longitudinal and lateral linearized systems are injected, is preceded by a first-order linear actuator model. This actuator model is built in feedback form in order to have direct access to the actuator rate (which is the input to the integrator). A dead-zone nonlinearity is placed between  $z_2$  and  $w_2$  and fulfills the function of the actuator rate saturation.

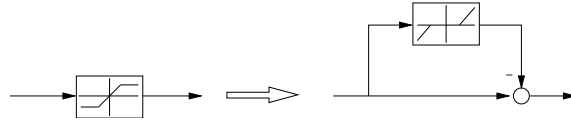


Figure 8.2: Transformation of saturation into dead-zone nonlinearity.

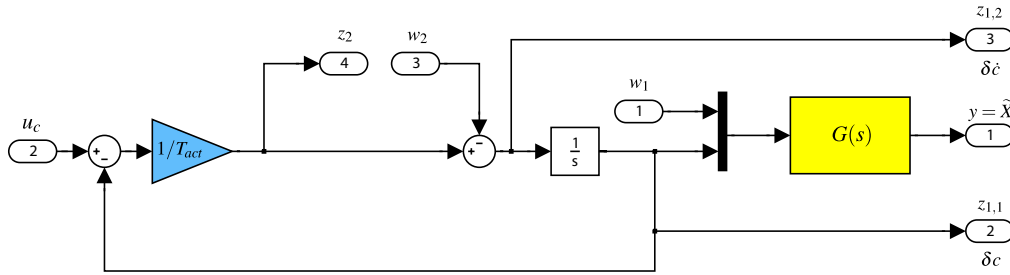


Figure 8.3: Plant model used for controller design.

The actuator model corresponds to a transfer function

$$H_{act}(s) = \frac{1}{T_{act}s + 1} \quad (8.10)$$

where  $T_{act} = 0.06$  s. For more information on why this actuator model has been chosen, kindly refer to Section 4.1.

According to the respective dynamics, the complete plant has three states in the longitudinal motion and six states in the lateral one (including the actuator states):

$$\mathcal{X}_{lon} = \underbrace{(\tilde{n}_z, q, \delta c_{lon})^T}_{\tilde{X}_{lon}} \quad (8.11)$$

$$\mathcal{X}_{lat} = \underbrace{(\tilde{n}_y, r, p, \phi, \delta c_{lat})^T}_{\tilde{X}_{lat}} \quad (8.12)$$

with

$$\delta c_{lon} = \delta m \quad (8.13)$$

$$\delta c_{lat} = (\delta l, \delta n)^T \quad (8.14)$$

Due to the presented modifications the problem turns out to be very close to a state-feedback one. Thus, the state-feedback controller is computed according to

$$u_c = K \cdot \begin{bmatrix} \tilde{X} \\ \delta c \end{bmatrix} \quad (8.15)$$

with respect to Figure 8.3. The feedback on the actuator position(s)  $\delta c$  will be zeroed *a posteriori*. The final controller  $K^*$  can then be applied to the original linear models as well as to the nonlinear model as

$$u_c = K^* \cdot Y \quad (8.16)$$

for validation purposes. One has to note that, since synthesis and validation model are different, it has to be verified *a posteriori* that the input/output criteria are realized when implementing the final controller in the validation model. As will be demonstrated, the performance does not suffer from this manipulation.

The design demands based on the presented plant for the longitudinal and the lateral aircraft controllers are subject of the next section.

## 8.2 Control Objectives

### 8.2.1 Summing Up

Part I of this dissertation delivers the analysis of the flight mechanics and dynamics influenced by a reduced natural stability of the aircraft. To exploit the potentials that lie within accepting a reduced stability, recommendations were given that are transformed here into a list of requirements for a stabilizing back-up control law.

The configuration retained is the VELA aircraft with a wide range of accessible center of gravity positions and a drastically reduced size of the vertical tailplane. This will allow for less structural mass and area drag (and hence less fuel burn) as well as more flexibility with regard to load charges. Placing the c.o.g. in the proximity to the aircraft's neutral point ( $dx_g \approx 0$ ) will reduce trim drag significantly.

This leads to four distinguishable groups of requirements:

- At low speed (i.e. the critical approach and landing phases), the aircraft is longitudinally unstable for aft and laterally for all c.o.g. positions. But official norms require minimum handling qualities for certification. The back-up controller must therefore guarantee the specified handling qualities for each allowable c.o.g. position.

- As shown in Chapter 4, c.o.g. positions distant from the neutral point trigger disadvantageously high actuator activity of the artificially stabilized airplane in turbulent atmosphere. Notably, aft positions cause high amplitudes in actuator position and rate. As a result, the actuators will suffer from strongly increased fatigue damage compared to a stable configuration with small c.o.g. ranges. It is thus necessary to incorporate a reduction of actuator activity as a control objective.
- Since the unstable configuration triggers high actuator activity, the actuators are likely to saturate. It must therefore be guaranteed that the system stays stable in case of saturation. The stability in the presence of saturation is hence the third objective.
- Finally, the control law obtained is to be as simple as possible. Since a back-up system is conceived no sophisticated gain scheduling or dynamic controllers are considerable. Still, all above points have to be realized.

Translating this list into automatic control vocabulary leads to distinguishing modal and input/output (I/O) criteria. Furthermore, the controller would ideally be static and robust over the whole range of c.o.g. positions at the same time.

### 8.2.2 Control Objectives

The following list represents the specifications for both longitudinal and lateral controllers w.r.t. the plant model shown in Figure 8.3 in Section 8.1:

1. The closed-loop poles should stay inside a defined region of the complex plane, to fulfill the *handling quality* requirements.
2. The *single, fixed, static controller* should be *robust* for a fixed target range of c.o.g. positions:

$$dx_g \in [-7\%; +5\%] \quad (8.17)$$

to stay within limits that make sense in the flight-mechanical context of this aircraft, [35]. Gain scheduling is to be avoided.

3. In order to keep *actuator activity* to a minimum, the  $H_\infty$  norm of the transfer function  $T_{w_1 \rightarrow z_1}$  between the wind input and the actuator position and rate outputs is limited to  $\gamma_1$ . See Section 9.2 for a definition of the  $H_\infty$  norm.
4. To ensure *stability in the presence of actuator saturations* a positivity objective<sup>2</sup>  $\gamma_2$  is considered for the transfer function  $T_{w_2 \rightarrow z_2}$ . The resulting domain of attraction is to be of sufficient size. For details on the positivity criterion, refer to Section 9.2.

---

<sup>2</sup>Section 5.2.2 already demonstrated the idea of analyzing the positivity characteristics of the system to assess its robustness in the presence of nonlinearities. Still, it did not provide any means to modify the closed-loop positivity characteristics. This issue is treated in the next chapter.

5. Since it is a key specification to preserve as much as possible stability and performance a static anti-windup controller may be added to minimize the sensitivity of the performance of the closed-loop system to actuator saturation. See Section 9.5 for details.

The next chapter will tackle the presented problem and deliver the corresponding design technique.

## Chapter 9

# Robust Multi-Objective Feedback and Anti-Windup Design Technique

Chapter 8 concluded in specifications for a back-up control law for the future project VELA1 aircraft (see Section 8.2). These specifications call for a multi-model multi-objective approach and at the same time demand a high degree of simplicity for the final controller. This chapter is dedicated to the presentation of a design technique satisfying these requirements.

### 9.1 Introduction to the Control Philosophy

Following the specifications indicated in Section 8.2, a flight control law has to be synthesized that gives satisfactory performance on a large range of c.o.g. positions in the presence of actuator saturations. Multiple criteria have to be realized simultaneously, i.e. modal and input/output ( $H_\infty$  and positivity) criteria. Since the controller is to be implemented as a back-up system, the final control law has to be as simple as possible.

Thus, a multi-objective feedback design technique is to be used: see e.g. [84] where the longitudinal system is decoupled so that the phugoid (slow) and short period (fast) modes can be independently controlled with respectively  $H_2$  and  $H_\infty$  techniques. The obtained controllers are dynamic and scheduled as a function of the Mach number. See also [83] whose objective is to minimize an  $H_2$  criterion under a positivity robustness constraint (in the specific context of collocated control of large space structures), noting that an observed state feedback controller is designed where the observer gain is fixed, i.e. just the state feedback gain is to be synthesized. More generally, see e.g. [79, 80, 45, 33] for multi-objective design techniques of a dynamic controller.

Nevertheless, these techniques cannot be applied to our problem since a back-up con-

troller must be as simple as possible, ideally static. Moreover, a multi-model design technique must be used. In this context, the polytopic design technique [23, 16, 36] appears especially suitable since its goal is to synthesize one state-feedback controller simultaneously satisfying modal, I/O, and robustness criteria on several plant models. A convex LMI optimization problem is obtained.

An additional anti-windup scheme, see e.g. [86, 87, 101], can then be considered if the stability domain and performance of the closed-loop system are not satisfactory due to actuator saturation. Takaba [86, 87] and Wu and Soto [101] propose the design of dynamic controllers for a single plant model or an LFT one. Here, a static anti-windup controller is designed with positivity and  $H_\infty$  criteria using a simple convex multi-model design technique.

This chapter is organized as follows: Section 9.2 gives the necessary theory on how to cast the relevant criteria into an LMI form. Section 9.3 presents the actual control design technique: a *polytopic* design technique guarantees performance over a large range of center of gravity positions via a multi-objective multi-model approach. For validation purposes, Section 9.4 deals with the *a posteriori* assessment of stability and performance in the presence of actuator saturations. An LMI based technique [43, 26, 17] computes the stability domain and the tracking quality to an external performance signal of the saturated closed-loop system. Additional techniques for the stability assessment of the saturated closed-loop system are presented. If it is considered necessary to improve performance, Section 9.5 presents a design technique for a static multi-model multi-objective anti-windup controller.

## 9.2 Modal and I/O Criteria

Basically, three modal and two I/O control objectives can be distinguished, each of which can be described by an individual criterion in linear matrix inequality form. Section 9.2.1 shows how handling quality demands are translated into LMI constraints representing modal constraints. Section 9.2.2 then presents a generalized framework from which  $H_\infty$  and positivity criteria are deduced in LMI form. The  $H_\infty$  criterion corresponds to the need for a reduction of the actuator activity. Furthermore, the positivity objective is used as an indirect means to maximize the stability domain of the closed-loop system in the presence of actuator saturations. Both I/O criteria are the consequence of high actuator activity triggered by the degree of instability (as shown in Chapter 4).

### 9.2.1 Modal Criterion (Pole Placement in an LMI Region of the Complex Plane)

Handling quality demands, as stated in certification norms, are often expressed in terms of ranges of acceptable damping ratios and frequencies of a certain airplane mode. In other

words, the eigenvalues in question have to stay inside a region of the complex plane. A damping constraint is represented by a sector stretching out from the origin in direction of the negative real axis. A maximum frequency constraint is translated into a circle in the complex plane. The minimum degree of stability<sup>1</sup> constraint, resembling the half plane left to a specified real value, can be understood as a minimum response time of the system.

The intersection of these three area constraints defines a region (see Figure 9.1) which can be formulated as an LMI region [23, 24]. The following proposition presents the corresponding LMI criteria.

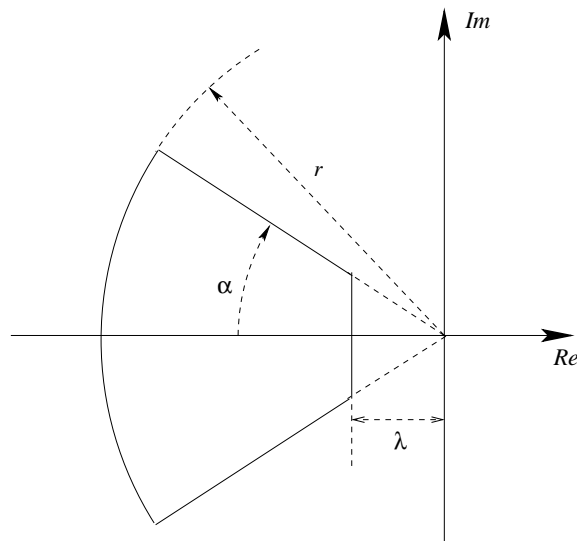


Figure 9.1: An LMI region of the complex plane.

**Proposition 9.1** *The eigenvalues of the state matrix  $A$  stay inside the LMI region of the complex plane of Figure 9.1, where  $\lambda$  is a minimal degree of stability,  $\xi = \cos(\alpha)$  a minimal damping ratio and  $r$  a maximal module/frequency, if there exists a Lyapunov matrix  $X = X^T > 0$  satisfying (see page 898 of [23]):*

$$AX + XA^T + 2\lambda X < 0 \quad (9.1)$$

$$\begin{pmatrix} -rX & AX \\ \star & -rX \end{pmatrix} < 0 \quad (9.2)$$

$$\begin{pmatrix} \sin \alpha (AX + XA^T) & \cos \alpha (AX - XA^T) \\ \star & \sin \alpha (AX + XA^T) \end{pmatrix} < 0 \quad (9.3)$$

<sup>1</sup>The degree of stability of a state matrix  $A$  is  $-\max_i \operatorname{Re}(\lambda_i)$ , where the  $\lambda_i$  are the eigenvalues of  $A$ .

or equivalently if there exists a Lyapunov matrix  $Y = Y^T > 0$  satisfying:

$$YA + A^T Y + 2\lambda Y < 0 \quad (9.4)$$

$$\begin{pmatrix} -rY & YA \\ \star & -rY \end{pmatrix} < 0 \quad (9.5)$$

$$\begin{pmatrix} \sin \alpha (YA + A^T Y) & \cos \alpha (YA - A^T Y) \\ \star & \sin \alpha (YA + A^T Y) \end{pmatrix} < 0 \quad (9.6)$$

$\star$  denotes the conjugate part of the hermitian matrix.

**Remark.** The use of a single Lyapunov function for all three criteria is not conservative since they correspond to the same LMI region [23].  $Y = X^{-1}$  in the above inequalities. Indeed, Eq. (9.4) is obtained by multiplying Eq. (9.1) on the left and on the right by  $X^{-1}$ . In the same way, Eq. (9.5) and Eq. (9.6) are obtained by multiplying Eq. (9.2) and Eq. (9.3) on the left and on the right by  $\text{blockdiag}(X^{-1}, X^{-1})$ .

## 9.2.2 U-V-W Dissipativity Criterion

The following paragraph presents a generalized framework called *U-V-W* dissipativity [80]. This framework is used to deduce and prove LMI based  $H_\infty$  and positivity criteria.

Let a state-space representation of a *stable* transfer matrix  $H(s)$  be

$$\dot{x}(t) = Ax(t) + Bw(t) \quad (9.7)$$

$$z(t) = Cx(t) + Dw(t). \quad (9.8)$$

**Definition 9.1** Given fixed matrices  $U = U^T \geq 0$ ,  $V = V^T$  and  $W$ , the state-space system (9.7),(9.8) is said to be *U-V-W dissipative* if it satisfies  $\forall T > 0$ ,  $\forall w \in L_2$  and  $x(0) = 0$

$$\int_0^T \begin{pmatrix} z(t) \\ w(t) \end{pmatrix}^T \begin{pmatrix} U & W \\ W^T & V \end{pmatrix} \begin{pmatrix} z(t) \\ w(t) \end{pmatrix} dt << 0, \quad (9.9)$$

i.e. there exists  $\epsilon > 0$  s.t.

$$\int_0^T \begin{pmatrix} z(t) \\ w(t) \end{pmatrix}^T \begin{pmatrix} U & W \\ W^T & V \end{pmatrix} \begin{pmatrix} z(t) \\ w(t) \end{pmatrix} dt \leq -\epsilon \int_0^T w^T(t)w(t)dt. \quad (9.10)$$

First note that

$$\begin{aligned} \begin{pmatrix} z(t) \\ w(t) \end{pmatrix}^T \begin{pmatrix} U & W \\ W^T & V \end{pmatrix} \begin{pmatrix} z(t) \\ w(t) \end{pmatrix} \\ = z^T(t)Uz(t) + z^T(t)Ww(t) + w^T(t)W^Tz(t) + w^T(t)Vw(t), \end{aligned}$$

so that important special cases include:

- The  $H_\infty$  norm of  $H(s)$  is less than  $\gamma$ , i.e.

$$\int_0^T z^T(t)z(t)dt < \gamma^2 \int_0^T w^T(t)w(t)dt, \quad (9.11)$$

corresponds to  $U = I$ ,  $V = -\gamma^2 I$  and  $W = 0$ , or  $U = I/\gamma$ ,  $V = -\gamma I$  and  $W = 0$ .

- $H(s)$  has dissipativity  $\gamma$ , i.e.

$$\int_0^T (w^T(t)z(t) - \gamma w^T(t)w(t)) dt > 0, \quad (9.12)$$

corresponds to  $U = 0$ ,  $V = 2\gamma I$ ,  $W = -I$ .

- $H(s)$  belongs to the sector  $[\alpha, \beta]$ , i.e.

$$\int_0^T (z(t) - \alpha w(t))^T (z(t) - \beta w(t)) dt < 0, \quad (9.13)$$

corresponds to  $U = I$ ,  $V = \alpha\beta I$  and  $W = -\frac{\alpha+\beta}{2}I$ , since  $(z(t) - \alpha w(t))^T (z(t) - \beta w(t)) = z^T(t)z(t) - \alpha w^T(t)z(t) - \beta z^T(t)w(t) + \alpha\beta w^T(t)w(t)$ .

Scherer et al. [80] (page 898) propose an LMI characterization of the  $U$ - $V$ - $W$  dissipativity.

**Proposition 9.2**  $H(s)$  is  $U$ - $V$ - $W$  dissipative if the following LMI w.r.t.  $Y = Y^T > 0$  holds

$$\begin{aligned} \begin{pmatrix} YA + A^T Y & YB \\ \star & 0 \end{pmatrix} + \begin{pmatrix} C & D \\ 0 & I \end{pmatrix}^T \begin{pmatrix} U & W \\ W^T & V \end{pmatrix} \begin{pmatrix} C & D \\ 0 & I \end{pmatrix} \\ = \begin{pmatrix} YA + A^T Y + C^T U C & YB + C^T U D + C^T W \\ \star & D^T U D + D^T W + W^T D + V \end{pmatrix} < 0. \end{aligned} \quad (9.14)$$

If  $U = Q\Sigma^{-1}Q^T$ , with  $\Sigma > 0$ , the LMI condition above can be rewritten as

$$\begin{pmatrix} YA + A^T Y & YB + C^T W & C^T Q \\ \star & D^T W + W^T D + V & D^T Q \\ \star & \star & -\Sigma \end{pmatrix} < 0. \quad (9.15)$$

**Proof.** It is only proved here that Eq. (9.14) implies Eq. (9.9), i.e. the LMI condition is a sufficient condition for U-V-W dissipativity. Proving that the LMI condition is necessary is more technical [80]. Suppose that Eq. (9.14) is satisfied. Let  $V(x(t)) = x^T(t)Yx(t)$  be a Lyapunov function. A straightforward computation gives

$$\dot{V}(x(t)) = \begin{pmatrix} x(t) \\ w(t) \end{pmatrix}^T \begin{pmatrix} A^T Y + YA & YB \\ B^T Y & 0 \end{pmatrix} \begin{pmatrix} x(t) \\ w(t) \end{pmatrix}.$$

To prove this, just note that  $\dot{V}(x(t)) = \dot{x}^T(t)Yx(t) + x^T(t)Y\dot{x}(t)$ , with  $\dot{x}(t) = Ax(t) + Bw(t)$ . Next, using  $z(t) = Cx(t) + Dw(t)$  (9.14) implies

$$\dot{V}(x(t)) + \begin{pmatrix} z(t) \\ w(t) \end{pmatrix}^T \begin{pmatrix} U & W \\ W^T & V \end{pmatrix} \begin{pmatrix} z(t) \\ w(t) \end{pmatrix} < 0 \quad (9.16)$$

Eq. (9.14) is to be multiplied on the left by  $[x^T(t), w^T(t)]$  and on the right by  $\begin{bmatrix} x(t) \\ w(t) \end{bmatrix}$ .

Integration from  $t = 0$  to  $t = T$  yields

$$x^T(T)Yx(T) + \int_0^T \begin{pmatrix} z(t) \\ w(t) \end{pmatrix}^T \begin{pmatrix} U & W \\ W^T & V \end{pmatrix} \begin{pmatrix} z(t) \\ w(t) \end{pmatrix} dt < 0 \quad (9.17)$$

Since  $x^T(T)Yx(T) \geq 0$ , Eq. (9.9) is obtained.

Eq. (9.15) is deduced from Eq. (9.14) using the notion of Schur complement. Indeed, Eq. (9.14) can be rewritten as

$$\begin{pmatrix} YA + A^T Y & YB + C^T W \\ B^T Y + W^T C & D^T W + W^T D + V \end{pmatrix} + \begin{pmatrix} C^T \\ D^T \end{pmatrix} Q \Sigma^{-1} Q^T \begin{pmatrix} C & D \end{pmatrix} < 0.$$

**Remark:** A necessary condition for Eq. (9.14) to hold is  $YA + A^T Y + C^T U C < 0$ . Because of the condition  $U = U^T \geq 0$ , this implies that all of the eigenvalues of the state-matrix  $A$  are in the LHP.

### 9.2.3 $H_\infty$ Criterion (Bounded Real Lemma)

The  $H_\infty$  norm stems from the induced  $L_2$  norm (a definition is given in Section 5.2.1) which is originally defined in the time domain, see Eq. (9.11). Still, in automatic control the importance of the  $H_\infty$  norm is more palpable from a frequency domain view point.

Let  $\|T_{w_i \rightarrow z_j}\|_\infty$  denote the  $H_\infty$  norm of the transfer function  $T_{w_i \rightarrow z_j}$ , that is, its largest gain from input channel  $w_i$  to output channel  $z_j$  across frequency in the singular value norm [28, 40]:

$$\|T_{w_i \rightarrow z_j}\|_\infty := \sup_{\omega} \sigma_{max}[T_{w_i \rightarrow z_j}(j\omega)] \quad (9.18)$$

where

$$\sigma_{max} := \text{maximum singular value} \quad (9.19)$$

Thus, the  $H_\infty$  norm is a measure of the system input/output gain for finite energy input signals. A constraint  $\|T_{w_i \rightarrow z_j}\|_\infty < \gamma$  can therefore be interpreted as a disturbance rejection performance for the selected I/O channels. Furthermore, it guarantees that the closed-loop system remains stable for all perturbations  $w_i = \Delta \cdot z_j$ , where  $\Delta$  has a gain not larger than  $1/\gamma$ .

The well known Bounded Real Lemma, see e.g. [10, 40, 78], allows for a description of an  $H_\infty$  related constraint in LMI notation.

**Proposition 9.3** *The  $H_\infty$  norm of the transfer matrix  $H(s)$  is less than  $\gamma$  if the following LMI w.r.t.  $X = X^T > 0$  holds*

$$\begin{pmatrix} AX + XA^T + BB^T & XC^T + BD^T \\ \star & DD^T - \gamma^2 I \end{pmatrix} < 0, \quad (9.20)$$

or equivalently:

$$\begin{pmatrix} AX + XA^T & XC^T & B \\ \star & -\gamma I & D \\ \star & \star & -\gamma I \end{pmatrix} < 0. \quad (9.21)$$

**Proposition 9.4** *The  $H_\infty$  norm of the transfer matrix  $H(s)$  is less than  $\gamma$  if the following LMI w.r.t.  $Y = Y^T > 0$  holds (see page 26 of [21])*

$$\begin{pmatrix} YA + A^T Y + C^T C & YB + C^T D \\ \star & D^T D - \gamma^2 I \end{pmatrix} < 0, \quad (9.22)$$

or equivalently (see page 898 of [80])

$$\begin{pmatrix} YA + A^T Y & YB & C^T \\ \star & -\gamma I & D^T \\ \star & \star & -\gamma I \end{pmatrix} < 0. \quad (9.23)$$

**Proof.** Eq. (9.22) can be obtained as a special case of Eq. (9.14) with  $U = I$ ,  $V = -\gamma^2 I$  and  $W = 0$ . In the same way, Eq. (9.23) is a special case of Eq. (9.15) with  $U = I/\gamma$ ,  $Q = I$ ,  $\Sigma = \gamma I$ ,  $V = -\gamma I$  and  $W = 0$ . Eq. (9.23) can also be deduced directly from Eq. (9.22) using the notion of Schur Complement (with  $\gamma = 1$  to simplify the computation).

Eqs. (9.20) and (9.21) are deduced from Eqs. (9.22) and (9.23), respectively, using the fact that  $H^T(s)$  and  $H(s)$  have the same  $H_\infty$  norm. The following substitutions are to be done:  $A \leftrightarrow A^T$ ,  $B \leftrightarrow C^T$ ,  $C \leftrightarrow B^T$ ,  $D \leftrightarrow D^T$ .

Last, note that for example Eq. (9.21) can be equivalently transformed into

$$\begin{pmatrix} AX + XA^T & B & XC^T \\ \star & -\gamma I & D^T \\ \star & \star & -\gamma I \end{pmatrix} < 0.$$

using the fact that

$$\begin{pmatrix} I & 0 & 0 \\ 0 & 0 & I \\ 0 & I & 0 \end{pmatrix} \begin{pmatrix} A_1 & A_2 & A_3 \\ A_2^T & A_4 & A_5 \\ A_3^T & A_5^T & A_6 \end{pmatrix} \begin{pmatrix} I & 0 & 0 \\ 0 & 0 & I \\ 0 & I & 0 \end{pmatrix} = \begin{pmatrix} A_1 & A_3 & A_2 \\ A_3^T & A_6 & A_5^T \\ A_2^T & A_5 & A_4 \end{pmatrix}.$$

#### 9.2.4 Positivity Criterion (Positive Real Lemma)

The next proposition presents the LMI criterion equivalent to a positivity constraint.

**Proposition 9.5** *The transfer matrix  $H(s)$  satisfies*

$$H(j\omega) + H^*(j\omega) > 2\gamma I \quad \forall \omega$$

if the following LMI w.r.t.  $X = X^T > 0$  holds

$$\begin{pmatrix} AX + XA^T & B - XC^T \\ \star & 2\gamma I - D - D^T \end{pmatrix} < 0 \quad (9.24)$$

or equivalently if the following LMI w.r.t.  $Y = Y^T > 0$  holds (see page 25 of [21])

$$\begin{pmatrix} YA + A^T Y & YB - C^T \\ \star & 2\gamma I - D - D^T \end{pmatrix} < 0. \quad (9.25)$$

**Proof.** Again, the corresponding proof is shown in Section 9.2.2. Note that Eq. (9.25) is a special case of Eq. (9.14) with  $U = 0$ ,  $V = 2\gamma I$ ,  $W = -I$ . Then, Eq. (9.24) is obtained from Eq. (9.25) by noting that  $H^T(s)$  and  $H(s)$  have the same degree of positivity.

**Remark.** When  $\gamma = 0$  the system is said to be passive (or positive). In the general case it is said to be dissipative, with dissipativity  $\gamma$  (see pages 93-94 of [21]).

### 9.3 Polytopic Multi-Objective Robust Control Design

The preceding sections build the basis for the controller design in LMI formulation. So far, modal and I/O criteria have been presented. In order to tackle robustness issues versus the c.o.g. position, a polytopic approach is considered. This approach allows for synthesizing a state-feedback controller satisfying multiple constraints on a polytope of linear state-space models. Model parameters vary within a convex polytope of the model parameter space where the vertices of the polytope are defined by the parameters of locally valid linear models [12]. The following proposition presents the technique [21, 23, 16, 36].

**Proposition 9.6** *Consider the open-loop state-space models ( $i \in [1, N]$ ):*

$$\begin{aligned}\dot{x} &= A_i x + B_{1,i} w_1 + B_{2,i} w_2 + B_{3,i} u \\ z_1 &= C_{1,i} x + D_{11,i} w_1 + D_{12,i} w_2 + D_{13,i} u \\ z_2 &= C_{2,i} x + D_{21,i} w_1 + D_{22,i} w_2 + D_{23,i} u\end{aligned}$$

*As a sufficient condition, there exists a state-feedback controller  $u = Kx$  satisfying:*

1. *The closed-loop eigenvalues of  $A_i + B_{3,i}K$  stay inside the LMI region of the complex plane of Fig. 9.1.*
2. *The  $H_\infty$  norm of the closed loop transfer matrix  $T_{w_1 \rightarrow z_1}$  between  $w_1$  and  $z_1$  is less than  $\gamma_1$ .*
3. *The closed-loop transfer matrix  $T_{w_2 \rightarrow z_2}$  between  $w_2$  and  $z_2$  satisfies:*

$$T_{w_2 \rightarrow z_2}(j\omega) + T_{w_2 \rightarrow z_2}^*(j\omega) > 2\gamma_2 \quad \forall \omega \in [0, +\infty)$$

*if there exists a Lyapunov matrix  $X = X^T > 0$  and a matrix  $W = KX$  satisfying the*

LMI:

$$L_i(X, W) + L_i^T(X, W) + 2\lambda X < 0 \quad (9.26)$$

$$\begin{pmatrix} -rX & L_i(X, W) \\ \star & -rX \end{pmatrix} < 0 \quad (9.27)$$

$$\begin{pmatrix} \sin \alpha (L_i(X, W) + L_i^T(X, W)) & -\cos \alpha (L_i(X, W) - L_i^T(X, W)) \\ \star & \sin \alpha (L_i(X, W) + L_i^T(X, W)) \end{pmatrix} < 0 \quad (9.28)$$

$$\begin{pmatrix} L_i(X, W) + L_i^T(X, W) & B_{1,i} & XC_{1,i}^T + W^T D_{13,i}^T \\ \star & -\gamma_1 I & D_{11,i}^T \\ \star & \star & -\gamma_1 I \end{pmatrix} < 0 \quad (9.29)$$

$$\begin{pmatrix} L_i(X, W) + L_i^T(X, W) & B_{2,i} - XC_{2,i}^T - W^T D_{23,i}^T \\ \star & 2\gamma_2 I - D_{22} - D_{22}^T \end{pmatrix} < 0 \quad (9.30)$$

with  $L_i(X, W) = A_i X + B_{3,i} W$ .  $\star$  denotes the conjugate part of the hermitian matrix.

In the above proposition, Eqs. (9.26)–(9.28) correspond to the LMI region defining acceptable aircraft handling qualities. Eq. (9.29) corresponds to the  $H_\infty$  criterion and Eq. (9.30) to the positivity one. The specifications/criteria can be set for each selected model (i.e. position of the c.o.g.) individually.

**Remarks:**

(i) In the above proposition  $\gamma_1$  or  $\gamma_2$  is fixed, while the other one is to be minimized with regard to  $W$  and  $X$  under LMI constraints with an LMI solver [41].  $K = WX^{-1}$  is deduced.

(ii) Several Lyapunov matrices should be used instead of a single one for all criteria and models, but the optimization problem is then not convex anymore. The minimized value of  $\gamma_1$  or  $\gamma_2$  is thus pessimistic, i.e. overestimated if more than one criterion (a modal,  $H_\infty$ , or positivity one) or more than one model are considered. It may happen that no solution to the LMI problem is found, though there exists a state feedback controller satisfying the design specifications. The number of criteria and models is thus kept as small as possible.

(iii)  $r = +\infty$  is generally chosen. When the design is satisfactory,  $r$  can be modified as an indirect means to reduce the norm of the feedback  $K$ .

(iv) The positivity constraint, Eq. (9.30), is incorporated into the LMI problem toward the end to manipulate the robustness against nonlinearities (like saturations). The aim is to indirectly maximize the domain of stability by maximizing positivity. How to compute the corresponding domain of attraction, i.e. the stability domain, is shown in Section 9.4.

(v) In the case of multiple diagonal saturations or dead zones, a multiplier can be introduced in Eq. (9.30) to reduce the conservatism of the technique [101].

## 9.4 Stability and Performance Analysis in the Presence of Nonlinearities

Linear unstable open-loop systems incorporating nonlinear saturation operators on their control input signals cannot globally be stabilized by a feedback controller.

*Example:* Consider a linear plant model which is asymptotically stable only in closed-loop (thus with integrated control laws). If now the plant model is initialized in such a way that the controller computes a control input superior to that of a saturation limit, the plant will behave as if it were open-loop with a constant input (= saturation value). Due to the still remaining constant input, two options<sup>2</sup> are possible: either the system converges to an equilibrium condition or it diverges completely. The reader can already guess that there exist initialization states which determine whether the system is stable (even though saturated) or unstable.

It is therefore reasonable to define a stability domain<sup>3</sup>, describing the set of initial system states for which the saturated system tends to converge back to an equilibrium condition. Furthermore, it can be assumed that the tendency to return to an equilibrium state, i.e. the convergence speed, differs for different initial states.

Section 9.4.1 deals with the computation of a stability domain for systems incorporating saturations on their control input. This technique addresses the internal stability of autonomous systems as well as the  $L_2$  properties of their exogenous outputs (for a definition of the  $L_2$  norm, see Section 5.2.1). In Section 9.4.2 a simple method is presented which can be used to modify/tune the shape of the stability domain by introducing weighting factors on system states. Section 9.4.3 introduces the notion of convergence speed as a performance parameter. Finally, Section 9.4.4 presents a method to address the  $L_2$  input/output stability and performance of a saturated closed-loop system by inserting filter states into the system.

### 9.4.1 Stability Analysis

Using the fact that symmetric saturations can be represented by the complementary dead-zone nonlinearity (as shown in Section 8.1.3, Figure 8.2), the following proposition presents an LMI based technique for computing the domain of attraction (stability domain) of the interconnection of a linear system with dead-zone blocks.

The proposition is adapted from [26] and based on the representation of a dead-zone nonlinearity via generalized sector conditions. Such a representation leads to less conservative results than previous techniques. For more details, see [26, 17].

---

<sup>2</sup>Actually, three options exist: under certain circumstances the system can enter limit-cycles. Further readings on this classical research subject can be found in, e.g. [98, 13, 46, 70, 62].

<sup>3</sup>Often, the term *domain of attraction* is used in literature.

**Proposition 9.7** Consider the following system, where state matrix  $A$  is assumed to be Hurwitz:

$$\begin{cases} \dot{x} = Ax + B_2\phi(y) \\ z = C_1x + D_1\phi(y) \\ y = C_2x \end{cases} \quad (9.31)$$

where  $x \in \mathbf{R}^n$  denotes the system state,  $z \in \mathbf{R}^p$  the exogenous output, and  $y \in \mathbf{R}^m$  the internal input of the normalized nonlinear dead-zone operator  $\phi(\cdot)$ :

$$\phi(y_i) = \begin{cases} 0 & \text{if } |y_i| \leq 1 \\ y_i - 1 & \text{if } y_i > 1 \\ y_i + 1 & \text{if } y_i < -1 \end{cases} \quad (9.32)$$

If there exist a symmetric, positive definite matrix  $Q \in \mathbf{R}^{n \times n}$ , a positive diagonal matrix  $S \in \mathbf{R}^{m \times m}$ , and a full rectangular matrix  $Z \in \mathbf{R}^{m \times n}$  such that the following LMI conditions hold (where  $Z_i$  and  $C_i$  denote the  $i^{\text{th}}$  rows of  $Z$  and  $C$  respectively):

$$\begin{pmatrix} AQ + QA^T & B_2S - Z^T \\ SB_2^T - Z & -2S \end{pmatrix} < 0 \quad (9.33)$$

$$\begin{pmatrix} Q & Z_i^T + QC_{2i}^T \\ Z_i + C_{2i}Q & I \end{pmatrix} > 0, \quad i = 1 \dots m \quad (9.34)$$

then the ellipsoid:

$$\mathcal{E}_{Q-1} = \{x \in \mathbf{R}^n / x^T Q^{-1} x \leq 1\} \quad (9.35)$$

defines a domain of attraction of system (9.31).

Furthermore, if the following LMI condition holds

$$\begin{pmatrix} AQ + QA^T & B_2S - Z^T & QC_1^T \\ SB_2^T - Z & -2S & D_1^T \\ C_1Q & D_1 & -\gamma I \end{pmatrix} < 0 \quad (9.36)$$

then for all  $x \in \mathcal{E}_{Q-1}$  the  $L_2$  norm of output  $z$  is bounded by  $\sqrt{\gamma}$ :

$$\|z(t)\|_{L_2} = \left[ \int_0^\infty z(t)^T z(t) dt \right]^{1/2} \leq \sqrt{\gamma} \quad (9.37)$$

**Remarks:**

- (i) If LMI condition (9.33) holds, then the LMI (9.36) is satisfied for a finite value of  $\gamma$ .
- (ii) The above proposition is based on a quadratic approach:

$$V(x) = x^T P x \quad (9.38)$$

where  $P \in \mathbf{R}^{n \times n}$  is a symmetric, positive definite matrix. A maximization of the stability domain  $\mathcal{E}_P = \{x \in \mathbf{R}^n / x^T P x \leq 1\}$  corresponds to the *minimization* of the determinant  $\det(P)$ . For computational reasons, in the above proposition the optimization variable is  $Q = P^{-1}$ . The objective is thus the maximization of the determinant  $\det(Q)$ , which is known to be a convex problem.

(iii) Alternatively, the shape of the ellipsoid  $\mathcal{E}_{Q^{-1}}$  can be optimized in such a way that it contains the farthest point in a given direction  $v$  of the state space [43]. In that case, the problem reduces to the maximization of a linear objective  $\beta$  under LMI constraint:

$$\begin{pmatrix} Q & \beta v \\ \beta v^T & 1 \end{pmatrix} > 0 \quad (9.39)$$

See Section 9.4.4 for an application.

(iv) With  $v = [1 \cdots 1]^T$  and  $v \in \mathbf{R}^n$  the maximization of the linear objective  $\beta$  under LMI constraint (9.39) leads to computing the largest hypercube inside  $\mathcal{E}_{Q^{-1}}$ , since the stability domain is homogeneously maximized in all state directions.

(v) The corresponding energy upper-bound for output  $z$  can also be computed via minimizing the linear objective  $\gamma$  in Eq. (9.36).

Another method to modify the shape of the stability domain is given in the next section.

### 9.4.2 Modification of the Stability Domain

The idea consists in introducing weighting factors on selected system states and then maximizing the volume of the stability ellipsoid. The technique presents an extension of Proposition 9.7. The procedure turns out to be a fairly simple modification of the system states.

Consider an autonomous system:

$$\begin{cases} \dot{x} = Ax + B_2 \phi(y) \\ y = C_2 x \end{cases} \quad (9.40)$$

with system state

$$x = \begin{bmatrix} x_1 \\ x_2 \end{bmatrix} \in \mathbf{R}^n \quad (9.41)$$

Now,  $x_2$  is substituted by  $\hat{x}_2 = \alpha x_2$ . Partitioning  $A, B$ , and  $C$  according to Eq. (9.41) yields

$$\begin{cases} \dot{x}_1 = A_{11} x_1 + A_{12} \frac{\hat{x}_2}{\alpha} + B_{21} \phi(y) \\ \dot{\hat{x}}_2 = \alpha A_{21} x_1 + A_{22} \hat{x}_2 + \alpha B_{22} \phi(y) \\ y = C_{21} x_1 + C_{22} \frac{\hat{x}_2}{\alpha} \end{cases} \quad (9.42)$$

Proposition 9.7 can now be applied to this new system in order to compute a stability domain. In the context of our aeronautical application, a trade-off can thus be achieved between, e.g. actuator states and aerodynamic states by applying corresponding weighting factors.

### 9.4.3 Convergence Speed

The convergence speed  $\mu$  is the guaranteed exponential contraction speed of the region of attraction toward the origin for a given initial system state  $x$ . In contrast to simple quadratic stability

$$\dot{V} < 0$$

with  $V = x^T P x$ , the convergence speed is determined by computing the domain of attraction by imposing (with  $\mu > 0$ ):

$$\dot{V} + \mu V < 0 \tag{9.43}$$

Note that Eq. (9.43) implies

$$\forall t \geq 0, \quad V(t) = x(t)^T P x(t) < V_0 e^{-\mu t} \tag{9.44}$$

The expected response time of the system is hence  $T_R = \mu^{-1}$ . The convergence speed is limited by the degree of stability  $\lambda$  of the linear system ( $\mu \leq \lambda$ ).

### 9.4.4 Stability in the Face of Exogenous Inputs

Up to this point, only the autonomous system has been regarded. In practice, a performance analysis issue would most likely be to determine the input/output properties of a system. To that aim, a method is presented which leads to incorporating external input signals into the stability analysis.

The computation of the stability domain can easily be extended to consider a certain class of  $L_2$ -bounded input signals. An  $L_2$ -bounded input signal  $w(t)$ , which represents a very slowly decreasing signal close to a step input, can be described by a first-order linear filter with non-zero initial state  $w_0$ .  $\mathcal{W}(\epsilon, \rho)$  is defined as the set of signals

$$\forall t \geq 0, \quad w(t) = w_0 e^{-\epsilon t}, \quad |w_0| \leq \rho \tag{9.45}$$

where  $\epsilon > 0$  is close to zero.

Consider the following system with state matrix  $A$  being Hurwitz:

$$\begin{cases} \dot{x} = Ax + B_1 w + B_2 \phi(y) \\ z = C_1 x + D_{11} w + D_{12} \phi(y) \\ y = C_2 x + D_{21} w \end{cases} \tag{9.46}$$

where  $x \in \mathbf{R}^n$ ,  $w \in \mathbf{R}^p$ ,  $z \in \mathbf{R}^p$ , and  $y \in \mathbf{R}^m$  denote the system state, the exogenous input, the exogenous output, and the internal input of the dead-zone operator  $\phi(\cdot)$ , respectively. Consider furthermore the augmentation of the system state  $x$  by filter state  $w$  such that:

$$\xi = \begin{bmatrix} x \\ w \end{bmatrix} \in \mathbf{R}^{n_a}, \begin{cases} \dot{\xi} = \mathcal{A}\xi + \mathcal{B}_2\phi(y) \\ z = \mathcal{C}_1\xi + \mathcal{D}_1\phi(y) \\ y = \mathcal{C}_2\xi \end{cases} \quad (9.47)$$

with:

$$\begin{aligned} \mathcal{A} &= \begin{bmatrix} A & B_1 \\ 0 & -\epsilon I \end{bmatrix} & \mathcal{B}_2 &= \begin{bmatrix} B_2 \\ 0 \end{bmatrix} \\ \mathcal{C}_1 &= [C_1 \quad D_{11}] & \mathcal{D}_1 &= D_{12} \\ \mathcal{C}_2 &= [C_2 \quad D_{21}] \end{aligned}$$

This augmented system can now be injected into Proposition 9.7. The goal is thus to find either the maximum initial state  $w_0 = \rho_{max}$  for which system (9.46) is still guaranteed to be stable, or to compute a stability domain for a fixed value  $w_0 = \rho$  in combination with any objective proposed in Proposition 9.7 and/or Section 9.4.2.

As an example, the following application is proposed:

- In a first step, the domain of attraction is maximized in the direction of the added performance signal state, i.e.  $\xi = [\mathbf{0} \quad w]^T$ , in such a way that the performance domain  $\mathcal{E}_{perf}$  contains the state  $\xi = [\mathbf{0} \quad \rho]^T$  for a maximized value  $\rho_{max}$ , i.e.

$$\max \rho / \begin{pmatrix} Q & [\mathbf{0} \quad \rho]^T \\ [\mathbf{0} \quad \rho] & 1 \end{pmatrix} > 0 \quad (9.48)$$

In that way, system (9.46) remains stable for all exogenous inputs  $w \in \mathcal{W}(\epsilon, \rho_{max})$  and all initial conditions  $x_0 \in \mathcal{E}_{perf}$ , where

$$\mathcal{E}_{perf} = \left\{ x \in \mathbf{R}^n / \begin{bmatrix} x \\ \rho_{max} \end{bmatrix}^T Q^{-1} \begin{bmatrix} x \\ \rho_{max} \end{bmatrix} \leq 1 \right\}. \quad (9.49)$$

- In a second step, for a fixed value  $\rho < \rho_{max}$  the corresponding energy upper-bound for output  $z$  can be computed via minimizing  $\gamma$  in LMI (9.36). Division by the input energy of the exogenous signal  $w(t) = \rho e^{-\epsilon t}$ , delivers an  $L_2$  gain of system (9.46) from  $w$  to  $z$ :

$$\gamma_{L_2} = \frac{\|z(t)\|_{L_2}}{\|w(t)\|_{L_2}} \quad (9.50)$$

This result can also be interpreted as a measure of the tracking quality of the system to some exogenous input signal.

A different mix or combination of techniques is thinkable. An application to a practical

aeronautical problem is shown in Chapter 10, Section 10.3.

For example, note that Section 9.4.1 only deals with internal stability while Section 9.4.4 essentially deals with input/output stability: when solving problem (9.48), an augmented stability domain in the space of

$$\xi = \begin{bmatrix} x \\ w \end{bmatrix}$$

is obtained. Still, the size of the stability domain (9.49) in the space of  $x$  is expected to be small since the issue was to maximize the augmented stability domain in the direction of  $[\mathbf{0} \ w]^T$ . Applying the technique of Section 9.4.2 would allow to study a trade-off between internal stability in the space of state vector  $x$  and input/output stability, by applying Proposition 9.7 to the augmented system (9.47) with a weighting factor on  $w$ . If  $w$  is heavily weighted, this reduces to optimizing the shape of the stability domain in direction of  $w$ . If  $w$  is less heavily weighted a larger stability domain is obtained in the space of state vector  $x$ . Remember moreover that a guaranteed upper bound on the energy of output  $z$  can be computed.

## 9.5 Static Anti-Windup Control Scheme Toward Enhanced Performance

It is desirable to preserve as much as possible stability and performance of the linear closed-loop system despite input saturation. If the resulting stability domain and the performance assessment are not satisfactory, an anti-windup control scheme can be introduced in addition to the a priori fixed feedback controller.

To this end, the additional anti-windup controller uses the outputs of the saturation blocks, or the difference of inputs and outputs, in order to minimize the sensitivity to saturation [86, 87, 101]. In the context of a robust back-up flight control law, unlike e.g. . Takaba [86, 87] and Wu and Soto [101] who synthesize dynamic controllers for a single plant model or an LFT one, a simple convex multi-model design technique of a static anti-windup controller is proposed, incorporating a positivity and an  $H_\infty$  criterion. This synthesis is performed after the main control law synthesis. Again, the design problems reduce to solving a set of linear matrix inequalities [41]. The next subsection presents the technique.

### 9.5.1 Plant Model for Anti-Windup Controller

Figure 9.2 presents the closed-loop structure including the robust static feedback controller  $K$  computed beforehand. Here, the actuator model between  $u_c$  and  $u$  (a first-order filter  $\frac{1}{1+T_{acts}}$ ) is extended, including now saturations both on actuator rate and position. It

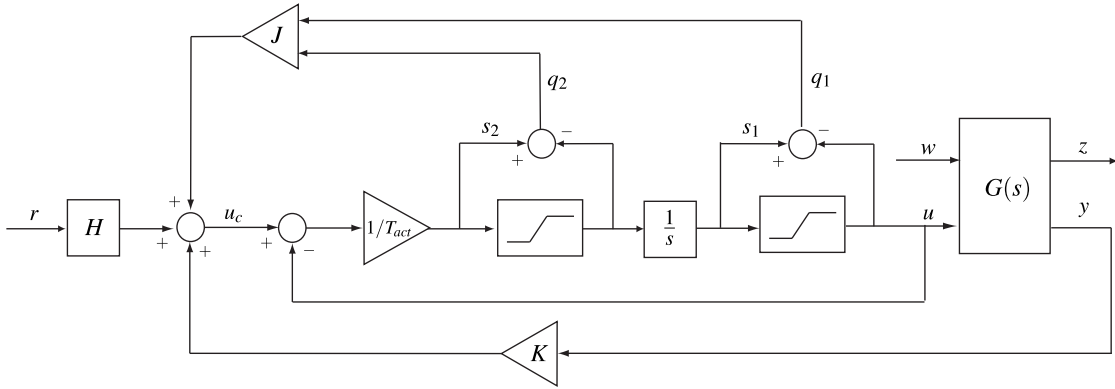


Figure 9.2: Closed-loop structure with anti-windup controller.

is possible to consider multiple actuators. The difference between the desired and real actuator position (resp. rate output) is supposed to be measured and noted as  $q_1$  (resp.  $q_2$ ). The (LTI) aircraft model  $G(s)$  has the control inputs  $u$  and wind inputs  $w$ , possibly filtered by a Von Dryden filter.  $z$  represents a set of plant outputs used for design specifications.

Let

$$q = \begin{bmatrix} q_1 \\ q_2 \end{bmatrix} \quad (9.51)$$

The flight control law is

$$u_c = Ky + Jq + Hr. \quad (9.52)$$

The static output feedback  $K$  is fixed as well as  $H$ , a static feedforward controller ( $r$  is a reference input). The static anti-windup controller is denoted as  $J$  and is only active if the saturations are active (i.e.  $q \neq 0$ ).

After transforming the saturation blocks into dead-zone ones Figure 9.2 becomes Figure 9.3, where the dead-zone blocks are omitted (they could be inserted between  $s_i$  and  $q_i$ ).

*Remember:* The use of a dead-zone block allows us to obtain a stable nominal closed-loop, under the assumption of a stabilizing static output-feedback  $K$ , noting that some open-loop models are unstable depending on the c.o.g. position.

It is worth emphasizing that the feedforward controller  $H$  and the anti-windup controller  $J$  do not affect the stability of the linear closed loop of Figure 9.3, even if the anti-windup controller  $J$  obviously modifies the stability of the real closed-loop system of Figure 9.2. Therefore, on the basis of Figure 9.3 the design of  $J$  is very close to a feedforward design problem.

Let

$$s = \begin{bmatrix} s_1 \\ s_2 \end{bmatrix} \quad (9.53)$$

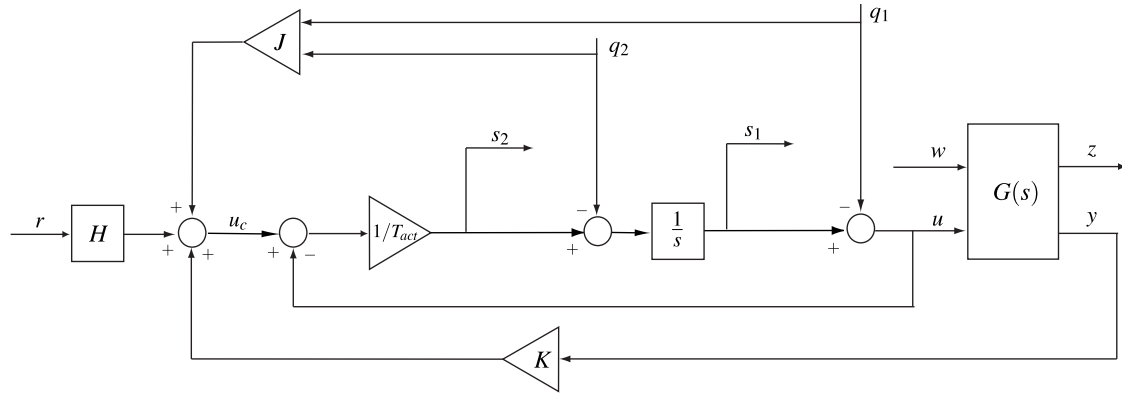


Figure 9.3: Transformed plant structure with anti-windup control scheme.

The closed-loop system of Figure 9.3 with a fixed static output-feedback  $K$  is transformed into the one of Figure 9.4. Exogenous inputs  $r$  and  $w$  are omitted as they are not relevant for the anti-windup control scheme.

The design specifications for the anti-windup controller w.r.t. Figure 9.4 can now be detailed:

1. A positivity criterion for transfer function  $T_{q \rightarrow s}$  is considered to ensure robustness of the closed-loop system in the presence of saturations.
2. The anti-windup controller is to be simple and robust versus c.o.g. displacements.

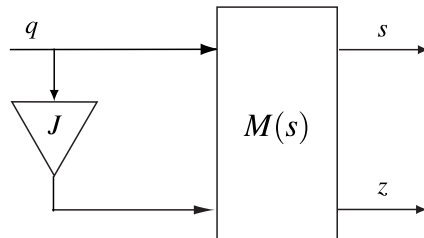


Figure 9.4: Plant for anti-windup control design.

### 9.5.2 Design of a Robust Anti-Windup Controller

The next proposition, which describes the LMI design technique of the static anti-windup controller  $J$ , is an application of Proposition 9.5.

**Proposition 9.8** Consider the closed-loop state-space models ( $i \in [1, N]$ ) as indicated in Figure 9.4, with Hurwitz state matrices  $A_i$ :

$$\begin{aligned} \dot{x} &= A_i x + B_{1,i} q + B_{2,i} J q \\ s &= C_{1,i} x + D_{11,i} q + D_{12,i} J q \\ z &= C_{2,i} x + D_{21,i} q + D_{22,i} J q \end{aligned}$$

All matrices above are fixed, except  $J$ . The positivity criterion

$$T_{q \rightarrow s}(j\omega) + T_{q \rightarrow s}^*(j\omega) > 2\gamma_3 I \quad \forall \omega$$

is satisfied if and only if there exist a matrix gain  $J$  and a positive definite matrix  $Q_1 = Q_1^T > 0$  satisfying

$$\begin{pmatrix} A_i Q_1 + Q_1 A_i^T & B_{1,i} + B_{2,i} J - Q_1 C_{1,i}^T \\ \star & 2\gamma_4 I - (D_{11,i} + D_{12,i} J) - (D_{11,i} + D_{12,i} J)^T \end{pmatrix} < 0.$$

**Remarks:**

(i) Contrary to the polytopic control design where one Lyapunov matrix is used for multiple criteria and models, here different Lyapunov functions can be used. The anti-windup control design is thus non-conservative.

(ii) The robust static anti-windup controller  $J$  allows to improve the stability and performance properties in the presence of saturations compared to those obtained with the static back-up controller only. The size of the domain of attraction is modified as well as the convergence speed of the system.

(iii) In the above proposition, the way to describe dead-zone blocks is less sophisticated than in Proposition 9.7 since dead-zone blocks are considered as generic nonlinearities inside a sector  $[0, 1/\gamma_3]$ .



# Chapter 10

## Controller Design and Application

This chapter is dedicated to the application of the presented design technique. As an introduction and for better comprehension Section 10.1 presents two preliminary designs in order to demonstrate the impact of modal constraints onto actuator activity. Section 10.2 then delivers the final longitudinal and lateral controllers.

The closed-loop poles and frequency responses are shown as well as the obtained maximum singular values (denoting the actuator activity) and positivity characteristics (denoting the robustness to saturations). The corresponding stability domains are computed in Section 10.3 which also sets out to assess the closed-loop performance. Section 10.4 deals with the simulation of the complete nonlinear three-axis model of the VELA aircraft stabilized by the developed controllers. Finally, a conclusion on the design technique is given in Section 10.5.

### 10.1 Preliminary Designs

In order to demonstrate the impact of modal constraints onto actuator activity two preliminary control designs are presented for both aircraft motions. One controller is synthesized for each c.o.g. position within the range specified in Eq. (8.17) of Section 8.2. This procedure allows for computing the optimal static controller in terms of  $H_\infty$  norm minimization at each c.o.g. position. Non-conservative values of the minimized actuator activity  $\gamma_{1,min}$  are hence obtained. In a second step, modal constraints are introduced and the impact on the actuator activity becomes thus tangible. The respective constraints for both preliminary designs are displayed in Tables 10.1 and 10.2.

| #  | $\lambda$ | $\xi$ | $r$      |
|----|-----------|-------|----------|
| 1. | 0         | 0     | $\infty$ |
| 2. | 0.7       | 0.7   | $\infty$ |

Table 10.1: Longitudinal motion. Sector constraints for preliminary designs.

| #  | $\lambda$ | $\xi$ | $r$      |
|----|-----------|-------|----------|
| 1. | 0         | 0     | $\infty$ |
| 2. | 0.1       | 0.1   | $\infty$ |

Table 10.2: Lateral Motion. Sector constraints for preliminary designs.

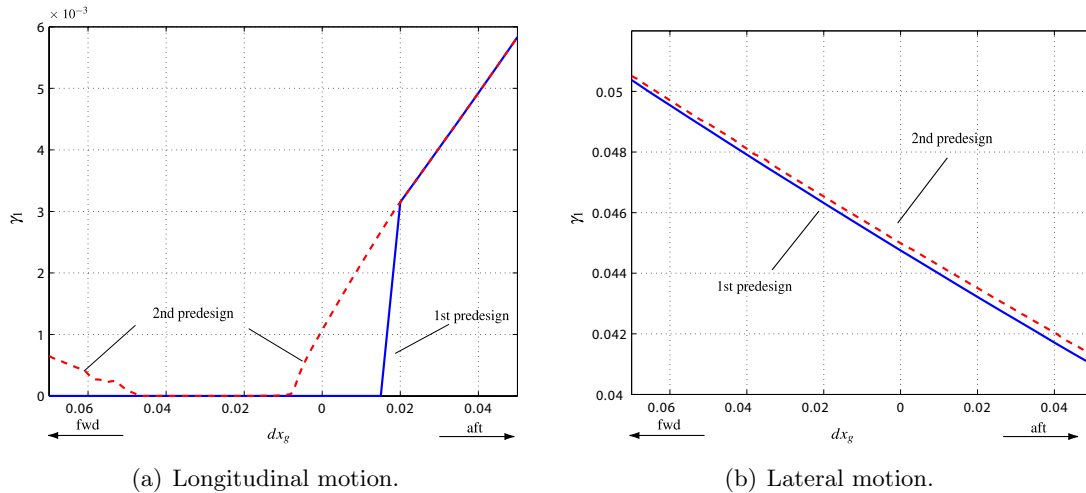
### 10.1.1 Preliminary Design for Minimized Activity $\gamma_{1,min}$

The aim of this subsection is to compute a controller at each  $X_g$  that minimizes the actuator activity, i.e. the transfer function  $T_{w_1 \rightarrow z_1}$  is minimized in Figure 8.3.  $w_1$  is an external wind input, whereas  $z_1$  is associated to the actuator position and rate outputs.

The real non-conservative minimized values for  $\gamma_1$  are achieved by considering minimal modal constraints, as specified in Tables 10.1 and 10.2, #1. The closed loop poles of the system are only required to be stable, i.e. they stay within the LHP.

In the longitudinal motion, the system is naturally stable for c.o.g. positions  $dx_g < +1.8\%$ , Figure 8.1. Therefore, a minimized value of  $\gamma_{1,min} = 0$  is expected to be computed in that range, that is the feedback on the elevator  $K_{\delta m} = \mathbf{0}$  is the optimal solution. Figure 10.1(a) shows exactly the described behavior with  $\gamma_{1,min}$  rising only for naturally unstable c.o.g. positions  $dx_g > +1.8\%$ .

With regard to the lateral aircraft motion, the dutch roll mode is naturally unstable for all c.o.g. positions. Thus a non-zero  $\gamma_{1,min}$  is expected throughout (Figure 10.1(b)). The minimal activity is notably higher than for the longitudinal motion.

Figure 10.1:  $\gamma_1$  for two preliminary designs.

### 10.1.2 Preliminary Design Introducing Modal Constraints

The FAR [96] and JAR [30] state that the SPO of the aircraft during take-off and landing has to be *heavily damped* in order to comply to certification rules. This leaves space for interpretation. Nonetheless, an arbitrary example fulfilling these vague specifications will be presented (see #2 in Table 10.1). A minimum damping to the SPO as well as a minimum time response will be imposed, the results being presented in Figures 10.1(a) and 10.2(a).

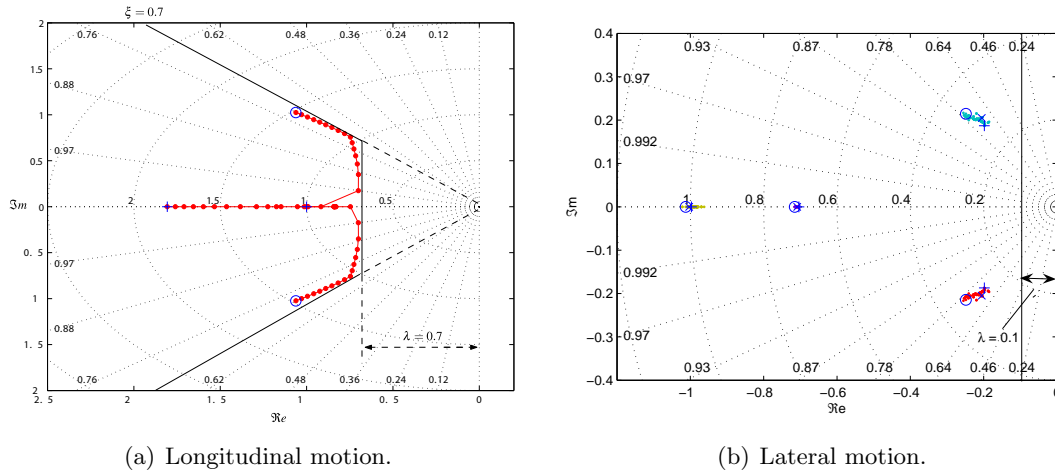


Figure 10.2: Closed-loop poles for preliminary design #2 as a function of  $X_g$ .

As concerns handling quality criteria for the dutch roll motion, FAR/JAR only require it positively damped. Airbus constraints are somewhat tighter, demanding a 10 % damping ratio (see #2 in Table 10.2). The increase in activity is minor in the lateral case because the modal constraints are not very demanding, see Figure 10.1(b). Figure 10.2(b) shows the lateral modes as a function of the c.o.g. position.

#### Remarks:

- (i) Introducing a stability degree constraint which also resembles imposing a minimum time response, accelerates the system and thus leads to an increase in actuator activity which is condensed in the increase of the  $H_\infty$  norm.
- (ii) It is interesting to see that imposing a minimum stability degree does not affect longitudinal  $\gamma_1$  at  $X_g$  positions that are unstable in the open-loop case, i.e.  $dx_g > +1.8\%$ . Thus, the actuator activity is not increased for aft positions. Still, it can be discovered that approximately neutral c.o.g. positions become more and more affected by imposing this constraint.
- (iii) In the longitudinal motion, an increase in actuator activity for the most fwd c.o.g. positions is noticeable. This effect is to be ascribed to the damping constraint, which of course only affects  $X_g$  positions for which the natural damping ratio of the open-loop model is  $\xi < 0.7$ .
- (iv) This example shows that the effects of damping and stability degree constraints can

be superposed. The information gathered with these two preliminary designs will now come in useful when deriving one robust state feedback.

## 10.2 Robust Back-Up Controllers

The longitudinal and lateral controllers are synthesized separately. Both control laws are designed according to the control objectives presented in Section 8.2. The design has been carried out on the plant model with modified system states  $\tilde{X}_{lon}$  and  $\tilde{X}_{lat}$ , see Eqs. (8.11) and (8.12). The corresponding design parameters are detailed in the respective sections.

The results shown in this section have been obtained by injecting the designed controller into the validation model, i.e. the model with original states and real outputs:

$$\begin{aligned} X_{lon} &= (\alpha, q, \delta m)^T & Y_{lon} &= (n_z, q)^T \\ X_{lat} &= (\beta, r, p, \phi, \delta l, \delta n)^T & Y_{lon} &= (n_y, r, p, \phi)^T \end{aligned} \quad (10.1)$$

and thus with

$$u_c = K^* \cdot Y \quad (10.2)$$

where  $K^*$  is the designed feedback controller  $K$  without the feedback on the actuator states.

### 10.2.1 Longitudinal Controller

The longitudinal controller has been computed with two extremal models, one for  $-7\%$  fwd and another one for  $+5\%$  aft. The LMI optimization objective is the maximisation of positivity  $\gamma_2$  of the transfer matrix  $T_{w_2 \rightarrow z_2}$ . In order to keep actuator activity to a minimum an  $H_\infty$  constraint is imposed with  $\gamma_1 < 0.2$ . Simple LHP stability is sufficient as an LMI region constraint. A maximum module  $r$  is only introduced to reduce the norm of the feedback gain. The parameter-settings are displayed in Table 10.3.

| Models | $(dx_g)$ | $\lambda$ , rad/s | $r$ , rad/s | $\xi$ | Objective  | Constraint       |
|--------|----------|-------------------|-------------|-------|------------|------------------|
| fwd    | $-7\%$   | 0                 | 16          | 0     | positivity | $H_\infty :$     |
| aft    | $+5\%$   | 0                 | 16          | 0     |            | $\gamma_1 < 0.2$ |

Table 10.3: Parameter-setting for the longitudinal control design.

The synthesized static state-feedback controller figures in Table 10.4. The final output-feedback controller is obtained by zeroing the feedback on the actuator state  $\delta m$ .

The controller is valid for the whole range of  $X_g$  positions. Table 10.5 shows the values obtained for the actuator activity  $\gamma_1$  of the transfer matrix  $T_{w_1 \rightarrow z_1}$  and the positivity  $\gamma_2$

$(T_{w_2 \rightarrow z_2})$ , as well as the modal properties of the *short-period oscillation*. As demanded in the certification norms, the motion is more than sufficiently damped.

Figure 10.3 displays the closed-loop poles of the system using the feedback on the real outputs  $n_z$  and  $q$ , only. Frequency responses are shown in Figure 10.4. The actuator pole does not lie within the specified LMI region. This does not surprise since the feedback on this state has been zeroed. Hence, the actuator pole is not controlled.  $r$  is used here as an indirect means to modify the feedback norm of  $K_{\delta m}$ .

$$K_{\delta m} = \begin{matrix} & n_z & q & \delta m \\ \hline & 0.26793 & 1.4906 & (1.3156) \end{matrix}$$

Table 10.4: Longitudinal static robust controller.

|           | $\gamma_1$ | $1/\gamma_2$ | $\lambda$ , rad/s | $r$ , rad/s | $\xi$ , % |
|-----------|------------|--------------|-------------------|-------------|-----------|
| fwd $X_g$ | .12        | .99          | .94               | 1.24        | 75.6      |
| aft $X_g$ | .12        | .98          | .63               | 1.16        | 100.0     |

Table 10.5: Results for the longitudinal robust control law. Valid for  $dx_g \in [-7\%; +5\%]$ .

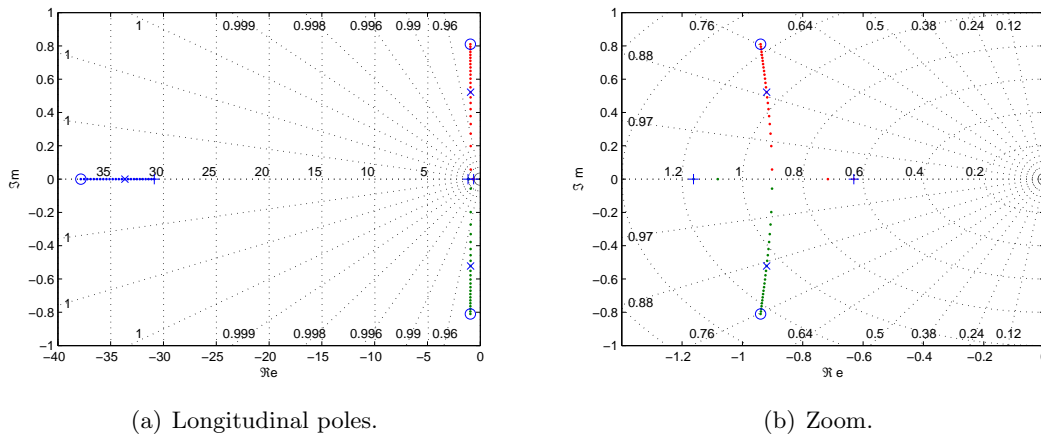


Figure 10.3: Closed-loop poles.  $\circ$ :  $-7\%$  fwd,  $+$ :  $+5\%$  aft. Longitudinal motion.

**Remark.** The positivity of the system with the designed feedback controller is very close to one, yet it cannot attain this asymptotic value. We recall, that for  $1/\gamma_2 = 1$  global stability would be obtained, which is impossible since the open-loop can be unstable. Nevertheless, the associated region of stability is expected to be very large.

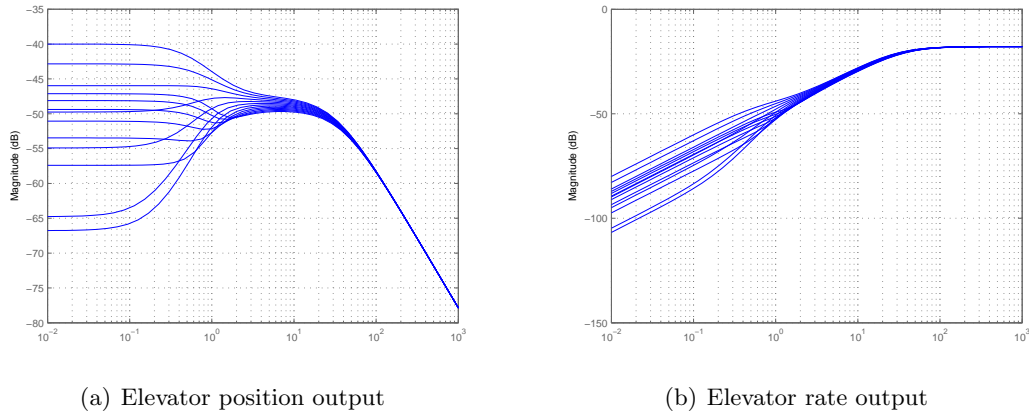


Figure 10.4: Magnitude (frequency response) of wind input to actuator outputs  $T_{w_1 \rightarrow z_1}$  as a function of  $dx_g$ . Longitudinal motion.

### 10.2.2 Lateral Controller

The lateral controller has also been computed using the same two extremal models. The same LMI optimization objective (positivity) applies. The  $H_\infty$  constraint is set to  $\gamma_1 < 0.1$ . The LMI sector conditions can be found in Table 10.6.

| Models | $(dx_g)$ | $\lambda$ , rad/s | $r$ , rad/s | $\xi$ | Objective  | Constraint                       |
|--------|----------|-------------------|-------------|-------|------------|----------------------------------|
| fwd    | -7 %     | 0.3               | $\infty$    | 0.3   | positivity | $H_\infty$ :<br>$\gamma_1 < 0.1$ |
| aft    | +5 %     | 0.3               | $\infty$    | 0.3   |            |                                  |

Table 10.6: Parameter-setting for the lateral control design.

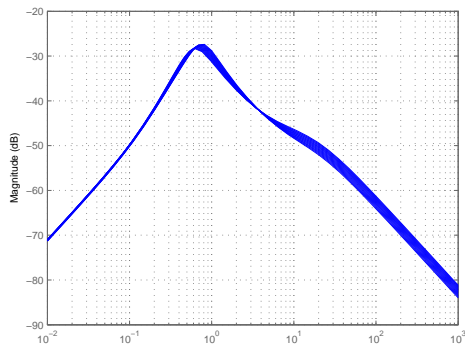
The synthesized static state-feedback controller figures in Table 10.7. Again, the final output-feedback controller is obtained by zeroing the feedback on the actuator states  $\delta l$  and  $\delta n$ .

|                  | $n_y$    | $r$     | $p$     | $\phi$ | $\delta l$ | $\delta n$ |
|------------------|----------|---------|---------|--------|------------|------------|
| $K_{\delta l} =$ | -0.71055 | 0.84715 | 4.2449  | 3.1964 | (0.049292) | (0.09115)  |
| $K_{\delta n} =$ | 0.11756  | 4.1335  | 0.10618 | 1.3366 | (-0.35831) | (0.26383)  |

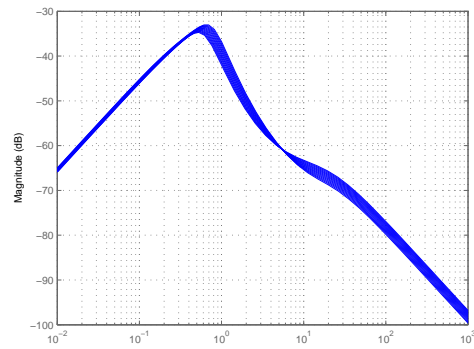
Table 10.7: Lateral static robust controller.

The controller is valid for the whole range of  $X_g$  positions except for the  $\lambda = 0.3$  stability degree constraint in aft position. Whereas the full state-feedback controller realizes this constraint, zeroing the actuator feedback leads to a small loss in stability degree of  $\Delta\lambda = 0.03$ , compare with Table 10.8. With *dutch roll* being the critical mode in lateral dynamics, the properties of this mode are displayed in Table 10.8 (next to activity  $\gamma_1$

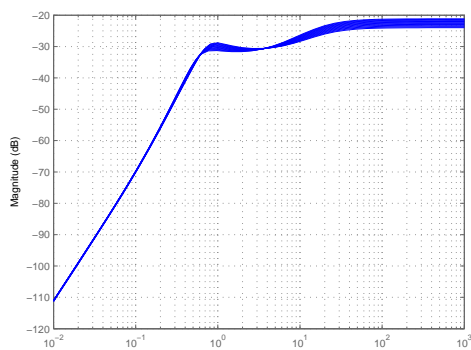




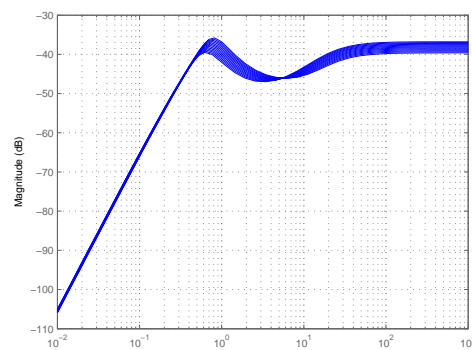
(a) Aileron position output



(b) Aileron rate output



(c) Rudder position output



(d) Rudder rate output

Figure 10.6: Magnitude (frequency response) of wind input to actuator outputs  $T_{w_1 \rightarrow z_1}$  as a function of  $dx_g$ . Lateral motion.

### 10.3 Stability and Performance Analysis

This section deals with the examination of the stability and performance characteristics of the airplane, stabilized with the robust back-up controller in the presence of rate saturations. The stability domains are computed as well as the  $L_2$  gain and convergence speed of the closed-loop system. Longitudinal and lateral motions are presented separately. Since very good results for positivity have been obtained, the resulting stability domains are expected to be of more than sufficient size.

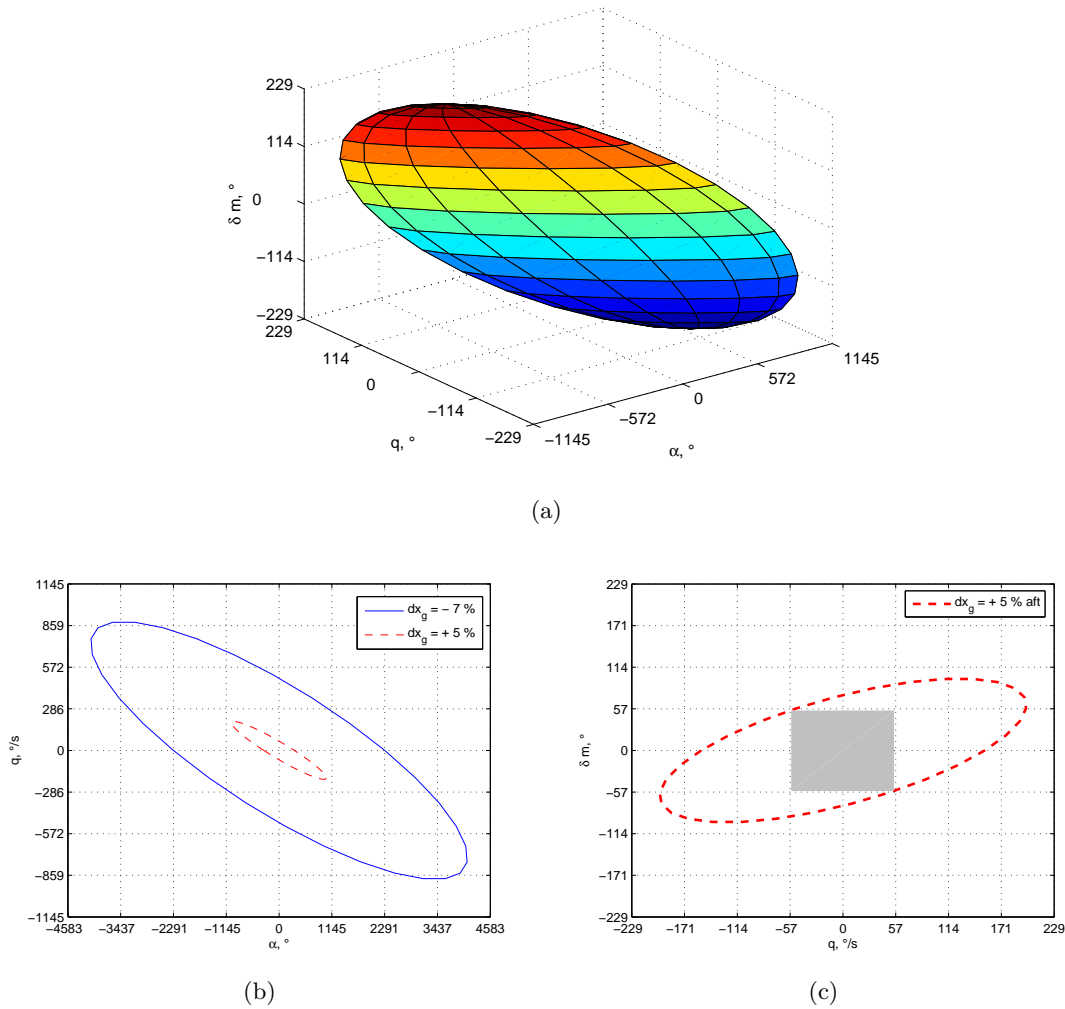


Figure 10.7: Domain of attraction. Longitudinal motion.

### 10.3.1 Longitudinal Stability and Performance

#### Stability Domain

Figure 10.7(a) depicts the stability ellipsoid for a +5% aft position in all three state dimensions, including the actuator state. Since a 3D view is not very satisfying, Figure 10.7(b) shows the projection of the stability domain on the  $\alpha - q$ -plane for two extremal  $X_g$  positions. The  $X_g$  dependence of the domain is clearly visible. The domain shrinks significantly for aft positions but is still more than sufficiently large for all  $X_g$ .

Since this 2D projection does not deliver complete information, Figure 10.7(c) shows the projection on the  $q - \delta m$ -plane for the smaller stability domain, i.e. for the aft c.o.g. position. We notice that the actuator state  $\delta m$  is the most constraining one.

It is thus useful to compute the dimensions of a cube maximized in volume that lies completely within the ellipsoid, centered at the origin. The computation method for this cube is straightforward from Proposition 9.7: the domain is maximized in all state directions homogeneously. The cube is found for the maximized value of the first state reaching the stability limit.

Thus, the cube describes a space of equally maximized system states for which stability is guaranteed. This space belongs to the larger stability domain, hence larger values with guaranteed stability for some (not all) states exist. One face of such a cube is sketched in Figure 10.7(c) for a rate saturation value of  $30^\circ/s$ . The reader notices, that the cube only covers a fraction of the guaranteed stability domain.

The state space defined by the cube is given by:

$$\begin{cases} -45.9^\circ & \leq \alpha & \leq +45.9^\circ \\ -45.9^\circ/s & \leq q & \leq +45.9^\circ/s \\ -45.9^\circ & \leq \delta m & \leq +45.9^\circ \end{cases} \quad (10.3)$$

The values are more than sufficiently large, especially when considering a large civil transport aircraft.

It is interesting to notice that the cube side length, i.e. in this case  $2 \times 45.9$ , is linearly dependent on the saturation value, as can be directly seen from Eq. (9.33). Since the dead-zone is normalized and the technique examines the linear part of the system, an increase in rate saturation translates directly into an increase in volume of the ellipsoid.

This fact is especially interesting from a conceptual point of view when determining minimum actuator characteristics. The exchange rate for one degree per second rate saturation  $sat(1^\circ/s)$  to cube side length increase  $\Delta l_{c,lon}$  corresponds to

$$\frac{\Delta l_{c,lon}}{sat(1^\circ/s)} = 3.06 \quad (10.4)$$

### Maximum Commanded Input and Convergence Speed

Figure 10.8 deals with performance issues and was computed by maximizing the performance stability domain in the direction of an added performance signal state  $w$ , as in Eqs. (9.47) to (9.49). The exogenous input signal is set to be a pilot load factor command  $w = n_{z,c}$ , rate saturation is again at  $30^\circ/s$ . In the upper plot, the convergence speed  $\mu$  of the stability domain is given as a function of the commanded pilot input. The maximum commanded value is reached, when the stability domain no longer converges (or contracts), and thus has a speed of zero. In the lower plot, the associated  $L_2$  gain (or induced norm) is presented as a performance parameter for output  $n_z$ .

The resulting maximum command values are again more than sufficient. A value of  $n_{z,max} = 14g$  is to be considered unrealistic. Even  $n_{z,max} = 2.8g$  for aft c.o.g. suffices

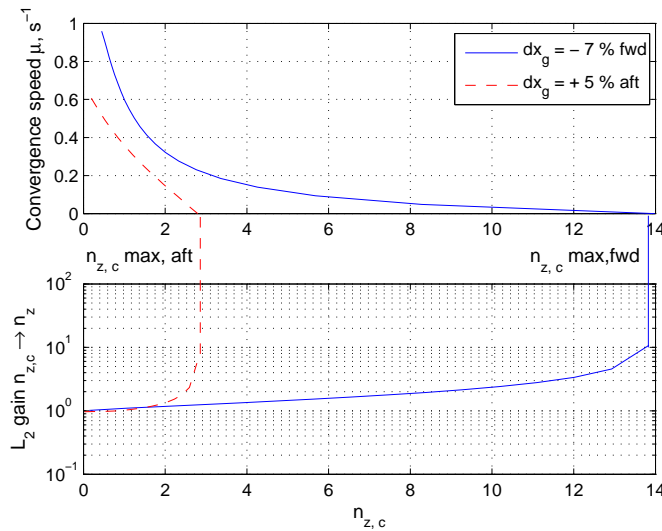


Figure 10.8: System performance. Longitudinal motion.

largely, especially in the context of a back-up control law for a civil airplane.

### 10.3.2 Lateral Stability and Performance

#### Stability Domain

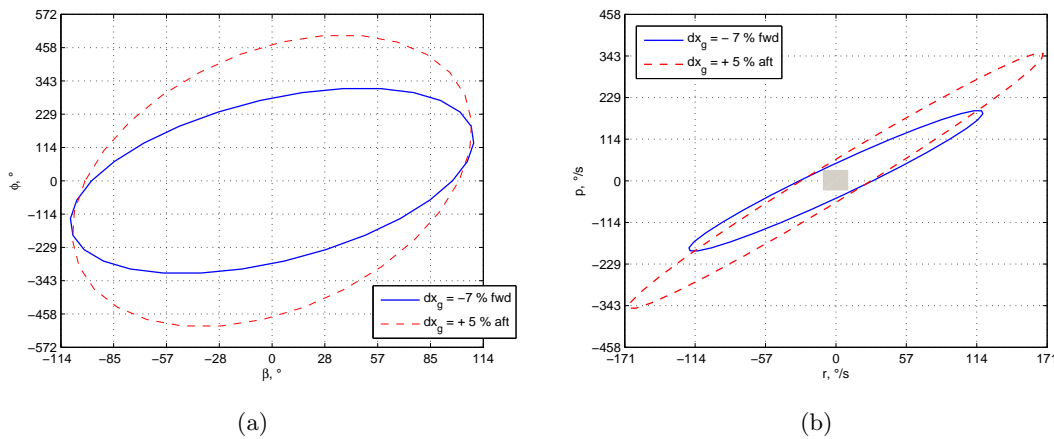


Figure 10.9: Domain of attraction. Lateral motion.

The same explanations as in the previous subsection apply. Since the ellipsoid is now a hyper-ellipsoid in the six-dimensional state space, only 2D projections on the  $\beta - \phi$ -plane (Figure 10.9(a)) and the  $r - p$ -plane (Figure 10.9(b)) are presented for two extremal  $X_g$ . Interestingly, in this case the fwd c.o.g. seems to reduce the size of the stability domain.

For a better comprehension, one has to consider the lateral open- and closed-loop poles for both c.o.g. positions: the natural spiral mode is less unstable for aft positions, hence the larger domain of attraction.

The projection on the  $r - p$ -plane shows the limiting case. One face of the hypercube corresponding to the smallest stability domain is sketched. The state variables are limited to:

$$\begin{cases} -8.7^\circ & \leq \beta & \leq +8.7^\circ \\ -8.7^\circ/s & \leq r & \leq +8.7^\circ/s \\ -8.7^\circ/s & \leq p & \leq +8.7^\circ/s \\ -8.7^\circ & \leq \phi & \leq +8.7^\circ \\ -8.7^\circ & \leq \delta l & \leq +8.7^\circ \\ -8.7^\circ & \leq \delta n & \leq +8.7^\circ \end{cases} \quad (10.5)$$

These values seem to be small, or even insufficient, especially with regard to roll rate  $p$  and maximum elevator deflections  $\delta l$  and  $\delta n$ . One should keep in mind, that the technique of computing the hypercube is conservative as it describes only a small space within the region of attraction. It will be thus very interesting to apply the technique described in Section 9.4.2. A possible application would be to give more weight to the actuators and roll rate before maximizing the domain.

The exchange rate of cube volume per saturation degree is significantly lower compared to the longitudinal case. When changing the rate saturation of both aileron and rudder actuators by one degree per second, the cube side length increase is:

$$\frac{\Delta l_{c,lat}}{sat(1^\circ/s)} = 0.58 \quad (10.6)$$

One has to consider as well that in the lateral motion two saturations are considered (aileron and rudder), thus the problem is more constrained. Furthermore, the aircraft is laterally unstable for all  $X_g$  positions whereas in the longitudinal motion only aft positions are unstable. Using actuators with higher saturation limits, e.g.  $60^\circ/s$  leads to a cube with a side length of  $2 \times 17.5$ . Remarkably, changing the aileron or rate saturation individually does not deliver the same exchange rates. Table 10.9 shows the resulting cube side length for a combination of aileron and rudder rate saturations. The aileron actuator seems more influencing, hence more constraining.

|                       |    | $sat_{rud}, ^\circ/s$ |                 |                 |
|-----------------------|----|-----------------------|-----------------|-----------------|
|                       |    | 15                    | 30              | 60              |
| $sat_{ail}, ^\circ/s$ | 15 | $2 \times 4.4$        | $2 \times 4.5$  | $2 \times 4.6$  |
|                       | 30 | $2 \times 7.5$        | $2 \times 8.7$  | $2 \times 9.2$  |
|                       | 60 | $2 \times 9.4$        | $2 \times 14.9$ | $2 \times 17.5$ |

Table 10.9: Lateral exchange rates.

## Maximum Commanded Input and Convergence Speed

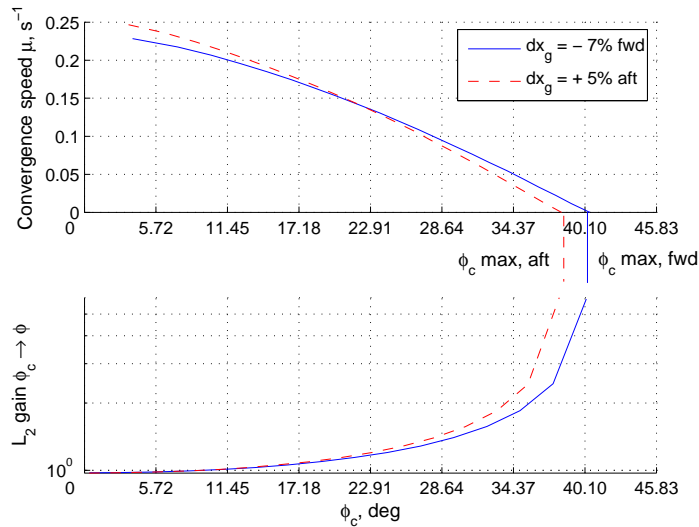


Figure 10.10: System performance. Lateral motion.

Figure 10.10 shows the convergence speed as a function of a commanded input  $w = \phi_c$ . A maximum command in bank angle is reached when the convergence speed becomes zero or the  $L_2$  gain from command input to bank angle output tends to infinity. The maximum allowable commanded bank angle is, again, more than sufficient for a back-up system.

## 10.4 Simulations

Figures 10.11 and 10.12 show the closed-loop performance of the system by the means of a nonlinear simulation with the complete coupled three-axis model. A pilot command of  $\phi_c = 30^\circ$  is given. The aileron, rudder, and elevator actuators are subject to saturation at  $sat = \pm 30^\circ/s$ .

Moreover, in Figures 10.13 and 10.14 the aircraft with controller is exposed to a turbulent atmosphere in both lateral and longitudinal directions. White Gaussian noise passing a Dryden spectral filter set to ‘stormy’ conditions is placed at wind inputs  $w_y$  and  $w_z$ . The turbulent scale lengths are set to  $L_{y,z} = 50\text{ m}$  and the turbulence intensity to  $\sigma_{y,z} = 5\text{ m/s}$ . Good flying qualities are obtained despite rate saturation on all three actuators (strong saturation on aileron rate).

## 10.5 Conclusion on the Robust Design Technique

The design of a robust static back-up control law for the naturally unstable VELA aircraft has been demonstrated. The controller is valid for a large range of center of gravity

positions and results from a multi-objective synthesis with guaranteed minimal flying qualities, minimization of actuator activity and a guaranteed performance within a large stability domain in the presence of actuator-rate saturations for the longitudinal motion as well as for the lateral one. The control law has been validated with a three-axis nonlinear simulator.

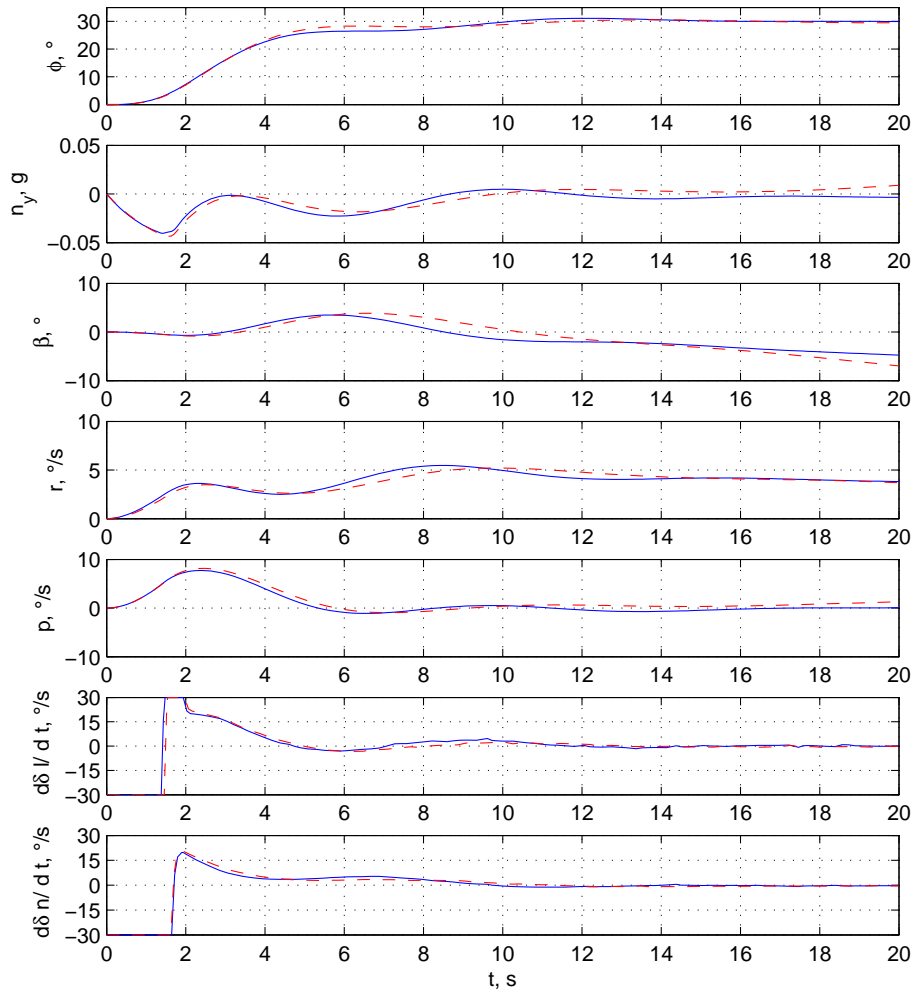


Figure 10.11: Time response to command  $\phi_c = 30^\circ$ .

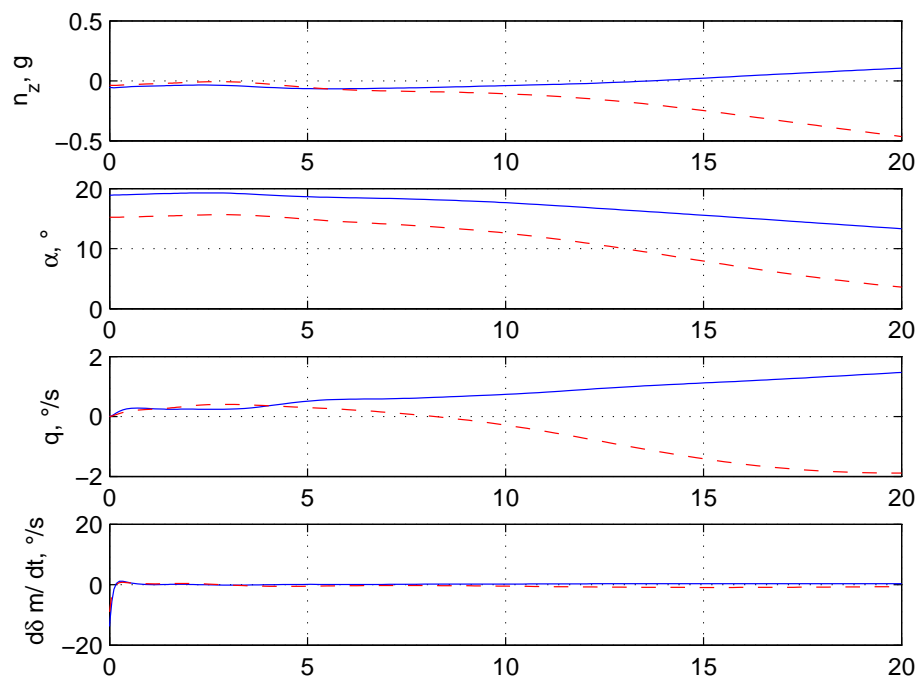


Figure 10.12: Time response to command  $\phi_c = 30^\circ$ .

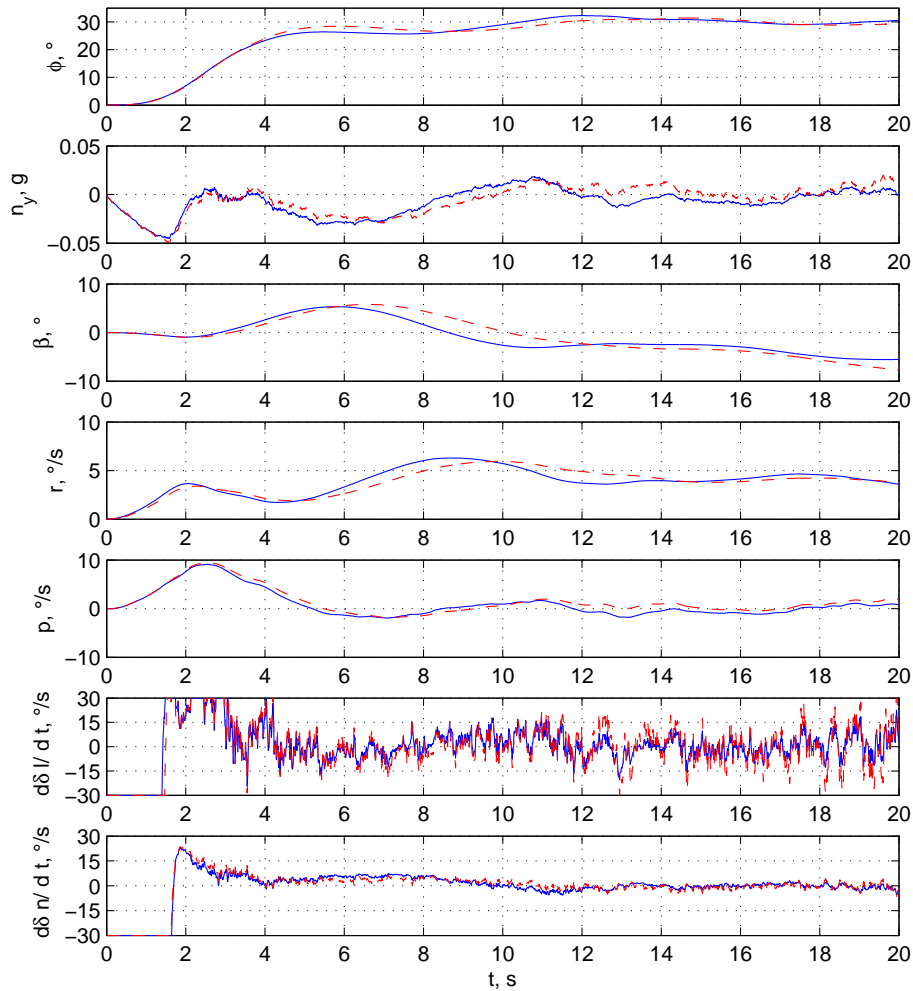


Figure 10.13: Time response to command  $\phi_c = 30^\circ$  in turbulent atmosphere.

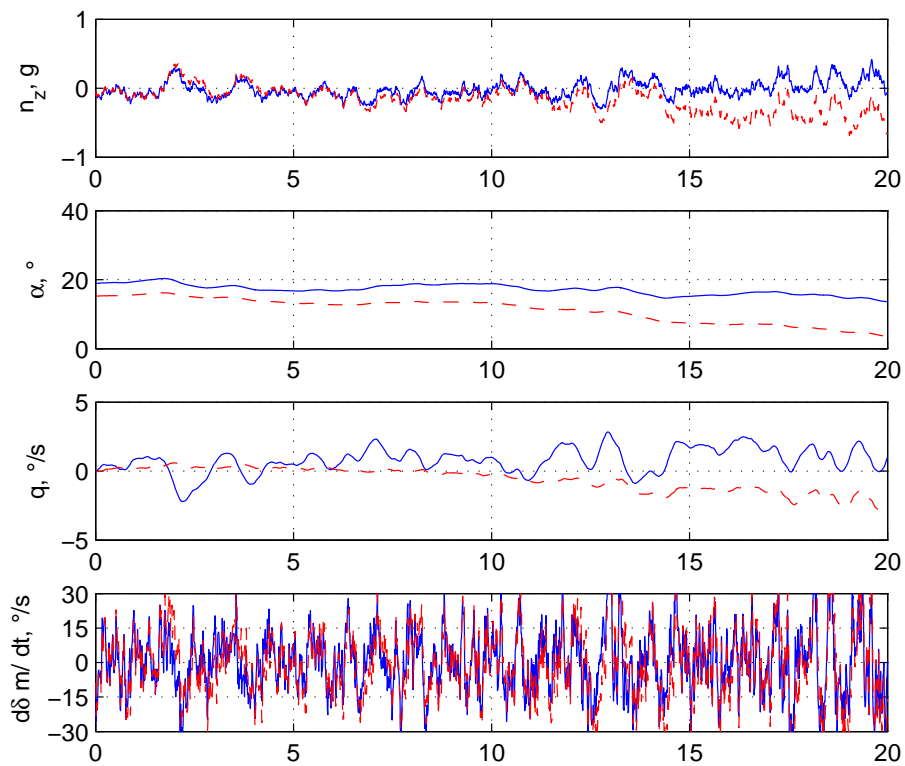


Figure 10.14: Time response to command  $\phi_c = 30^\circ$  in turbulent atmosphere.



**Part III**

**Synthesis**



## Chapter 11

# Gains and Potentials

Two overarching objectives defined the road map for this dissertation. The first one has been the assessment of the impact of reduced stability on airplane flight mechanics and dynamics, with a special focus on the size of the vertical tailplane and aft center of gravity positions. Methods and tools have been developed in view of achieving this first goal.

The second objective has been the design of a static robust back-up control law for the specified unstable aircraft design. This control law has been computed with the specifications in mind that were derived from the flight dynamics analysis. The degree of considered natural instability condensed in a multi-objective design approach taking into account a large range of center of gravity positions, the reduction of actuator activity, as well as stability in the presence of saturations.

A third objective remains. It is the logical consequence to demonstrate the benefits of accepting a reduced stability for the given aircraft. More precisely, an estimation of gains in mass, drag, and fuel consumption of the unstable aircraft in combination with the back-up controller is formulated as a final goal. Therefore, this chapter sets out to demonstrate that the potentials of reduced stability in civil transport aviation are assessable, under certain assumptions, with the developed methods and tools at an early stage of airplane conception.

To this aim, Section 11.1 gives the parameter settings for two VELA1 designs which differ in their natural degree of stability. A minimized fin size as well as an optimized c.o.g. range will result in potential mass and drag reductions. An estimation of these gains is presented in Sections 11.2 and 11.3, respectively. Finally, Section 11.4 demonstrates how these gains translate into possible fuel savings for a long range aircraft.

Simplified formulas for a rapid estimation of the gains in mass, drag, and fuel consumption are used. The applied techniques are derived from basic airplane design procedures, [56, 53, 67, 75, 51, 69]. Other valuable sources are [11, 88, 1].

## 11.1 Parameters of a Naturally Stable and an Unstable Airplane Design

Two principle parameters determine the degree of stability of the VELA1 aircraft: the size of the vertical tailplane (VTP) which consists of two vertical fins, and the allowable range of center of gravity positions. Thus, a stable and an unstable version of the same airplane can be compared easily by adjusting these parameters. This section briefly juxtaposes an aircraft that is naturally stable in the two most critical modes *short-period oscillation* (SPO) and *dutch roll* (DR), and the examined unstable concept incorporating the stabilizing back-up control law. The corresponding settings for both parameters figure in Table 11.1. Figure 11.1 depicts the open-loop poles of the aircraft at low speed with augmented fins and a reduced range of c.o.g. positions.

|           | stable               | unstable          |
|-----------|----------------------|-------------------|
| $dx_g$    | $[-7\% - 2\%]$       | $[-7\% + 5\%]$    |
| $S_{vtp}$ | $2 \times 122.3 m^2$ | $2 \times 45 m^2$ |

Table 11.1: Range of c.o.g. displacements  $dx_g$  and reference surfaces of the fins  $S_{vtp}$  for two VELA1 designs.

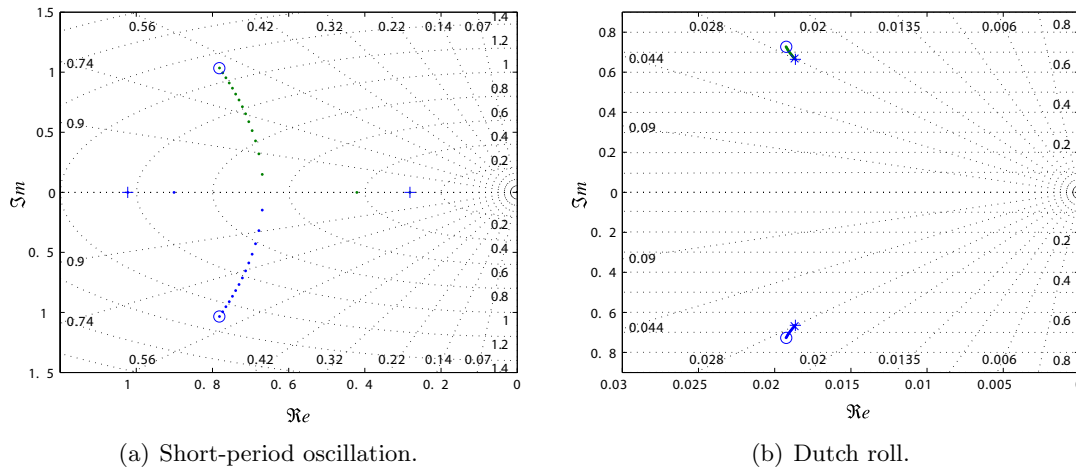


Figure 11.1: Open-loop poles of a VELA1 concept naturally stable in SPO and DR.

The augmented fin size of  $122.3 m^2$  has been chosen for facilitated comparison with the VTP of the Airbus A380 airplane and suffices to stabilize the dutch-roll mode. The surface ratio  $\tau_{vtp}$  of minimized to augmented fins is

$$\tau_{vtp} = \frac{S_{vtp,u}}{S_{vtp,s}} = 0.37 \quad (11.1)$$

The aft c.o.g. limit for the stable design corresponds to the neutral point position during cruise flight. The degree of stability of the SPO suffices largely up to  $-2\%$  fwd in

c.o.g. position. The next section will estimate the reduction in mass due to the minimized fins.

## 11.2 Estimation of the Gain in Mass

The construction of the VELA fins is assumed to be comparable to the Airbus A380 VTP which is very similar in size w.r.t. the naturally stable version of the VELA1 concept. The A380 rudder is composed of two panels with two electrical backup hydrostatic actuators (EBHA) each [50, 64, 82]. These are powered by a segregated electrical circuit if hydraulic systems fail. The amount of flight control hardware might be subject to change for the unstable VELA1 aircraft since the aircraft is, unlike the A380, laterally unstable.

Let us assume that a stable VELA configuration has two A380 VTPs as vertical fins. The corresponding data for one A380 VTP are given in Table 11.2.

|                   |                  |          |        |
|-------------------|------------------|----------|--------|
| Reference surface | $S_{vtp}$ ,      | $m^2$    | 122.30 |
| Reference length  | $l_{vtp}$ ,      | $m$      | 8.92   |
| Height or span    | $H_{vtp}$ ,      | $m$      | 14.59  |
| Aspect ratio      | $\Lambda_{vtp}$  |          | 1.74   |
| Taper ratio       | $\lambda_{vtp}$  |          | 0.39   |
| Root chord        | $rc_{vtp}$ ,     | $m$      | 12.06  |
| Tip chord         | $tc_{vtp}$ ,     | $m$      | 4.70   |
| 25 % sweep angle  | $\varphi_{25}$ , | $^\circ$ | 40.00  |

Table 11.2: A380 vertical tailplane specifications, [50, 5].

Mass estimation procedures are usually based on statistic data taken from a considerable number of airplanes already built. Thus, the introduction of recent developments, like new light-weight materials and/or the implementation of modern additional flight control hardware into a stabilizing surface is often not covered by these formulas. The reason for this is simply that not enough aircraft have been built in order to incorporate statistically significant data incorporating these new technologies [15].

Nonetheless, well known estimation formulas are used here for a first approximation. The mass of the VTP shall here be estimated with Eq. (11.2), [53, 58].

$$m_{vtp} = 0.00506 S_{vtp} (S_{vtp} + 3.25)^{1/4} (\Lambda_{vtp} + 25) \left( \frac{0.025}{\delta_{vtp}} + \delta_D \right)^{1/4} \cdot (\varphi_{25}^2 + 2) \left( \frac{2 + \sqrt{\tau}}{S_{vtp, str}/S_{vtp}} \right)^{1/4} \left( \frac{V_D}{100} + 5.18 \right)^{5/4} \quad (11.2)$$

$S_{vtp, str}$  in  $m^2$  denotes the surface of the supporting structure of the VTP, as in Fig-

ure 11.2. That is, the surface of the fin minus all actuated parts (rudder).  $S_{vtp, str}$  is here roughly estimated to  $0.7 \cdot S_{vtp}$ .

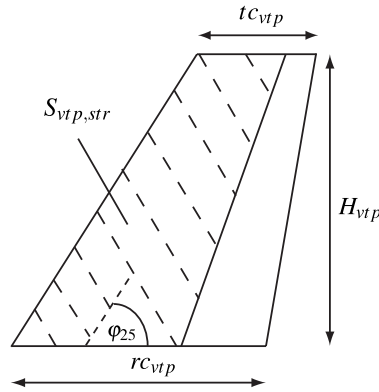


Figure 11.2: VTP dimensions and surface of supporting structure.

$\delta_{vtp}$  is the mean thickness to chord ratio and is determined via

$$\delta_{vtp} = \frac{3\delta_r + \delta_t}{4} \approx 0.188 \quad (11.3)$$

This equation weights the root thickness ratio  $\delta_r$  and tip thickness ratio  $\delta_t$  and determines an overall mean thickness of the VTP.

The last term needed for a mass estimation is  $V_D$  designating the design diving speed in equivalent airspeed ( $EAS$ ,  $km/h$ ). This speed is an important factor when determining the structural strength of the VTP.  $V_D$  is determined by a 20 s dive at  $7.5^\circ$  slope, starting from the maximum operating speed. When knowing the design cruising speed  $V_C$  this speed can also be computed with [67]

$$V_D = 1.25 \cdot V_C \quad (11.4)$$

The factor of 1.25 represents a safety margin between cruise flight and maximum structural load at  $V_D$ . The design cruise speed in true air speed ( $TAS$ ) is set to approximately

$$V_{C, TAS} \approx 260.0 \text{ m/s} \quad (11.5)$$

Conversion to  $EAS$  via factor  $k$

$$k = \sqrt{\frac{\rho}{\rho_0}} \approx 0.55 \quad (11.6)$$

results in

$$V_{C, EAS} = 143.0 \text{ m/s} \quad (11.7)$$

The resulting design diving speed becomes

$$V_{D,EAS} = 178.8 \text{ m/s} = 643.5 \text{ km/h} \quad (11.8)$$

Inserting all parameters into Eq. (11.2) delivers a first simplified mass estimation for the A380 VTP:

$$m_{vtp,A380} \approx 3215 \text{ kg} \quad (11.9)$$

This mass estimate is in the proximity of the actual weight of a fully equipped A380 VTP (3500 kg, [65]). The mass of a fin for a stable configuration is thus assumed to be roughly equal to the mass of the A380 VTP.

When now estimating the mass of a VTP with smaller dimensions, the mass of the flight control hardware will not reduce. Since the surface of the VTPs is reduced drastically for the unstable but more efficient configuration, the rudders of the two VTPs are supposed to incorporate only one panel each but each with two actuators for back-up reasons (redundancy/security [19]). Thus, the mass for an additional set of actuators will be added onto the mass estimate of smaller fins.

Corresponding to [11, 88, 1, 64] the additional mass associated to a modern actuator is somewhere between 130 kg and 180 kg.

The dimensions of the new reduced VTP are scaled with  $\tau_{vtp} = 0.37$ . The specifications detail in Table 11.3

|                   |                 |          |       |
|-------------------|-----------------|----------|-------|
| Reference surface | $S_{vtp}$       | $m^2$    | 45.00 |
| Reference length  | $l_{vtp}$       | $m$      | 3.28  |
| Height or span    | $H_{vtp}$       | $m$      | 5.37  |
| Aspect ratio      | $\Lambda_{vtp}$ |          | 0.64  |
| Taper ratio       | $\lambda_{vtp}$ |          | 0.39  |
| Root chord        | $rc_{vtp}$      | $m$      | 4.43  |
| Tip chord         | $tc_{vtp}$      | $m$      | 1.73  |
| 25 % sweep angle  | $\varphi_{25}$  | $^\circ$ | 40.00 |

Table 11.3: VELA1 reduced vertical tailplane specifications.

The structural mass computes to

$$m_{vtp,vela,str} \approx 1027 \text{ kg} \quad (11.10)$$

Adding the estimated mass of two actuators of roughly 300 kg delivers

$$m_{vtp,vela} \approx 1327 \text{ kg} \quad (11.11)$$

The final mass gain for two vertical fins can thus be computed:

$$\Delta_{mass} = 2 \cdot (3500 - 1340) \text{ kg} = 4320 \text{ kg} \quad (11.12)$$

### 11.3 Estimation of Drag Reduction

Generally speaking, two superordinate types of airplane drag can be distinguished: one depending on the generated lift and the other independent of the lift production. A general description is given by the well-known lift/drag polar, Eq. (11.13), see also Figure 11.3:

$$C_X = C_{X0} + k \cdot (C_Z - C_{ZC_{X0}})^2 \quad (11.13)$$

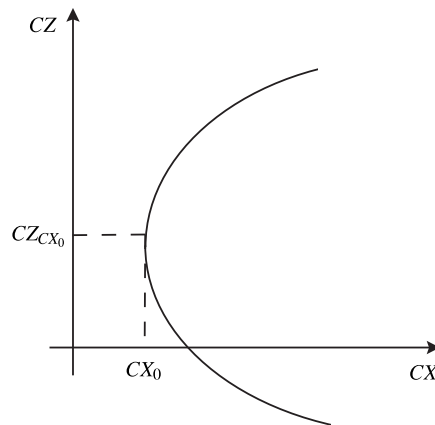


Figure 11.3: Typical lift/drag polar.

The lift independent part  $C_{X0}$  can basically be broken down into friction and form (or pressure) drag as well as interference drag and other drag types, also known as parasite drag.

The part depending on lift increases quadratically with the lift coefficient  $C_Z$  (minus the value of  $C_Z$  corresponding to  $C_{X0}$ ) multiplied with factor  $k$ , being

$$k = \frac{1}{e \cdot \pi \cdot \Lambda} \quad (11.14)$$

Here,  $\Lambda$  is the airfoil aspect ratio and  $e$  the Oswald factor, which is around 0.8 to 0.9 for cruise flight of common jet airplanes [49]. The lift dependent part is known as induced drag.

Finally, the trim of the airplane in cruise flight adds as well to the total drag. The so called trim drag is produced by the deflection of aerodynamic surfaces in order to keep the aircraft equilibrated. Since the overall lift balance is not changed the trim drag represents extra pressure or form drag.

Figure 11.4 breaks down the overall drag for a common jet airplane into the different

drag types and their typical contribution [49].

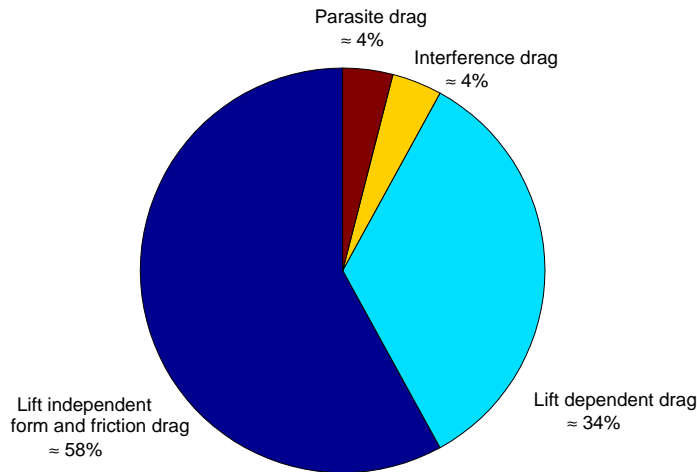


Figure 11.4: Typical contribution of different drag types.

The influence of a minimized fin size or a modification of the c.o.g. range can now be estimated. The reader will expect of course a significant reduction of friction and form drag due to a smaller fin surface. Furthermore, the reduced VTP mass will call for less necessary lift in cruise flight and hence less induced drag is expected. Finally, a modified allowable c.o.g. range can yield optimized cruising trim points and therefore reduce the trim drag due to smaller trim deflections.

The next subsections will treat each point individually and present a final overall estimation of the attainable reduction in fuel burn. The drag reduction will be measured in *drag counts dc*. One drag count equals  $dc = \Delta C_X = 1 \cdot 10^{-4}$ .

### 11.3.1 Friction and Form Drag

The computation of the gain in friction drag is straightforward. The dimensions of the fins are just scaled and so is the drag coefficient for the fins.

The fins, as concerns their surface, are assumed to produce only lift independent drag, i.e. friction and form drag. The drag coefficients for straight and symmetric flight for two small ( $2 \times 45 m^2$ ) fins and two enlarged fins ( $2 \times 122.3 m^2$ ) are given with [6]

$$C_{X0_{45}} = 3.59 \cdot 10^{-4} \quad (11.15)$$

$$C_{X0_{122.3}} = 9.7568 \cdot 10^{-4} \quad (11.16)$$

The achievable reduction in friction and pressure drag sums up to

$$\Delta C_X = 6.1668 dc \quad (11.17)$$

With  $C_{X0,nf} = 8.2 \cdot 10^{-3}$  for the flying-wing body without fins, the lift independent drag parts for a stable and an unstable VELA configuration are:

$$C_{X0,unstable} = 8.5 \cdot 10^{-3} \quad (11.18)$$

$$C_{X0,stable} = 9.2 \cdot 10^{-3} \quad (11.19)$$

### 11.3.2 Induced Drag

For the computation of gains in induced drag it is assumed that the payload and fuel amount stay unchanged. Only the operational empty weight (OWE) of the aircraft is smaller due to smaller fins. Therefore, the necessary lift coefficient  $C_Z$  for cruise flight decreases as well. It is true that for equilibrated cruise the aircraft weight equals its lift force  $L$

$$m \cdot g = L = \frac{1}{2} \rho V^2 S C_Z \quad (11.20)$$

Thus, a change in  $C_Z$  with a reduced VTP mass is determined by

$$\Delta C_Z = \frac{2 \Delta m_{fins} g}{\rho V^2 S} \quad (11.21)$$

With Eq. (11.13) the reduction in induced drag therefore computes to:

$$\begin{aligned} \Delta C_{Xind} &= k \cdot \left[ \left( C_Z - C_{ZC_{X0}} \right)^2 - \left( (C_Z - \Delta C_Z) - C_{ZC_{X0}} \right)^2 \right] \\ &= k \cdot \Delta C_Z \cdot \left[ 2 C_Z - \Delta C_Z - 2 C_{ZC_{X0}} \right] \end{aligned} \quad (11.22)$$

For the VELA1 blended-wing body aircraft the Oswald factor is 0.99 and  $k$  becomes 0.0652 with  $\Lambda = 4.93$ . The value of the lift coefficient at minimum drag  $C_{ZC_{X0}}$  is assumed to be negligible [6].

For flight at 36000 *ft*,  $Mach = 0.86$ ,  $C_Z = 0.29$ , and with  $\Delta m_{fins} = 4320$  *kg*, see Eq. (11.12), the lift coefficient diminishes by

$$\Delta C_Z = 1.8 \cdot 10^{-3} \quad (11.23)$$

The potential saving on induced drag sums up to

$$\Delta C_{Xind} = 0.69 dc \quad (11.24)$$

### 11.3.3 Trim Drag

The VELA aircraft does not have a separate horizontal plane for trimming, i.e. the airplane needs to be trimmed with the elevators. It is assumed here that trim drag is principally determined by the amount of elevator deflection necessary to trim the aircraft in cruise flight. It is therefore obvious that c.o.g. positions close the aircraft neutral point are beneficial for a reduced trim deflection.

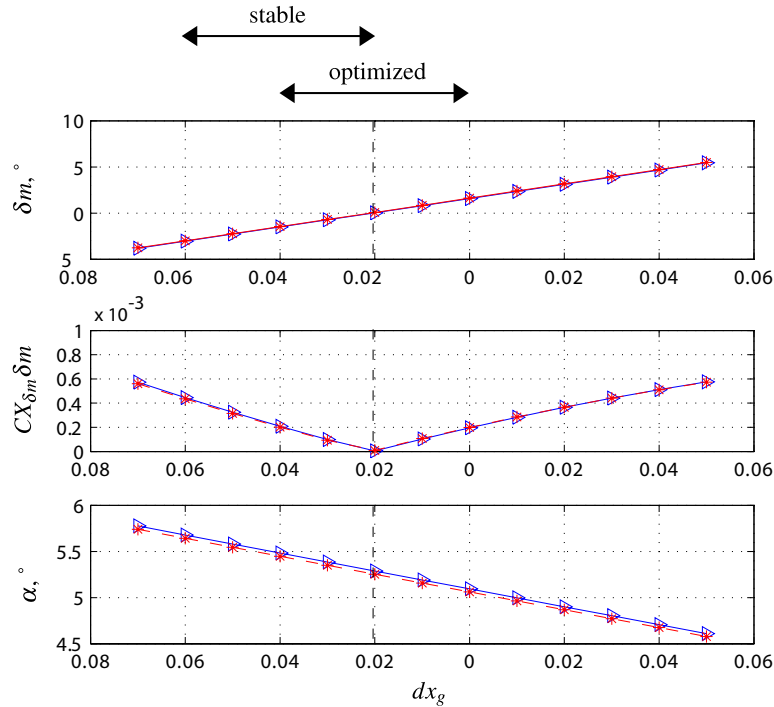


Figure 11.5: Elevator trim deflection and drag in cruise flight. Two exemplary c.o.g. ranges are indicated as well as the position of the neutral point.

Figure 11.5 shows the required elevator deflections for a range of c.o.g. positions as well as for the two specified fin sizes for cruise flight at  $Mach = 0.86$  and  $36.000 ft$ . A mass of  $m = 700 t$  is assumed for the aircraft with larger fins and  $m - \Delta m_{fins}$  for that with smaller ones. The corresponding drag coefficient  $C_{X\delta m}\delta m$  is displayed as well as the corresponding angle of attack  $\alpha$ .

The curves for the two masses and fin surfaces nearly coincide. The neutral point moves forward for higher speeds and altitude ( $dx_g = -2\%$ ).

The selection of a c.o.g. range around the neutral point is beneficial. Keeping the c.o.g. within the neutral point's proximity ( $\pm 2\%$ ) keeps the trim drag under 2 drag counts. More fwd or aft positions increase drag significantly. An average gain of 1 drag count for a 4%-c.o.g. range seems realistic for an aircraft with c.o.g. positions centered around the neutral point compared to a naturally stable aircraft being trimmed to fwd positions only.

$$\Delta C_{Xtrim} \approx 1 dc \quad (11.25)$$

## 11.4 Estimation of the overall Gain in Fuel Burn

Now, that the gains in mass and drag are roughly determined the actual reduction in fuel burn for a long range flight can be estimated. It will be assumed that flight phases other than cruise flight can be neglected in the course of this estimation.

### 11.4.1 Fuel Consumption and Drag

In steady state, symmetric, and horizontal flight, thrust  $F$  equals the total drag force  $D$  and lift  $L$  equals the aircraft weight  $W$ :

$$F = D \quad L = W \quad (11.26)$$

With *glide angle*  $\varepsilon$  the thrust becomes:

$$F = \varepsilon \cdot L = \varepsilon \cdot G \quad \varepsilon = \frac{D}{L} \quad (11.27)$$

The fuel mass is denoted as  $m_F$ , the fuel consumption  $\dot{m}_F$  and the **thrust specific fuel consumption** (TSFC)  $b_F$ . The definitions read:

$$\dot{m}_F = \frac{dm_F}{dt} \quad b_F = \frac{\dot{m}_F}{F} \quad (11.28)$$

During flight the aircraft weight reduces by the amount of fuel burned. Using Eqs. (11.27) and (11.28) the weight change ratio is given by

$$\frac{1}{g} \frac{dW}{dt} = -\frac{dm_F}{dt} = -b_F \cdot \varepsilon \cdot W \quad (11.29)$$

Separation of variables and integration delivers the flight time  $t_R$ :

$$t_R = -\frac{1}{g} \int_{W_0}^{W_E} \frac{1}{\varepsilon \cdot b_F} \cdot \frac{dW}{W} \quad (11.30)$$

where  $W_0$  is the *weight at the beginning* and  $W_E$  the *weight at the end* of the cruise flight phase. It is now assumed that the product of specific fuel burn and glide angle stays constant:  $\varepsilon \cdot b_F = \text{const} = \bar{\varepsilon} \cdot \bar{b}_F$  (the ‘bar’ denotes the mean value over cruise flight).

After integration the flight time becomes

$$t_R = \frac{1}{g \cdot \bar{b}_F \bar{\varepsilon}} \cdot \ln \frac{W_0}{W_E} \quad (11.31)$$

With  $W_F$  being the fuel weight

$$\frac{W_0}{W_E} = \frac{1}{1 - \frac{W_F}{W_0}} = \frac{1}{1 - \frac{m_F}{m_0}}$$

the total cruise flight time becomes

$$t_R = -\frac{1}{g \cdot \bar{b}_F \bar{\varepsilon}} \cdot \ln\left(1 - \frac{m_F}{m_0}\right) \quad (11.32)$$

Note that Eq. (11.32) is the well-known Breguet range equation when multiplying with mean cruise speed  $\bar{V}_c$ .

The goal is now to infer from this formula the fuel savings due to drag reduction. Therefore, Eq. (11.32) is solved for fuel mass  $m_F$ , which is then a function of the mean glide angle  $\bar{\varepsilon}$ :

$$m_F(\bar{\varepsilon}) = m_0 \cdot \left(1 - e^{(-g t_R \bar{b}_F \bar{\varepsilon})}\right) \quad (11.33)$$

Using the first term of a Taylor series expansion for Eq. (11.33) in terms of  $\bar{\varepsilon}$  delivers the approximated change in fuel  $\Delta m_F$  due to a change  $\Delta \bar{\varepsilon}$  in mean glide angle:

$$\underbrace{m_F(\bar{\varepsilon}) - m_F(\bar{\varepsilon}_0)}_{\Delta m_F} \approx g m_0 t_R \bar{b}_F e^{(-g t_R \bar{b}_F \bar{\varepsilon}_0)} \cdot \underbrace{(\bar{\varepsilon} - \bar{\varepsilon}_0)}_{\Delta \bar{\varepsilon}} \quad (11.34)$$

The error for considering only the first Taylor series term is smaller  $< 1\%$ . In the following, the ‘bars’ will be omitted for the sake of legibility. In order to obtain the change in fuel  $\Delta m_F$  due to a change in mean drag  $\Delta C_X$  the following relation is used:

$$\Delta \varepsilon = \frac{\Delta F}{W}, \quad \text{and} \quad \Delta F = \Delta D = \frac{\Delta C_X}{C_X} \cdot D = \frac{\Delta C_X}{C_X} \cdot \varepsilon_0 \cdot W \quad (11.35)$$

Finally, the expression for the fuel burn savings due to a change in drag  $\Delta C_X$  reads:

$$\Delta m_F = t_R b_F W_0 \varepsilon_0 \cdot \frac{\Delta C_X}{C_X} \cdot e^{(-g t_R b_F \varepsilon_0)} \quad (11.36)$$

### 11.4.2 Fuel Burn Due to One Drag Count

The VELA aircraft is assumed to operate engines that exhibit a slightly better performance in terms of specific fuel consumption than the Engine Alliance GP7270 engine of the Airbus A380. Furthermore, the average glide angle in cruise flight is assumed to be significantly better than for classical transonic aircraft. The flight distance is set similar to a long range mission profile used by the Airbus technical marketing division for the A380 [65].

$$C_{Xc} = 0.015 \quad t_R = 7.1 \text{ h} \quad W_0 = 6867 \cdot 10^3 \text{ N} \quad (11.37)$$

$$C_{Zc} = 0.27 \quad V_c = 255 \text{ m/s} \quad \varepsilon = \frac{1}{18} \quad (11.38)$$

$$\Delta C_X = 1 \text{ dc} = 0.0001 \quad R = 6500 \text{ km} \quad b_F = 0.045 \frac{\text{kg}}{\text{N h}} \quad (11.39)$$

An estimation of the fuel burn saving due a 1 *dc* reduction in drag is now possible. The saved fuel mass computes to

$$\Delta m_F = 7.1 \text{ h} \cdot 0.045 \frac{\text{kg}}{\text{N h}} \cdot 6867 \cdot 10^3 \text{ N} \cdot \frac{1}{18} \cdot \frac{0.0001}{0.015} \cdot e^{(-9.81 \cdot 7.1 \cdot 0.045 \cdot \frac{1}{18})} \quad (11.40)$$

resulting in mass per drag count *dc* and trip

$$\Delta m_F = 683 \frac{\text{kg}}{\text{dc} \cdot \text{trip}} \quad (11.41)$$

### 11.4.3 Potential Fuel Burn Savings with Reduced Stability

This section presents the potential of savings on fuel when accepting a reduced stability due to a minimization of the vertical tailplane and placing the range of accessible center of gravity positions symmetrically around the neutral point. Of course, this implies the installation of an autonomously operating back-up control system, like the one being developed in the 2nd part of this dissertation.

A drag reduction of 1 *dc* translates into a fuel saving of  $\Delta m_F = 683 \text{ kg}$  per trip for the VELA aircraft. Fuel savings are expected due to a reduction in friction and form drag, induced drag, and trim drag, see Section 11.3. Table 11.4 lists each drag type and the corresponding potential on drag/fuel/cost savings. The fuel price is assumed to be  $P_f = 0.5 \text{ \$/kg}$  [65]. The aircraft is assumed to perform 650 missions per year, which equals to  $t_a = 7.1 \text{ h} \cdot 650 = 4615 \text{ h}$ .

## 11.5 Synthesis

The possible gains presented in Table 11.4 are impressive. Figure 11.6 sketches the contribution of each drag type that is modified with a change of c.o.g. position and fin area. Whereas the the VTP contributes to both friction and induced drag (fin surface and mass) the c.o.g. position influences the trim drag of the aircraft.

The estimate is based on the fact that the aircraft is certified with a back-up control system which implies the redundant installation of control hardware, such as additional

| drag type            | $\Delta C_X, dc$ | <i>kg/trip</i> | <i>\$/trip</i> | <i>kg/year</i> | <i>\$/year</i> |
|----------------------|------------------|----------------|----------------|----------------|----------------|
| friction<br>and form | 6.17             | 4281           | 2140           | 2 782 650      | 1 391 325      |
| induced              | 0.69             | 471            | 236            | 153 400        | 76 700         |
| trim                 | 1.0              | 683            | 342            | 443 950        | 221 975        |
| total                | 7.86             | 5368           | 177.4          | 3 489 200      | 1 744 600      |

Table 11.4: Potential fuel savings.

actuators for rudder, elevator, and ailerons and the associated infrastructure (hydraulic pipes, electrical pumps, etc.). The additional mass of automatic control hardware and its associated costs, including development and installation costs, might cancel out the savings due to a reduced VTP mass.

Still, resizing the VTP entails the largest potential in cost saving as it reduces the friction and form drag. However, as Chapter 6 showed, certification criteria linked to the  $V_{MC}$  will pose a problem when reducing the fin surface area. This implies certification for higher speeds or other extensive design changes, e.g. engine installation, to equilibrate the aircraft with one engine being inoperative. Moreover, a reduced fin size will call for the implementation of additional rudder and aileron hardware to stabilize the lateral motion.

Therefore, the best trade-off in terms of simplicity seems to be the optimization of the c.o.g. position. In contrast to the lateral motion, only one back-up set has to be installed for the elevator actuator due to reduced stability. Even though not representing the largest potential in fuel burn savings, the gain in trim drag is considerable<sup>1</sup>. One can argue, that an increase in activity and fatigue damage inflicted upon the actuators due to aft c.o.g. positions has to be expected, as shown in Chapter 4. But this problem is solved with the developed control design method. The actuator activity is reduced significantly and so is the fatigue damage. In addition, no special elevator actuator characteristics which might result in heavier and more expensive hardware are necessary as the conceived controller is robust against standard saturations and works with standard actuators thanks to its multi-objective design.

---

<sup>1</sup>Remember that the considered aircraft is a blended-wing body concept and not a classical airplane.

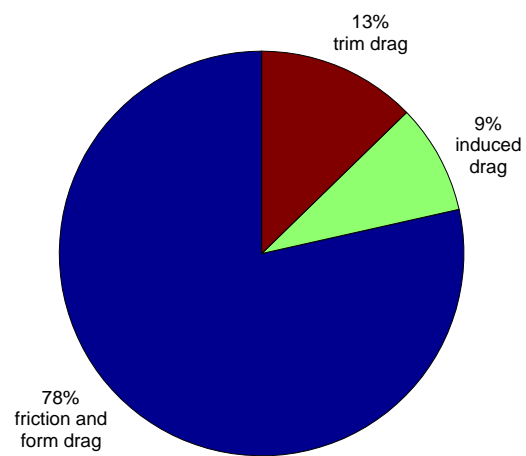


Figure 11.6: Distribution of total drag/cost reduction onto drag types.

## Chapter 12

# Conclusion and Outlook

After an introduction to the research topic and the formulation of objectives, a framework of certification criteria and aircraft modeling aspects has been presented, building the starting point for this dissertation. The interdisciplinary nature of the subject then led to a natural division into two main parts of the thesis: one part, analyzing flight mechanics and dynamics in the context of reduced stability and another, dealing with automatic control design.

The flight dynamics analysis part opened with the examination of the effects of reduced stability on the longitudinal aircraft motion. A worthwhile contribution has been the analytic description of the airplane's short period oscillation within the framework of a stabilizing feedback law, actuator characteristics, and robustness against center of gravity displacements. Built on the results of this approach a numerical tool has been developed allowing for an estimation of control system activity and actuator fatigue damage caused by artificial stabilization. This technique was then applied to an exemplary vertical mission profile for a long range aircraft. Moreover, nonlinear actuator characteristics were considered which condensed in the development of a criterion relating minimum linear and nonlinear actuator requirements to a given degree of longitudinal instability.

The next step has been to take into consideration the lateral aircraft motion, and more specifically the criteria related to the *minimum control speed*. An analytical approach to these criteria led to the development of yet another numerical tool. This tool proved valuable when assessing the capability of an aircraft to fulfill these certification relevant criteria at an early design stage. Both static and dynamic criteria have been examined. The first part of the dissertation resulted in recommendations for the VELA flying-wing body design, demonstrating the applicability of the presented approach.

The automatic control part started with a short introduction to the problem and presented a specification list for a robust back-up control law. The control objectives were directly derived from the outcome of the flight mechanics and dynamics part.

A brief review of several possible design approaches was followed by the description of

the theory relevant to the polytopic state-feedback design technique. Due to the diversity of control demands several objectives had to be incorporated into the control design. A contribution has been the integration of modal,  $H_\infty$ , positivity, and robustness criteria into a one-shot convex design procedure. In addition, a static anti-windup control design technique was proposed allowing also for the integration of multiple criteria and models. A stability and performance analysis method has been adapted to assess the closed-loop properties in the presence of actuator saturations. The relation between actuator saturation characteristics and size of the stability domain has been demonstrated. Finally, good results were obtained on the naturally unstable VELA aircraft.

The third part of the dissertation sketches the estimation of potentials in mass, drag, and fuel consumption when exploiting reduced stability for civil transport aircraft. As concerns the considered blended-wing body concept, the largest gain would result from a minimization of the fin size. However, this entails major modifications not only on the rudder and aileron control but also on the aircraft design itself due to minimum control speed criteria. Therefore, it can be concluded that opting for an optimization of the center of gravity position while installing only a longitudinal robust back-up control system seems to be the best trade-off in terms of simplicity and cost savings.

The perspectives for ongoing research are twofold. Following the same direction as the assessment technique for control system activity and actuator fatigue, a promising research field is the representation of general flight maneuvers, e.g. take-off, climb, turns, and landing as a set of filters. Using transfer functions to filter a random signal in order to model pilot inputs would be a straightforward extension to the presented method and allow not only for rapid fatigue damage estimates but also for a definition of control system requirements corresponding to a mission profile. Of course, a validation of the developed tools on real aircraft is necessary in order to define a range of possible application.

Within the context of controlling a wide body long range airplane with reduced stability, future research can focus on the integration of flexible aircraft structures into the robust back-up control design. The degree of instability will certainly excite structural modes and it will be a challenging task keeping these controlled with a simple structured control law.

# Bibliography

- [1] AGARD (1974). Impact of active control technology on airplane design. Technical Report AGARD-CP-157, AGARD, Paris, France.
- [2] AGARD (1995). Aerodynamics of 3-d aircraft afterbodies. Technical report, AGARD.
- [3] Airbus (2002). Technical Report L07D1.169.0098/2002, Airbus.
- [4] Airbus (2003). Technical Report L27D1.169.1433/2003, Airbus.
- [5] Airbus (2005a). A380 specifications. Technical report, Airbus Industrie.
- [6] Airbus (2005b). Vela specifications. Technical report, AIRBUS.
- [7] Airbus (2006). A340-500/-600 elevators servocontrol - duty cycles update. Technical Report LR2734RP0602384, Airbus/EYCAA.
- [8] Alles, W. (2001). *Flugmechanik und Flugregelung*. RWTH Aachen.
- [9] Ananthkrishnan, N. and Unnikrishnan, S. (2001). Literal approximation to aircraft dynamic modes. *Journal of Guidance, Control, and Dynamics*, 24:1196–1203.
- [10] Anderson, B. and Vongpanitred, S. (1973). *Network Analysis*. Prentice-Hall, Englewood Cliffs, NJ.
- [11] Anderson, R. D., Flora, C. C., Nelson, R. M., Raymond, E. T., and Vincent, J. H. (1976). Development of weight and cost estimates for lifting surfaces with active controls. Technical Report NAS1-14064, NASA - National Aeronautics and Space Administration, Langley Research Center, Developed under contract by Boeing Commercial Airplane Company, Seattle, Washington.
- [12] Angelis, G., Kamidi, R., Molengraft, R., and Nijmeijer, H. (2000). Optimal polytopic control system design. *Proceedings of the 15th IEEE International Symposium on Intelligent Control (ISIC)*, pages 43–48.
- [13] Arnold, V. I. (1973). *Ordinary Differential Equations*. MIT Press, Cambridge, MA.
- [14] Bernard, C. (2002). Expressions analytiques des modes latéraux et longitudinaux d'un avion. Master's thesis, SUPAERO.

- [15] Böhm, M. (2007). *Gesamtentwurf eines ökonomischen und ökologischen Lufttransportsystems unter ausnutzung von Synergieeffekten*. PhD thesis, Universität der Bundeswehr, München.
- [16] Biannic, J., Roos, C., and Knauf, A. (2006a). Design and robustness analysis of fighter aircraft control laws. *European Journal of Control - special issue on LMI techniques in Control*, 12(1):71–85.
- [17] Biannic, J., Tarbouriech, S., and Farret, D. (2006b). A practical approach to performance analysis of saturated systems with applications to fighter aircraft flight controllers. *Proc. of the IFAC Symposium on Robust Control*.
- [18] Biannic, J.-M. (1998). Stability analysis of multivariable feedback systems with control input saturations. *Proceedings of IEE Control'98, Swansea, UK*.
- [19] Birk, T. (2007). Personal communication. *EADS Apsys, Risk Analysis Dept., Toulouse, France*.
- [20] Boiffier, J.-L. (1998). *Dynamique du Vol*. SUPAERO, Notes de cours.
- [21] Boyd, S., Ghaoui, L. E., Feron, E., and Balakrishnan, V. (1994). *Linear matrix inequalities in systems and control theory*. SIAM.
- [22] Brockhaus, R. (1994). *Flugregelung*. Springer-Verlag, Heidelberg, Berlin.
- [23] Chilali, M. and Gahinet, P. (1996).  $H_\infty$  design with pole placement constraints: an LMI approach. *IEEE Transactions on Automatic Control*, 41(3):358–367.
- [24] Chilali, M., Gahinet, P., and Apkarian, P. (1999). Robust pole placement in LMI regions. *IEEE Transactions on Automatic Control*, 44(12):2257–2269.
- [25] Covert, E. (1985). *Thrust and Drag: its Prediction and Verification*. AIAA, New York.
- [26] da Silva, J. G. and Tarbouriech, S. (2005). Antiwindup design with guaranteed regions of stability: an LMI-based approach. *IEEE Transactions on Automatic Control*, 50(1):106–111.
- [27] Döll, C. and Feuersänger, A. P. (2005-2006). MISCO - Minimization of the Control Function Cost. Progress Report. Technical Report Subtask B.1.2.2, ONERA - Airbus.
- [28] Doyle, J., Glover, K., Khargonekar, P., and Francis, B. (1989). State-space solutions to standard  $H_2$  and  $H_\infty$  control problems. *IEEE Transactions on Automatic Control*, 34(8):831–845.
- [29] EASA - European Aviation Safety Agency (2007a). Joint Aviation Requirements, Part23 - Normal, Utility, Aerobatic and Commuter Category Aeroplanes. Technical report, Joint Aviation Authorities, Cologne, Germany.

- [30] EASA - European Aviation Safety Agency (2007b). Joint Aviation Requirements, Part25 - Large Aeroplanes. Technical report, Joint Aviation Authorities, Cologne, Germany.
- [31] Eraydin, E. (1994). *Domaine de validité des équations de la dynamique du vol: decouplage*. PhD thesis, SUPAERO.
- [32] Etkins, B. and Reid, L. D. (1995). *Dynamics of Flight: Stability and Control*. Wiley, 3rd edition.
- [33] Ferreres, G. and Puyou, G. (2006). Flight control law design for a flexible aircraft: limits of performance. *Journal of Guidance, Control and Dynamics*, 29(4):870–878.
- [34] Feuersänger, A. (2004). Control of an aircraft with reduced stability. Master's thesis, SUPAERO, Toulouse, France.
- [35] Feuersänger, A. P., Döll, C., and Toussaint, C. (2006). Actuator influence on flying qualities of a naturally unstable aircraft. *Proceedings of the ICAS, Hamburg, Germany*.
- [36] Feuersänger, A. P. and Ferreres, G. (2006). Design of a robust back-up controller for an aircraft with reduced stability. *Guidance, Navigation, and Control Conference and Exhibit, Keystone, CO, USA*.
- [37] Feuersänger, A. P. and Ferreres, G. (2007). Robust back-up control design for an aircraft with reduced stability and saturated actuators. *IFAC Symposium: Automatic Control in Aerospace, Toulouse, France*.
- [38] Feuersänger, A. P., Toussaint, C., and Döll, C. (2005). The impact of reduced lateral stability on the  $v_{MC}$  equilibrium and manoeuvres during early design phases of an aircraft. *Deutscher Luft-und Raumfahrtkongress, Friedrichshafen, Germany*.
- [39] Feuersänger, A. P., Ferreres, G., and Toussaint, C. (2006). Synthèse d'un correcteur robuste de type back-up pour un avion à stabilité réduite. *Actes du congrès des doctorants EDSYS, Tarbes, France*.
- [40] Francis, B. A. (1987). *A course in  $H_\infty$  Control Theory*. Number 88 in Lecture Notes in Control and Information Sciences. Springer-Verlag, Berlin.
- [41] Gahinet, P., Nemirovski, A., Laub, A., and Chilali, M. (1995). *LMI control toolbox*. The Mathworks, Inc.
- [42] Gaulocher, S., Knauf, A., and Feuersänger, A. P. (2007). Self-scheduled controller design for relative motion control of a satellite formation. *In Proceedings: IMSM-IMAACA Multiconference, Buenos Aires, Argentina*.
- [43] Gomes da Silva, J. and Tarbouriech, S. (1999). Stability regions for linear systems with saturating controls. In *Proceedings of the ECC, Karlsruhe, Germany*.

- [44] Hafer, X. and Sachs, G. (1993). *Flugmechanik*. Springer, Berlin.
- [45] Hindi, H., Hassibi, B., and Boyd, S. (1998). Multi-objective  $H_2/H_\infty$ -optimal control via finite dimensional Q-parametrization and Linear Matrix Inequalities. *Proceedings of the ACC*, pages 3244–3249.
- [46] Hirsch, M. W. and Smale, S. (1974). *Differential Equations, Dynamical Systems and Linear Algebra*. Academic Press, New York.
- [47] Hoblit, F. (1988). *Gust loads on aircraft: concepts and applications*. Education Series. AIAA.
- [48] Imbert, N. and Mouyon, P. (2007). Calcul prédictif de la fatigue des actionneurs. Technical Report 1/11970 DCSD, ONERA-DCSD.
- [49] Jakob, D. (2000). *Flugzeugbau I und II und Flugzeugsysteme*. ILR, RWTH Aachen.
- [50] Jane's (2007). *Jane's: All the World's Aircraft*. Jane's Information Group.
- [51] Jenkinson, L., Simpkin, P., and Rhodes, D. (1999). *Civil Jet Aircraft Design*. Arnold, London.
- [52] Knauf, A., Gaulocher, S., and Feuersänger, A. P. (2006). Innovative controller design for systems with parameter variations. In *Proceedings: Deutscher Luft-und Raumfahrtkongress, Braunschweig, Germany*.
- [53] Kossira, H. (2002). *Flugzeugbau II, Arbeitsblätter zur Vorlesung*. Technische Universität Braunschweig.
- [54] Lalanne, C. (1999a). *Dommages par fatigue*, volume 4 of *Vibrations et chocs mécaniques*. Hermes Science Publications, Paris, London, 1st edition.
- [55] Lalanne, C. (1999b). *Vibrations aléatoires*, volume 3 of *Vibrations et chocs mécaniques*. Hermes Science Publications, Paris, London, 1st edition.
- [56] Lemaignan, B. (2002). Mise en place de méthodes de comparaison des qualités de vol au stade avant-projet. Technical report, SupAéro- Airbus France.
- [57] Lemaignan, B. (2003). Vela stability and control criteria list for the flying wing. Technical Report VELA-AF-310-001, Airbus EYCD.
- [58] LHT - Arbeitskreis Masseanalyse (MA) (2007). *Luftfahrttechnisches Handbuch - Masseanalyse*. IABG mbH.
- [59] Livneh, R. (1995). Improved literal approximation for lateral-directional dynamics of rigid aircraft. *Journal of Guidance, Control, and Dynamics*, 18:925–927.

- [60] Losser, Y. and Mouyon, P. (2004). Ajustement de lois de pilotage pour la réduction du dommage par fatigue des servocommandes d'un avion. In *Conférence Internationale Francophone d'Automatique CIFA 2004*, Douz, Tunisia.
- [61] Magni, J.-F. (2002). *Robust Modal Control with a Toolbox for Use with Matlab*. Kluwer Academic/Plenum Publishers.
- [62] Marquez, H. (2003). *Nonlinear control systems: analysis and design*. Wiley Interscience.
- [63] McCormick, B. (1995). *Aerodynamics, Aeronautics, and Flight Mechanics*. John Wiley & Sons, Inc., New York.
- [64] Messier-Bugatti (2007). Electro hydro static actuator. *Messier-Bugatti*, , *SAFRAN Group*.
- [65] Müller, S. (2007). Personal communication. *Airbus Central Entity, Marketing Division - CSMAW, Toulouse/Blagnac, France*.
- [66] Mouyon, P. and Gaillet, A. (2004). Critère de dommage par fatigue pour les servocommandes d'un avion. In *Conférence Internationale Francophone d'Automatique CIFA 2004*, Douz, Tunisia.
- [67] Nguewo, D. (2006). *Entwurfseminar Flugzeugbau*. Universität Stuttgart.
- [68] Pac, J. (1999). *Les processus stochastiques*. SUPAERO, Toulouse, France.
- [69] Pamadi, B. N. (2004). *Performance, Stability, Dynamics, and Control of Airplanes*. American Institut of Aeronautics and Astronautics (AIAA).
- [70] Perko, L. (1991). *Differential Equations and Dynamical Systems*. Springer-Verlag, New York.
- [71] Phillips, W. F. (2000). Improved closed-form approximation for dutch-roll. *Journal of Aircraft*, 37:484–490.
- [72] Pialat, E. and Loubignac, H. (2003). Étude comparative des VMC sur les avions Airbus et Boeing. Internal report, SUPAERO, Toulouse, France.
- [73] Pittet, C. S., Tarbouriech, S., and Burgat, C. (1997). Stability regions for linear systems with saturating controls via circle and popov criteria. *Proceedings of the IEEE CDC, Sam Diego, CA*, pp.4518-4523.
- [74] Rageade, L. and Delporte, M. (2004). Simulation des missions de fatigue actionneurs a340-500 a340-600. Technical Report F070SP040403996, Airbus/EYCDA.
- [75] Raymer, D.-P. (1999). *Aircraft Design: A Conceptual Approach*. AIAA Education Series, Washington D.C.

- [76] Roskam, J. (1987-1990). *Airplane Design, Part I - VIII*. Roskam Aviation and Engineering Corporation, Ottawa, Kansas.
- [77] Ruijgrok, D. (1990). *Elements of Airplane Performance*. Delft University Press.
- [78] Scherer, C. (1990). *The Riccati Inequality and State-Space  $H_\infty$ -Optimal Control*. PhD thesis, University of Würzburg, Germany.
- [79] Scherer, C. (1995). Multiobjective  $H_2/H_\infty$  control. *IEEE Transactions on Automatic Control*, 40(6):1054–1062.
- [80] Scherer, C., Gahinet, P., and Chilali, M. (1997). Multiobjective output-feedback control via LMI optimization. *IEEE Transactions on Automatic Control*, 42(7):896–911.
- [81] Schlichting, U.-J. and Truckenbrodt, E. (1967). *Aerodynamik des Flugzeuges, Band 1 und 2*. Springer, Berlin.
- [82] Schneider, H. (2007). Personal communication. *Universität Karlsruhe, Germany*.
- [83] Shimomura, T. and Pullen, S. (2002). Strictly positive real  $H_2$  controller synthesis via iterative algorithms for convex optimisation. *Journal of Guidance, Control and Dynamics*, 25(6):1003–1011.
- [84] Shue, S., Sawan, M., and Rokhsaz, K. (1997). Mixed  $H_2/H_\infty$  method suitable for gain-scheduled aircraft control. *Journal of Guidance, Control and Dynamics*, 20(4):699–706.
- [85] Simon, D. and Servoles, S. (2001). Analytical expression of the lateral modes of an aircraft. Studyproject, SUPAERO.
- [86] Takaba, K. (1999). Anti-windup control system design based on Youla parametrization. *Proceedings of the ACC*, pages 2012–2017.
- [87] Takaba, K. (2002). Analysis and synthesis of anti-windup control system based on Youla parametrization. *Proceedings of the IEEE CDC*, pages 2692–2697.
- [88] Thayer, W. J. (1967). Supply pressure considerations for servocontrols. *Meeting 63, SAE Commitee A-6, Aerospace Fluid Power and Control Technologies, Phoenix, Arizona*.
- [89] Torenbeek, E. (1986). *Synthesis of Subsonic Airplane Design*. Delft University Press, Martinus Nijhoff Publishers.
- [90] Toussaint, C. and Gimonet, B. (2007). Flybig, tache c.3.2: contrôle longitudinal de l'aile volante. Technical Report RF 1/09626 DAAP/DCSD, ONERA.

- [91] Toussaint, C., Renier, O., and L.Planckaert (2004). Qualités de vol d'une aile volante naturellement instable. Technical Report RT 211/07505 DAAP-DCSD, ONERA Toulouse, France.
- [92] U.S. Department of Defense (1975). Flight control systems - design, installation and test of piloted aircraft. Technical report, USAF.
- [93] U.S. Department of Defense (1980). Military specification, flying qualities of piloted airplanes. MIL-F-8785C. Technical report, Department of Defense Military Specifications and Standards, Philadelphia, Pennsylvania.
- [94] U.S. Department of Defense (1990). Department of defense interface standard, flying qualities of piloted aircraft. MIL-STD-1797A. Technical report, Department of Defense Military Specifications and Standards, Philadelphia, Pennsylvania.
- [95] U.S. Department of Defense (1995). Department of defense interface standard, flying qualities of piloted aircraft. MIL-STD-1797A update. Technical report, Wright-Patterson Air Force Base, Ohio: Systems Engineering Division, Aeronautical Systems Center.
- [96] U.S. Department of Transportation (2001). Federal Aviation Regulations, Part 25 - Airworthiness Standards: Transport Category Airplanes. Technical report, FAA - Federal Aviation Administration, Washington, DC.
- [97] U.S. Department of Transportation (2002). Federal Aviation Regulations, Part 23 - Airworthiness Standards: Normal, Utility, Acrobatic, and Commuter Category Airplanes. Technical report, FAA - Federal Aviation Administration, Washington, DC.
- [98] van der Pol, B. (1920). *Radio Review*, 1:704–754.
- [99] Wanner, J.-C. (1984). *Dynamique du vol et pilotage des avions*. ONERA/SUPAERO.
- [100] Wokurka, N. (2004). Long range - handling qualities fatigue missions sizing for actuators duty cycles - update. Technical Report LR070RP0413950, Airbus/EYCDA.
- [101] Wu, F. and Soto, M. (2004). Extended anti-windup control schemes for LTI and LFT systems with actuator saturations. *International Journal of Robust and Nonlinear Control*, 14:1255–1281.
- [102] Young, A. D., Paterson, J. H., and Lloyd, J. J. (1995). Aircraft excrescence drag. Technical Report AGARDograph No.264, AGARD, London.



# Appendix A

## Aircraft Data

### A.1 VELA1 Blended-Wing Body

#### A.1.1 Geometry and Mass Inertia

|  |     |       |            |       |
|--|-----|-------|------------|-------|
| Mass range   | $M$ | $\in$ | [550; 770] | $t$   |
| Reference surface                                      | $S$ | $=$   | 2012       | $m^2$ |
| Mean aerodynamic chord<br>( $\equiv$ Reference length) | $l$ | $=$   | 35.93      | $m$   |
| Wing span  | $b$ | $=$   | 99.60      | $m$   |

Table A.1: VELA reference values.

The used mass inertia are based on empirical estimates provided by Airbus and are displayed in Table A.2.

|              |     |                    |                |
|--------------|-----|--------------------|----------------|
| $m$          | $=$ | $700 \cdot 10^3$   | $kg$           |
| $I_{xx} = A$ | $=$ | $5.88 \cdot 10^6$  | $kg \cdot m^2$ |
| $I_{yy} = B$ | $=$ | $44.8 \cdot 10^6$  | $kg \cdot m^2$ |
| $I_{zz} = C$ | $=$ | $238.1 \cdot 10^6$ | $kg \cdot m^2$ |
| $I_{xz} = E$ | $=$ | $0.36 \cdot 10^6$  | $kg \cdot m^2$ |

Table A.2: Mass inertia.

The inertia can be taken to be proportional to the mass of the aircraft. To have the option of studying different mass cases (reduced mass) a factor is introduced. It is multiplied with the aircraft mass and its inertia in all relevant terms for modeling the aircraft dynamics correctly.

The aerodynamic data is given for a reference point  $X_{ref}$  that is placed at 30.7% of the *mean aerodynamic chord* (*mac*). This equals 23.7  $m$  behind the geometric reference

| "cz "    |           |           |           |           |           |          |
|----------|-----------|-----------|-----------|-----------|-----------|----------|
| " Alpha" | -0,1      | -0,05     | 0         | 0,05      | 0,1       | " Beta " |
| -0,1     | 0,314795  | 0,317944  | 0,318997  | 0,317944  | 0,314795  |          |
| -0,05    | 0,159622  | 0,161599  | 0,16226   | 0,161599  | 0,159622  |          |
| 0        | 0,002687  | 0,003479  | 0,003744  | 0,003479  | 0,002687  |          |
| 0,05     | -0,154441 | -0,154835 | -0,154967 | -0,154835 | -0,154441 |          |
| 0,1      | -0,310189 | -0,31176  | -0,312285 | -0,31176  | -0,310189 |          |
| 0,15     | -0,463001 | -0,465726 | -0,466637 | -0,465726 | -0,463001 |          |
| 0,2      | -0,611349 | -0,615194 | -0,61648  | -0,615194 | -0,611349 |          |
| 0,25     | -0,753748 | -0,758668 | -0,760314 | -0,758668 | -0,753748 |          |
| 0,3      | -0,888774 | -0,894714 | -0,896701 | -0,894714 | -0,888774 |          |

Table A.3: Coefficient  $C_Z$  as a function of  $\alpha$  and  $\beta$ .

point.  $dx_g$  describes then the non-dimensional displacement of the center of gravity along the x-axis:

$$dx_g = \frac{X_g - X_{ref}}{l}, \quad (\text{A.1})$$

where  $l$  is the length in  $[m]$  of  $mac$ ,  $X_{ref}$  the reference point position and  $X_g$  the position of the center of gravity in  $[m]$ .

### A.1.2 Full Aerodynamic Model

All six aerodynamic coefficients ( $C_X, C_Y, C_Z, Cl, Cm$  and  $Cn$ ) are reconstructed from tables where these are noted as functions of the angle of attack  $\alpha$ , successively combined with yaw angle  $\beta$ , rotational velocities  $p, q$  and  $r$ , accelerations  $\dot{\alpha}$  and  $\dot{\beta}$ , and finally the control surface deflections (elevator, rudders - left and right - and wing control surfaces A1 to A10 - ailerons and spoilers). An example of one coefficient table is shown in Table A.3.

### A.1.3 Simplified Aerodynamic Model

The simplified longitudinal aerodynamic model is based on the following equations in aerodynamic coordinates:

$$C_Z = C_{Z0} + C_{Z\alpha}\alpha + C_{Zq}\frac{ql}{V} + C_{Z\delta m}\delta m \quad (\text{A.2})$$

$$C_X = C_{X0} + k_i C_Z^2 + C_{X\delta m}\delta m \quad (\text{A.3})$$

$$Cm = Cm_0 + Cm_\alpha\alpha + Cm_q\frac{ql}{V} + Cm_{\delta m}\delta m \quad (\text{A.4})$$

The lateral equations are written in the body frame:

$$C_Y = C_{Y\beta}\beta + C_{Yp}\frac{p^l}{V} + C_{Yr}\frac{r^l}{V} + C_{Y\delta l}\delta l + C_{Y\delta n}\delta n \quad (\text{A.5})$$

$$Cl = Cl_\beta\beta + Cl_p\frac{p^l}{V} + Cl_r\frac{r^l}{V} + Cl_{\delta l}\delta l + Cl_{\delta n}\delta n \quad (\text{A.6})$$

$$Cn = Cn_\beta\beta + Cn_p\frac{p^l}{V} + Cn_r\frac{r^l}{V} + Cn_{\delta l}\delta l + Cn_{\delta n}\delta n \quad (\text{A.7})$$

Using linear regression, the complete aerodynamic tables are simplified, resulting in coefficients linearized in  $\alpha$ . The corresponding coefficients figure in Tables A.4 and A.5.

|                 | $\alpha = 0$ | $\partial./\partial\alpha$ |
|-----------------|--------------|----------------------------|
| $C_Z$           | -0.0036      | 3.115                      |
| $C_{Zq}$        | 1.131        | -0.113                     |
| $C_{Z\delta m}$ | 0.4          | -0.078                     |
| $C_X$           | 0.0085       | $k_i=0.0652$               |
| $C_{X\delta m}$ | -0.004       | 0.125                      |
| $C_m$           | 0.0043       | 0.015                      |
| $C_{mq}$        | -0.275       | -0.007                     |
| $C_{m\delta m}$ | -0.210       | 0.027                      |

Table A.4: Simplified longitudinal coefficients.

|                 | $\alpha = 0$ | $\partial./\partial\alpha$ |
|-----------------|--------------|----------------------------|
| $C_{Y\beta}$    | -0.104       | 0.209                      |
| $C_{Yp}$        | -0.055       | 1.634                      |
| $C_{Yr}$        | 0.083        | 0.077                      |
| $C_{Y\delta l}$ | -0.004       | 0.091                      |
| $C_{Y\delta n}$ | 0.064        | -0.011                     |
| $Cl_\beta$      | -0.071       | -0.933                     |
| $Cl_p$          | -0.924       | 0.136                      |
| $Cl_r$          | 0.007        | 1.388                      |
| $Cl_{\delta l}$ | -0.179       | 0.044                      |
| $Cl_{\delta n}$ | 0.011        | -0.005                     |
| $Cn_\beta$      | 0.064        | -0.175                     |
| $Cn_p$          | 0.055        | -2.148                     |
| $Cn_r$          | -0.063       | 0.012                      |
| $Cn_{\delta l}$ | -0.002       | -0.150                     |
| $Cn_{\delta n}$ | -0.050       | 0.010                      |

Table A.5: Simplified lateral coefficients.

## A.2 Douglas DC8

### A.2.1 Geometry and Mass Inertia

|  |     |       |           |       |
|--|-----|-------|-----------|-------|
| Mass range   | $M$ | $\in$ | [63; 120] | $t$   |
| Reference surface                                      | $S$ | $=$   | 240       | $m^2$ |
| Mean aerodynamic chord<br>( $\equiv$ Reference length) | $l$ | $=$   | 6.5       | $m$   |
| Wing span  | $b$ | $=$   | 44.8      | $m$   |

Table A.6: DC8 reference values.

|              |     |                    |                |
|--------------|-----|--------------------|----------------|
| $m$          | $=$ | $120 \cdot 10^3$   | $kg$           |
| $I_{xx} = A$ | $=$ | $5.88 \cdot 10^6$  | $kg \cdot m^2$ |
| $I_{yy} = B$ | $=$ | $9.72 \cdot 10^6$  | $kg \cdot m^2$ |
| $I_{zz} = C$ | $=$ | $11.1 \cdot 10^6$  | $kg \cdot m^2$ |
| $I_{xz} = E$ | $=$ | $-0.33 \cdot 10^6$ | $kg \cdot m^2$ |

Table A.7: Mass inertia.

The inertia are assumed to be proportional to the mass of the aircraft. The aerodynamic data is given for a reference point  $X_{ref} = 0.6$ . The non-dimensional c.o.g. displacement is given with  $dx_g = \frac{X_g - X_{ref}}{l}$ .

### A.2.2 Simple Aerodynamic Model

The same simplified equations as for the VELA model are used. The following coefficients are injected:

|                 | $\alpha = 0$ | $\partial./\partial\alpha$ |
|-----------------|--------------|----------------------------|
| $C_Z$           | 0.6          | 5                          |
| $C_{Zq}$        | 0            | 0                          |
| $C_{Z\delta m}$ | 0.44         | 0                          |
| $C_X$           | 0.02         | $k_i = 0.06$               |
| $C_{X\delta m}$ | 0            | 0                          |
| $C_m$           | -0.1         | 0                          |
| $C_{mq}$        | -13.52       | 0                          |
| $C_{m\delta m}$ | -1.46        | 0                          |

Table A.8: Simplified longitudinal coefficients.

|                 | $\alpha = 0$ | $\partial./\partial\alpha$ |
|-----------------|--------------|----------------------------|
| $C_{Y\beta}$    | -0.65        | 0                          |
| $C_{Yp}$        | 0            | 0                          |
| $C_{Yr}$        | 0            | 0                          |
| $C_{Y\delta l}$ | 0            | 0                          |
| $C_{Y\delta n}$ | 0.19         | 0                          |
| $Cl_{\beta}$    | -0.92        | 0                          |
| $Cl_p$          | -18.6        | 0                          |
| $Cl_r$          | 5.89         | 0                          |
| $Cl_{\delta l}$ | -0.56        | 0                          |
| $Cl_{\delta n}$ | 0.13         | 0                          |
| $Cn_{\beta}$    | 0.98         | 0                          |
| $Cn_p$          | -1.37        | 0                          |
| $Cn_r$          | -7.18        | 0                          |
| $Cn_{\delta l}$ | -0.02        | 0                          |
| $Cn_{\delta n}$ | -0.56        | 0                          |

Table A.9: Simplified lateral coefficients.



# Appendix B

## Certification Criteria and Norms

### B.1 Classical Criteria

The VELA1 aircraft is naturally unstable in its longitudinal and lateral motions. The following two subsections present the most relevant criteria drawn from the ‘classical sources’: *Military Specifications* and *Federal / Joint Aviation Regulations*.

#### B.1.1 Military Specifications

The below-mentioned criteria refer to the ‘*lateral directional flying qualities*’ of MIL-F-8785 CMIL2, MIL-STD-1797 [94, 95] respectively. The specifications distinguish between numerous classes of aircraft, quality, flight phase categories and level of flying qualities. The VELA1-configuration will be categorized as follows:

- ‘Class III: Large, heavy, low-to-medium maneuverability airplanes’
- ‘Category B: Those nonterminal Flight Phases that are normally accomplished (...), like climb, cruise, descend ...’
- ‘Category C: Terminal flight phases are normally accomplished using gradual maneuvers (...), like take-off, landing ...’
- ‘Level 1: Flying qualities clearly adequate for the mission Flight Phase.’

This categorization leads to the following restrictions:

1. Lateral-directional oscillations (Dutch roll).

The natural frequency  $\omega_{nd}$  and damping ratio  $\zeta_d$  have the following minimum values:

$$\begin{aligned}\omega_{nd} &\geq 0.4 \\ \zeta_d &\geq 0.19 \\ \zeta_d \omega_{nd} &\geq 0.35.\end{aligned}$$

## 2. Roll mode.

A maximum roll-mode time constant  $\tau_r$  in seconds [s] is given by

$$\tau_r \leq 1.4 \text{ s}.$$

## 3. Roll performance.

The limitations represent the maximum time  $T$  in seconds [s] to achieve a bank angle of  $30^\circ$ :

$$\begin{aligned}T &\leq 2.3 \text{ s} && \text{for cruise and} \\ T &\leq 2.5 \text{ s} && \text{for take-off and landing.}\end{aligned}$$

## 4. Spiral stability

After a disturbance in bank of up to  $20^\circ$  the time  $T_{sp2}$  in seconds [s] to double the bank angle shall be greater than:

$$\begin{aligned}T_{sp2} &\geq 12 \text{ s} && \text{for approach, landing and} \\ T_{sp2} &\geq 20 \text{ s} && \text{for cruise.}\end{aligned}$$

### B.1.2 FAR / JAR guidelines

The FAR/JAR [96, 30] guidelines provide other interesting criteria with respect to the aircraft's particular design. It refers to the one-engine-failure case where, in a critical flight phase, suddenly the critical engine is made inoperative. For multi engine aircraft, the critical engine is typically an outboard engine due to the length of the associated thrust lever arm. Unlike propeller airplanes, there is no left/right outboard engine difference for jet airplanes as far as subsystems are neglected.

1. A summary of FAR/JAR Part 25 §149 '*minimum control speed*' is given below:

$V_{MC}$  is the calibrated airspeed at which, when the critical engine is suddenly made inoperative, it is still possible to maintain control of the aircraft and straight flight with a bank angle of not more than  $5^\circ$ .

$V_{MC}$  may not exceed  $1.13 V_{SR}$  with

- maximum take-off thrust,
- aircraft trimmed for take-off,
- most unfavorable center of gravity and
- maximum sea-level take-off weight, or any lesser weight necessary to show  $V_{MC}$ ,
- airplane airborne, landing gear retracted and ground effect negligible.

$V_{SR}$  is a calibrated airspeed defined by the applicant and may not be less than a 1-g stall speed.  $V_{SR}$  is expressed as:

$$V_{SR} \geq \frac{V_{C_{Lmax}}}{\sqrt{n_{ZW}}}. \quad (\text{B.1})$$

- $V_{C_{Lmax}}$  is the calibrated airspeed when the load factor-corrected lift coefficient  $\left(\frac{n_{ZW}W}{\bar{q}S}\right)$  is a first maximum when using the longitudinal control to decelerate the airplane from a stabilized trim condition at a rate of  $1kt/s$ ,
- $n_{ZW}$  is the load factor normal to the flight path at  $V_{C_{Lmax}}$ ,
- $W$  is the airplane gross weight,
- $S$  is the aerodynamic reference wing area and
- $\bar{q}$  the dynamic pressure.

Additionally, it should be possible to roll the aircraft, from initial steady flight, through an angle of  $20^\circ$  in the direction necessary to initiate a turn away from the inoperative engine in not more than  $5s$ .

2. Lateral control with one engine inoperative is given in FAR/JAR Part 25 §147. A summary is displayed below:

*Banked turns* with an angle  $20^\circ$  must be possible with and against the inoperative critical engine from a steady flight at  $1.3V_{SR}$  with:

- the remaining engines at maximum continuous power,
- the most unfavorable center of gravity,
- maximum take-off weight,
- wing-flaps in most favorable climb position and landing gear retracted.

3. FAR/JAR Part25 §181 describes the dynamic stability, and interestingly, the stability of combined lateral-directional oscillations, the ‘*Dutch Roll*’.

*Lateral-directional oscillations*, occurring between  $1.3V_{SR}$  and maximum allowable speed, must be positively damped.

The above-mentioned guidelines will suffice for a first basis of classical performance criteria. Additional guidelines delivered by the VELA work group are given in the next section.

## B.2 Criteria Proposed within the Framework of the VELA Project

This section addresses performance criteria and amendments to JAR guidelines furnished by the VELA work group [57]. In this case, the description of certain speeds is facilitated and some definitions are presented differently. The goal is to provide an alternative, facilitated way of expressing the requirements. Furthermore, during the work conducted on the VELA project tighter constraints had to be introduced with regard to take-off and landing due to the special aircraft design.

Section B.2 details the supplement of the VELA group to JAR guidelines whereas Section B.2.1 refers to take-off and landing issues.

### Supplement to Lateral Criteria

For all lateral criteria, expressions that include  $V_{SR}$  are replaced by terms incorporating  $V_S$  or  $V_{S1g}$  in order to facilitate use of the  $V_{MC}$  related criteria.  $V_{S1g}$  reads (with  $W = m \cdot g$ ):

$$V_{S1g} = \sqrt{\frac{W}{S} \frac{2}{\rho} \frac{1}{C_{Lmax}}}. \quad (\text{B.2})$$

And  $V_S$  is defined by:

$V_S$  = stalling speed  
 = speed, at which the aeroplane decelerates with engines in ‘idle’ position  
 at a rate of  $1 \text{ kt/s}$ .

$$V_S \approx 0.94 V_{S1g}$$

1. According to the approximation for  $V_S$  the guideline for the *minimum control speed* becomes:

$V_{MC}$  may not exceed  $1.2 V_S$  with

- maximum take-off thrust,
- aeroplane trimmed for take-off,
- ... (see subsection B.1.2)

2. The compliance with the FAR/JAR guideline for *lateral control* (FAR/JAR Part 25 §147) can be shown differently. An acceptable method is as follows:

*With one engine (critical engine) inoperative*, from a steady  $30^\circ$  banked turn it should be possible to roll the aeroplane through an angle of  $60^\circ$  in a reverse direction in no more than 11 s with  $V_2$ .

$V_2$  is the *secure take-off speed* of the aeroplane on its take-off path when flying over the 35 ft obstacle.

$$V_2 \geq 1.2 V_S \rightarrow V_{2min} = 1.2 V_S$$

Hence, the criterion for the roll time  $T_R$  at  $V_{2min} = 1.2 V_S$  is as follows:

$$\phi : +30^\circ \rightarrow -30^\circ \quad T_R \leq 11 s$$

3. Another roll criterion demanded by Airbus is to roll the aeroplane at  $V_{MC}$  under the below-mentioned conditions with all engines operative:

$$\phi : +5^\circ \rightarrow +25^\circ \quad T_R \leq 7 s$$

4. Finally, the *lateral dynamics* criterion is tightened. Instead of demanding only a positive damping of the *Dutch Roll*, the damping minimum should be greater than 10% with a back-up yaw damper in case of flight control computer failures.

### B.2.1 Supplement to Take-Off and Landing Criteria

With the initial design of the VELA1 aircraft the necessary approach and take-off speeds were too high which called for a higher lift coefficient:

- The approach speed should be, in comparison to *Concorde*, less or equal to 160 kt ( $\approx 82.3 m/s$ ).
- Tailstrike has to be considered at an angle of incidence of  $14.4^\circ$ .

A small safety margin for the tailstrike criterion of  $0.4^\circ$  has been introduced so that it should be feasible to land the aircraft at a maximum incidence of  $14.0^\circ$ . Therefore a high-lift configuration<sup>1</sup> is necessary raising the lift coefficient sufficiently to achieve lower approach speeds approximately to  $Mach = 0.2$  or roughly  $70 m/s$ .

---

<sup>1</sup>The high-lift configuration is set to  $0^\circ / 15^\circ / 25^\circ$  for outboard/midboard/inboard wing flaps with a  $25^\circ$  droop nose.



## Appendix C

# $V_{MC}$ Equilibrium: Parametric Study in Detail

**How does the term  $\varepsilon_D \cdot (\kappa + v)$  influence  $V_{MC}$  ?** The expressions  $V_{MC_{s2}}$  and  $V_{MC_{s3}}$  distinguish themselves from the most simplified formulation by the above-mentioned term. Consider the following reasoning (always within the body frame):

The sign of  $\sin \phi$  will depend on  $\delta n$ , and thus on  $y_{eng}$ . That way,  $v < 0$  is always true. Since  $\kappa > 0$ , the following is true (mind the case differentiation):

---

*Consider*

$$V_{MC_{s2}} = \sqrt{\kappa + \varepsilon_D \cdot (\kappa + v)}, \quad \text{with } \kappa > 0 \quad \text{and} \quad v < 0 :$$

*if*

$$|\kappa| < |v| \quad | \quad |\kappa| > |v|$$

*and if*

$$0 < \varepsilon_D < -\frac{\kappa}{\kappa+v} \quad | \quad -\frac{\kappa}{\kappa+v} < \varepsilon_D < 0$$

*then*

$$\kappa + \varepsilon_D \cdot (\kappa + v) < \kappa$$

*and thus*

$$V_{MC_{s2}} < V_{MC_{s3}}. \tag{C.1}$$


---

This reasoning establishes a guideline w.r.t. parameters  $v$  and  $\varepsilon_D$  allowing for an optimization of the  $V_{MC}$ . The closer  $\varepsilon_D$  is in the proximity of  $-\frac{\kappa}{\kappa+v}$ , the smaller is the resulting  $V_{MC}$ . Considering again Eq. (6.29), we notice that  $V_{MC_{s2}} < V_{MC_{s3}}$  is either true for  $|\kappa|/|v| < 1$  for laterally statical stable airplanes, or for  $|\kappa|/|v| > 1$  for unstable airplanes<sup>1</sup>. Thus,  $V_{MC_{s2}}$  depends greatly on  $v$  and therewith on the mass.

---

<sup>1</sup>Still, the chances of encountering a civil laterally statical unstable airplane are low.

**How do secondary effects and roll and yaw coupling influence  $V_{MC}$ ?** New parameters  $\gamma$  and  $\sigma$  are introduced which regroup secondary coupling effects of control surface deflections, including ailerons. Again, rules will be derived that show possibilities of how to exploit a given configuration or change conceptual parameters in order to obtain an optimized  $V_{MC}$ .

---

Consider

$$V_{MC_{s1}} = \sqrt{\kappa\gamma + \varepsilon_D\sigma \cdot (\kappa\gamma + v)}, \quad \text{with } \kappa\gamma > 0 \quad \text{and } v < 0 :$$

if

$$|\kappa\gamma| < |v| \quad | \quad |\kappa\gamma| > |v|$$

and if

$$\frac{\kappa(1-\gamma)}{\sigma(\kappa\gamma+v)} < \varepsilon_D < -\frac{1}{\sigma(1+\frac{v}{\kappa\gamma})} \quad | \quad -\frac{1}{\sigma(1+\frac{v}{\kappa\gamma})} < \varepsilon_D < \frac{\kappa(1-\gamma)}{\sigma(\kappa\gamma+v)}$$

then

$$V_{MC_{s1}} < V_{MC_{s3}}.$$

If furthermore

$$\frac{\kappa(1-\gamma)}{\kappa(\sigma\gamma-1)+v(\sigma-1)} < \varepsilon_D < -\frac{1}{\sigma(1+\frac{v}{\kappa\gamma})} \quad | \quad -\frac{1}{\sigma(1+\frac{v}{\kappa\gamma})} < \varepsilon_D < \frac{\kappa(1-\gamma)}{\kappa(\sigma\gamma-1)+v(\sigma-1)}$$

then

$$V_{MC_{s1}} < V_{MC_{s2}}. \tag{C.2}$$


---

This is true since (condition for  $V_{MC_{s1}} < V_{MC_{s3}}$ ):

$$\begin{aligned} \tilde{\kappa} + \tilde{\varepsilon}_D \cdot (\tilde{\kappa} + v) &< \kappa \\ \kappa \cdot \gamma + \varepsilon_D \cdot \sigma \cdot (\kappa \cdot \gamma + v) &< \kappa \\ \varepsilon_D &> \frac{\kappa(1-\gamma)}{\sigma(\kappa\gamma+v)}, \quad \text{for } |\tilde{\kappa}| < |v| \end{aligned} \tag{C.3}$$

$$\varepsilon_D < \frac{\kappa(1-\gamma)}{\sigma(\kappa\gamma+v)}, \quad \text{for } |\tilde{\kappa}| > |v| \tag{C.4}$$

and (condition for  $V_{MC_{s1}} < V_{MC_{s2}}$ )

$$\begin{aligned} \tilde{\kappa} + \tilde{\varepsilon}_D \cdot (\tilde{\kappa} + v) &< \kappa + \varepsilon_D \cdot (\kappa + v) \\ \kappa \cdot \gamma + \varepsilon_D \cdot \sigma \cdot (\kappa \cdot \gamma + v) &< \kappa + \varepsilon_D \cdot (\kappa + v) \\ \varepsilon_D &> \frac{\kappa(1-\gamma)}{\kappa(\sigma\gamma-1)+v(\sigma-1)}, \quad \text{for } |\tilde{\kappa}| < |v| \end{aligned} \tag{C.5}$$

$$\varepsilon_D < \frac{\kappa(1-\gamma)}{\kappa(\sigma\gamma-1)+v(\sigma-1)}, \quad \text{for } |\tilde{\kappa}| > |v| \tag{C.6}$$

and (condition that  $V_{MC_{s1}}$  exists)

$$\begin{aligned} 0 &< \tilde{\kappa} + \tilde{\varepsilon}_D \cdot (\tilde{\kappa} + \nu) \\ \tilde{\varepsilon}_D &\leq -\frac{\tilde{\kappa}}{\tilde{\kappa} + \nu} \\ \varepsilon_D &< -\frac{1}{\sigma(1 + \frac{\nu}{\kappa\gamma})}, \quad \text{for } |\tilde{\kappa}| < |\nu| \end{aligned} \quad (\text{C.7})$$

$$\varepsilon_D > -\frac{1}{\sigma(1 + \frac{\nu}{\kappa\gamma})}, \quad \text{for } |\tilde{\kappa}| > |\nu|. \quad (\text{C.8})$$

**Remarks:**

(i) The above gives the theoretic boundaries which guarantee that a more precise  $V_{MC}$  expression will result in a smaller speed. This is meant as a guideline: the newly introduced abstract parameters regroup physical effects and therefore it can be quickly assessed if a certain group of physical factors leads to a reduction or augmentation of the  $V_{MC}$ .

(ii) The case differentiation is based on the ratio  $|\kappa|/|\nu|$ . Depending on whether this ratio is less or greater than one, the boundaries for pseudo-coefficient  $\varepsilon_D$  vary.  $\varepsilon_D$  is not a free parameter and is set for a given aircraft. Therefore it is to be understood as a help to exploit a fixed airplane concept. If the aircraft concept is not determined yet,  $\varepsilon_D$  adds another degree of freedom to an optimization of  $V_{MC}$ .

(iii) With  $\kappa$  fixed, the mass is an important factor determining the absolute value of  $\nu$ . As we noted before, the  $V_{MC}$  criteria are harder to realize with a lighter aircraft. Thus, the empty weight of an aircraft is an important factor to be considered in this context. Compare with the reasoning for Eq. (C.1): when deflection  $\delta n$  and attitude angles are fixed the mass is the determining factor for whether  $V_{MC_{s2}}$  is less or superior to  $V_{MC_{s3}}$ .

A list of the relevant boundaries is displayed in Table C.1 in order to enhance the comprehensibility of the upcoming parametric study. This table, even though with a focus on  $\varepsilon_D$ , has three possible uses:

- a) better comprehension of the factors determining  $V_{MC}$  by the means of the upcoming diagrams in the parametric study,
- b) when exploiting a given airplane concept, parameters can be modified following the guidelines,
- c) if the concept itself can be changed, modification not only of parameters but also of the pseudo-coefficient  $\varepsilon_D$  according to the guidelines.

The following figures show the results of the parametric analysis of the three simplified expressions for the minimum control speed. Principal factors ( $\kappa$ ,  $\nu$ ,  $\varepsilon_D$ ) will be varied and the influence of a varying fin size and a displacement of the center of gravity is demonstrated.

**Equations and coefficient modeling for parametric study**

$$V_{MC_{s1}} = \sqrt{\tilde{\kappa} + \tilde{\varepsilon}_D \cdot (\tilde{\kappa} + v)} \quad (C.9)$$

$$V_{MC_{s2}} = \sqrt{\kappa + \varepsilon_D \cdot (\kappa + v)} \quad (C.10)$$

$$V_{MC_{s3}} = \sqrt{\kappa} \quad (C.11)$$

with

$$\kappa = \frac{2y_{eng}F}{\rho S l C n_{\delta n} \delta n} \quad (C.12)$$

$$\tilde{\kappa} = \kappa \cdot \gamma, \quad \text{where } \gamma = \frac{1}{1 - \varepsilon_{\delta l \delta n}} \quad (C.13)$$

$$v = \frac{2mg \cos \theta \sin \phi}{\rho S C_{Y \delta n} \delta n} \quad (C.14)$$

$$\varepsilon_D = \frac{C_{Y \delta n} C n_{\beta}}{C n_{\delta n} C_{Y \beta}} \quad (C.15)$$

$$\tilde{\varepsilon}_D = \varepsilon_D \cdot \sigma, \quad \text{where } \sigma = \frac{1 - \varepsilon_{C n_{\beta}}}{(1 - \varepsilon_{C_{Y \beta}})(1 - \varepsilon_{\delta l \delta n})} \quad (C.16)$$

$$C_{Y \delta n}^* = C_{Y \delta n, nom} \cdot \frac{S_D}{S_{D, nom}} \quad (C.17)$$

$$C n_{\delta n}^* = C n_{\delta n, X_{ref}} \cdot \frac{S_D}{S_{D, nom}} + dx_g \cdot C_{Y \delta n, nom} \cdot \frac{S_D}{S_{D, nom}} \quad (C.18)$$

$$C_{Y \beta}^* = C_{Y \beta, fuselage} \cdot \left(1 + \frac{\Delta C_{Y \beta, fuselage}}{C_{Y \beta, fuselage}}\right) + C_{Y \beta, fin} \cdot \frac{S_D}{S_{D, nom}} \quad (C.19)$$

$$C n_{\beta}^* = C n_{\beta, fuselage} \cdot \left(1 + \frac{\Delta C n_{\beta, fuselage}}{C n_{\beta, fuselage}}\right) + C n_{\beta, fin} \cdot \frac{S_D}{S_{D, nom}} - dx_g \cdot C_{Y \beta, fin} \cdot \frac{S_D}{S_{D, nom}} \quad (C.20)$$

**Physical influence of parameters**

- $\kappa$  balance of rudder moment and engine thrust (in  $V_{MC_{s1}}$ ,  $V_{MC_{s2}}$ ,  $V_{MC_{s3}}$ )
- $v$  equilibrium angles and balance of mass and lateral force (in  $V_{MC_{s1}}$ ,  $V_{MC_{s2}}$ )
- $\varepsilon_D$  geometry, lateral neutral point (in  $V_{MC_{s1}}$ ,  $V_{MC_{s2}}$ )
- $\sigma, \gamma$  corrective terms and aileron effects (in  $V_{MC_{s1}}$  only)

| $\varepsilon_D$ |                             | $ \kappa / v  < 1$  | $ \kappa / v  > 1$  |
|-----------------|-----------------------------|---|---|
| B12:            | $V_{MC_{s1}} < V_{MC_{s2}}$ | $> \frac{\kappa(1-\gamma)}{\kappa(\sigma\gamma-1)+v(\sigma-1)}$ | $< \frac{\kappa(1-\gamma)}{\kappa(\sigma\gamma-1)+v(\sigma-1)}$ |
| B13:            | $V_{MC_{s1}} < V_{MC_{s3}}$ | $> \frac{\kappa(1-\gamma)}{\sigma(\kappa\gamma+v)}$             | $< \frac{\kappa(1-\gamma)}{\sigma(\kappa\gamma+v)}$             |
| B23:            | $V_{MC_{s2}} < V_{MC_{s3}}$ | $> 0$   | $< 0$   |
| C1:             | $\exists V_{MC_{s1}}$       | $< -\frac{1}{\sigma(1+\frac{v}{\kappa\gamma})}$                 | $> -\frac{1}{\sigma(1+\frac{v}{\kappa\gamma})}$                 |
| C2:             | $\exists V_{MC_{s2}}$       | $< -\frac{\kappa}{\kappa+v}$                                    | $> -\frac{\kappa}{\kappa+v}$                                    |

Table C.1: Boundaries for  $\varepsilon_D$  with  $\kappa > 0, v < 0$ .

### C.1 DC8

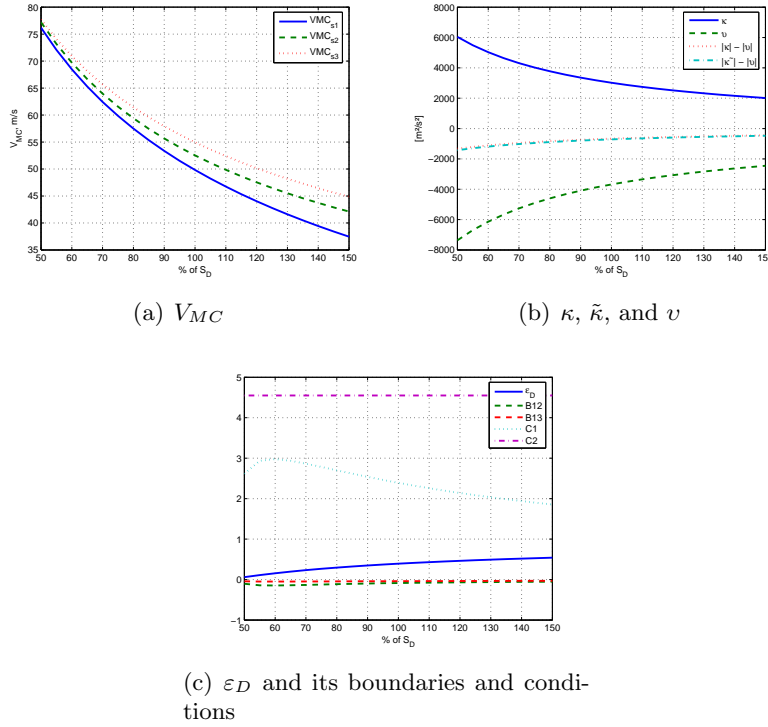


Figure C.1: DC8. Variation of the fin size.

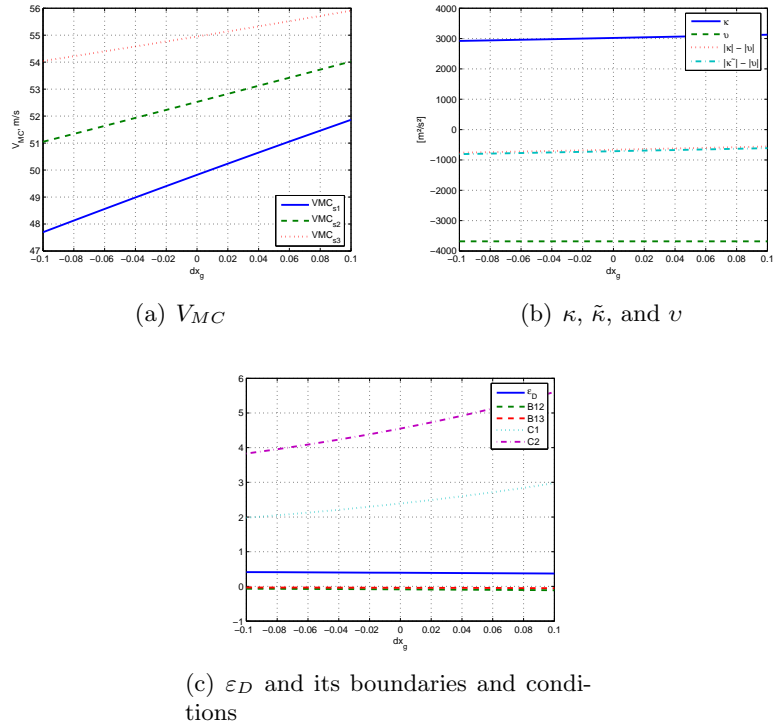


Figure C.2: DC8. Variation of the center of gravity position.

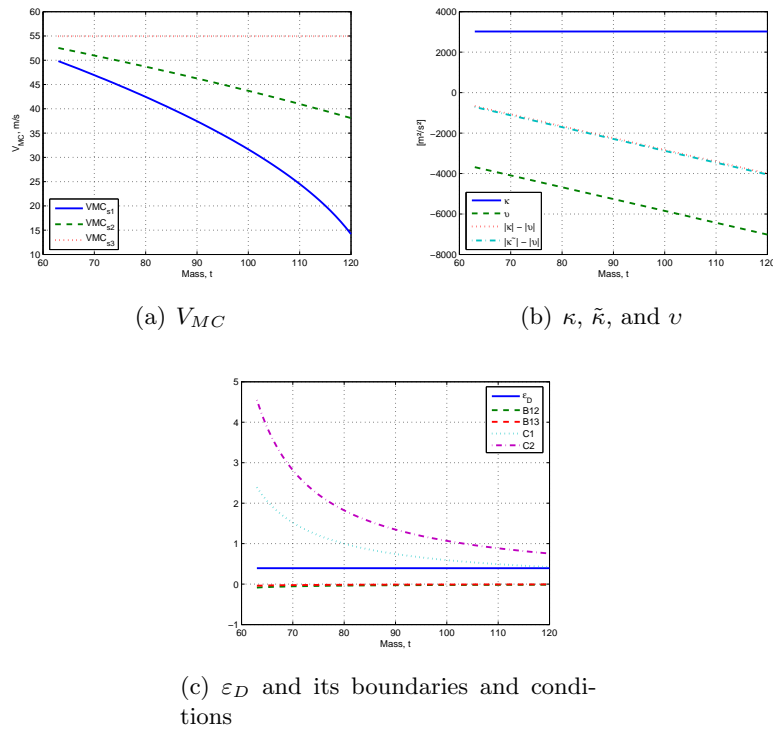


Figure C.3: DC8. Variation of the mass.

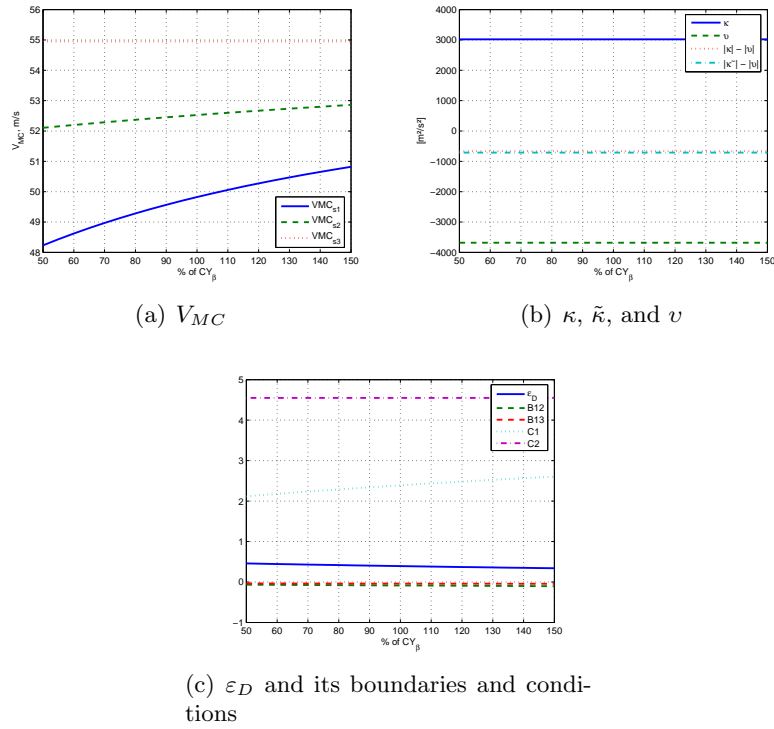


Figure C.4: DC8. Variation of  $CY_{\beta, fuselage}$ .

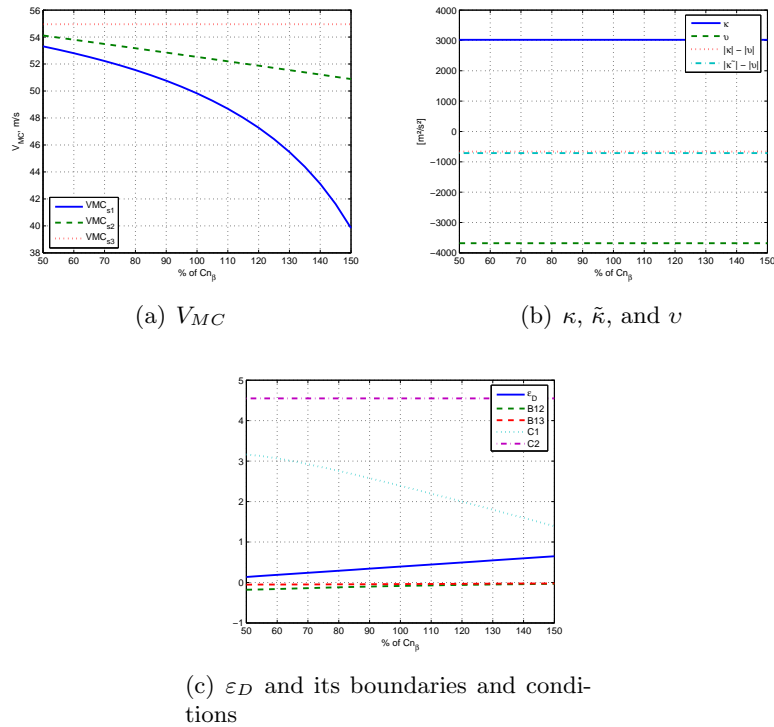
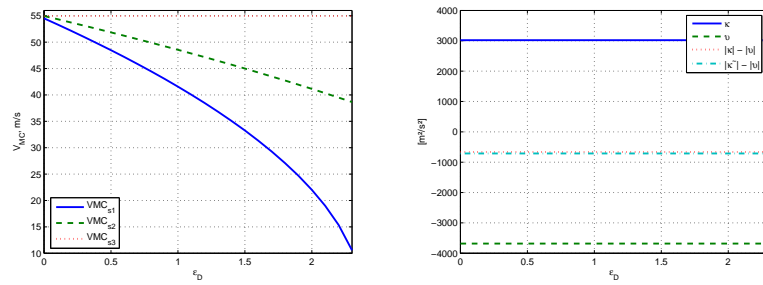
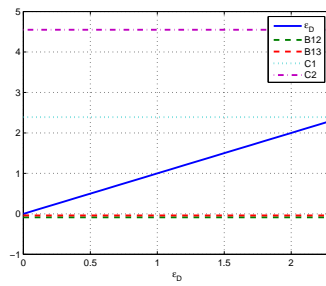


Figure C.5: DC8. Variation of  $Cn_{\beta, fuselage}$ .

(a)  $V_{MC}$ (b)  $\kappa$ ,  $\tilde{\kappa}$ , and  $v$ (c)  $\epsilon_D$  and its boundaries and conditionsFigure C.6: DC8. Variation of  $\epsilon_D$ .

## C.2 VELA1

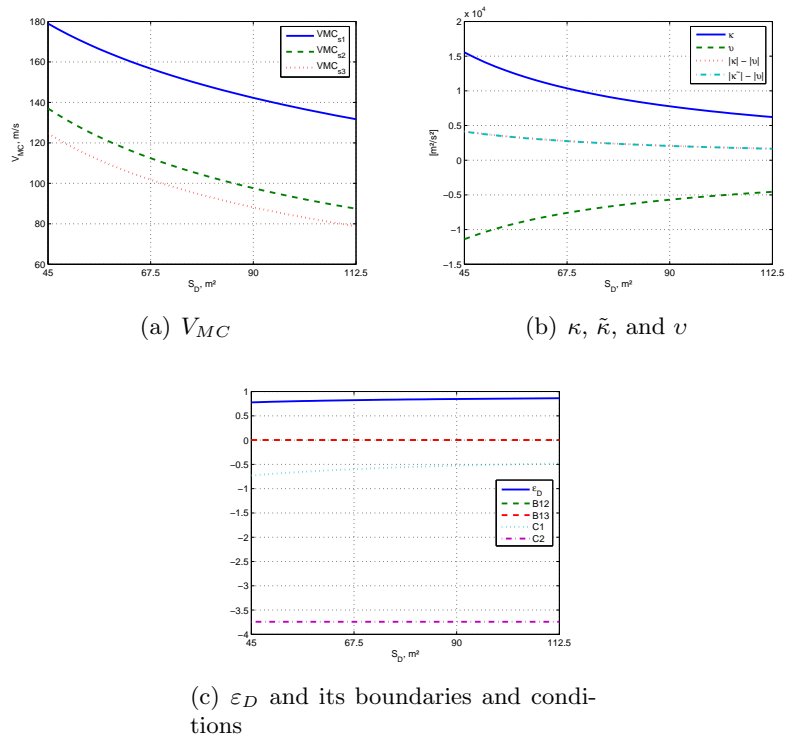


Figure C.7: VELA. Variation of the fin size.

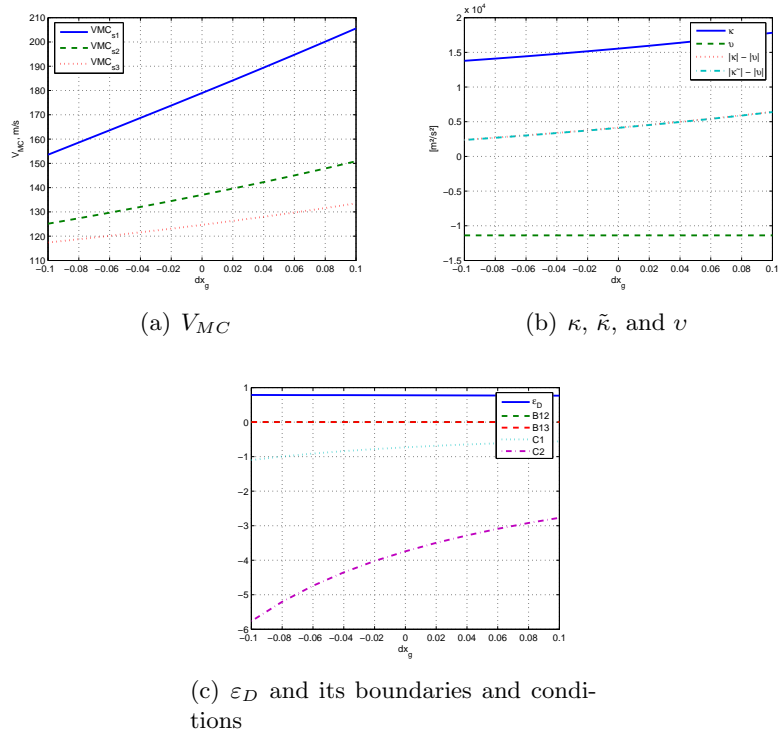


Figure C.8: VELA. Variation of the center of gravity position.

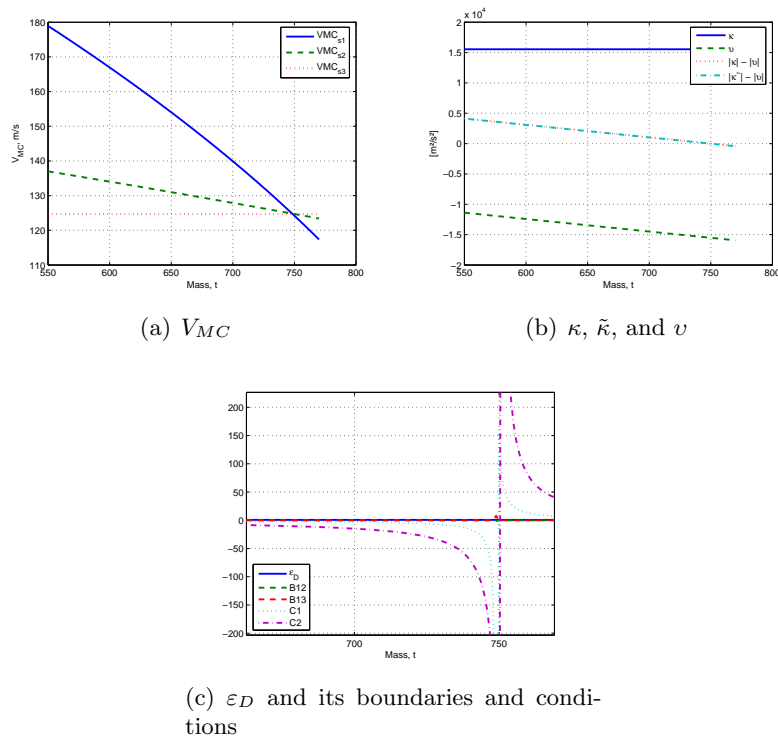


Figure C.9: VELA. Variation of the mass.

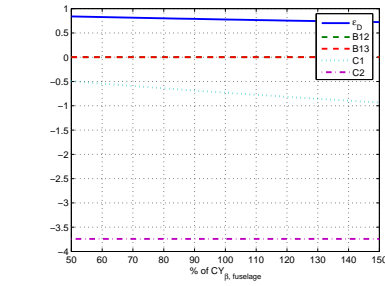
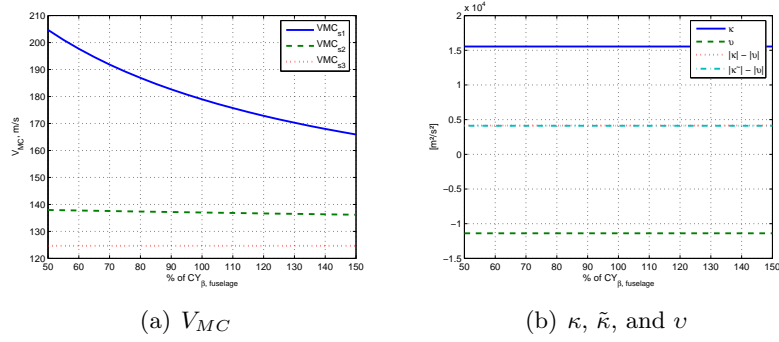


Figure C.10: VELA. Variation of  $CY_{\beta, fuselage}$ .

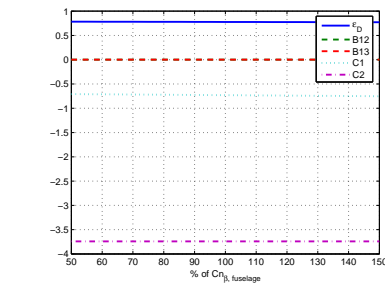
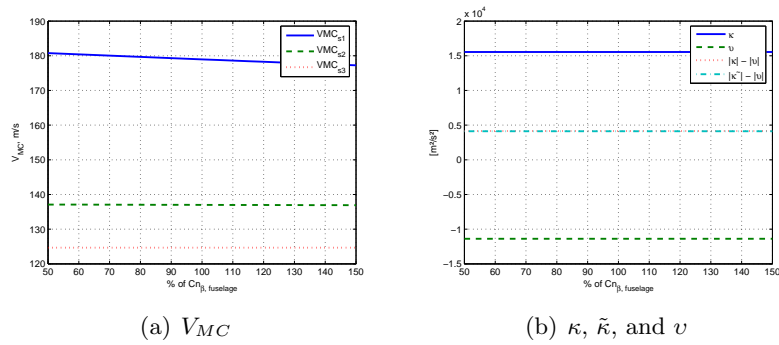
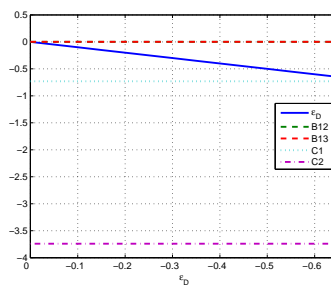
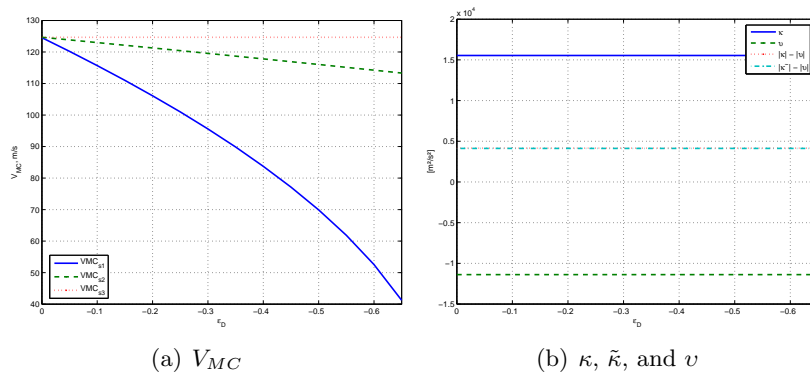


Figure C.11: VELA. Variation of  $Cn_{\beta, fuselage}$ .

Figure C.12: VELA. Variation of  $\varepsilon_D$ .

## Appendix D

# Aileron-Sideslip Coupling

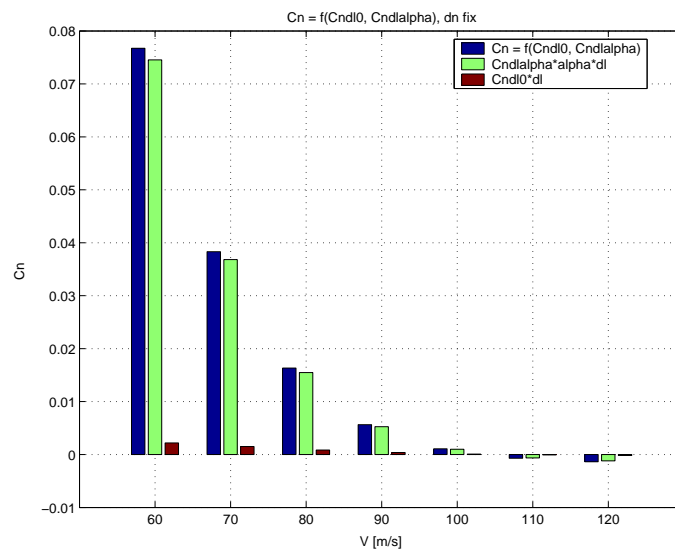


Figure D.1: VELA. Coefficient  $C_n^*$  as composition of aileron deflection and angle of attack ( $C_{n\delta l}$ ,  $C_{n\delta l, \alpha}$ ).  $S_D = 2 \times 45m^2$ ,  $dx_g = -8.35\%$ .

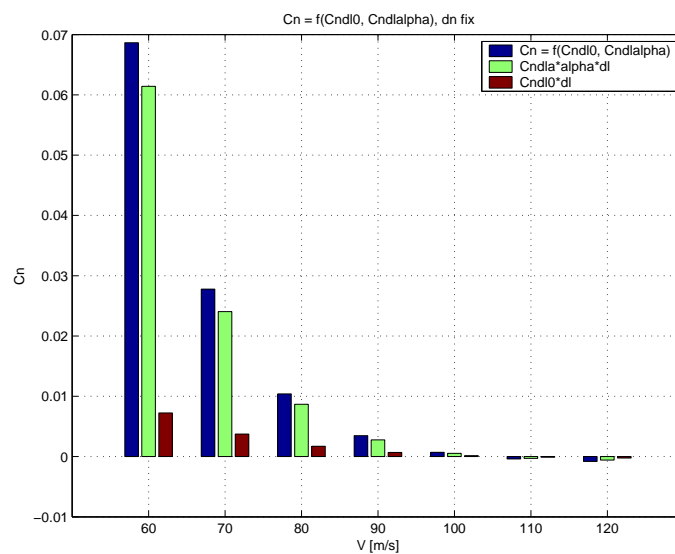


Figure D.2: VELA. Coefficient  $C_n^*$  as composition of aileron deflection and angle of attack with reduced derivative  $C_{n\delta l, \alpha}$ .  $S_D = 2 \times 45m^2$ ,  $dx_g = -8.35\%$ .

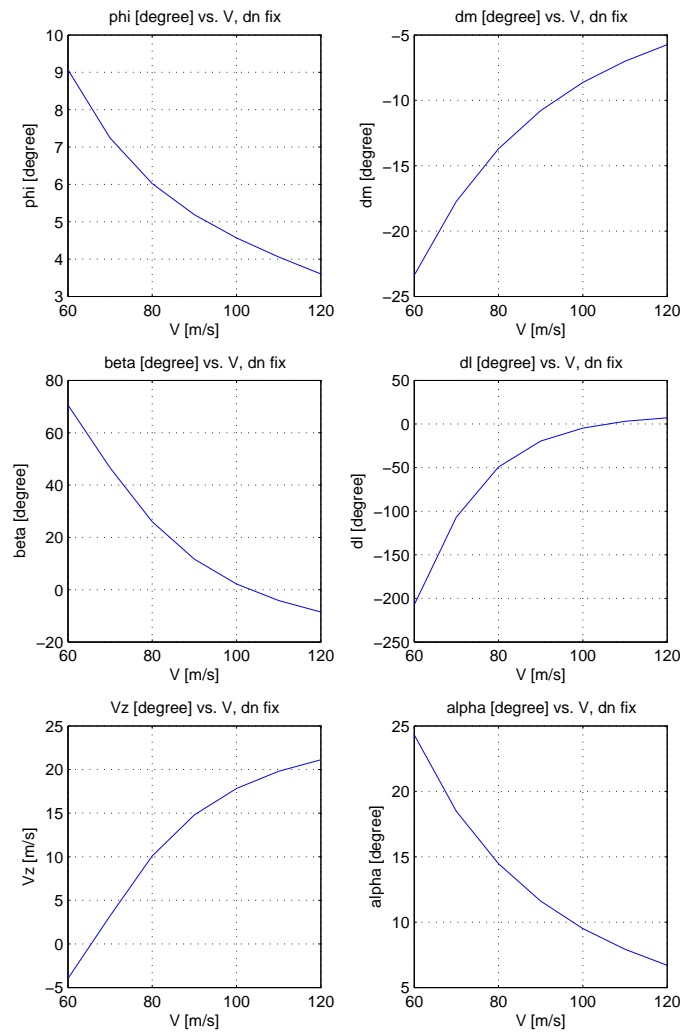


Figure D.3: VELA. Equilibrium at  $\delta n = -30^\circ$ ,  $S_D = 2 \times 45 \text{ m}^2$ ,  $dx_g = -0.0835$  and reduced  $C_{n\delta l, \alpha}$ .

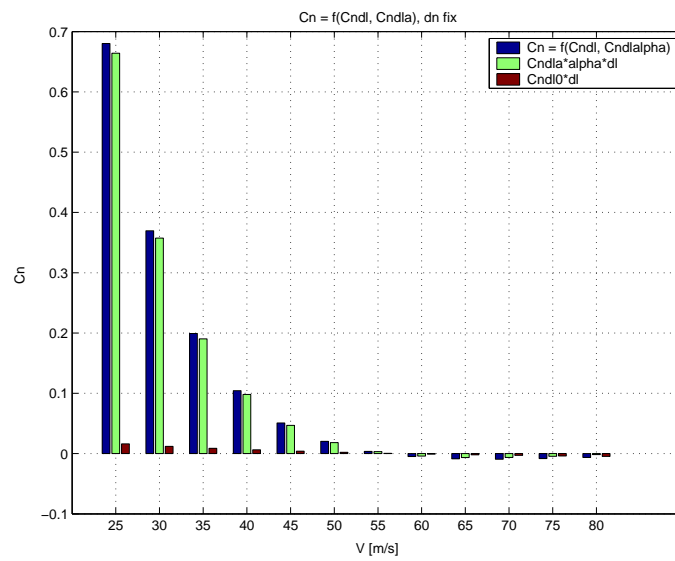


Figure D.4: DC8. Introduction of derivative  $C_{n\delta l, \alpha}$  into aircraft model.

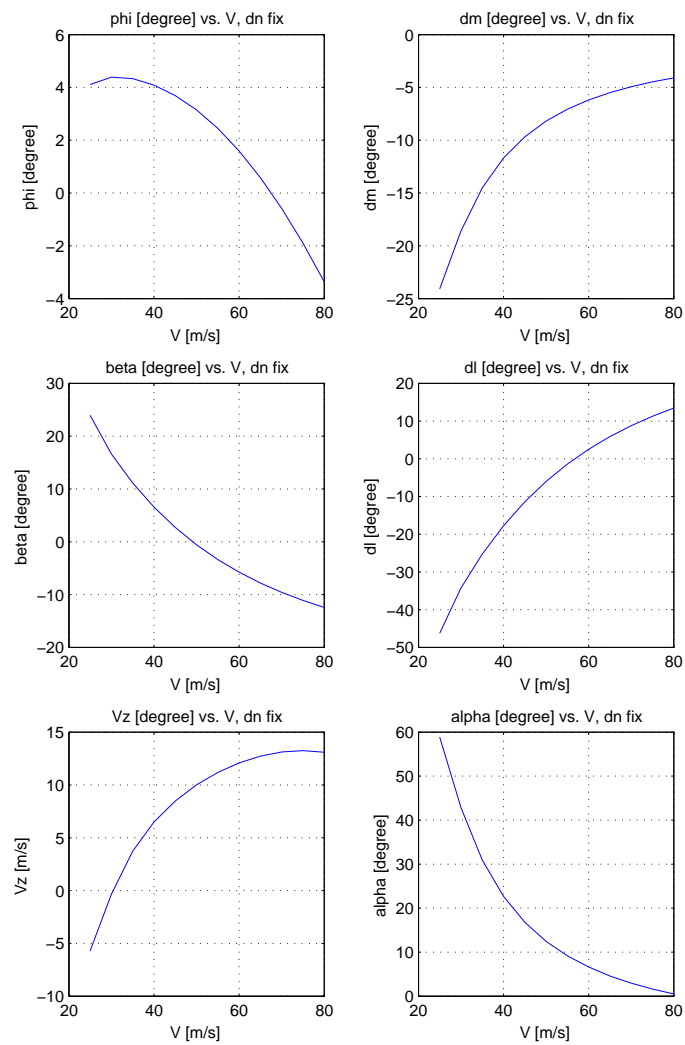


Figure D.5: DC8. Equilibrium at  $\delta n = -30^\circ$  with modified modeling of aileron-sideslip-angle of attack coupling.





# THÈSE

En vue de l'obtention du

## DOCTORAT DE L'UNIVERSITÉ DE TOULOUSE

Délivré par **l'Institut Supérieur de l'Aéronautique et de l'Espace**  
Spécialité : Systèmes automatiques

---

Présentée et soutenue par **Alexander Peter FEUERSÄNGER**  
le 4 décembre 2007

**Contrôle d'un avion à stabilité réduite**  
**Control of Aircraft with Reduced Stability**

Résumé

---

### JURY

M. Benoît Bergeon, président du jury - rapporteur  
M. Laurent Bovet  
M. Gilles Ferrères, co-directeur de thèse  
M. Dieter Schmitt, rapporteur  
M. Clément Toussaint, co-directeur de thèse  
M. Daniel Walker, rapporteur

---

École doctorale : **Systèmes**

Unité de recherche : **Équipe d'accueil SUPAERO-ONERA CSDV (ONERA-DCSD, centre de Toulouse)**

Co-directeurs de thèse : **M. Gilles Ferrères, M. Clément Toussaint**



*À mes parents  
et à mon frère*



---

## Remerciements

J'aimerais commencer par remercier la fondation ERICH-BECKER (aéroport de Francfort), le *Deutscher Akademischer Austausch Dienst* (DAAD), et l'*Office National d'Études et de Recherches Aérospatiales* (ONERA). C'est grâce à leur soutien financière que cette thèse a pu être achevée sous des conditions vivables.

J'exprime ma gratitude envers Prof. Dr. Benoît BERGEON de l'*Université de Bordeaux*, Prof. Dr.-Ing. Dr. hc. Dieter SCHMITT de l'*Université de Munich* (TUM) et d'Airbus, et Dr. Daniel WALKER de l'*Université de Liverpool* pour avoir accepté d'être rapporteurs et pour avoir pris le temps d'étudier mon rapport de thèse. Je remercie aussi Dr. Laurent BOVET d'Airbus pour sa participation au jury de soutenance.

Que soient remerciés mes encadrants Dr. Gilles FERRERES et Clément TOUSSAINT de l'ONERA. J'ai particulièrement apprécié leur approche méthodique et structurée qui a contribué de manière significative au résultat de cette thèse.

Remercées soient les équipes entières du DCSD (Department Commande des Systèmes et Dynamique du Vol) à l'ONERA, en particulier Dr. Jean-Marc BIANNIC et Dr. Carsten DÖLL pour la collaboration enrichissante. De plus, j'aimerais remercier Carsten particulièrement pour son aide avec tous ce qui vient avec vivre en France étant étranger.

Merci beaucoup à Prof. Dr.-Ing. Wolfgang SCHRÖDER, Prof. Dr.-Ing. Wolfgang ALLES, et Prof. Dr.- Ing. Dieter JACOB, tous *Université d'Aix-la-Chapelle* (RWTH Aachen), pour leurs conseils et recommandations.

J'aimerais dire merci à tous les autres doctorants et stagiaires au DCSD, en particulier à Patrice ANTOINETTE et Nicolas FEZANS pour les conversations intéressantes et leur aide linguistique pour le présent résumé français de ma thèse.

Je ne veux pas oublier mes collègues et amis Andreas KNAUF et Sebastian GAULOCHER avec qui j'ai pu passer tous les hauts et les bas de la vie d'un doctorant à Toulouse : des moments heureux et tristes, laborieux et paresseux, drôles et sérieux, de peur et de l'espoir, le début et la fin.

Pour finir, j'aimerais remercier les personnes qui me sont les plus chères dans ma vie : ma famille, mes parents Hortange Antoinette et Gert-Peter, et mon frère Grischa Peter, qui m'ont encouragé et motivé ma vie entière et qui m'ont donné le nécessaire (et plus que ça !) pour poursuivre mon chemin et pour arriver là où je suis maintenant. Et à Andrea, pour son amour et sa patience, merci.

Toulouse, décembre 2007

Alexander Peter FEUERSÄNGER



## Résumé

Afin d'améliorer les performances et l'efficacité des avions civils, les développements actuels sont toujours plus orientés vers la réduction de la stabilité naturelle en combinaison avec un système de stabilisation automatique. Ceci permet de réduire de façon significative la traînée de l'avion en minimisant les surfaces stabilisatrices ou de voler avec des centrages plus avantageux.

Deux objectifs principaux définissent l'orientation de cette thèse. En première partie, on propose un ensemble de méthodes et d'outils pour évaluer l'impact d'une réduction de la stabilité naturelle de l'avion. Dans le cadre des critères de certification, nous examinons les paramètres qui jouent simultanément sur une augmentation de l'efficacité et une réduction de la stabilité, notamment la surface de la dérive et le centrage. En faisant cette évaluation dans le contexte d'avant-projet, nous aboutissons à des recommandations pour la conception de l'avion.

La deuxième partie traite de la synthèse d'un correcteur robuste de type *back-up*. On utilise une technique de synthèse polytopique qui garantit les qualités de vol nécessaires sur une large plage de centrages. Cette approche multi-objectif a pour but de limiter l'activité des actionneurs (critère  $H_\infty$ ) ainsi que de maximiser la positivité du système en boucle fermée pour garantir la stabilité en présence des saturations. Nous calculons les domaines d'attraction correspondants et proposons de synthétiser un correcteur de type *anti-windup* pour améliorer la performance du système saturé.

Finalement, une dernière partie traite des gains que l'on peut attendre avec les concepts d'avion à stabilité réduite. Sous quelques hypothèses, nous estimons les gains en masse, traînée et consommation de carburant pour démontrer l'intérêt des outils développés et de l'approche choisie.



# Contents

|          |   |          |
|----------|---|----------|
| <b>1</b> | <b>Introduction</b>   | <b>1</b> |
| 1.1      | Motivation . . . . .  | 1        |
| 1.2      | Analyse de la mécanique et de la dynamique du vol . . . . .           | 2        |
| 1.2.1    | Objectifs . . . . .   | 2        |
| 1.2.2    | Plan . . . . .  | 2        |
| 1.3      | Synthèse d'un correcteur robuste de type back-up . . . . .            | 4        |
| 1.3.1    | Objectifs . . . . .   | 4        |
| 1.3.2    | Plan . . . . .  | 4        |
| 1.4      | Synthèse et comparaison . . . . .                                     | 5        |
| <b>2</b> | <b>Analyse de la dynamique du vol d'un avion à stabilité réduite</b>  | <b>7</b> |
| 2.1      | Approche analytique vers la stabilité réduite longitudinale . . . . . | 7        |
| 2.1.1    | Stabilité statique longitudinale . . . . .                            | 7        |
| 2.1.2    | Stabilité dynamique longitudinale . . . . .                           | 8        |
| 2.1.3    | Contrôle de l'oscillation d'incidence . . . . .                       | 10       |
| 2.1.4    | Actionneurs et stabilité réduite . . . . .                            | 11       |
| 2.1.5    | Illustration . . . . .  | 13       |
| 2.2      | Activité/fatigue des actionneurs et stabilité réduite . . . . .       | 15       |
| 2.2.1    | Activité des actionneurs et dommage par fatigue . . . . .             | 15       |
| 2.2.2    | Application à une mission . . . . .                                   | 17       |
| 2.3      | Stabilité longitudinale et saturations . . . . .                      | 21       |
| 2.4      | Équilibre $V_{MC}$ . . . . .  | 22       |
| 2.4.1    | Résultats analytiques . . . . .                                       | 23       |
| 2.4.2    | Résultats numériques . . . . .  | 25       |
| 2.5      | Critères dynamiques . . . . .   | 26       |

---

|          |  |           |
|----------|--|-----------|
| 2.6      | Recommandation pour l'avion VELA . . . . .   | 27        |
| <b>3</b> | <b>Synthèse multi-modèle multi-objectif d'un correcteur de type back-up et anti-windup</b> | <b>29</b> |
| 3.1      | Objectifs . . . . .  | 29        |
| 3.2      | Philosophie . . . . .  | 30        |
| 3.3      | Correcteur robuste de type retour d'état multi-objectif . . . . .                          | 31        |
| 3.4      | Évaluation de la stabilité et de la performance . . . . .                                  | 33        |
| 3.5      | Correcteur robuste de type anti-windup multi-objectif . . . . .                            | 34        |
| 3.6      | Synthèse du correcteur et application . . . . .  | 36        |
| 3.6.1    | Correcteur robuste de type back-up . . . . .   | 36        |
| 3.6.2    | Analyse de la stabilité et de la performance de la boucle fermée saturée                   | 38        |
| 3.6.3    | Simulation . . . . .   | 40        |
| <b>4</b> | <b>Gains et potentiels</b>   | <b>43</b> |
| <b>5</b> | <b>Conclusion et perspectives</b>  | <b>45</b> |

# Publications

A. P. Feuersänger, G. Ferreres [37]

Robust Back-Up Control Design for an Aircraft with Reduced Stability and Saturated Actuators

In Proceedings: *IFAC Symposium: Automatic Control in Aerospace*

Toulouse, France, 2007

S. Gaulocher, A. Knauf, A. P. Feuersänger [42]

Self-Scheduled Controller Design for Relative Motion Control of a Satellite Formation

In Proceedings: *IMSM-IMAACA Multiconference*

Buenos Aires, Argentina, 2007

A. Knauf, S. Gaulocher, A. P. Feuersänger [52]

Innovative Controller Design for Systems with Parameter Variations

In Proceedings: *Deutscher Luft- und Raumfahrtkongress*

Braunschweig, Germany, 2006

A. P. Feuersänger, C. Döll, C. Toussaint [35]

Actuator Influence on Flying Qualities of a Naturally Unstable Aircraft

In Proceedings: *International Council of the Aeronautical Sciences, ICAS*

Hamburg, Germany, 2006

A. P. Feuersänger, G. Ferreres [36]

Design of a Robust Back-Up Controller for an Aircraft with Reduced Stability

In Proceedings: *Guidance, Navigation, and Control Conference and Exhibit*

Keystone, CO, USA, 2006

A. P. Feuersänger, G. Ferreres, C. Toussaint [39]

Synthèse d'un correcteur robuste de type back-up pour un avion à stabilité réduite

*Actes du congrès des doctorants EDSYS*

Tarbes, France, 2006

A. P. Feuersänger, C. Toussaint, C. Döll [38]

The Impact of Reduced Lateral Stability on the VMC Equilibrium and Manoeuvres during early Design Phases of an Aircraft

In Proceedings: *Deutscher Luft- und Raumfahrtkongress*

Friedrichshafen, Germany, 2005



# Chapter 1

## Introduction

### 1.1 Motivation

La recherche permanente d'une meilleure efficacité a mené les principaux constructeurs d'aéronefs à concevoir des avions à stabilité réduite, voire négative. Alors que les concepts habituels satisfaisaient naturellement presque tous les critères de qualité de vol et de performances ces nouveaux concepts nécessitent un système de contrôle automatique.

Tandis que la famille A320 est naturellement stable, les avions de type A330/A340 sont déjà pour certaines conditions de vol à la limite de la stabilité naturelle avec un système mécanique de dernier secours (*back-up*) pour le cas où l'ordinateur de bord tomberait en panne. L'A380 abandonne presque tous les systèmes mécaniques de back-up pour des systèmes électriques et automatiques.

Cette nouvelle tendance est la conséquence de la recherche d'efficacité et de performance. La philosophie d'une stabilisation naturelle implique une certaine taille des empennages horizontaux et verticaux engendrant un certain niveau de masse structurelle. Accepter une stabilité réduite dans l'aviation civile permettrait de réduire les empennages et de mettre à disposition une plus large plage de centrages admissibles. Ceci est bénéfique pour la traînée, la consommation de kérosène et la souplesse au niveau du chargement de l'avion.

En contrepartie, l'avion à stabilité réduite ne satisfait plus les critères de qualité de vol nécessaires pour sa certification. L'avion peut même devenir complètement incontrôlable si les systèmes de stabilisation tombent en panne.

Un objectif important est alors l'évaluation de l'impact d'une stabilité réduite sur la dynamique de vol de l'avion. Nous devons examiner l'influence des paramètres augmentant l'efficacité mais réduisant la stabilité dans le contexte des normes et critères de certification.

Par ailleurs, un deuxième objectif est la conception d'un système autonome de type back-up pour un avion à stabilité réduite ne satisfaisant plus les critères de qualité de vol. Les besoins pour ce système sont plus sophistiqués que pour les systèmes habituels (par

exemple : *Back-Up Yaw Damper Units - BYDUs*) parce que le degré d'instabilité peut engendrer des accélérations de l'avion naturel d'une amplitude très importante quand des perturbations, comme la turbulence, apparaissent. Néanmoins, ce système doit être le plus simple possible.

Un troisième objectif est l'évaluation générale des gains potentiels et des inconvénients provenant d'une stabilité réduite pour concevoir un avion plus efficace. Cette évaluation devrait prendre en compte les deux parties, analyse de la dynamique du vol et synthèse d'un correcteur de type dernier secours, afin de tirer une conclusion générale sur ce sujet.

Étant donné la nature pluridisciplinaire de ces objectifs, nous proposons une répartition de ce manuscrit en trois parties que nous présentons ci-après.

## 1.2 Analyse de la mécanique et de la dynamique du vol

### 1.2.1 Objectifs

Deux paramètres ont été identifiés comme les facteurs dominants du compromis entre efficacité et stabilité : la position du centre de gravité et la taille du plan vertical. Les deux ont une influence significative sur la traînée d'équilibrage, la traînée de surface/friction, la masse ou encore la souplesse du chargement de l'avion [81, 76, 89, 102, 75, 77, 2].

Une optimisation de ces deux paramètres mène à une dégradation des qualités de vol ou à une violation des critères de certification, ce qui doit être quantifié pour en déduire des recommandations ou des besoins pour une stabilisation artificielle. En outre, le degré de stabilité (resp. d'instabilité) affecte non seulement la dynamique de l'aéronef, mais aussi le système de stabilisation lui-même, plus précisément les actionneurs [35]. Ce point mérite d'être approfondi car les actionneurs représentent le lien physique entre le système de commande et l'activité des surfaces aérodynamiques de contrôle.

L'impact d'une stabilité naturelle réduite est à quantifier au stade d'avant-projet de la conception d'un avion pour formuler à temps des recommandations. Le concept d'aéronef retenu est le modèle de VELA<sup>1</sup> qui a été développé dans le cadre d'un projet de recherche européen. Il s'agit d'une configuration d'aile-fuselage intégrés à doubles empennages, qui dépasse l'actuel A380 en masse/capacité ainsi qu'en dimensions géométriques [91, 6].

La première partie de la thèse est dédiée au développement de méthodes et d'outils permettant d'évaluer l'impact de la stabilité réduite à ce stade préliminaire de conception d'avion.

### 1.2.2 Plan

Précédant la partie I du manuscrit complet, le chapitre 2 résume brièvement le cadre des normes et critères de certification et détaille quelques aspects de la modélisation de l'avion.

---

<sup>1</sup>VELA - Very Efficient Large Aircraft. Avion à grande capacité très efficace.

Des références classiques [94, 95, 93, 92, 96, 97, 30, 29] ainsi que des critères spécifiques développés par l'industrie [57] ont servis de base bibliographique.

Le chapitre 3 concerne l'analyse de la dynamique du vol et examine l'effet de la stabilité réduite sur le mouvement longitudinal d'un avion. Une approche analytique pour la description de l'oscillation d'incidence de l'avion aboutit à un ensemble d'équations permettant d'évaluer l'impact de la position du centre de gravité, des caractéristiques d'actionneur et du contrôle de l'avion. Voir aussi [90] pour une approche similaire. Pour les équations de la mécanique du vol, nous suggérons les livres [22, 63, 44, 76, 89, 8, 20].

Le chapitre 4 développe les outils numériques permettant une estimation de l'activité du système de commande et la fatigue des actionneurs provoquée par la stabilisation artificielle [35, 48, 60, 66]. Cette technique est ensuite utilisée pour calculer l'estimation de la fatigue globale sur tout un profil vertical de mission typique, ce qui illustre la faisabilité de cette approche pour la conception d'avion au stade d'avant-projet. Contrairement aux techniques actuellement utilisées par l'industrie aéronautique [7], la méthode proposée ici fournit rapidement des résultats sans faire appel à des simulations numériques lourdes de longue durée.

Le chapitre 5 introduit ensuite une relation entre la position du centre de gravité et les besoins minimaux pour les actionneurs en utilisant des critères de stabilité classiques d'automatique. En particulier, la relation entre la position longitudinale du centre de gravité et le niveau minimal de saturation des actionneurs de la gouverne de profondeur est mise en évidence [27].

Le chapitre 6 traite les critères du mouvement latéral de l'avion et plus précisément les critères associés à l'équilibre d'avion à la vitesse minimale de contrôle ( $V_{MC}$ ). Ces critères concernent le vol rectiligne avec une panne de moteur externe et sont habituellement dimensionnants pour la taille du plan vertical. De nouveau, nous abordons le problème par une approche analytique. La combinaison des expressions analytiques obtenues et d'un outil développé [38] permet d'évaluer très tôt dans la phase de conception la capacité de l'avion à satisfaire les critères liés à la vitesse minimale de contrôle.

Une sélection de critères dynamiques - notamment ceux liés à la  $V_{MC}$  - sont examinés dans le chapitre 7. Ceux-ci concernent des manœuvres [57, 27] ainsi que des spécifications sur les qualités de vol qui sont analysées d'une manière analytique et numérique. Ce chapitre et la partie sur la mécanique et dynamique du vol s'achèvent par une liste de recommandations pour la conception de VELA en illustrant les atouts des approches présentées.

## 1.3 Synthèse d'un correcteur robuste de type back-up

### 1.3.1 Objectifs

Comme l'avion naturel à stabilité réduite est difficilement voire incontrôlable, un système de commande de type *back-up* doit être développé. Les spécifications opérationnelles sont très contraignantes dans la mesure où l'on s'attend à une activité importante du système de commande, comme illustré dans le chapitre 4 du manuscrit, et à une saturation des gouvernes de commande. De plus, le correcteur final doit être très simple.

La synthèse de ce système de dernier secours doit donc intégrer plusieurs objectifs de commande : il doit d'abord garantir les qualités de vol minimales indispensables pour la certification, et ceci sur toute la plage des positions possibles du centre de gravité. Les amplitudes des signaux de commande pouvant être importantes, les caractéristiques non-linéaires des actionneurs doivent aussi être considérées. Les saturations sur la position et la vitesse de gouvernes sont notamment à prendre en compte, et leur influence sur la stabilité et les performances en boucle fermée doit être minimisée lors de la synthèse. On souhaite obtenir une loi de commande statique robuste aux saturations et au centrage, compte tenu de la nécessaire simplicité de l'architecture d'un système de commande de dernier secours.

### 1.3.2 Plan

La partie sur la synthèse robuste commence par une courte introduction au problème d'un point de vue Automatique et présente une liste de spécifications pour une loi de commande de type back-up (chapitre 8). Cette liste est directement déduite des recommandations pour la conception d'aéronefs de la partie précédente.

Compte tenu des objectifs de commande spécifiés, le chapitre 9 détaille une technique de synthèse polytopique d'un retour d'état [23, 16, 36, 37] qui s'avère adaptée à ce problème et qui fournit rapidement des résultats satisfaisants. Les objectifs de commande sont transformés en LMIs (inégalités matricielles linéaires) [78, 21, 41, 23, 24]. Une attention particulière est portée à l'évaluation a posteriori du domaine de stabilité et des performances en boucle fermée en présence de saturations [101, 17]. Une solution pour minimiser l'impact des saturations est également proposée par ajout d'une commande de type *anti-windup*. Contrairement aux travaux de [86, 87, 101] par exemple, on synthétise un correcteur anti-windup statique en utilisant une technique convexe multi-modèles multi-objectifs.

Le chapitre 10 est entièrement dédié à la synthèse et à la validation du correcteur et à la présentation des résultats. Des remarques concluent la partie commande.

## 1.4 Synthèse et comparaison

Dans cette dernière partie de la thèse, deux configurations du même type d'avion ont été comparées pour illustrer les gains rendus possibles en acceptant une stabilité réduite. L'une des configurations est naturellement stable et satisfait les critères de certification sans avoir recours à un système supplémentaire d'augmentation de stabilité. L'autre configuration a, quant à elle, un plan vertical de taille réduite ainsi qu'une plage de variation du centre de gravité plus large. Cette configuration naturellement instable intègre le correcteur robuste de dernier secours synthétisé précédemment.

Sur la base de procédures classiques de conception d'aéronefs [25, 89, 76, 75, 63, 51, 49, 53], les gains en masse, traînée et consommation de kérosène ont pu être estimés dans le chapitre 11. Il a été montré que les gains potentiels résultant de l'acceptation d'une stabilité réduite dans l'aviation civile pouvaient être quantifiés au stade d'avant-projet de la conception d'un avion par les méthodes et outils développés.

Une conclusion sur l'ensemble des travaux réalisés et des perspectives prometteuses pour de futurs travaux de recherches terminent cette thèse.



## Chapter 2

# Analyse de la dynamique du vol d'un avion à stabilité réduite

Ce chapitre résume les principaux résultats de la partie analyse de la dynamique du vol. La section 2.1 résume les développements analytiques identifiant les principaux enjeux d'une stabilité longitudinale réduite dans le cadre de la contrôlabilité de l'oscillation d'incidence. La section 2.2 présente les résultats liés à une analyse linéaire du vol en turbulence d'un avion artificiellement stabilisé. L'activité du système de contrôle et la fatigue des actionneurs y sont notamment examinées. La section 2.3 donne un bref aperçu d'un critère que nous avons développé afin d'incorporer des non-linéarités d'actionneur dans l'évaluation d'un domaine de contrôlabilité. La section 2.4 récapitule les résultats de l'analyse de l'équilibre à la vitesse minimum de contrôle qui se situe dans le contexte d'un vol asymétrique avec un moteur non-opérationnel. La section finale de ce chapitre traite du mouvement latéral de l'avion et examine la dynamique latérale vis-à-vis d'une stabilité réduite.

### 2.1 Approche analytique vers la stabilité réduite longitudinale

On peut définir une stabilité statique et une stabilité dynamique de l'avion. Les deux notions forment la base pour la suite de l'étude.

#### 2.1.1 Stabilité statique longitudinale

La stabilité statique longitudinale provient de l'équilibrage de l'avion pour une certaine valeur de l'angle d'incidence  $\alpha$  et du fait que la dérivée partielle du moment de tangage par rapport à  $\alpha$  est négative :

$$\begin{aligned}\frac{\partial M}{\partial \alpha} &< 0 \\ M(\alpha_{trim}) &= 0\end{aligned}\tag{2.1}$$

Cette condition mène à définir une marge statique de stabilité  $s_m$  qui dénote la distance adimensionnée suivant l'axe avion entre la position de centre de gravité  $X_g$  et le foyer  $X_N$ . Ce dernier représente le centrage auquel l'avion est statiquement neutre. Si le centrage est avant ce point (fwd), l'avion est statiquement stable ( $s_m > 0$ ), si le centrage est derrière ce point (aft), l'avion est instable ( $s_m < 0$ ) :

$$s_m = -\frac{Cm_\alpha}{C_{L\alpha}} = -(x_g - x_N) = -\frac{X_g - X_N}{l}\tag{2.2}$$

$l$  est la longueur de référence de l'avion,  $Cm_\alpha$  et  $C_{L\alpha}$  sont des dérivatives aérodynamiques. Plus de détails sont disponibles à la section 3.1 du manuscrit complet.

### 2.1.2 Stabilité dynamique longitudinale

Nous nous penchons ici sur l'oscillation d'incidence (OI) qui est très difficile à gérer pour un pilote si elle est en limite de stabilité, voire instable. Les équations de l'OI sont obtenues par les équations de portance et de moment de tangage (les notations sont celles du manuscrit complet):

$$mV \frac{d\gamma}{dt} = L - W \cos \gamma + F \sin(\alpha + \sigma)\tag{2.3}$$

$$I_{yy} \frac{d^2\theta}{dt^2} = \sum M_Y\tag{2.4}$$

où  $L$  est la portance,  $W$  le poids et  $\sigma$  l'angle entre le vecteur de poussée et l'axe  $x$  de l'avion. Après quelques simplifications et substitutions les équations deviennent en notation matricielle :

$$\begin{pmatrix} \dot{\alpha} \\ \dot{q} \end{pmatrix} = \begin{pmatrix} -b_1 C_{L\alpha} & 1 - \varepsilon \\ b_2 C_{m\alpha} & b_2 \frac{l}{V} C_{m_q} \end{pmatrix} \begin{pmatrix} \alpha \\ q \end{pmatrix} + \begin{pmatrix} -b_1 C_{L\delta m} \\ b_2 C_{m\delta m} \end{pmatrix} \delta m\tag{2.5}$$

avec

$$b_1 = \frac{\bar{q}S}{mV}, \quad b_2 = \frac{\bar{q}Sl}{I_{yy}}, \quad \varepsilon = b_1 \frac{l}{V} C_{Lq}\tag{2.6}$$

Ceci permet de déterminer les valeurs propres du système.

En dérivant les expressions et en substituant, on obtient deux équations différentielles de deuxième ordre en  $\alpha$  et  $q$  qui nous serviront à trouver la limite de stabilité dynamique :

Équations différentielles linéaires non-homogènes de l'oscillation de l'incidence:

$$a_2 \ddot{x} + a_1 \dot{x} + a_0 x = \mathcal{F}_x(\delta m) \quad (2.7)$$

où

$$a_0 = -b_2 [(1 - \varepsilon) C m_\alpha + b_1 \frac{l}{V} C m_q C_{L\alpha}] \quad (2.8)$$

$$a_1 = b_1 C_{L\alpha} - b_2 \frac{l}{V} C m_q \quad (2.9)$$

$$a_2 = 1 \quad (2.10)$$

avec

$$b_1 = \frac{\bar{q}S}{mV}, \quad b_2 = \frac{\bar{q}Sl}{I_{yy}}, \quad \varepsilon = b_1 \frac{l}{V} C_{Lq} \quad (2.11)$$

Les parties non-homogènes  $\mathcal{F}_x(\delta m)$  pour  $x = \alpha$  et  $x = q$  sont :

$$\mathcal{F}_\alpha(\delta m) = b_2 [(1 - \varepsilon) C m_{\delta m} + b_1 \frac{l}{V} C m_q C_{L\delta m}] \delta m - b_1 C_{L\delta m} \delta \dot{m} \quad (2.12)$$

$$\mathcal{F}_q(\delta m) = b_1 b_2 [C_{L\alpha} C m_{\delta m} - C m_\alpha C_{L\delta m}] \delta m + b_2 C m_{\delta m} \delta \dot{m} \quad (2.13)$$

Selon le critère de Hurwitz, pour assurer la stabilité il faut que

$$a_n > 0, \quad n \in [0, 1, 2]$$

Ceci nous amène à deux critères de stabilité en termes de la marge statique  $s_m$  :

$$\begin{array}{l} 1. \quad s_m > \frac{\rho S l}{2m} C m_{q,x_N} \\ 2. \quad s_m > \frac{C m_{q,x_N}}{C_{Lq}} - \frac{I_{yy}}{m l^2} C_{L\alpha} \end{array} \quad (2.14)$$

La première condition définit le centrage en terme de marge statique où l'avion se trouve à la limite de stabilité. La deuxième condition n'est pas une contrainte physique puisque  $C m_{q,x_N} < 0$ .

De la première condition découle directement la limite générale de la stabilité dynamique, qui s'appelle également *point de manœuvre*  $X_{MP}$ . Ce point se situant à  $|\frac{\rho S l}{2m} C m_{q,x_N}|$  derrière le foyer  $X_N$ , sa position s'écrit :

$$X_{MP} = X_N - \frac{\rho S l^2}{2m} C m_{q,x_N} \quad (2.15)$$

On en déduit la marge dynamique  $d_m$  :

$$d_m = -\frac{X_g - X_{MP}}{l} \quad (2.16)$$

Comme indiqué dans le manuscrit principal, il est maintenant tout à fait possible de tracer l'évolution des qualités de vol en fonction du centrage. Nous disposons de l'expression suivante pour l'évolution de l'amortissement  $\xi$  et de la pulsation  $\omega$  pour un déplacement du centrage d'en arrière (aft)  $s_{m-}$  vers une position plus en avant (fwd)  $s_m$  en fonction des caractéristiques de l'OI ( $\xi_{s_{m-}}, \omega_{s_{m-}}$ ) en  $s_{m-}$  :

$$\omega_{s_m} = \sqrt{\omega_{s_{m-}}^2 + [s_m - s_{m-}] b_2 C_{L\alpha}} \quad (2.17)$$

$$\xi_{s_m} = \frac{2 \xi_{s_{m-}} \omega_{s_{m-}} + [s_m - s_{m-}] C_{Lq}}{2 \sqrt{\omega_{s_{m-}}^2 + [s_m - s_{m-}] b_2 C_{L\alpha}}} \quad (2.18)$$

### 2.1.3 Contrôle de l'oscillation d'incidence

Nous proposons ici un ensemble d'expressions pour un retour individuel des variables aérodynamiques  $\alpha$  et  $q$ , ainsi que d'une combinaison des deux afin d'atteindre un objectif en termes de pulsation et d'amortissement en boucle fermée.

#### Retour de $\alpha$

La loi de retour s'écrit :

$$\delta m = K_\alpha \cdot \alpha \quad (2.19)$$

Après quelques développements on obtient l'expression du gain qui stabilise le système avec un retour pur en  $\alpha$  :

$$K_\alpha^{stab} = \frac{C_{L\alpha} d_m}{(1 - \varepsilon) C_{m\delta m, x_N} + C_{L\delta m} d_m} \quad (2.20)$$

#### Retour de $q$

La loi de retour s'écrit :

$$\delta m = K_q \cdot q \quad (2.21)$$

Le gain de retour en  $q$  stabilisant le système est :

$$K_q^{stab} = \frac{d_m}{b_1 C_{m\delta m, x_N}} \quad (2.22)$$

### Combinaison d'un retour en $\alpha$ et $q$ avec un objectif modal

Considérons le retour

$$\delta m = (K_\alpha, K_q) \cdot (\alpha, q)^T \quad (2.23)$$

Nous proposons les expressions suivantes pour un objectif de pulsation  $\omega_{obj}$  et d'amortissement  $\xi_{obj}$  sous l'hypothèse que  $C_{L\delta m} \approx 0$  :

$$K_q = \frac{a_1 - 2\xi_{obj}\omega_{obj}}{b_2 C_{m_{\delta m, x_N}}} \quad (2.24)$$

$$K_\alpha = \frac{a_0 - \omega_{obj}^2 + (2\xi_{obj}\omega_{obj} - a_1)}{b_2(1 - \varepsilon) C_{m_{\delta m, x_N}}} \quad (2.25)$$

Ce résultat, combiné avec les Eqs. (2.17) and (2.18), permet de calculer un gain robuste vis-à-vis du centrage de l'avion. Plus de détails figurent dans le manuscrit.

#### 2.1.4 Actionneurs et stabilité réduite

##### Intégration du modèle d'actionneur

Considérons un modèle d'actionneur du premier ordre :

$$T_{act}\delta\dot{m} + \delta m = u_c \quad (2.26)$$

L'actionneur est caractérisé par sa constante de temps  $T_{act}$ ,  $u_c$  est la commande calculée par la loi de retour

$$u_c = K_\alpha \alpha + K_q q \quad (2.27)$$

et  $\delta m$  est en boucle fermée à la fois la position actuelle de l'actionneur et l'entrée du système linéaire de l'avion. Par la transformée de Laplace nous obtenons dans le domaine fréquentiel pour un transfert entre l'entrée du système  $U(s)$  et la position du profondeur  $\delta m$  dans la boucle ouverte :

$$\frac{\delta m(s)}{U(s)} = G(s) = \frac{g_1 \cdot s + g_0}{(T_{act}s + 1)(s^2 + a_1 s + a_0)} \quad (2.28)$$

avec

$$g_0 = K_q z_{1q} + K_\alpha z_{1\alpha} \quad (2.29)$$

$$g_1 = K_q z_{2q} - K_\alpha z_{2\alpha} \quad (2.30)$$

où

$$z_{1\alpha} = b_2 [(1 - \varepsilon) C m_{\delta m} + b_1 \frac{l}{V} C m_q C_{L\delta m}] \quad z_{2\alpha} = b_1 C_{L\delta m} \quad (2.31)$$

$$z_{1q} = b_1 b_2 [C_{L\alpha} C m_{\delta m} - C m_\alpha C_{L\delta m}] \quad z_{2q} = b_2 C m_{\delta m} \quad (2.32)$$

Il est maintenant possible d'analyser l'influence de l'actionneur sur deux caractéristiques de la boucle fermée qui ont une signification importante dans le contexte de la stabilité : la marge de gain et la marge de phase.

### Marge de gain

Selon le critère de Bode, la marge de gain  $GM$  se définit à la fréquence  $\omega_{pc}$  pour laquelle l'argument  $\varphi_0 = -\pi$ . Avec la variable de Laplace  $s = j\omega$  on obtient :

$$\omega_{pc} = \sqrt{\frac{T_{act} a_0 g_0 + a_1 g_0 - a_0 g_1}{T_{act} (g_0 - a_1 g_1) - g_1}} \quad (2.33)$$

ce qui nous amène à l'expression suivante pour la marge de gain :

$$GM = \frac{1}{A_0} = \frac{a_1^2 T_{act} + a_1 a_0 T_{act}^2 + a_1}{a_1 g_1 T_{act} - g_0 T_{act} + g_1} \quad (2.34)$$

Pour un actionneur idéal ( $T_{act} \rightarrow 0$ ) la marge de gain devient :

$$GM = \frac{a_1}{g_1} \quad (2.35)$$

Une condition de l'existence de  $GM$  est donc  $\frac{a_1}{g_1} > 0$ , ce qui nous donne une relation entre les gains de retour  $K_q$  et  $K_\alpha$  (notons que  $z_{2q} < 0$ ) :

$$K_q < K_\alpha \frac{z_{2\alpha}}{z_{2q}} \quad \Rightarrow \quad K_q < K_\alpha \frac{b_1 C_{L\delta m}}{b_2 C m_{\delta m}}$$

Nous procédons d'une manière similaire pour évaluer l'impact de la bande passante de l'actionneur. Nous proposons ici deux conditions : la première donne seulement une limite pour  $T_{act}$  si l'avion est instable ( $a_0 < 0$ ), la deuxième indique la constante de temps pour laquelle la marge n'est pas définie.

$$1. \quad T_{act_{max}} < -\frac{a_1}{2a_0} + \sqrt{\left(\frac{a_1}{2a_0}\right)^2 - \frac{1}{a_0}} \quad (2.36)$$

$$2. \quad 0 < T_{act} \neq \frac{g_1}{g_0 - a_1 g_1} \quad (2.37)$$

### Marge de phase

La marge de phase se trouve à la fréquence  $\omega_{gc}$  pour laquelle l'amplitude du système

$$|G(j\omega_{gc})| = \frac{|j\omega_{gc} g_1 + g_0|}{|(j\omega_{gc} T_{act} + 1)((j\omega_{gc})^2 + j\omega_{gc} a_1 + a_0)|} = 1 \quad (2.38)$$

Pour un actionneur idéal ( $T_{act} \rightarrow 0$ ) la marge de phase  $PM$  est :

$$PM = \pi + \varphi_0 = \pi + \arctan\left(\frac{g_1\omega_{gc}}{g_0}\right) - \arctan\left(\frac{a_1\omega_{gc}}{a_0 - \omega_{gc}^2}\right) \quad (2.39)$$

Une marge de retard maximale de la boucle en découle directement :

$$\tau_{max} = \frac{PM}{\omega_{gc}} \quad (2.40)$$

Pour estimer l'impact de la bande passante de l'actionneur on trace les pulsations  $\omega$  qui satisfont simultanément les Eqs. (2.38) and (2.41) en fonction de  $T_{act}$ .

$$\arctan\left(\frac{g_1\omega}{g_0}\right) - \arctan\left(\frac{a_1\omega}{a_0 - \omega^2}\right) - \arctan(\omega T_{act}) = -\pi \quad (2.41)$$

#### 2.1.5 Illustration

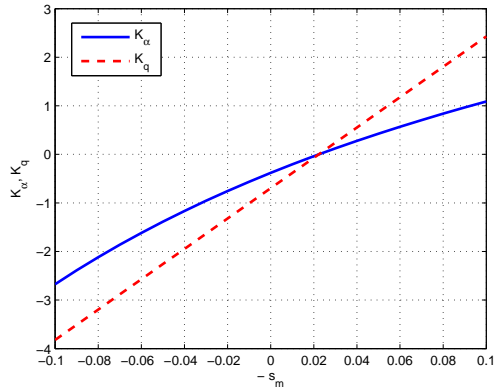
Nous présentons ici les résultats obtenus avec les expressions analytiques. L'avion de l'application est le modèle VELA à faible masse ( $m = 550t$ ), équilibré à basse vitesse ( $Mach = 0.2$ ).

La Figure 2.1(a) présente le gain nécessaire pour mener le système en limite de stabilité, Eqs. (2.20) and (2.22). La Figure 2.1(b) montre l'évolution de gains suivant un objectif en termes d'amortissement et de pulsation. Nous avons fixé  $\omega = 0.8 rad/s$  et fait varier l'amortissement  $\xi$  entre 0.1 et 1. Un amortissement élevé produit une norme réduite du gain nécessaire. Pour un objectif de 70% (grasse, rouge) à un centrage de 7% en arrière nous avons  $K_\alpha = 1.32$  et  $K_q = 0.03$ .

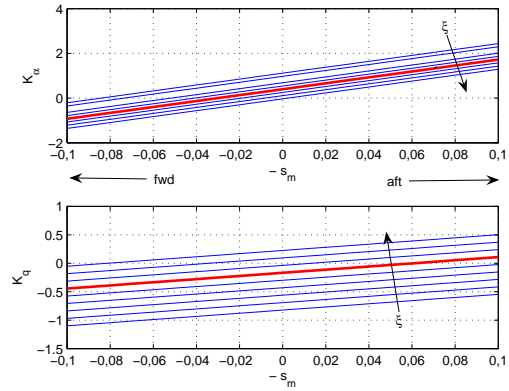
Les valeurs propres calculées analytiquement sont représentées à la Figure 2.1(c) (boucle ouverte) et à la Figure 2.1(d) (boucle fermée) pour les gains indiqués ci-dessus.

La Figure 2.1(e) présente l'évolution de la pulsation et de l'amortissement avec la position du centre de gravité pour  $\omega = 0.8 rad/s$  et  $\xi = 0.7$  à  $dx_g = 7\%$  en arrière du foyer.

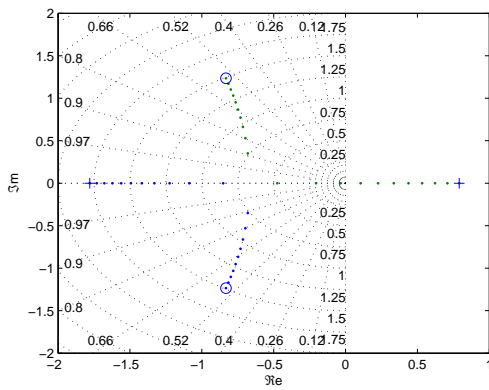
Finalement, la Figure 2.1(f) représente l'évolution de la relation entre marge de retard  $\tau$  et la constante de temps de l'actionneur par rapport l'amortissement  $\xi$ . On constate qu'un amortissement élevé permet d'obtenir une meilleure marge de retard.



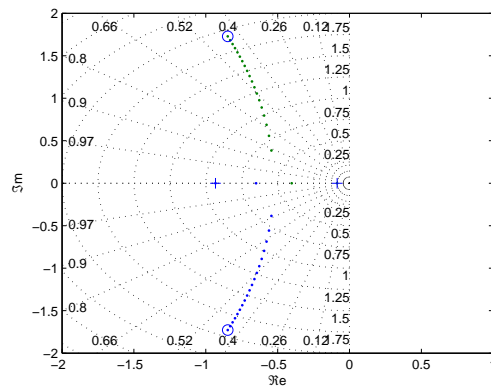
(a) Gains limites de stabilité.



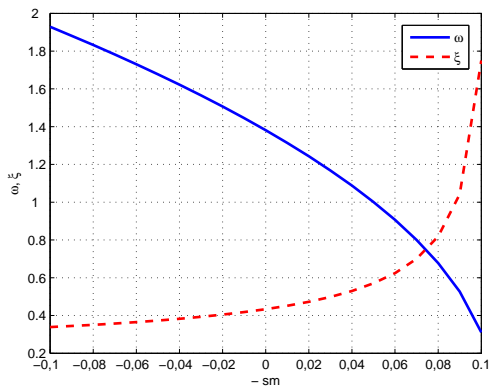
(b) Gains objectifs amortissement et pulsation.



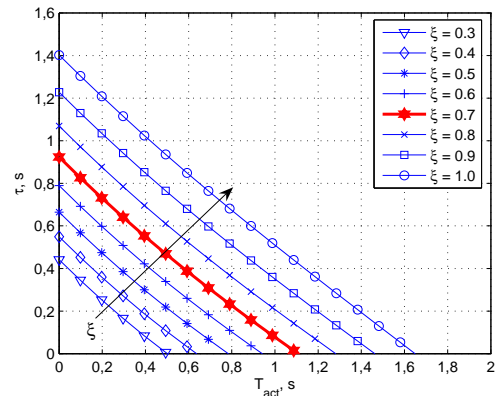
(c) Valeurs propres en boucle ouverte.



(d) Valeurs propres en boucle fermée.



(e) Évolution amortissement et fréquence.



(f) Marge de retard.

## 2.2 Activité/fatigue des actionneurs et stabilité réduite

Dans cette section nous présentons un bref aperçu des contributions présentées au chapitre 4 du manuscrit complet. À la base des résultats analytiques, l'approche choisie traite du vol en turbulence avec un modèle d'avion linéarisé ainsi qu'un modèle d'actionneur. Nous nous intéressons ici explicitement à l'actionneur qui transforme les commandes d'une loi stabilisante en forces aérodynamiques.

Une simple loi de commande garantit des spécifications modales pour toute la plage des centrages examinée, c'est-à-dire que les valeurs propres sont placées au même endroit dans le plan complexe pour tous centrages avec la méthode de la commande modale.

Puisque l'atmosphère turbulente est modélisée comme un bruit blanc passant à travers un filtre incorporant les spécifications atmosphériques à l'entrée de l'avion en boucle fermée, nous pouvons estimer la réaction du système de commande aux perturbations atmosphériques.

Cette réaction que l'on obtient en calculant les déviations des sorties par la résolution de l'équation de Lyapunov est une mesure de l'activité des actionneurs.

À partir de ces résultats nous avons étendu la méthode pour en déduire la fatigue des actionneurs due à leur activité. Il est donc désormais possible de faire le lien direct entre le degré d'instabilité (centrage), l'activité du système de contrôle et la fatigue associée des actionneurs.

Finalement, la méthode développée démontre son intérêt par une application à une mission entière d'un avion long courrier.

### 2.2.1 Activité des actionneurs et dommage par fatigue

À titre d'exemple, on présente dans cette section les résultats obtenus pour l'activité des actionneurs en fonction du centrage au vol à forte turbulence et basse vitesse.

La Figure 2.1 montre les limites de fluctuation pour la position de l'élévateur. Puisque le modèle de VELA1 ne possède pas un plan de trim séparé, l'avion doit s'équilibrer avec l'élévateur. En conséquence, les fluctuations s'ajoutent à une position d'équilibre initiale. Les courbes pointillées dénotent  $1\sigma$ , c'est-à-dire elles couvrent 68% de toutes les fluctuations anticipées pendant un vol en turbulence. Les courbes en continu dénotent  $3\sigma$  couvrant 99.7%. Elles sont fonction du centrage et de la constante de temps de l'actionneur. La courbe rouge correspond à  $T_{act} = 0.06$  s. La Figure 2.2 montre les fluctuations en vitesse de l'actionneur.

Les lignes pointillées horizontales indiquent la valeur de saturation classique d'un actionneur. Nous pouvons donc donner une estimation sur la plage des centrages admissibles, c'est-à-dire les positions qui ne sont pas sujettes aux saturations.

On montre également dans le manuscrit complet l'influence des spécifications modales

de la loi de commande sur l'activité de l'actionneur. On peut retenir qu'il est préférable de viser un amortissement assez élevé afin d'élargir la plage de centrage admissible.

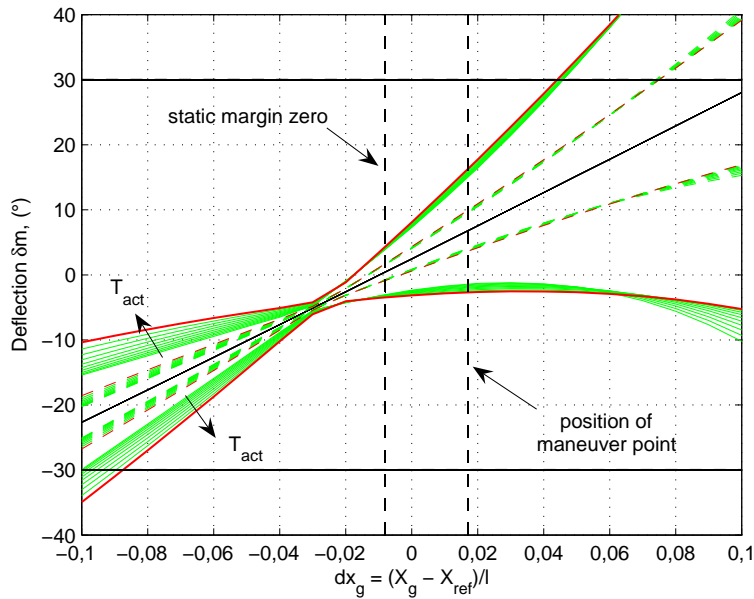


Figure 2.1: Limites des fluctuations en position de l'élévateur  $\delta m$ .  $T_{act} \in [0.06 \text{ s}; 0.48 \text{ s}]$ .

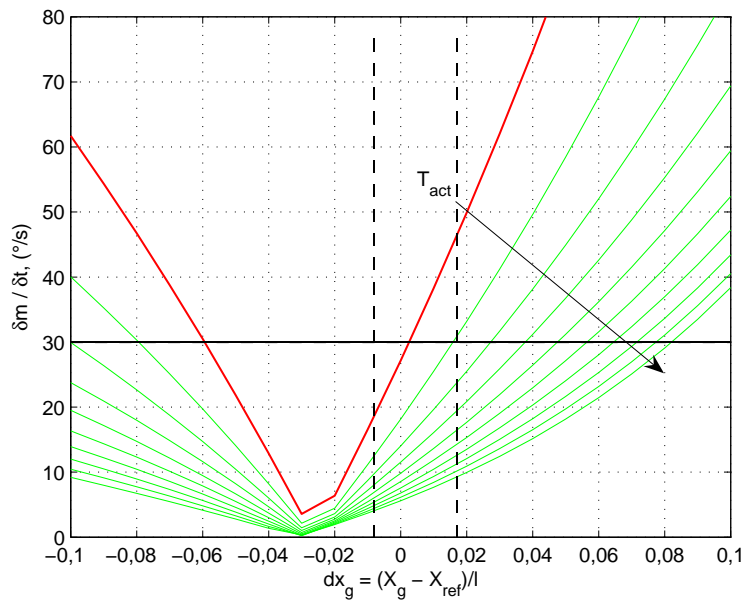


Figure 2.2: Limites des fluctuations en vitesse de l'élévateur  $\delta \dot{m}$ .  $T_{act} \in [0.06 \text{ s}; 0.48 \text{ s}]$ .

La Figure 2.3 présente le dommage relatif infligé à l'élévateur en fonction du centrage et

de la bande passante. Les valeurs  $D_N$  sont normalisées par rapport un point de référence à amortissement faible  $X_g = X_{ref}$ ,  $\xi = 0.3$  et  $T_{act} = 0.06 s$ . On remarque la forte croissance du dommage pour des centrages en arrière ainsi que l'influence de la bande passante. Nous percevons également l'importance du choix des qualités de vol imposées : un amortissement plus élevé réduit le dommage de manière significative.

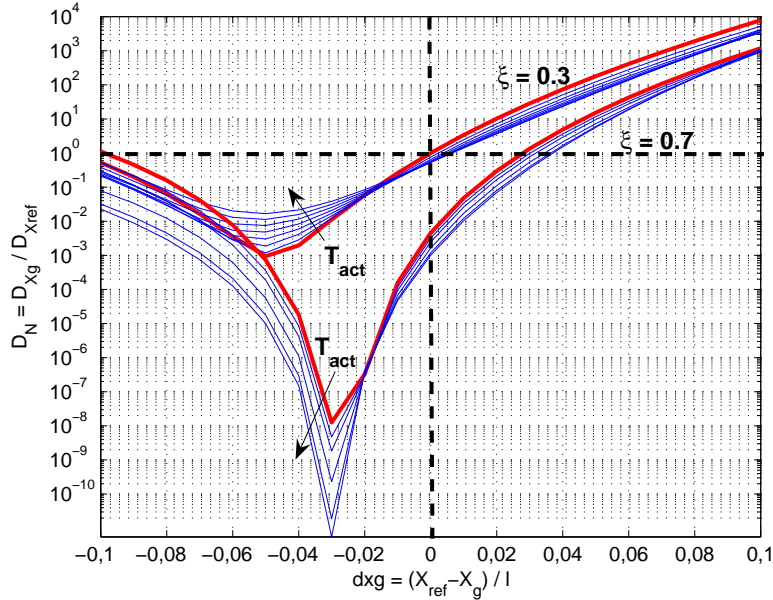


Figure 2.3: Dommage normalisé  $D_N = \frac{D_{X_g}}{D_{X_{ref}, \xi=0.3, T_{act}=0.06 s}}$  en fonction de  $dx_g$ .  $T_{act} \in [0.06 s; 0.48 s]$ . Rouge (gras):  $T_{act} = 0.06 s$ .

### 2.2.2 Application à une mission

Dans cette section nous résumons l'application de la méthode développée pour estimer le dommage infligé par l'activité du système de stabilisation d'un avion à stabilité réduite pour une mission entière. Cette approche est tout à fait intéressante dans une phase d'avant-projet puisque l'estimation se fait classiquement à travers de simulations qui peuvent durer plusieurs jours [7]. Notre méthode permettra, une fois validée et étalonnée, de donner des résultats en quelques minutes.

Les spécifications d'une mission type figurent dans la Table 2.1 [74, 100] : la Figure 2.4 montre le profil vertical correspondant. Ce profil, légèrement simplifié, est représentatif d'un profil d'évaluation de la fatigue des actionneurs d'un avion de type A340-600. La durée de la mission est de  $362 min$ , ce qui correspond à peu près à un vol de Francfort à Dubaï.

La Figure 2.5 montre le dommage absolu de chaque phase de vol pour deux centrages et deux amortissements différents. On note que le dommage pour des centrages en arrière

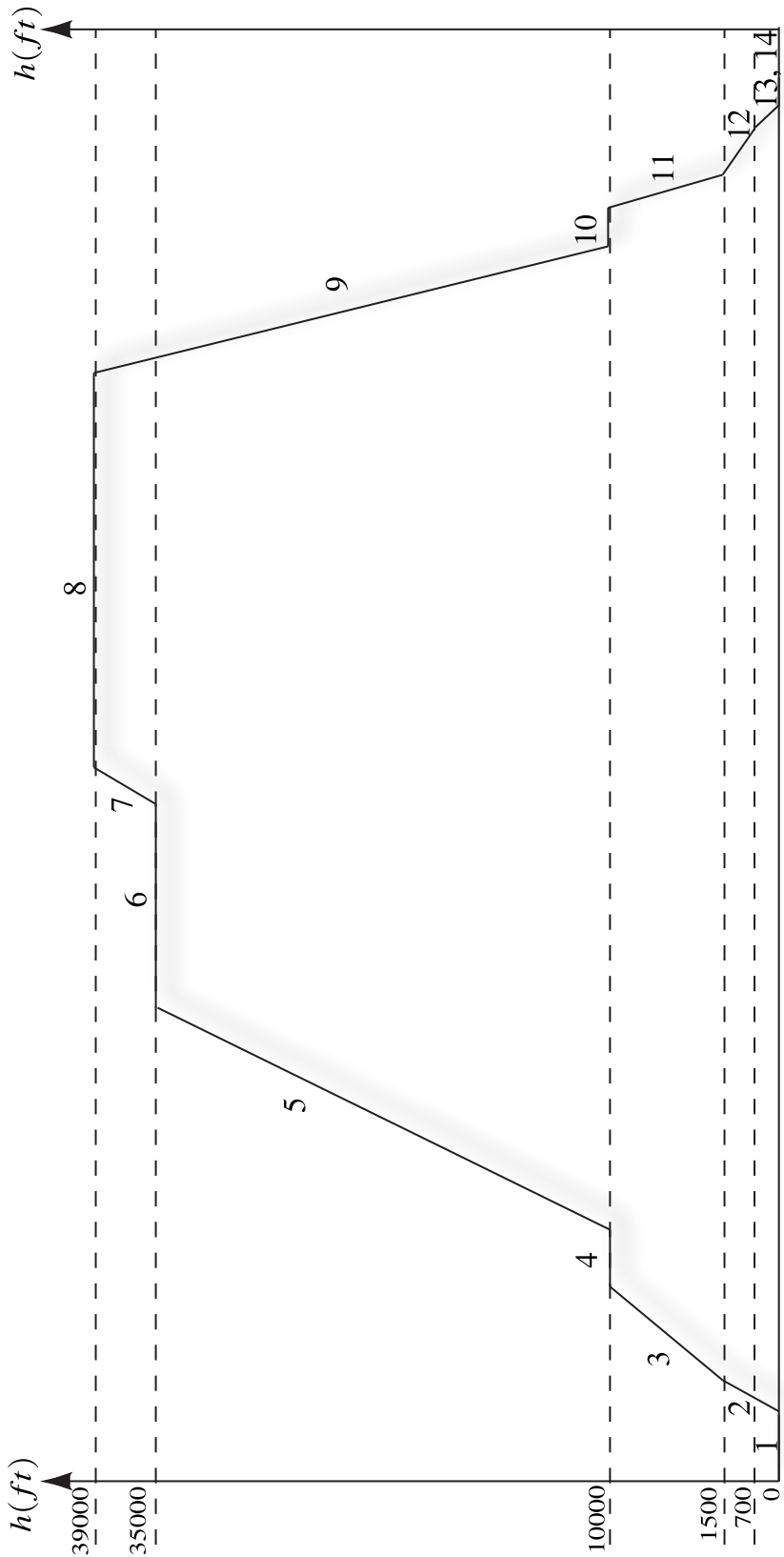


Figure 2.4: Profil dimensionnant simplifié.

| phase | description                  | $V$ , [kt]/Mach | altitude $h$ , [ft] | durée $t_p$ , [s] |
|-------|------------------------------|-----------------|---------------------|-------------------|
| 1     | startup and taxi             | 10, 25          | 0                   | 540               |
| 2     | take-off and initial climb   | 80, 220         | 0, 1500             | 96                |
| 3     | climb                        | 220, 250        | 1500, 10000         | 162               |
| 4     | acceleration in level flight | 250, 320        | 10000               | 42                |
| 5     | climb                        | 320/0.82        | 10000, 35000        | 816               |
| 6     | cruise flight                | 0.83            | 35000               | 2334              |
| 7     | climb                        | 0.83            | 39000               | 276               |
| 8     | cruise flight                | 0.83            | 39000               | 16524             |
| 9     | descend                      | 0.83            | 39000, 10000        | 738               |
| 10    | deceleration at level flight | 310, 250        | 10000               | 60                |
| 11    | descend                      | 250             | 10000, 1500         | 390               |
| 12    | approach                     | 250, 147        | 1500, 700           | 240               |
| 13    | landing                      | 147, 45         | 700, 0              | —                 |
| 14    | taxi-in                      | 30, 20          | 0                   | 300               |

Table 2.1: Profil dimensionnant simplifié.

est plus élevé qu'en avant. En outre, la plupart du dommage se produit pendant les phases de décollage et d'atterrissage. Même si la phase de croisière dure beaucoup plus longtemps, le fait de voler à basse vitesse (moins d'efficacité de l'élévateur) et avec une turbulence intense à basse altitude ont l'impact principal. Nous démontrons également avec la Figure 2.6 que la contribution des différentes phases au dommage varie en fonction du centrage.

Finalement, la Figure 2.7 montre le dommage total pour une mission en fonction du centrage. L'espérance de vie de l'actionneur est également représentée (en supposant que l'avion effectue 650 voyages par an [65]). Si le dommage est seulement dû au fait de voler dans une atmosphère turbulente, la figure s'interprète de la manière suivante : pour une espérance de vie de 100 ans, un amortissement de  $\xi = 0.7$  de l'OI permet des centrages 2% plus en arrière que pour un amortissement de  $\xi = 0.3$ .

Nous disposons donc d'une technique pour déterminer l'activité, la fatigue et l'espérance de vie d'un actionneur, notamment dans la phase d'avant projet à partir d'une spécification des qualités de vol. On peut étendre cette approche afin d'y inclure non seulement le vol en turbulence mais aussi des manœuvres ainsi que d'autres commandes du pilote.

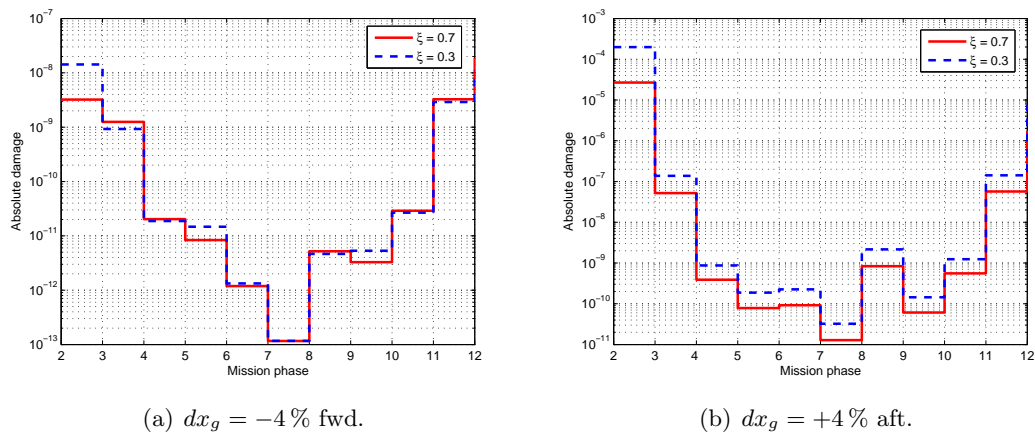


Figure 2.5: Dommage absolu selon les phases du vol pour deux centrages différents.

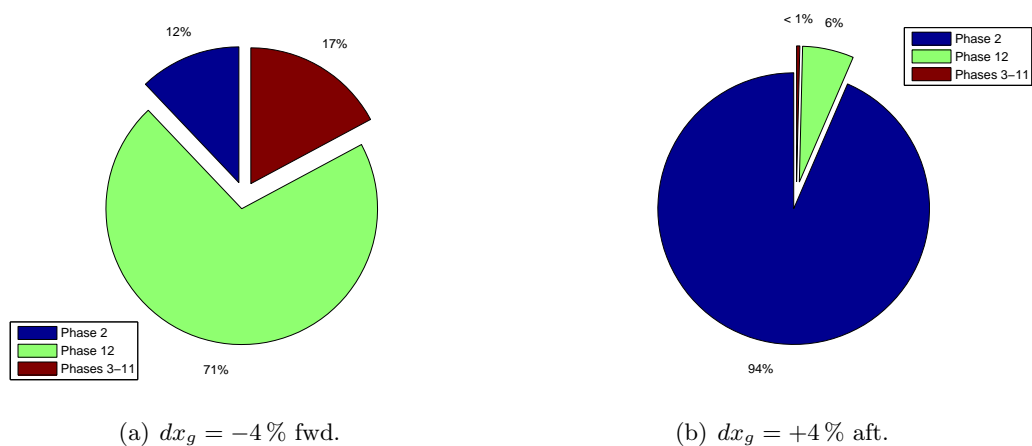


Figure 2.6: Contribution des phases du vol au dommage total ( $\xi = 0.7$ ).

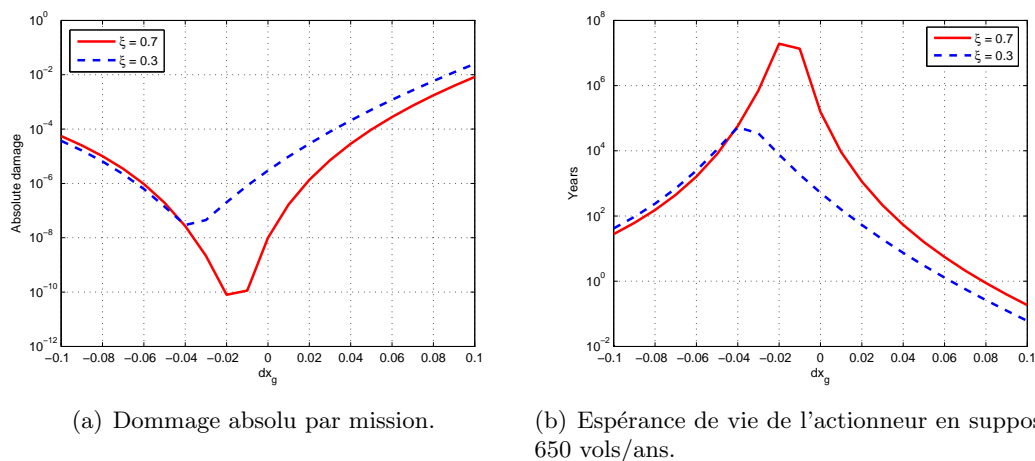


Figure 2.7: Dommage de l'actionneur par vol et espérance de vie.

## 2.3 Stabilité longitudinale et saturations

On résume dans cette section un critère développé dans le chapitre 5 du manuscrit. Des simulations non-linéaires ont montré qu'une saturation en position est à éviter. Dans ce cas, la méthode d'estimation de l'activité en position de l'actionneur donne la plage des centrages admissibles. Par contre, les simulations ne permettent pas de faire un énoncé au sujet des saturations en vitesse, si ce n'est qu'elles semblent être moins critiques.

Afin de disposer d'un critère qui fait la relation entre la saturation en vitesse et la plage des centrages admissibles, nous avons développé une méthode qui fait appel à la notion du gain  $L_2$  et le critère de Popov/cercle provenant de la théorie de la commande automatique.

Plus précisément, il s'agit de transformer le système linéarisé de l'avion en forme de Lur'e, c'est-à-dire que le système est transformé en forme *feedback*, les entrées et sorties étant les sorties et entrées correspondantes de la saturation en vitesse. Il suffit maintenant d'analyser la réponse fréquentielle de ce système qui dépend à la fois du modèle avion (centrage) ainsi que des spécifications de la loi stabilisante.

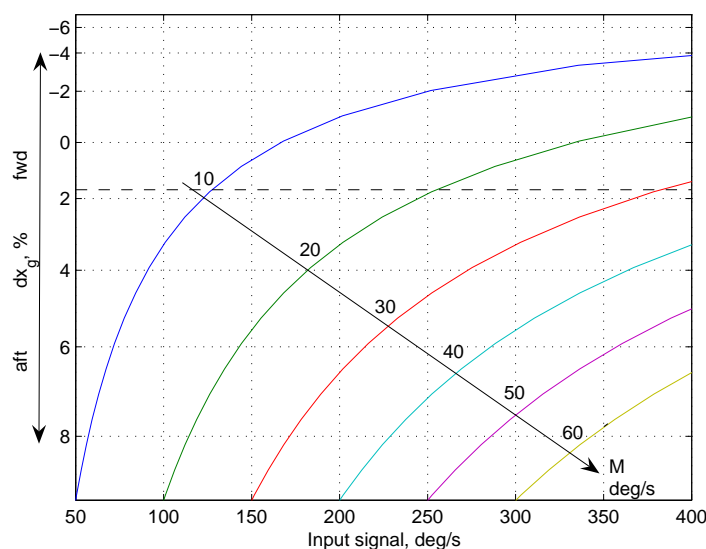


Figure 2.8: Centrages admissibles on fonction de saturation en vitesse et amplitude des signaux d'entrée.

Nous avons condensé ce critère dans la Figure 2.8 où l'on note la relation entre les signaux à l'entrée de l'actionneur, des propriétés de saturation en différentes vitesses  $M$  et la position du centre de gravité la plus en arrière possible  $dx_g$ . Pour une estimation de l'amplitude des signaux nous utilisons la méthode d'estimation d'activité d'actionneur.

La figure s'interprète de la manière suivante : si par exemple on s'attend à des valeurs commandées en vitesse jusqu'à  $300^\circ/s$ , un actionneur qui peut traiter des signaux jusqu'à

$60^\circ/s$  permet de centrages jusqu'à 10% en arrière, cependant un actionneur qui gère  $30^\circ/s$  permet des centrages jusqu'à 3% en arrière seulement.

## 2.4 Équilibre $V_{MC}$

Dans le contexte de la vitesse minimale de contrôle  $V_{MC}$  nous avons notamment analysé l'impact d'une variation de la taille de la dérive et la position du centrage. Ceci est important parce que les critères associés à la  $V_{MC}$  sont critiques pour la certification d'un avion. Dans le cadre d'une stabilité réduite évoquée par une surface réduite de la dérive ou par des centrages en arrière, il semble donc intéressant d'examiner l'influence de ces paramètres.

$V_{MC}$  est la vitesse à laquelle l'avion peut encore poursuivre un vol droit et rectiligne avec un moteur externe non-opérationnel. La poussée du moteur externe encore opérationnel doit être contrée, notamment avec la dérive et sa gouverne (cf. figures 2.9(a) et 2.9(b)). Le poids de l'avion peut être utilisé afin de contrer les forces latérales en inclinant l'appareil. Néanmoins, une limite de  $5^\circ$  en angle de gîte doit être respectée.

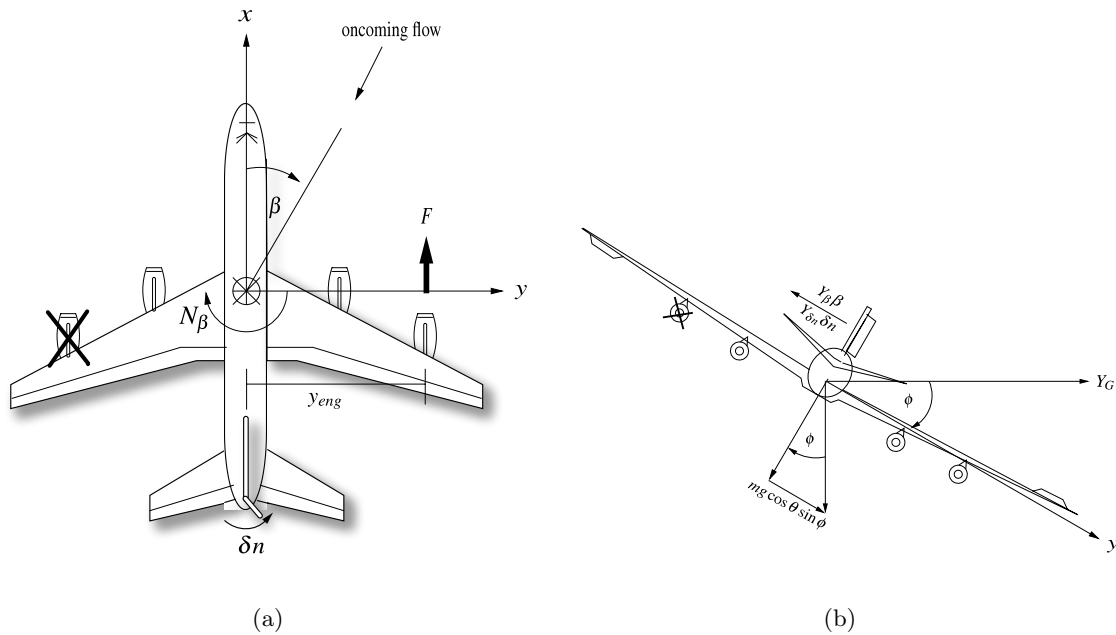


Figure 2.9: Équilibre de l'avion avec moteur non-opérationnel.

### 2.4.1 Résultats analytiques

Basées sur des équations du vol latéral, et avec les termes correctifs

$$\varepsilon_{\delta l \delta n} = \frac{C_{n_{\delta l}} C_{l_{\delta n}}}{C_{l_{\delta l}} C_{n_{\delta n}}} \quad (2.42)$$

$$\varepsilon_{C_{n_{\beta}}} = \frac{C_{l_{\beta}} C_{n_{\delta l}}}{C_{n_{\beta}} C_{l_{\delta l}}} \quad (2.43)$$

$$\varepsilon_{C_{Y\beta}} = \frac{C_{Y_{\delta n}} C_{n_{\beta}}}{C_{Y_{\beta}} C_{n_{\delta n}}} \frac{1 - \varepsilon_{C_{n_{\beta}}}}{1 - \varepsilon_{\delta l \delta n}} \quad (2.44)$$

nous proposons trois formules de degrés de complexité différents pour calculer la vitesse minimale de contrôle. La page suivante présente un résumé de ces formules, ainsi que les effets physiques en jeux. Une paramétrisation qui sert à effectuer des études paramétriques y figure également.

**Équations et modélisation des coefficients pour une étude paramétrique**

$$V_{MC_{s1}} = \sqrt{\tilde{\kappa} + \tilde{\varepsilon}_D \cdot (\tilde{\kappa} + v)} \quad (2.45)$$

$$V_{MC_{s2}} = \sqrt{\kappa + \varepsilon_D \cdot (\kappa + v)} \quad (2.46)$$

$$V_{MC_{s3}} = \sqrt{\kappa} \quad (2.47)$$

avec

$$\kappa = \frac{2y_{eng}F}{\rho S l C n_{\delta n} \delta n} \quad (2.48)$$

$$\tilde{\kappa} = \kappa \cdot \gamma, \quad \text{où } \gamma = \frac{1}{1 - \varepsilon_{\delta l \delta n}} \quad (2.49)$$

$$v = \frac{2mg \cos \theta \sin \phi}{\rho S C_{Y \delta n} \delta n} \quad (2.50)$$

$$\varepsilon_D = \frac{C_{Y \delta n} C_{n_{\beta}}}{C_{n_{\delta n}} C_{Y_{\beta}}} \quad (2.51)$$

$$\tilde{\varepsilon}_D = \varepsilon_D \cdot \sigma, \quad \text{où } \sigma = \frac{1 - \varepsilon_{C_{n_{\beta}}}}{(1 - \varepsilon_{C_{Y_{\beta}}})(1 - \varepsilon_{\delta l \delta n})} \quad (2.52)$$

$$C_{Y \delta n}^* = C_{Y \delta n, nom} \cdot \frac{S_D}{S_{D, nom}} \quad (2.53)$$

$$C_{n_{\delta n}}^* = C_{n_{\delta n}, X_{ref}} \cdot \frac{S_D}{S_{D, nom}} + dx_g \cdot C_{Y \delta n, nom} \cdot \frac{S_D}{S_{D, nom}} \quad (2.54)$$

$$C_{Y_{\beta}}^* = C_{Y_{\beta}, fuselage} \cdot \left(1 + \frac{\Delta C_{Y_{\beta}, fuselage}}{C_{Y_{\beta}, fuselage}}\right) + C_{Y_{\beta}, fin} \cdot \frac{S_D}{S_{D, nom}} \quad (2.55)$$

$$C_{n_{\beta}}^* = C_{n_{\beta}, fuselage} \cdot \left(1 + \frac{\Delta C_{n_{\beta}, fuselage}}{C_{n_{\beta}, fuselage}}\right) + C_{n_{\beta}, fin} \cdot \frac{S_D}{S_{D, nom}} - dx_g \cdot C_{Y_{\beta}, fin} \cdot \frac{S_D}{S_{D, nom}} \quad (2.56)$$

**Effets physiques**

- $\kappa$  relation entre moment de la gouverne et poussée (dans  $V_{MC_{s1}}$ ,  $V_{MC_{s2}}$ ,  $V_{MC_{s3}}$ )
- $v$  angles de l'équilibre, balance entre masse et forces latéral (dans  $V_{MC_{s1}}$ ,  $V_{MC_{s2}}$ )
- $\varepsilon_D$  géométrie, foyer latérale (dans  $V_{MC_{s1}}$ ,  $V_{MC_{s2}}$ )
- $\sigma, \gamma$  termes correctifs et effets ailerons (dans  $V_{MC_{s1}}$  seule)

Sans entrer dans les détails, la Figure 2.10 montre de manière synthétique les résultats d'une étude paramétrique qu'on présente dans le manuscrit complet à la section 6.2. L'influence de plusieurs paramètres sur la  $V_{MC}$  y figure pour un avion classique de type DC8 et pour le modèle VELA1. La section 6.2 du manuscrit complet contient de plus amples informations et explications.

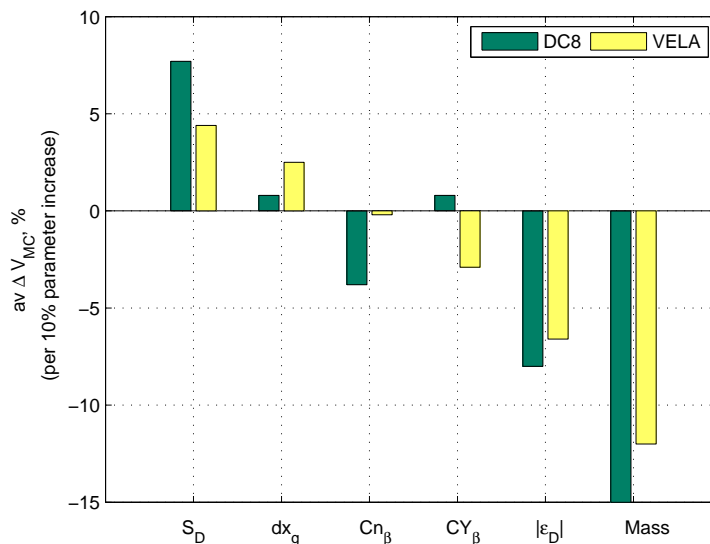


Figure 2.10: Impact des paramètres sur la  $V_{MC}$  pour un avion classique et le modèle VELA.

L'approche analytique permet d'identifier les facteurs principaux influençant l'équilibre avec un moteur non-opérationnel. La juxtaposition de facteurs qui augmentent l'efficacité (réduction de la surface de la dérive, centrages plus reculés) et qui contraignent l'équilibre (vitesse, limitations physiques) aide à trouver un compromis au niveau de la conception de l'avion.

Nous notons que pour une analyse de la  $V_{MC}$  en phase avant projet d'un avion atypique, il est nécessaire d'utiliser l'expression analytique complète qui a été développée au cours de cette thèse.

### 2.4.2 Résultats numériques

Nous avons développé un outil qui résout les équations du vol pour calculer des points d'équilibre sous contraintes physiques (moteur non-opérationnel, centrage, taille de la dérive). Ensuite, le domaine de vol est visualisé sur un plan vitesse-dérapiage, ce qui permet d'identifier d'autres contraintes difficilement perceptibles avec l'approche analytique.

Plus particulièrement, dans le cas de VELA, on note l'existence de deux points de vol qui réalisent les contraintes liées à la  $V_{MC}$ . La Figure 2.11 montre que le plan  $\beta - V$

est séparé en deux par le critère de l'angle de gîte. Nous pouvons identifier deux vitesses minimales de contrôle, une à faible dérapage mais à grande vitesse et l'autre à basse vitesse mais à fort dérapage. Par ailleurs, une contrainte longitudinale s'ajoute qui est l'existence d'un angle maximal d'incidence afin d'éviter que l'arrière de l'avion touche le sol avant les roues. Ce plan permet également d'en déduire une autre contrainte : il semble important de définir une limitation de l'angle de dérapage pour éviter un décrochage de la dérive. On propose la limitation  $\beta \leq 15^\circ$ .

Naturellement, nous avons analysé l'impact du centrage et de la surface de la dérive sur l'équilibre  $V_{MC}$  avec cet outil.

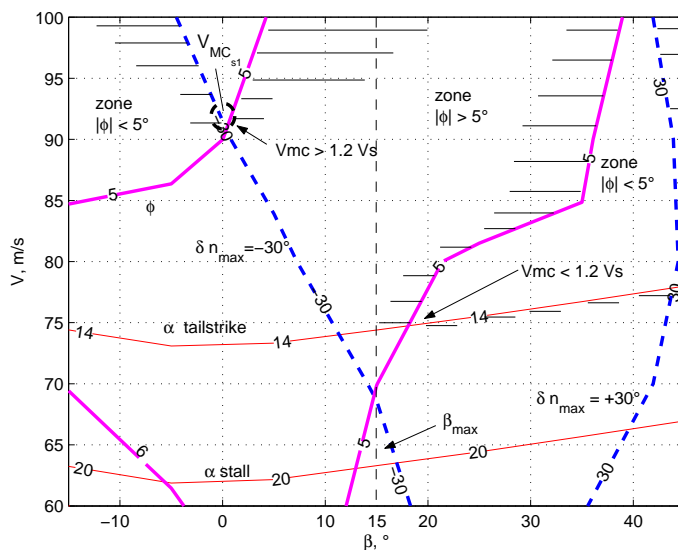


Figure 2.11: Plan  $\beta - V$  pour l'avion VELA avec un moteur externe non-opérationnel.

Par ailleurs, une analyse complémentaire permet de trouver la raison pour laquelle le domaine est séparé en deux. Ce phénomène est lié à l'évolution de l'angle de gîte, comme démontré dans la section 6.4 de la thèse. Il y est également démontré, comment l'évolution des autres paramètres s'explique et pourquoi il est important de considérer le couplage entre le longitudinal et le latéral pour l'avion VELA. En combinaison avec l'approche analytique nous disposons ainsi d'une méthode d'analyse qui permet d'identifier les enjeux principaux et la physique du vol à moteur non-opérationnel.

## 2.5 Critères dynamiques

Le chapitre 7 de la thèse traite des critères latéraux dynamiques dans le contexte d'une stabilité réduite. Il s'agit à la fois des critères modaux et des critères liés à la vitesse minimale de contrôle (manœuvres).

On a d'abord développé des expressions analytiques et examiné l'impact d'une variation de la surface de la dérive et du centrage pour le DC8 et le VELA à travers une paramétrisation simple. On a également développé un modèle générique de manœuvre de roulis afin de pouvoir estimer l'évolution de l'angle de dérapage dans le cas où un moteur tombe en panne. Ceci est surtout intéressant, si l'avion doit effectuer un manœuvre de roulis avec la gouverne de la dérive saturée : il n'est dans ce cas plus possible de contrôler le dérapage d'avion. Des simulations et manipulations numériques valident l'approche choisie.

## 2.6 Recommandation pour l'avion VELA

La partie dynamique du vol conclut avec des recommandations pour la conception de l'avion VELA. Ces recommandations ont servi de base pour la partie automatique qui suit, ainsi que pour la dernière partie de la thèse. Les recommandations sont faites pour permettre exploiter de manière optimale les bénéfices d'une stabilité réduite. Elles sont résumées ci-après.

- + Sélection d'une petite dérive, approximativement entre  $2 \times 45 m^2$  et  $2 \times 64 m^2$ .
- + Une plage de centrage centrée autour de la position du foyer.
- Pour compenser la dégradation des qualités de vol naturelles, il est obligatoire de concevoir un système de type *back-up* pour garantir un niveau de contrôlabilité suffisant pour les spécifications (dérive, centrage) choisies pour le cas où l'ordinateur de bord tombe en panne.
- Pour contrer statiquement les effets néfastes d'une petite dérive, l'avion est certifié pour des vitesses de décollage et d'atterrissage plus élevées. Il est également possible de considérer une modification de l'installation motrice pour réduire le moment induit par la poussée.

D'autres remarques et recommandations se trouvent dans le rapport principal.



## Chapter 3

# Synthèse multi-modèle multi-objectif d'un correcteur de type back-up et anti-windup

Ce chapitre résume les points principaux de la partie commande et traite de la synthèse d'un correcteur robuste de type *back-up* pour l'avant-projet d'une aile volante (VELA – Very Efficient Large Aircraft) qui est très sensible à la position du centre de gravité. On utilise une technique de synthèse polytopique qui garantit les qualités de vol nécessaires pour une large plage de centrage, notamment pour des centrages arrières. Ce sont ces derniers qui réduisent la stabilité longitudinale de l'avion et imposent des contraintes fortes sur l'actionneur de l'élévateur. Concernant le mouvement latéral, l'avion possède des dérives de taille réduite ce qui rend les modes latéraux instables pour toute la plage de centrage. La stabilité est garantie malgré des saturations des actionneurs. Pour une amélioration de la performance nous proposons également une technique de type *anti-windup*.

### 3.1 Objectifs

Afin d'améliorer les performances des avions civils les développements actuels incorporent de plus en plus une réduction de la stabilité naturelle en combinaison avec un système de stabilisation automatique. Selon les recommandations données dans la partie dynamique du vol, on présente ici le cahier des charges pour la synthèse d'un correcteur de type back-up. On fait référence à la Figure 3.1 : une zone morte est intégrée entre  $z_2$  et  $w_2$ . Ceci correspond à une saturation en vitesse. Il est tout à fait possible de considérer une saturation en position en déplaçant  $z_2$  et  $w_2$  juste après l'entrée commande  $u_c$ . La section 8.1 de la thèse donne des informations plus précises.

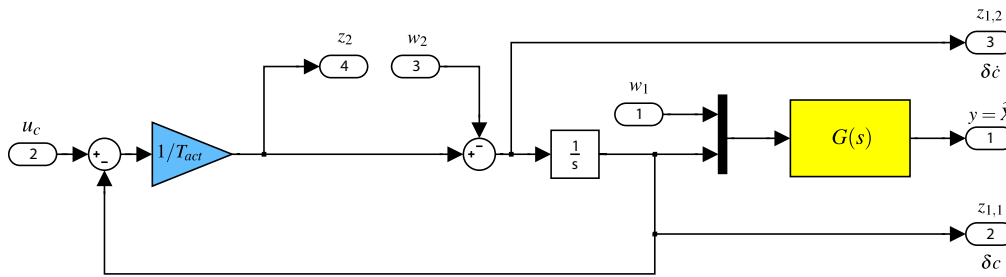


Figure 3.1: Modèle de synthèse.

1. Les valeurs propres de la boucle fermée doivent rester dans une région définie du plan complexe afin de réaliser les besoins au niveau des qualités de vol.
2. Le correcteur statique doit être robuste par rapport aux centrages dans la plage ciblée :

$$dx_g \in [-7\%; +5\%] \quad (3.1)$$

On préfère éviter d'auto-séquencer le correcteur.

3. Afin de minimiser l'activité de l'actionneur la norme  $H_\infty$  du transfert  $T_{w_1 \rightarrow z_1}$  entre l'entrée vent et les sorties position et vitesse de l'actionneur est limitée à  $\gamma_1$ .
4. Afin d'assurer la stabilité en présence des saturations, un objectif  $\gamma_2$  de positivité pour le transfert  $T_{w_2 \rightarrow z_2}$  est considéré. Le domaine d'attraction doit avoir une taille suffisante.
5. Puisqu'il est crucial de préserver au maximum la stabilité et la performance un correcteur statique de type anti-windup peut être ajouté pour réduire la dégradation de la performance du système en boucle fermée en présence de saturations.

## 3.2 Philosophie

Compte tenu du cahier des charges on doit synthétiser une loi de commande donnant une performance satisfaisante pour une large plage de centrages et en présence des saturations des actionneurs. Cette loi doit réaliser pour plusieurs modèles à la fois des spécifications modales et entrée/sortie (placement des pôles dans une région du plan complexe, contraintes  $H_\infty$  et de positivité pour des fonctions de transfert). Puisqu'on implante le correcteur final comme un système de type back-up il doit être le plus simple possible.

On applique donc une technique multi-objectif : voir par exemple [84] où le système longitudinal est découplé et l'on contrôle l'OI et la phugoïde séparément avec des correcteurs  $H_\infty$  et  $H_2$  respectivement. Les correcteurs obtenus sont dynamiques et séquencés en fonction du *Mach*. Voir également [83] où l'objectif est la minimisation d'un critère  $H_2$  sous une contrainte de positivité (robustesse). L'idée est de synthétiser un correcteur

de type retour d'état observé, où le gain d'observation est fixé, c'est-à-dire que l'on ne synthétise qu'un retour d'état. [79, 80, 45, 33] donnent un aperçu général des techniques de synthèse d'un correcteur multi-objectif dynamique.

Néanmoins, ces techniques ne sont pas adaptées à notre problème puisque le correcteur de type back-up doit être le plus simple possible et donc idéalement statique. De plus, il est nécessaire d'appliquer une technique multi-modèle. Dans ce contexte, une technique polytopique [23, 16, 36] semble adaptée puisque son but est de satisfaire simultanément des critères modaux, entrée/sortie et de robustesse pour plusieurs modèles. Le problème se ramène à la résolution d'un problème d'optimisation convexe sous forme LMI.

Dans le cas où le domaine d'attraction ou la performance du système saturé en boucle fermée ne sont pas satisfaisants, nous proposons également une technique de type anti-windup. [86, 87, 101] proposent la synthèse de correcteurs dynamiques pour un seul modèle ou un modèle LFT. Nous proposons ici une technique de synthèse convexe multi-modèle d'un correcteur avec des critères de positivité et  $H_\infty$ .

La section 9.2 du manuscrit explique plus particulièrement comment transformer les critères considérés en LMI. Dans la suite de ce résumé nous allons brièvement présenter la technique polytopique. Nous allons également résumer la technique permettant d'évaluer la performance du système saturé en boucle fermée en calculant entre autres des domaines d'attraction [43, 26, 17]. Finalement, on donne un aperçu de la technique pour synthétiser un correcteur de type anti-windup.

### 3.3 Correcteur robuste de type retour d'état multi-objectif

La section 9.2 de la thèse décrit les critères modaux et entrée/sortie. Ceci est la base de la technique que nous résumons ici. Afin d'être robuste par rapport aux différents modèles, on a utilisé une technique polytopique. Cette technique permet de synthétiser un correcteur de type retour d'état qui satisfait plusieurs contraintes sur un *polytope* de modèles linéaires. Les paramètres du modèle varient à l'intérieur d'un ensemble convexe de l'espace des paramètres du modèle dont les sommets sont définis par les valeurs extrêmes des paramètres des modèles linéaires localement valides [12]. La proposition 3.1 présente la technique [21, 23, 16, 36].

**Proposition 3.1** *Considérons les modèles d'état en boucle ouverte ( $i \in [1, N]$ ):*

$$\begin{aligned}\dot{x} &= A_i x + B_{1,i} w_1 + B_{2,i} w_2 + B_{3,i} u \\ z_1 &= C_{1,i} x + D_{11,i} w_1 + D_{12,i} w_2 + D_{13,i} u \\ z_2 &= C_{2,i} x + D_{21,i} w_1 + D_{22,i} w_2 + D_{23,i} u\end{aligned}$$

*Une condition suffisante pour qu'il existe un retour d'état  $u = Kx$  satisfaisant :*

1. *Les valeurs propres de la boucle fermée  $A_i + B_{3,i}K$  sont placées à l'intérieur d'une*

région LMI du plan complexe (figure 3.2) :  $\lambda$  étant le degré de stabilité<sup>1</sup>,  $\xi = \cos(\alpha)$  un amortissement minimum et  $r$  un module maximum.

2. La norme  $H_\infty$  de la matrice de transfert entre  $w_1$  et  $z_1$  est inférieure à  $\gamma_1$ .

3. La matrice de transfert  $T_{w_2 \rightarrow z_2}$  entre  $w_2$  et  $z_2$  satisfait :

$$T_{w_2 \rightarrow z_2}(j\omega) + T_{w_2 \rightarrow z_2}^*(j\omega) > 2\gamma_2 \quad \forall \omega \in [0, +\infty) \quad (3.2)$$

est qu'il existe une matrice de Lyapunov  $X = X^T > 0$  et une matrice  $W = KX$  satisfaisant les LMIs :

$$L_i(X, W) + L_i^T(X, W) + 2\lambda X < 0 \quad (3.3)$$

$$\begin{pmatrix} -rX & L_i(X, W) \\ \star & -rX \end{pmatrix} < 0 \quad (3.4)$$

$$\begin{pmatrix} \sin \alpha (L_i(X, W) + L_i^T(X, W)) & -\cos \alpha (L_i(X, W) - L_i^T(X, W)) \\ \star & \sin \alpha (L_i(X, W) + L_i^T(X, W)) \end{pmatrix} < 0 \quad (3.5)$$

$$\begin{pmatrix} L_i(X, W) + L_i^T(X, W) & B_{1,i} & XC_{1,i}^T + W^T D_{13,i}^T \\ \star & -\gamma_1 I & D_{11,i}^T \\ \star & \star & -\gamma_1 I \end{pmatrix} < 0 \quad (3.6)$$

$$\begin{pmatrix} L_i(X, W) + L_i^T(X, W) & B_{2,i} - XC_{2,i}^T - W^T D_{23,i}^T \\ \star & 2\gamma_2 I - D_{22} - D_{22}^T \end{pmatrix} < 0 \quad (3.7)$$

avec  $L_i(X, W) = A_i X + B_{3,i} W$ .  $\star$  représente la partie conjuguée de la matrice hermitienne.

Dans la proposition, les éqs. (3.3)–(3.5) correspondent à la région LMI du plan complexe définissant des qualités de vol acceptables. L'Eq. (3.6) correspond au critère  $H_\infty$  et l'Eq. (3.7) au critère de positivité. Il est possible de spécifier individuellement les spécifications/critères pour chaque modèle (c'est-à-dire pour des centrages différents).

*Remarques :*

(i) Dans la proposition  $\gamma_1$  ou  $\gamma_2$  est fixé, tandis que l'autre valeur sera minimisée en fonction de  $W$  et  $X$  [41]. On en déduit  $K = WX^{-1}$ .

(ii) Différentes matrices de Lyapunov devraient être utilisées au lieu d'une seule matrice pour tous les critères et modèles, mais le problème d'optimisation n'est alors plus convexe. La valeur de  $\gamma_1$  ou  $\gamma_2$  minimisée est donc pessimiste, c'est-à-dire surestimée si plus d'un seul critère ou modèle est considéré. Il peut arriver qu'aucune solution ne soit trouvée, même s'il existe un correcteur satisfaisant les spécifications. On a donc intérêt à minimiser le nombre de critères et de modèles.

(iii) En général,  $r = +\infty$ . Quand la synthèse est proche d'être satisfaisante,  $r$  peut être modifié afin de réduire la norme de la matrice de retour  $K$ .

<sup>1</sup>Le degré de stabilité d'une matrice d'état  $A$  est  $-\max_i \operatorname{Re}(\lambda_i)$ , où les  $\lambda_i$  sont les valeurs propres de  $A$ .

(iv) La contrainte de positivité, Eq. (3.7), sert à assurer la robustesse par rapport aux saturations. Le but est de maximiser indirectement le domaine d'attraction en maximisant la positivité du système en boucle fermée.

(v) Dans le cas de saturations multiples, il est possible d'injecter un *multiplieur* dans Eq. (3.7) afin de réduire le conservatisme de la technique [101].

(vi) Dans l'application d'un correcteur de type back-up, on enlève les retours sur les actionneurs. On vérifie a posteriori la réalisation des critères.

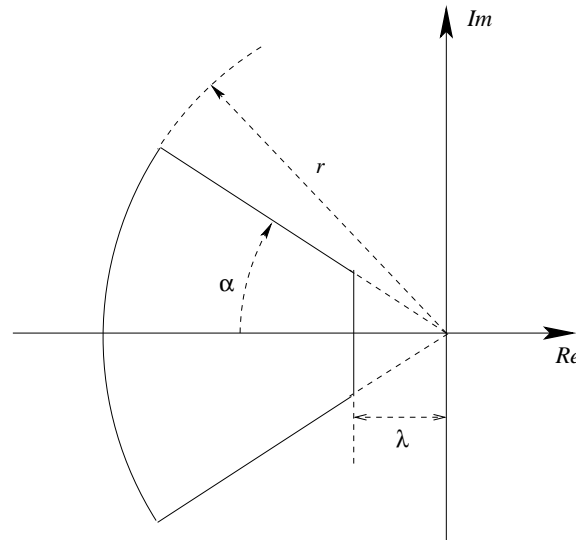


Figure 3.2: Une région LMI du plan complexe pour la synthèse polytopique (voir proposition 3.1).

### 3.4 Évaluation de la stabilité et de la performance

Comme expliqué dans la section 9.4 du manuscrit complet, les systèmes linéaires instables en boucle ouverte incorporant des saturations ne peuvent pas être stabilisés globalement par un correcteur rétroactif.

La même section propose une variété de techniques pour évaluer les limites de stabilité d'un système saturé en boucle fermée ainsi que des méthodes pour estimer sa performance. Il s'agit du calcul d'un domaine d'attraction du système autonome ainsi que la détermination des propriétés  $L_2$  de ses sorties exogènes [26, 17]. Nous avons également proposé une modification visant à façonner la forme du domaine de stabilité en introduisant des pondérations sur des états du système. De plus, on a fait appel à la notion de vitesse de convergence comme paramètre de performance et, finalement, à une méthode pour intégrer un critère de performance  $L_2$  entrée/sortie en augmentant les états du système par un état filtre [17]. Pour plus de détails et la formulation du problème sous forme LMI, on pourra consulter la section 9.4 du manuscrit complet.



on peut transformer le système en omettant les entrées exogènes de consigne  $r$  et de vent  $w$  pour obtenir la Figure 3.4 qui représente le modèle de synthèse du correcteur  $J$ .

Le cahier des charges pour la synthèse de ce correcteur est le suivant :

1. On considère un critère de positivité pour le transfert  $T_{q \rightarrow s}$  pour assurer la robustesse de la boucle fermée en présence des saturations.
2. Le correcteur doit être statique et robuste vis-à-vis d'une large plage de centrage de l'avion.

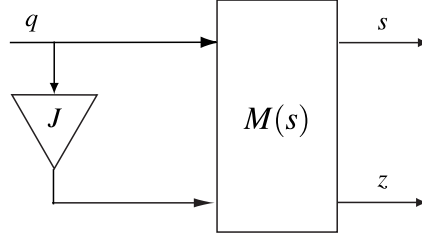


Figure 3.4: Modèle de synthèse pour le correcteur anti-windup.

On obtient les LMIs suivants, voire la section 9.2 du manuscrit complet.

**Proposition 3.2** *Considérons les modèles d'état en boucle fermée ( $i \in [1, N]$ ) comme indiqué dans la Figure 3.4, les matrices d'état  $A_i$  étant Hurwitz :*

$$\begin{aligned} \dot{x} &= A_i x + B_{1,i} q + B_{2,i} J q \\ s &= C_{1,i} x + D_{11,i} q + D_{12,i} J q \\ z &= C_{2,i} x + D_{21,i} q + D_{22,i} J q \end{aligned}$$

Toutes les matrices ci-dessus sont fixées, à l'exception de  $J$ . Le critère de positivité

$$T_{q \rightarrow s}(j\omega) + T_{q \rightarrow s}^*(j\omega) > 2\gamma_3 I \quad \forall \omega$$

est satisfait si et seulement s'il existe un gain matriciel  $J$  et une matrice définie positive  $Q_1 = Q_1^T > 0$  satisfaisant :

$$\begin{pmatrix} A_i Q_1 + Q_1 A_i^T & B_{1,i} + B_{2,i} J - Q_1 C_{1,i}^T \\ \star & 2\gamma_4 I - (D_{11,i} + D_{12,i} J) - (D_{11,i} + D_{12,i} J)^T \end{pmatrix} < 0.$$

**Remarques:**

(i) Contrairement à la synthèse polytopique où l'on utilise une seule fonction de Lyapunov pour plusieurs critères et modèles, ici nous pouvons utiliser plusieurs fonctions de Lyapunov. La technique n'est donc pas conservatrice.

(ii) Le correcteur robuste statique  $J$  de type anti-windup permet d'améliorer la stabilité et la performance en présence des saturations par rapport aux résultats obtenus avec le correcteur initial. La taille du domaine d'attraction est modifiée ainsi que la vitesse de convergence.

Pour plus des détails, voir la section 9.5 du manuscrit.

## 3.6 Synthèse du correcteur et application

Dans une première partie du chapitre d'application nous avons démontré l'influence des contraintes modales sur le critère d'activité des actionneurs (norme  $H_\infty$ ). Ceci a également permis de trouver les valeurs optimales non-conservatives de la norme  $H_\infty$  en fonction du centrage. Ces valeurs permettent de définir les objectifs de minimisation pour la synthèse du correcteur de type back-up.

À titre d'exemple, nous présentons ici la synthèse et la validation du correcteur pour le mouvement latéral de l'avion. Les valeurs obtenues, l'analyse de stabilité et une simulation sont présentées. L'application complète est traitée dans le chapitre 10 du manuscrit complet.

### 3.6.1 Correcteur robuste de type back-up

Le correcteur est synthétisé pour deux modèles extrêmes de centrage en avant et en arrière. L'objectif d'optimisation est la positivité. Une contrainte  $H_\infty$  est fixée à  $\gamma_1 < 0.1$ . Les conditions de la région LMI figurent dans la Table 3.1.

| modèles | $(dx_g)$ | $\lambda$ , rad/s | $r$ , rad/s | $\xi$ | objectif   | contrainte       |
|---------|----------|-------------------|-------------|-------|------------|------------------|
| fwd     | -7%      | 0.3               | $\infty$    | 0.3   | positivité | $H_\infty :$     |
| aft     | +5%      | 0.3               | $\infty$    | 0.3   |            | $\gamma_1 < 0.1$ |

Table 3.1: Paramètres de synthèse du correcteur latéral.

Après synthèse, on obtient le correcteur final en retirant le retour sur les actionneurs  $\delta l$  et  $\delta n$ , comme l'indique la Table 3.2.

|                  | $n_y$    | $r$     | $p$     | $\phi$ | $\delta l$ | $\delta n$ |
|------------------|----------|---------|---------|--------|------------|------------|
| $K_{\delta l} =$ | -0.71055 | 0.84715 | 4.2449  | 3.1964 | (0.049292) | (0.09115)  |
| $K_{\delta n} =$ | 0.11756  | 4.1335  | 0.10618 | 1.3366 | (-0.35831) | (0.26383)  |

Table 3.2: Correcteur robuste statique latéral.

Nous présentons les résultats obtenus pour le roulis hollandais et les critères entrée/sortie dans la Table 3.3.

|           | $\gamma_1$ | $1/\gamma_2$ | $\lambda$ , rad/s | $r$ , rad/s | $\xi$ , % |
|-----------|------------|--------------|-------------------|-------------|-----------|
| fwd $X_g$ | .063       | .95          | .33               | .77         | 42.8      |
| aft $X_g$ | .087       | .95          | .27               | .60         | 45.8      |

Table 3.3: Résultats obtenus avec le correcteur robuste pour des centrages  $dx_g \in [-7\%; +5\%]$ .

Les Figures 3.5 and 3.6 montrent les valeurs propres en fonction du centrage en boucle fermée ainsi que les réponses fréquentielles. Le correcteur utilise uniquement les sorties  $n_y$ ,  $r$ ,  $p$  et  $\phi$ .

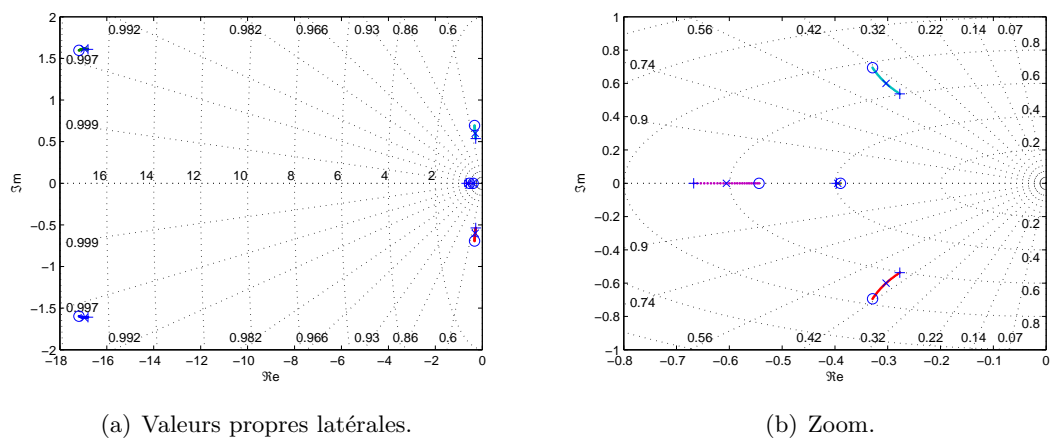
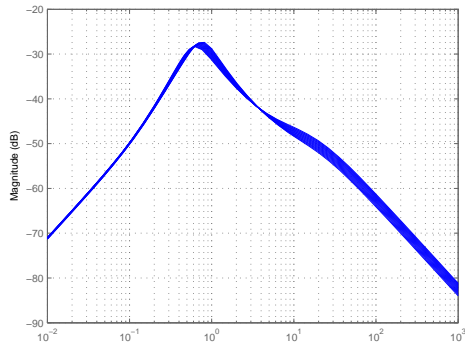
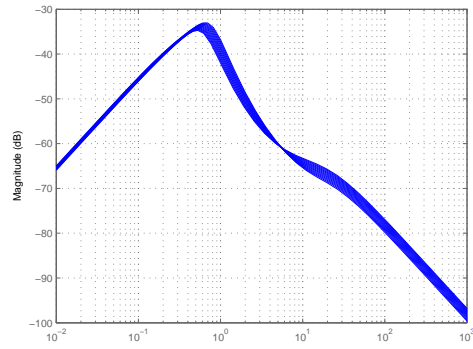


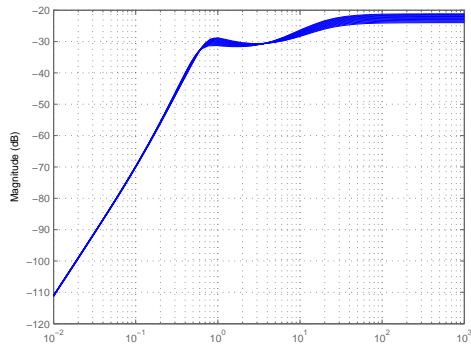
Figure 3.5: Valeurs propres en boucle fermée.  $\circ$ :  $-7\%$  fwd,  $+$ :  $+5\%$  aft.



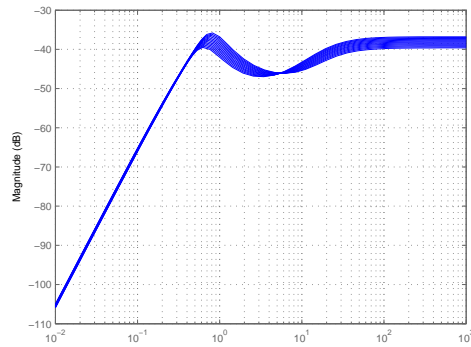
(a) Sortie position d'aileron.



(b) Sortie vitesse d'aileron.



(c) Sortie position de rudder.



(d) Sortie vitesse de rudder.

Figure 3.6: Diagrammes de Bode en magnitude des transferts de l'entrée vent vers les sorties actionneur  $T_{w_1 \rightarrow z_1}$  en fonction de  $dx_g$ .

### 3.6.2 Analyse de la stabilité et de la performance de la boucle fermée saturée

Le domaine d'attraction correspond à un hyper-ellipsoïde de six dimensions. Les Figures 3.7(a) and 3.7(b) montrent la projection de ce domaine sur les plans  $\beta - \phi$  et  $r - p$  pour les deux mêmes centrages extrêmes. Afin d'obtenir un domaine plus simple à utiliser, on calcule le plus grand hyper-cube inclu dans cet hyper-ellipsoïde. Ainsi, on obtient des

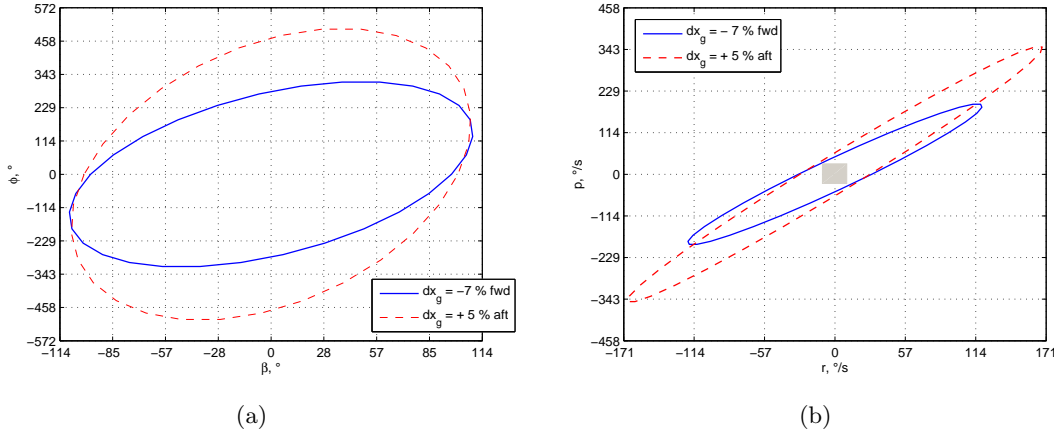


Figure 3.7: Domaine d'attraction.

valeurs limites (conservatives) pour les variables d'état :

$$\left\{ \begin{array}{l} -8.7^\circ \leq \beta \leq +8.7^\circ \\ -8.7^\circ/s \leq r \leq +8.7^\circ/s \\ -8.7^\circ/s \leq p \leq +8.7^\circ/s \\ -8.7^\circ \leq \phi \leq +8.7^\circ \\ -8.7^\circ \leq \delta l \leq +8.7^\circ \\ -8.7^\circ \leq \delta n \leq +8.7^\circ \end{array} \right. \quad (3.11)$$

Nous pouvons remarquer que : le ratio entre une variation simultanée des saturations en vitesse et la longueur du côté de l'hyper-cube est constant. Dans cet exemple :

$$\frac{\Delta l_{c,lat}}{sat(1^\circ/s)} = 0.58 \quad (3.12)$$

Il est à noter que l'influence de la saturation de l'aileron est plus importante que celle de la gouverne de la dérive. La Table 3.4 illustre ces variations pour 9 combinaisons différentes de saturation.

|                       |    | $sat_{rud}, ^\circ/s$ |                 |                 |
|-----------------------|----|-----------------------|-----------------|-----------------|
|                       |    | 15                    | 30              | 60              |
| $sat_{ail}, ^\circ/s$ | 15 | $2 \times 4.4$        | $2 \times 4.5$  | $2 \times 4.6$  |
|                       | 30 | $2 \times 7.5$        | $2 \times 8.7$  | $2 \times 9.2$  |
|                       | 60 | $2 \times 9.4$        | $2 \times 14.9$ | $2 \times 17.5$ |

Table 3.4: Lateral exchange rates.

Nous présentons également sur la Figure 3.8 la vitesse de convergence garantie du système saturé en boucle fermée en fonction d'une consigne de gîte  $\phi_c$ . Le gain  $L_2$  associé

entre l'entrée et la sortie  $\phi$  est également représenté. On obtient une consigne maximale en angle de gîte  $\phi_{c,max}$  valable pour toute la plage des centrages.

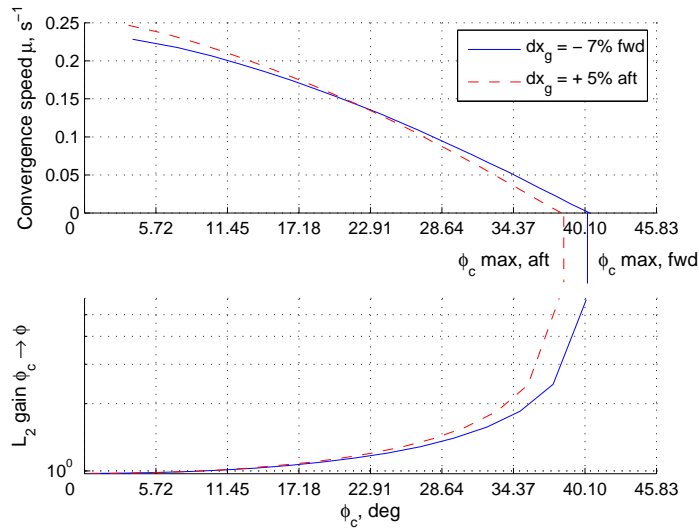


Figure 3.8: Performance du système.

### 3.6.3 Simulation

À titre d'exemple, nous présentons ici une simulation pour un échelon de gîte  $\phi_c = 30^\circ$  pour deux centrages différents. Les actionneurs sont saturés à  $sat = \pm 30^\circ/s$ . L'avion se trouve en atmosphère fortement turbulente.

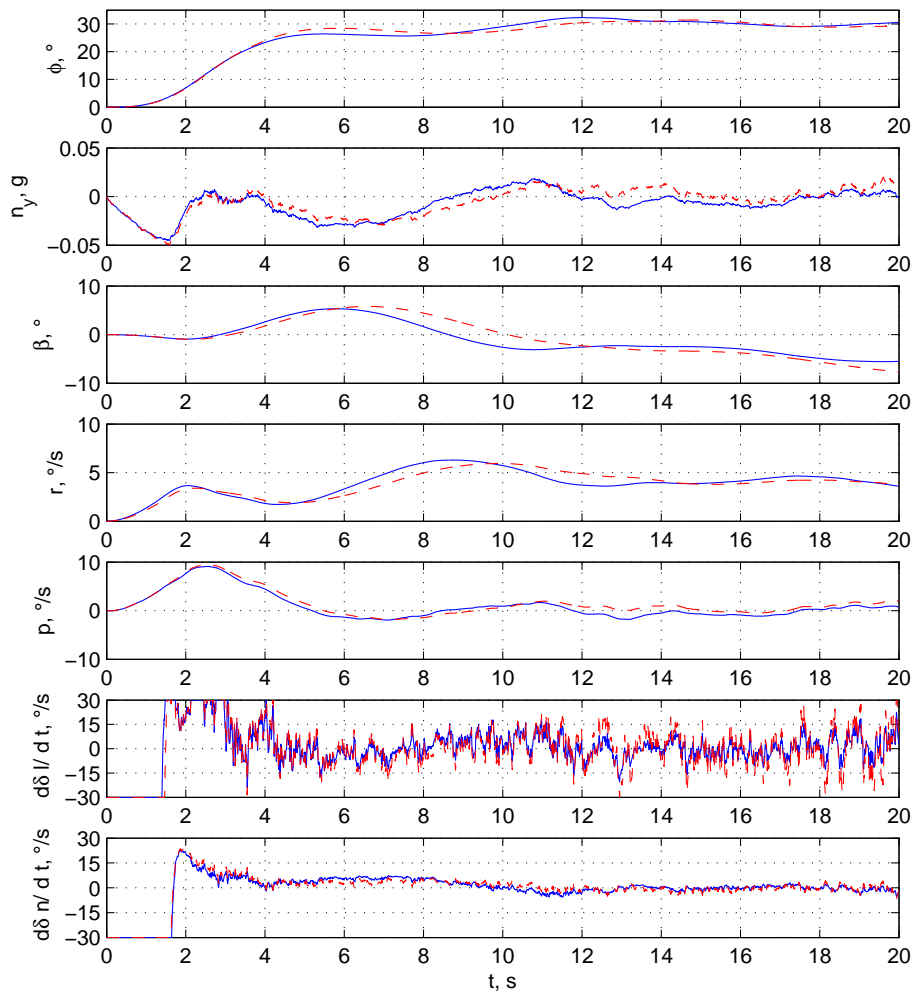


Figure 3.9: Commande  $\phi_c = 30^\circ$  dans une atmosphère turbulente.



## Chapter 4

# Gains et potentiels

La dernière partie de la thèse traite de l'estimation des avantages que l'on peut attendre d'une réduction de la stabilité naturelle d'un avion. Dans ce but, nous avons effectué une comparaison entre un modèle VELA naturellement stable, c'est-à-dire avec des centrages avant et une surface augmentée des dérives, et un modèle à efficacité maximisée (surface réduite, centrages autour du foyer).

Pour ceci on a effectué une estimation de masse des dérives. Le gain en masse d'une version à stabilité réduite n'a pas une grande influence sur la réduction de consommation de kérosène dans la mesure où il va falloir installer des actionneurs supplémentaires ainsi qu'une infrastructure pour le système de type back-up. Le gain en masse sera donc potentiellement compensé par la masse supplémentaire du système de contrôle.

Contrairement à la réduction de masse, l'effet d'une réduction de la traînée due à une surface réduite des dérives est très important. Nous avons appliqué la formule de Breguet afin de déduire une relation entre gain en traînée et gain en carburant. Le gain envisageable en centrant la plage des centrages autour du foyer n'est pas non plus à négliger, car cette modification est la plus simple à réaliser.

Pour un avion de type VELA, une différence de 1  $dc$  (variation de  $\pm 10^{-4}$  du coefficient de traînée) produit une consommation de  $\Delta m_F \approx 683$   $kg$  par vol long courrier. Pour un total de 650 vols par an et un prix de carburant de  $P_f = 0.5$   $\$/kg$  [65], la Table 4.1 montre la réduction des coûts d'un modèle VELA efficace instable par rapport à son équivalent stable.

Dans la Figure 4.1 on montre les contributions de chaque type de traînée pour une réduction de la surface de la dérive (traînée induite/ de friction) et d'une optimisation du centrage (traînée *trim*). Comme il a été annoncé précédemment, le gain en traînée induite dû à une masse réduite de la dérive peut être compensé par la masse associée à l'installation du système automatique. Par ailleurs, la réduction du plan vertical est sujette à des contraintes (notamment à cause des critères de vitesse minimale de contrôle). L'optimisation de la plage de centrage entraîne dans ce cas le minimum de modifications

| drag type         | $\Delta C_X, dc$ | <i>kg/trip</i> | <i>\$/trip</i> | <i>kg/year</i> | <i>\$/year</i> |
|-------------------|------------------|----------------|----------------|----------------|----------------|
| friction and form | 6.17             | 4281           | 2140           | 2 782 650      | 1 391 325      |
| induced           | 0.69             | 471            | 236            | 153 400        | 76 700         |
| trim              | 1.0              | 683            | 342            | 443 950        | 221 975        |
| total             | 7.86             | 5368           | 177.4          | 3 489 200      | 1 744 600      |

Table 4.1: Gains potentiels.

nécessaires et représente donc un compromis prometteur.

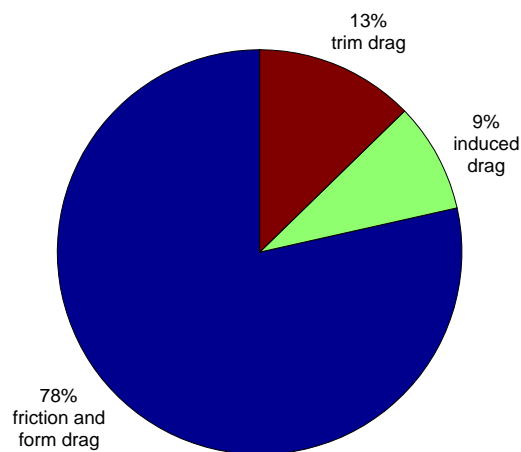


Figure 4.1: Contributions individuelles des différents types de traînée à une réduction potentielle des coûts.

## Chapter 5

# Conclusion et perspectives

Après la présentation de la motivation du sujet de recherche et la formulation des objectifs, le cadre de la certification et les aspects de la modélisation de l'avion ont été présentés, ce qui forme le point de départ de la thèse. La pluridisciplinarité du sujet a naturellement mené à diviser la thèse en deux parties majeures : une partie dédiée à l'analyse de la mécanique et de la dynamique du vol dans le contexte de la stabilité réduite et l'autre traitant de la synthèse d'un système de commande. Une troisième partie synthétise les résultats ainsi obtenus pour illustrer les gains possibles.

La partie sur l'analyse de la dynamique du vol a commencé par l'examen des effets de la stabilité réduite sur le mouvement longitudinal d'un avion. Une contribution majeure a été la description analytique de l'oscillation d'incidence de l'avion en présence d'une loi de commande stabilisante en fonction des caractéristiques de l'actionneur. Cette contribution permet d'aborder le problème de la robustesse par rapport aux variations du centre de gravité. Basé sur les résultats de cette approche, un outil numérique a été développé qui estime l'activité du système de commande et la fatigue de l'actionneur causées par la stabilisation artificielle. Cette technique a ensuite été appliquée à un profil d'une mission type d'un avion long courrier. De plus, les caractéristiques non-linéaires des actionneurs ont été prises en compte ce qui a abouti à la formulation d'un critère reliant les besoins minimaux en linéaire et non-linéaire sur les actionneurs pour un degré donné d'instabilité longitudinale.

Par la suite, nous avons étudié le mouvement latéral de l'avion et plus particulièrement les critères liés à la vitesse minimale de contrôle. Une approche analytique a mené à un outil numérique. Cet outil s'est montré d'une grande valeur pour l'évaluation de la capacité de l'avion à satisfaire les critères de certification lors d'une phase préliminaire de conception. Des critères statiques et dynamiques ont été examinés.

La première partie de la thèse s'est achevée par des recommandations pour le VELA - concept d'une configuration aile-fuselage intégrés - illustrant ainsi la faisabilité des approches proposées.

La partie commande a débuté par une courte introduction du problème en présentant la liste des spécifications pour la loi de commande robuste de dernier secours dite *back-up*. Les objectifs de commande étaient directement déduits des résultats de la partie sur la mécanique et la dynamique du vol.

La description théorique de la technique de synthèse polytopique d'un retour d'état a suivi un bref rappel des différentes approches possibles. À cause des multiples besoins de commande, plusieurs objectifs ont dû être simultanément pris en compte lors de la synthèse. Une contribution importante consistait en la combinaison de critères variés de type modal,  $H_\infty$ , de positivité et de robustesse en une seule procédure de synthèse convexe en une seule étape. De plus, une technique multi-critères multi-modèles de synthèse d'un correcteur statique de type anti-windup a été proposée. Une méthode d'analyse de stabilité et de performance a été adaptée afin d'évaluer les propriétés de la boucle fermée en présence de saturations. La relation entre les caractéristiques des saturations et la taille du domaine de stabilité a été illustrée. Enfin, nous avons obtenu des bons résultats pour l'aéronef naturellement instable VELA.

La troisième partie de la thèse illustre l'estimation des gains potentiels en masse, traînée et consommation de combustible en utilisant la stabilité réduite pour un avion de transport civil. En ce qui concerne le concept d'aile-fuselage intégrés, le gain le plus significatif viendrait de la réduction des plans verticaux. Ceci engendrerait néanmoins d'importantes modifications non seulement sur la commande de la dérive et des ailerons, mais aussi sur la conception de l'aéronef lui-même en raison des critères liés à la vitesse minimale de contrôle. Par conséquent, nous pouvons conclure qu'opter pour une optimisation de la plage de centrage tout en installant seulement un système de type back-up robuste longitudinal semble être le meilleur compromis entre simplicité et coût.

Il existe deux axes pour les perspectives : suivant le principe de l'évaluation de l'activité du système de commande et de la fatigue d'actionneur, un domaine de recherche prometteur est la représentation des manœuvres de vol sous la forme d'un ensemble de filtres, par exemple pour le décollage, la montée, les virages et l'atterrissage. Utiliser des fonctions de transfert pour filtrer des signaux aléatoires et modéliser les commandes du pilote pourrait être une extension directe de la méthode présentée. Elle permettrait non seulement l'estimation rapide de la fatigue, mais aussi la définition de besoins pour le système de commande correspondant à un profil de mission. Une validation des outils développés par rapport aux résultats obtenus sur l'avion réel est bien sûr nécessaire pour définir le domaine possible d'application.

Concernant le contrôle d'un avion long courrier à fuselage large et à stabilité réduite, les travaux futurs peuvent se focaliser sur la prise en compte de la partie flexible dans la synthèse du système de type back-up robuste. Maintenir les excitations des modes structuraux à un niveau acceptable avec une loi de commande à structure simple sera à coup sûr un défi, en particulier avec un degré d'instabilité naturelle élevé.

# Bibliography

- [1] AGARD (1974). Impact of active control technology on airplane design. Technical Report AGARD-CP-157, AGARD, Paris, France.
- [2] AGARD (1995). Aerodynamics of 3-d aircraft afterbodies. Technical report, AGARD.
- [3] Airbus (2002). Technical Report L07D1.169.0098/2002, Airbus.
- [4] Airbus (2003). Technical Report L27D1.169.1433/2003, Airbus.
- [5] Airbus (2005a). A380 specifications. Technical report, Airbus Industrie.
- [6] Airbus (2005b). Vela specifications. Technical report, AIRBUS.
- [7] Airbus (2006). A340-500/-600 elevators servocontrol - duty cycles update. Technical Report LR2734RP0602384, Airbus/EYCAA.
- [8] Alles, W. (2001). *Flugmechanik und Flugregelung*. RWTH Aachen.
- [9] Ananthkrishnan, N. and Unnikrishnan, S. (2001). Literal approximation to aircraft dynamic modes. *Journal of Guidance, Control, and Dynamics*, 24:1196–1203.
- [10] Anderson, B. and Vongpanitred, S. (1973). *Network Analysis*. Prentice-Hall, Englewood Cliffs, NJ.
- [11] Anderson, R. D., Flora, C. C., Nelson, R. M., Raymond, E. T., and Vincent, J. H. (1976). Development of weight and cost estimates for lifting surfaces with active controls. Technical Report NAS1-14064, NASA - National Aeronautics and Space Administration, Langley Research Center, Developed under contract by Boeing Commercial Airplane Company, Seattle, Washington.
- [12] Angelis, G., Kamidi, R., Molengraft, R., and Nijmeijer, H. (2000). Optimal polytopic control system design. *Proceedings of the 15th IEEE International Symposium on Intelligent Control (ISIC)*, pages 43–48.
- [13] Arnold, V. I. (1973). *Ordinary Differential Equations*. MIT Press, Cambridge, MA.
- [14] Bernard, C. (2002). Expressions analytiques des modes latéraux et longitudinaux d'un avion. Master's thesis, SUPAERO.

- [15] Böhm, M. (2007). *Gesamtentwurf eines ökonomischen und ökologischen Lufttransportsystems unter ausnutzung von Synergieeffekten*. PhD thesis, Universität der Bundeswehr, München.
- [16] Biannic, J., Roos, C., and Knauf, A. (2006a). Design and robustness analysis of fighter aircraft control laws. *European Journal of Control - special issue on LMI techniques in Control*, 12(1):71–85.
- [17] Biannic, J., Tarbouriech, S., and Farret, D. (2006b). A practical approach to performance analysis of saturated systems with applications to fighter aircraft flight controllers. *Proc. of the IFAC Symposium on Robust Control*.
- [18] Biannic, J.-M. (1998). Stability analysis of multivariable feedback systems with control input saturations. *Proceedings of IEE Control'98, Swansea, UK*.
- [19] Birk, T. (2007). Personal communication. *EADS Apsys, Risk Analysis Dept., Toulouse, France*.
- [20] Boiffier, J.-L. (1998). *Dynamique du Vol*. SUPAERO, Notes de cours.
- [21] Boyd, S., Ghaoui, L. E., Feron, E., and Balakrishnan, V. (1994). *Linear matrix inequalities in systems and control theory*. SIAM.
- [22] Brockhaus, R. (1994). *Flugregelung*. Springer-Verlag, Heidelberg, Berlin.
- [23] Chilali, M. and Gahinet, P. (1996).  $H_\infty$  design with pole placement constraints: an LMI approach. *IEEE Transactions on Automatic Control*, 41(3):358–367.
- [24] Chilali, M., Gahinet, P., and Apkarian, P. (1999). Robust pole placement in LMI regions. *IEEE Transactions on Automatic Control*, 44(12):2257–2269.
- [25] Covert, E. (1985). *Thrust and Drag: its Prediction and Verification*. AIAA, New York.
- [26] da Silva, J. G. and Tarbouriech, S. (2005). Antiwindup design with guaranteed regions of stability: an LMI-based approach. *IEEE Transactions on Automatic Control*, 50(1):106–111.
- [27] Döll, C. and Feuersänger, A. P. (2005-2006). MISCO - Minimization of the Control Function Cost. Progress Report. Technical Report Subtask B.1.2.2, ONERA - Airbus.
- [28] Doyle, J., Glover, K., Khargonekar, P., and Francis, B. (1989). State-space solutions to standard  $H_2$  and  $H_\infty$  control problems. *IEEE Transactions on Automatic Control*, 34(8):831–845.
- [29] EASA - European Aviation Safety Agency (2007a). Joint Aviation Requirements, Part23 - Normal, Utility, Aerobatic and Commuter Category Aeroplanes. Technical report, Joint Aviation Authorities, Cologne, Germany.

- [30] EASA - European Aviation Safety Agency (2007b). Joint Aviation Requirements, Part25 - Large Aeroplanes. Technical report, Joint Aviation Authorities, Cologne, Germany.
- [31] Eraydin, E. (1994). *Domaine de validité des équations de la dynamique du vol: decouplage*. PhD thesis, SUPAERO.
- [32] Etkins, B. and Reid, L. D. (1995). *Dynamics of Flight: Satability and Control*. Wiley, 3rd edition.
- [33] Ferreres, G. and Puyou, G. (2006). Flight control law design for a flexible aircraft: limits of performance. *Journal of Guidance, Control and Dynamics*, 29(4):870–878.
- [34] Feuersänger, A. (2004). Control of an aircraft with reduced stability. Master's thesis, SUPAERO, Toulouse, France.
- [35] Feuersänger, A. P., Döll, C., and Toussaint, C. (2006). Actuator influence on flying qualities of a naturally unstable aircraft. *Proceedings of the ICAS, Hamburg, Germany*.
- [36] Feuersänger, A. P. and Ferreres, G. (2006). Design of a robust back-up controller for an aircraft with reduced stability. *Guidance, Navigation, and Control Conference and Exhibit, Keystone, CO, USA*.
- [37] Feuersänger, A. P. and Ferreres, G. (2007). Robust back-up control design for an aircraft with reduced stability and saturated actuators. *IFAC Symposium: Automatic Control in Aerospace, Toulouse, France*.
- [38] Feuersänger, A. P., Toussaint, C., and Döll, C. (2005). The impact of reduced lateral stability on the  $v_{MC}$  equilibrium and manoeuvres during early design phases of an aircraft. *Deutscher Luft-und Raumfahrtkongress, Friedrichshafen, Germany*.
- [39] Feuersänger, A. P., Ferreres, G., and Toussaint, C. (2006). Synthèse d'un correcteur robuste de type back-up pour un avion à stabilité réduite. *Actes du congrès des doctorants EDSYS, Tarbes, France*.
- [40] Francis, B. A. (1987). *A course in  $H_\infty$  Control Theory*. Number 88 in Lecture Notes in Control and Information Sciences. Springer-Verlag, Berlin.
- [41] Gahinet, P., Nemirovski, A., Laub, A., and Chilali, M. (1995). *LMI control toolbox*. The Mathworks, Inc.
- [42] Gaulocher, S., Knauf, A., and Feuersänger, A. P. (2007). Self-scheduled controller design for relative motion control of a satellite formation. *In Proceedings: IMSM-IMAACA Multiconference, Buenos Aires, Argentina*.
- [43] Gomes da Silva, J. and Tarbouriech, S. (1999). Stability regions for linear systems with saturating controls. In *Proceedings of the ECC, Karlsruhe, Germany*.

- [44] Hafer, X. and Sachs, G. (1993). *Flugmechanik*. Springer, Berlin.
- [45] Hindi, H., Hassibi, B., and Boyd, S. (1998). Multi-objective  $H_2/H_\infty$ -optimal control via finite dimensional Q-parametrization and Linear Matrix Inequalities. *Proceedings of the ACC*, pages 3244–3249.
- [46] Hirsch, M. W. and Smale, S. (1974). *Differential Equations, Dynamical Systems and Linear Algebra*. Academic Press, New York.
- [47] Hoblit, F. (1988). *Gust loads on aircraft: concepts and applications*. Education Series. AIAA.
- [48] Imbert, N. and Mouyon, P. (2007). Calcul prédictif de la fatigue des actionneurs. Technical Report 1/11970 DCSD, ONERA-DCSD.
- [49] Jakob, D. (2000). *Flugzeugbau I und II und Flugzeugsysteme*. ILR, RWTH Aachen.
- [50] Jane's (2007). *Jane's: All the World's Aircraft*. Jane's Information Group.
- [51] Jenkinson, L., Simpkin, P., and Rhodes, D. (1999). *Civil Jet Aircraft Design*. Arnold, London.
- [52] Knauf, A., Gaulocher, S., and Feuersänger, A. P. (2006). Innovative controller design for systems with parameter variations. In *Proceedings: Deutscher Luft-und Raumfahrtkongress, Braunschweig, Germany*.
- [53] Kossira, H. (2002). *Flugzeugbau II, Arbeitsblätter zur Vorlesung*. Technische Universität Braunschweig.
- [54] Lalanne, C. (1999a). *Dommages par fatigue*, volume 4 of *Vibrations et chocs mécaniques*. Hermes Science Publications, Paris, London, 1st edition.
- [55] Lalanne, C. (1999b). *Vibrations aléatoires*, volume 3 of *Vibrations et chocs mécaniques*. Hermes Science Publications, Paris, London, 1st edition.
- [56] Lemaignan, B. (2002). Mise en place de méthodes de comparaison des qualités de vol au stade avant-projet. Technical report, SupAéro- Airbus France.
- [57] Lemaignan, B. (2003). Vela stability and control criteria list for the flying wing. Technical Report VELA-AF-310-001, Airbus EYCD.
- [58] LHT - Arbeitskreis Masseanalyse (MA) (2007). *Luftfahrttechnisches Handbuch - Masseanalyse*. IABG mbH.
- [59] Livneh, R. (1995). Improved literal approximation for lateral-directional dynamics of rigid aircraft. *Journal of Guidance, Control, and Dynamics*, 18:925–927.

- [60] Losser, Y. and Mouyon, P. (2004). Ajustement de lois de pilotage pour la réduction du dommage par fatigue des servocommandes d'un avion. In *Conférence Internationale Francophone d'Automatique CIFA 2004*, Douz, Tunisia.
- [61] Magni, J.-F. (2002). *Robust Modal Control with a Toolbox for Use with Matlab*. Kluwer Academic/Plenum Publishers.
- [62] Marquez, H. (2003). *Nonlinear control systems: analysis and design*. Wiley Interscience.
- [63] McCormick, B. (1995). *Aerodynamics, Aeronautics, and Flight Mechanics*. John Wiley & Sons, Inc., New York.
- [64] Messier-Bugatti (2007). Electro hydro static actuator. *Messier-Bugatti*, , *SAFRAN Group*.
- [65] Müller, S. (2007). Personal communication. *Airbus Central Entity, Marketing Division - CSMAW, Toulouse/Blagnac, France*.
- [66] Mouyon, P. and Gaillet, A. (2004). Critère de dommage par fatigue pour les servocommandes d'un avion. In *Conférence Internationale Francophone d'Automatique CIFA 2004*, Douz, Tunisia.
- [67] Nguewo, D. (2006). *Entwurfseminar Flugzeugbau*. Universität Stuttgart.
- [68] Pac, J. (1999). *Les processus stochastiques*. SUPAERO, Toulouse, France.
- [69] Pamadi, B. N. (2004). *Performance, Stability, Dynamics, and Control of Airplanes*. American Institut of Aeronautics and Astronautics (AIAA).
- [70] Perko, L. (1991). *Differential Equations and Dynamical Systems*. Springer-Verlag, New York.
- [71] Phillips, W. F. (2000). Improved closed-form approximation for dutch-roll. *Journal of Aircraft*, 37:484–490.
- [72] Pialat, E. and Loubignac, H. (2003). Étude comparative des VMC sur les avions Airbus et Boeing. Internal report, SUPAERO, Toulouse, France.
- [73] Pittet, C. S., Tarbouriech, S., and Burgat, C. (1997). Stability regions for linear systems with saturating controls via circle and popov criteria. *Proceedings of the IEEE CDC, Sam Diego, CA*, pp.4518-4523.
- [74] Rageade, L. and Delporte, M. (2004). Simulation des missions de fatigue actionneurs a340-500 a340-600. Technical Report F070SP040403996, Airbus/EYCDA.
- [75] Raymer, D.-P. (1999). *Aircraft Design: A Conceptual Approach*. AIAA Education Series, Washington D.C.

- [76] Roskam, J. (1987-1990). *Airplane Design, Part I - VIII*. Roskam Aviation and Engineering Corporation, Ottawa, Kansas.
- [77] Ruijgrok, D. (1990). *Elements of Airplane Performance*. Delft University Press.
- [78] Scherer, C. (1990). *The Riccati Inequality and State-Space  $H_\infty$ -Optimal Control*. PhD thesis, University of Würzburg, Germany.
- [79] Scherer, C. (1995). Multiobjective  $H_2/H_\infty$  control. *IEEE Transactions on Automatic Control*, 40(6):1054–1062.
- [80] Scherer, C., Gahinet, P., and Chilali, M. (1997). Multiobjective output-feedback control via LMI optimization. *IEEE Transactions on Automatic Control*, 42(7):896–911.
- [81] Schlichting, U.-J. and Truckenbrodt, E. (1967). *Aerodynamik des Flugzeuges, Band 1 und 2*. Springer, Berlin.
- [82] Schneider, H. (2007). Personal communication. *Universität Karlsruhe, Germany*.
- [83] Shimomura, T. and Pullen, S. (2002). Strictly positive real  $H_2$  controller synthesis via iterative algorithms for convex optimisation. *Journal of Guidance, Control and Dynamics*, 25(6):1003–1011.
- [84] Shue, S., Sawan, M., and Rokhsaz, K. (1997). Mixed  $H_2/H_\infty$  method suitable for gain-scheduled aircraft control. *Journal of Guidance, Control and Dynamics*, 20(4):699–706.
- [85] Simon, D. and Servoles, S. (2001). Analytical expression of the lateral modes of an aircraft. Studyproject, SUPAERO.
- [86] Takaba, K. (1999). Anti-windup control system design based on Youla parametrization. *Proceedings of the ACC*, pages 2012–2017.
- [87] Takaba, K. (2002). Analysis and synthesis of anti-windup control system based on Youla parametrization. *Proceedings of the IEEE CDC*, pages 2692–2697.
- [88] Thayer, W. J. (1967). Supply pressure considerations for servocontrols. *Meeting 63, SAE Commitee A-6, Aerospace Fluid Power and Control Technologies, Phoenix, Arizona*.
- [89] Torenbeek, E. (1986). *Synthesis of Subsonic Airplane Design*. Delft University Press, Martinus Nijhoff Publishers.
- [90] Toussaint, C. and Gimonet, B. (2007). Flybig, tache c.3.2: contrôle longitudinal de l’aile volante. Technical Report RF 1/09626 DAAP/DCSD, ONERA.

- [91] Toussaint, C., Renier, O., and L.Planckaert (2004). Qualités de vol d'une aile volante naturellement instable. Technical Report RT 211/07505 DAAP-DCSD, ONERA Toulouse, France.
- [92] U.S. Department of Defense (1975). Flight control systems - design, installation and test of piloted aircraft. Technical report, USAF.
- [93] U.S. Department of Defense (1980). Military specification, flying qualities of piloted airplanes. MIL-F-8785C. Technical report, Department of Defense Military Specifications and Standards, Philadelphia, Pennsylvania.
- [94] U.S. Department of Defense (1990). Department of defense interface standard, flying qualities of piloted aircraft. MIL-STD-1797A. Technical report, Department of Defense Military Specifications and Standards, Philadelphia, Pennsylvania.
- [95] U.S. Department of Defense (1995). Department of defense interface standard, flying qualities of piloted aircraft. MIL-STD-1797A update. Technical report, Wright-Patterson Air Force Base, Ohio: Systems Engineering Division, Aeronautical Systems Center.
- [96] U.S. Department of Transportation (2001). Federal Aviation Regulations, Part 25 - Airworthiness Standards: Transport Category Airplanes. Technical report, FAA - Federal Aviation Administration, Washington, DC.
- [97] U.S. Department of Transportation (2002). Federal Aviation Regulations, Part 23 - Airworthiness Standards: Normal, Utility, Acrobatic, and Commuter Category Airplanes. Technical report, FAA - Federal Aviation Administration, Washington, DC.
- [98] van der Pol, B. (1920). *Radio Review*, 1:704–754.
- [99] Wanner, J.-C. (1984). *Dynamique du vol et pilotage des avions*. ONERA/SUPAERO.
- [100] Wokurka, N. (2004). Long range - handling qualities fatigue missions sizing for actuators duty cycles - update. Technical Report LR070RP0413950, Airbus/EYCDA.
- [101] Wu, F. and Soto, M. (2004). Extended anti-windup control schemes for LTI and LFT systems with actuator saturations. *International Journal of Robust and Nonlinear Control*, 14:1255–1281.
- [102] Young, A. D., Paterson, J. H., and Lloyd, J. J. (1995). Aircraft excrescence drag. Technical Report AGARDograph No.264, AGARD, London.